THE UNIVERSITY
of EDINBURGH

How telomerase and Dna2 govern the fate of chromosome ends in *Saccharomyces cerevisiae*

Andrei Sukhareuski

Thesis presented for the degree of Doctor of Philosophy

Institute of Cell Biology
The University of Edinburgh
September 2019

Declaration

I declare that this thesis has been composed by myself and the work presented herein is my own, unless stated otherwise. This work has not been submitted for any other degree or professional qualification

Andrei Sukhareuski
September 2019

Acknowledgements

I would like to express gratitude to my supervisor Sveta Makovets, who gave me a unique chance to study and work in her lab in one of the world's most prestigious universities. Such opportunity can not be underestimated. Sveta's firm mentorship and helpful advice guided me through a lot of rocky patches during my PhD both inside and outside the lab environment.

My thanks also go to the members of my thesis committee, Sander Granneman, Heidrun Interthal and David Leach, who gave me essential feedback on my work, provided me with support and useful advice, when I needed it most.

I also want to thank my labmates, both former and present, my comrades and fellow warriors in the battle for science and survival in the lab. Caroline, Yulia, Lyosha, Vicky, Dima, Tadas, John, Raminta, Alina, Anton, Melanie and Alex were side-by-side with me during my hardest times. Together we shared a lot of memorable moments, inside jokes, beer pints, reagents and seminars, exchanged skills and ideas, had each other's back, when an occasional spec was left switched on, lived through highs and lows of the lab work. Together we matured as scientists, and just like any other major school in life, the PhD school will leave a lingering imprint in my memory of people with whom I shared this journey.

I should also thank the members of neighboring labs, who helped me with their expertise, provided valuable feedback and with whom I had many entertaining conversations: Xavier Zaoui, Jerko Rosko, Rob van Nues, Dani Wicaksono, Katerina Kapitonova, Trevor Ho, Lisa Iurchenko, Benura Azeroglu and Smitha Hegde. I want to thank the Belarusian undergraduate students, who made me feel at home in a foreign country: Alex Damenikan, Tanya Kapustenko, Nastya Malysheva, Sergei Gladkov and Katya Moskalenko.

Many thanks to my dear friends, who stayed in touch with me, when I was far from home, who made me company, when I was lonely and desperate, who had a lot of faith in me, when I had very little, who helped me to get through

the tough times and not give it all up: Anton Kovalevskiy, Oksana Kirsanova, Sergey Yanushkevich, Nikita Vasilyev, Natasha Khenkina, Anya Yablonskaya, Polina Sasinovich, Zhenya Anch, Pavel Platonov, Katya Gotina, Dima Kuzmin, Dasha Pavlova, Diana Lesnikova, Artyom Chizhik, Tanya Kostachka, Vika Staravoytova and Margarita Gotmanova. My special thanks go to my two best friends Vladimir Kerzikov and Lena Strelchenya. I cannot stress enough, how much their friendship and unrelenting support are appreciated.

I am very grateful to my parents and grandparents, unwaveringly supportive of my choices in life, to my school teachers Ludmila Semyonovna Mitskevich and Evegeniy Grigoryevich Terehov, who instigated my interest in biology and to my undergraduate supervisor Vasily Grinev for helping me to set up my research career.

My PhD would not have been possible without funding provided by the Darwin Trust of Edinburgh, established by Ken and Noreen Murray, brilliant scientists and wonderful people, whom I unfortunately never had a pleasure to meet. I also thank David Finnegan and Heather Hall, whose work makes Darwin Trust possible.

The smooth flow of scientific work within the Roger Land building relies on the members of university administration and management: George Mcmillan, Fiona Black, Graham Nicolson, David Sneddon and Margaret Martin to whom I also address my thanks.

I am thankful to all unknown readers of my thesis who found it, for giving me hope that my work was not in vain.

Finally, I would like to thank my examiners Dr Sara Buonomo and Dr Laura Maringele for the time and effort spent on helping me to improve my thesis and successfully complete my PhD.

Abstract

Genome stability in eukaryotic cells relies heavily on their ability to differentiate between telomeres - natural ends of linear chromosomes - and double strand breaks (DSBs), pathological lesions which can occur throughout the stretch of chromosomal DNA. The former are to be protected from fusions, recombination and recognition by DNA damage response, whereas the latter are to be detected by the checkpoint system and repaired by end joining or homologous recombination. Due to the end replication problem, continually dividing cells are confronted with an additional necessity to maintain stable telomere length, which in most eukaryotes is fulfilled by telomerase. Telomerase is downregulated in human somatic cells to limit their replicative capacity and prevent malignization, forcing pre-malignant cells to seek ways of re-establishing telomere length homeostasis. Most cancers perform it by reactivating telomerase. Recently, Makovets group found a yeast model for telomerase reactivation through aneuploidy in cells with temperature-induced telomerase insufficiency. Given that aneuploidy is a common feature of cancers, a deeper mechanistic understanding of aneuploidy-driven telomerase reactivation in yeast may shed more light on cancer telomere biology.

In telomerase-negative cancers telomere attrition is counteracted by alternative lengthening of telomeres (ALT). ALT is related to one of DSB repair pathways - break-induced replication (BIR), which operates on single-ended DSBs, such as those originating from broken replication forks. Phosphorylated Pif1 helicase has been reported to be essential for BIR, but the molecular mechanism of this requirement has not been ascertained. We found that the need for phosphorylated Pif1 in BIR is alleviated in yeast expressing an N-terminally truncated Dna2 nuclease/helicase. In my work I aim to gain insights into how yeast solve problems related to both natural chromosomal ends and DSBs by investigating mechanisms underlying aneuploidy-dependent telomerase reactivation in yeast cells with temperature-induced telomerase insufficiency and by studying the genetic interaction between Dna2 and Pif1 in BIR.

Lay summary

The human genetic makeup is composed of 46 chromosomes, each of them a linear DNA molecule with two ends. Bacterial genome is different in that regard, as in most bacterial species there is only one circular chromosome with no ends. Having two-ended chromosomes is a two-edged sword. As a species we benefit from the genetic diversity resulting from the constant reshuffling of genes between parental chromosomes in each generation, made easy by the linear topology of human chromosomes. But for an individual human cell, linear chromosomes present certain challenges, as the chromosome ends require protection from fusing and degradation. In addition, because of the properties of the machinery used by all living cells to copy their DNA, chromosomes with linear topology become ever shorter at the ends with each copying cycle. The ends of the chromosomes are called telomeres and consist of a stretch of repetitive DNA sequence, which is mostly meaningless in terms of informational content, but constitutes an essential reserve of chromosome length, which can be sacrificed for the greater good of DNA copying. Moreover, telomeres play essential role in protecting chromosomes from fusions and degradation. However, when many DNA replication cycles pass, the telomere reserve becomes exhausted and essential genes start being targeted by the chromosomal attrition. This attrition is considered to be one of the fundamental mechanisms of ageing both at the level of single cells and complex organisms, such as ourselves. Multicellular organisms die eventually, but their species prevail at the level of germline cells (which give rise to sperms and egg cells), while for single-celled organisms reproduction is tantamount to cellular division. Thus, in all eukaryotic species the continuation of life requires some way of restoring the telomeres lost in the process of DNA synthesis. This is made possible by a special molecular machine called telomerase, which adds on telomere repeats at chromosome ends. In humans telomerase is present in sufficient amounts in germline, embryonic and stem cells, while in the bulk of human cells the amount of telomerase diminishes at the embryonic stage and is kept low thought life. This is believed to be an evolved protective

mechanism, which prevents pre-cancerous cells from forming tumors by limiting their capacity to proliferate, as without telomerase such cells would eventually run out of telomere repeats to spare. However, cancers do occur in humans, which means that cancerous cells have ways of sustaining their telomeres. Most types of cancers do this by restoring the necessary amount of telomerase. The process of telomerase reactivation in cancer cells is thus of outmost interest for medical science and a major target of cancer therapy research.

A lot of telomere biology research has been performed on buddying yeast – a convenient model organism, which is easy to grow and manipulate genetically. Being single-celled organisms, yeast normally possess active telomerase in each cell, however it was discovered that a rise in the growth temperature produces a decrease in the amount of the telomerase in yeast. Makovets lab have developed a yeast model of telomerase reactivation, which occurs at elevated growth temperature as a result of a major genetic rearrangement in yeast cells. Similarities between this yeast model and human cancers can be drawn, as genetic rearrangements are commonplace in cancer cells and are known to cause telomerase activation. The precise mechanism of telomerase reactivation in this yeast model is the focus of one of my PhD projects.

The second project of my PhD addresses some aspects of the repair of chromosomal breaks. While the ends at the edges of chromosomes are a natural part of human life, the ends that are created as a result of chromosomal fragmentation are different and extremely dangerous for cells. Chromosomal breaks that produce such ends may result from radiation, toxins or simply as a consequence of metabolic processes in the cell. Luckily, cells possess an efficient machinery for tackling chromosomal breaks. Yet again, an extremely useful and life-giving process, such as chromosome break repair, may become hijacked by cancer cells for their malignant purposes, specifically, to maintain their telomeres in the absence of telomerase. At the same time, the reliance of cancer cells on specific types of chromosomal break repair for proliferation makes these types of repair cancer’s Achilles tendon, if only we were to learn how to target these processes. Many proteins are involved in chromosomal

break repair, Dna2 being one of them. My second PhD project is devoted to understanding some of the functions of Dna2 in break repair in yeast with the hope of contributing to finding more weak spots in cancer.

Abbreviations

5-FOA	5-fluoroorotic acid
ALT	alternative lengthening of telomeres
alt-NHEJ	alternative non-homologous end joining
APS	ammonium persulfate
ATP	adenosine triphosphate
BIR	break-induced replication
bp	base pair(s)
c-NHEJ	classic non-homologous end joining
DDC	DNA damage checkpoint
dHJs	double Holliday junctions
D-loop	displacement loop
DMSO	dimethyl sulfoxide
DNA	deoxyribonucleic acid
DNTA	*de novo* telomere addition
dNTP	deoxyribonucleotide triphosphate
DRC	DNA replication checkpoint
DSB	double-strand break
DSBR	double-strand break repair
dsDNA	double-stranded DNA
DTT	dithiothreitol
ECL	electrochemiluminescence
EDTA	ethylenediaminetetraacetic acid
FISH	fluorescent in situ hybridization
Gal	galactose
GC	gene conversion
h	hour(s)
HDR	homology-dependent repair
HJ	Holliday junction
HR	homologous recombination

IP	immunoprecipitation
kb	kilobase(s)
kDa	kilodalton(s)
LOH	loss of heterozygosity
min	minute(s)
MMEJ	microhomology-mediated end joining
NHEJ	non-homologous end joining
nt	nucleotide(s)
OD_{600}	optical density at 600 nm
o/n	overnight
PCR	polymerase chain reaction
PEG	polyethylene glycol
PMSF	phenylmethylsulfonyl fluoride
PVDF	polyvinylidene difluoride
PVP	polyvinylpyrrolidone
Raf	raffinose
REC	recombination execution checkpoint
RNA	ribonucleic acid
rpm	revolutions per minute
sec	second (s)
SDS	sodium dodecyl sulphate
SDSA	synthesis-dependent strand annealing
SDS-PAGE	SDS polyacrylamide gel electrophoresis
SSA	single-strand annealing
SSC	saline sodium citrate
ssDNA	single-stranded DNA
SSPE	saline sodium phosphate EDTA
T_a	temperature of annealing
TBE	Tris-borate-EDTA
TBST	Tris-buffered saline with Tween

TCA	trichloroacetic acid
TE	Tris-EDTA
TEMED	N,N,N’,N’-tetramethylethylenediamine
T_m	temperature of melting
TPE	telomere position effect
TRF	terminal restriction fragment
UV	ultraviolet light
v/v	volume per volume
WB	western blot
w/v	weight per volume

Contents

List of figures

List of tables

CHAPTER 1

General Introduction

1.1. Properties, functions and maintenance of natural eukaryotic chromosome ends

Telomeres are the ends of linear eukaryotic chromosomes and are crucial for maintaining genome stability (Kupiec, 2014). Two major components of telomeres are DNA (represented by TTAGG-type repeats in most eukaryotes, Palm and de Lange, 2008; Fulcher *et al.*, 2014) and associated proteins which prevent chromosomes from fusion (Pardo and Marcand, 2005), nucleolytic degradation and recombination (Polotnianka, Li and Lustig, 1998). The telomeric DNA consists of a centromere-proximal double-stranded region followed by a centromere-distal G-rich 3'-overhang which varies in length across different groups of eukaryotes.

1.1.1. An overview of mammalian telomeres

The structure and functions of mammalian and, more specifically, human telomeres are particularly relevant to understanding and treating human telomere-related diseases, ageing and cancer. Mammalian telomeres represent a stretch of tandem repeats of the sequence TTAGGG which may span as long as 50 kbp (Lejnine, Makarov and Langmore, 1995). The G-rich 3'-tail at the end of a human telomere is about 50-500 nucleotides long (Makarov, Hirose and Langmore, 1997; Stewart *et al.*, 2003) and is not present as a free ssDNA overhang, but is instead base-paired to the double-stranded part of the telomere DNA causing an eviction of a region of the G-reach strand in the form of a D-loop (Griffith *et al.*, 1999). The bigger loop that encompasses the D-loop and the terminal part of the telomere separated by the D-loop from the rest of the chromosome is termed the t-loop. As will be discussed below, the t-loop plays critical roles in telomere protection from checkpoint recognition, homologous recombination and telomere fusions.

Mammalian telomeres are covered by a six-protein complex, called shelterin (Figure 1.1, De Lange, 2005), which performs vital protective functions, including the formation of the t-loop (Stansel, De Lange and Griffith, 2001). Two evolutionarily related shelterin proteins TRF1 and TRF2 form homodimers

which interact with the double-stranded telomere sequence via their C-terminal Myb/SANT domains (Bianchi *et al.*, 1997; Broccoli *et al.*, 1997; Court *et al.*, 2005; Hanaoka, Nagadoi and Nishimura, 2009) and directly or indirectly recruit other shelterin components and non-shelterin accessory factors to telomeres (Kim *et al.*, 2009; reviewed in de Lange, 2018).

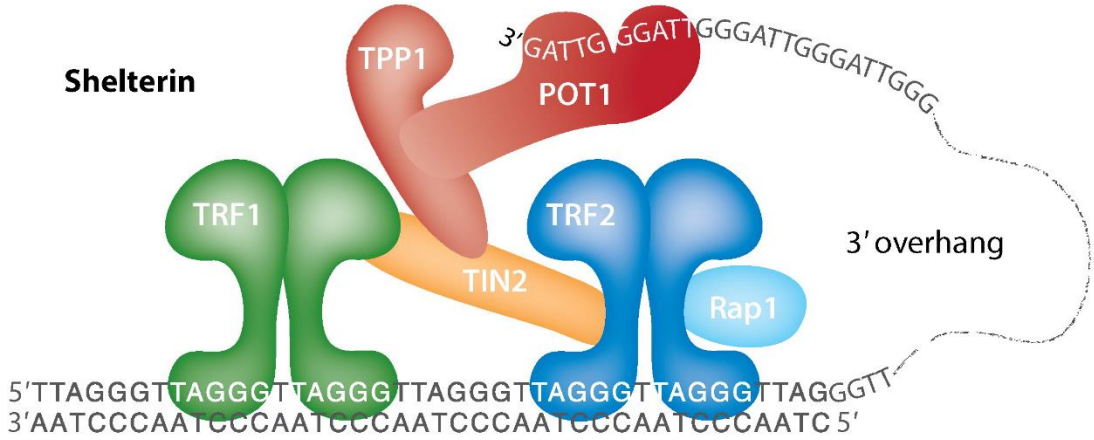

Figure 1.1: Schematic of human shelterin complex and its association with a telomere

From de Lange, 2018

The single-stranded parts of the telomere (including the ssDNA of the telomeric D-loop) are bound by the shelterin component POT1 which forms a heterodimer with another shelterin protein TPP1 (Baumann and Cech, 2001; Liu *et al.*, 2004; Loayza *et al.*, 2004). Rodent cells possess two POT1 paralogues – POT1a and POT1b, which have a partial separation of functions (Hockemeyer *et al.*, 2006; Wu, Takai and De Lange, 2012). TPP1 is bridged to TRF1 and TRF2 via another shelterin protein TIN2, which thus connects the dsDNA-interacting part of the shelterin complex to the ssDNA-interacting part (Ye *et al.*, 2004; Hu *et al.*, 2017). Noteworthy, POT1 depends on the interaction with TPP1 for its nuclear localization and recruitment to the telomeric ssDNA (Liu *et al.*, 2004; Ye *et al.*, 2004; Chen, Liu and Songyang, 2007). In addition, TPP1 has been shown to recruit telomerase to human telomeres (Abreu *et al.*, 2010).

Finally, the shelterin complex comprises RAP1, which is the only shelterin component with an ortholog among budding yeast telomere-capping proteins. Contrary to its *S. cerevisiae* counterpart, mammalian RAP1 demonstrates a low affinity to telomeric DNA, despite possessing a Myb domain (Hanaoka *et al.*, 2001; Arat and Griffith, 2012), and predominantly depends on TRF2 for telomere association (Zhu *et al.*, 2000; Celli and de Lange, 2005).

Shelterin performs a range of tasks pertinent to telomere protection and genome stability. TRF2 is believed to facilitate t-loop formation by virtue of its ability to wrap DNA around itself, thus creating a local area of unwound DNA in the double-stranded part of the telomere, which promotes the invasion by the G-tail and D-loop formation (Amiard *et al.*, 2007). Some models propose that the TRF2-dependent t-loop formation averts ATM activation by preventing the 3'-overhang from interacting with the MRN complex, thereby blocking the initial step of the ATM-dependent checkpoint cascade (see section 1.2.2 for the DNA damage checkpoint overview) (Palm and de Lange, 2008). Another checkpoint cascade, that is governed by the ATR kinase, is inhibited by POT1 at telomeres (Denchi and De Lange, 2007). POT1 associates with telomeric ssDNA thus rendering it inaccessible for RPA binding, which is required for ATR activation (Gong and de Lange, 2010). Deletion of either POT1 or TRF2 causes continuous checkpoint signalling, inhibiting the transition of cells into the S-phase or mitosis and eventually leading to senescence or apoptosis, depending on the cell type (Karlseder *et al.*, 1999; Smogorzewska and De Lange, 2002; Celli and de Lange, 2005; Denchi and De Lange, 2007).

Additionally, TRF2 hinders PARP1 signalling at telomeres by masking the 5' ds-ssDNA junctions at the base of the t-loop from PARP1 detection (Poulet *et al.*, 2009; Rai *et al.*, 2016; Schmutz *et al.*, 2017). When PARP1 is not restricted by TRF2 in its ability to recognize the 5' ds-ssDNA junction, such as when cellular TRF2 lacks part of its N-terminus, it may recruit Holiday junction resolvases to the t-loop, potentially resulting in large terminal deletions.

Apart from inhibiting checkpoint signalling at telomeres shelterin and the associated factors protect telomeres from the double-strand break (DSB)

repair processes, such as classic non-homologous end-joining (c-NHEJ), microhomology-mediated end-joining (MMEJ) and homologous recombination (see section 1.2.1 for the overview of DSB repair) (Van Steensel, Smogorzewska and De Lange, 1998; Celli, Denchi and de Lange, 2006; Mateos-Gomez *et al.*, 2015). TRF2-induced t-loop has been proposed to repress telomere fusions by sequestering the telomere end from the Ku70/80 protein complex (Doksani *et al.*, 2013). Homologous recombination at telomeres is averted by Ku70/80 complex (Celli, Denchi and de Lange, 2006), which has been shown to associate with TRF2 (Song *et al.*, 2000). Both shelterin complex and Ku70/80 have been implicated in alternative NHEJ (alt-NHEJ) inhibition at telomeres (Sfeir and De Lange, 2012; Mateos-Gomez *et al.*, 2015).

1.1.2. An overview of mammalian telomerase

Soon after deciphering the molecular mechanism of DNA replication it became apparent that telomeric ends of linear chromosomes cannot be completely copied by regular eukaryotic DNA-polymerases (as these enzymes require an RNA primer to initiate synthesis) and therefore must become ever shorter with each replication/division cycle (Olovnikov, 1973). This is actually the case for human somatic cells which hence divide only around 50 times in cell culture before they senesce and die (Hayflick, 1965; Gilson and Géli, 2007). But the fact that telomere length is maintained in germline cells, embryonic stem cells, cancer cells and unicellular organisms still required an explanation and it came with the discovery of *Tetrahymena* telomerase – the enzyme capable of extending telomeric DNA primer (Greider and Blackburn, 1985).

It has since been established that in most other eukaryotes telomere length is also sustained by telomerase, with some exceptions, such as *Drosophila melanogaster*, whose cells maintain their telomere-length homeostasis through retrotransposition (Mason, Frydrychova and Biessmann, 2008; Wellinger and Zakian, 2012).

Similarly to most other eukaryotes, mammalian cells maintain stable telomere length using telomerase enzyme (Morin, 1989; Meyerson *et al.*, 1997; Nakamura *et al.*, 1997). Mammalian telomerase core includes a reverse transcriptase polypeptide (TERT) and an RNA (TERC) containing a template region for telomere extension (Feng *et al.*, 1995; Beattie *et al.*, 2001). In large mammals, such as humans, TERT gene is transcriptionally downregulated in most somatic cells, limiting their proliferative capacity (Gorbunova and Seluanov, 2009). When several telomeres in a cell reach critically short length, it undergoes apoptosis or transitions into a senescence state, likely due to shelterin deprotection (Karlseder, Smogorzewska and De Lange, 2002; D'Adda Di Fagagna *et al.*, 2003; Zou *et al.*, 2004). Cellular senescence resulting from reduced telomerase activity in somatic cells is considered among the main reasons of ageing in humans (Harley *et al.*, 1992; Kim *et al*., 1994). Downregulation of telomerase gene is believed to serve the purpose of restricting proliferation of pre-cancerous cells in organisms with higher cell numbers and correspondingly a higher chance of cancer development (Gorbunova and Seluanov, 2009). However, human cells that have impaired DNA damage signalling due to the lack p53 and RB proteins are able to bypass senescence induced by telomere deprotection (Jacobs and De Lange, 2004). In cells with dysfunctional DNA damage signalling deprotected telomeres may initiate a cascade of severe genome rearrangements, which might result in malignant transformation (Chin *et al.*, 1999; Maser and DePinho, 2002; O'Hagan *et al.*, 2002). In the absence of cell cycle arrest repeated break-fusion-bridge cycles caused by telomere fusion may lead to translocations, gene amplifications and loss of heterozygosity (LOH) (Riboni *et al.*, 1997; Artandl *et al.*, 2000; Roger *et al.*, 2013). The consequences of telomere dysfunction also include chromothripsis and tetraploidization, the latter often followed by aneuploidy (Galipeau *et al.*, 1996; Davoli, Denchi and de Lange, 2010; Davoli and de Lange, 2012; Maciejowski *et al.*, 2015). All these kinds of genomic rearrangements have been connected to malignization (Artandl *et al.*, 2000; Dumur *et al.*, 2003; Davoli and de Lange, 2011; Li *et al.*, 2014). However, in the long run constant genome instability

may decrease cell viability and proliferative capacity due to extreme levels of genome deterioration (Jacobs and De Lange, 2004). Therefore, despite genome instability promoting cellular transformation at a certain step of cancer development, long-term survival of cancerous cells likely requires that genome instability is eventually restrained. This requirement has been postulated to create a selective pressure in cancerous cells to reestablish telomere protection by reactivating telomerase expression or switching to recombination-dependent alternative lengthening of telomeres (ALT) (Maciejowski and De Lange, 2017). Noteworthy, as many as 85% of cancers reactivate telomerase in order to overcome the end-replication problem limiting propagation (Shay and Bacchetti, 1997). Telomerase-positive cancers are often more aggressive than telomerase-negative variants (Tatsumoto *et al.*, 2000; Oh *et al.*, 2008; Peifer *et al.*, 2015). These notions underscore telomerase as both a relevant research object and a promising therapeutic target.

1.1.3. The structure and the biological role of *S. cerevisiae* telomeres

The structure of budding yeast telomeres has special properties (Figure 1.2) some of which are not shared by other model organisms. One of the key features of *S. cerevisiae* telomere dsDNA is that it is represented by a 300±75bp stretch of degenerate repeats with consensus $C_{1-3}A/TG_{1-3}$ (Shampay, Szostak and Blackburn, 1984) rather than a precisely repeated sequence. The terminal part of budding yeast double-stranded telomere region is juxtaposed to a single-stranded tail of G-rich strand. The latter sustains the length of 12-15 nt during most of the cell cycle (Larrivée, LeBel and Wellinger, 2004) except for a short period within late S/G_2 phase when it extends to ≥30-100 nt (Wellinger, Wolf and Zakian, 1993). Safe for specific circumstances (Cesare *et al.*, 2008), yeast telomeres are speculated to lack any base pairing between the relatively short overhang (the G-tail) and the double-stranded telomere stretch due to yeast telomeres being short and irregular in sequence (Tomaska *et al.*, 2004; Luke-Glaser, Poschke and Luke, 2012).

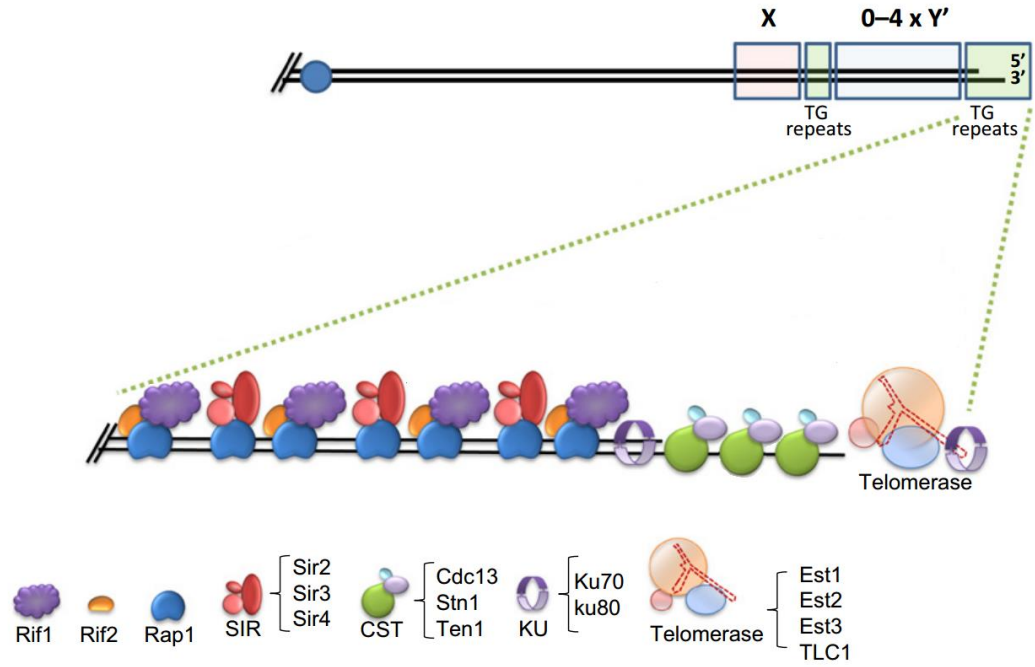

Figure 1.2: Schematic of a yeast telomere with associated proteins

Modified from Kupiec, 2014

Budding yeast telomeres are preceded by subtelomeric sequences of two types – X and Y' (Chan and Tye, 1983, see Figure 1.6). An X element is present on each *S. cerevisiae* telomere, whereas a Y' element can be usually found on half of telomeres and is always centromere distal with respect to the X element. Sometimes multiple copies of the Y' element occur on a single telomere. Two size classes of Y' elements exist - short (5.2 kb) and long (6.7 kb). Quite often a short stretch of telomeric GC-rich repeats can be observed at a junction between X and Y' elements and is always present between multiple copies of the Y' element (Wellinger and Zakian, 2012).

The proteins bound to the *S. cerevisiae* telomere region form two distinctive sets corresponding to either double-stranded or single-stranded regions of the telomere. Rap1 is a major telomere-associated protein covering the double-stranded area of telomeric repeats. The functions of this protein are diverse and are often mediated via its interaction with other proteins such as Rif1, Rif2, Sir2, Sir3, and Sir4. In the genome Sir (Silent Information Regulator) proteins play an important role in transcription repression and organization of heterochromatin (Rine *et al.*, 1979; Palladino *et al.*, 1993). At telomeres Sir

proteins participate in so-called telomere position effect (TPE) along with the Ku complex. TPE (silencing of a gene located next to a telomere) was discovered when a gene placed in a close proximity of a telomere was repressed regardless of its specific promoter sequence (Gottschling *et al.*, 1990; Pryde and Louis, 1999). The C-terminal domain of Rap1 protein is required for TPE and this effect is possibly explained by the fact that Sir proteins are recruited to the telomeres via their interaction with the Rap1 carboxy-terminus (Hardy, Sussel and Shore, 1992; Palladino *et al.*, 1993; Moretti *et al.*, 1994).

Among the key roles of Rap1 protein is protecting telomeres from fusions occurring by NHEJ. This function is executed via two parallel pathways involving proteins Rif2 and Sir4 (Marcand *et al.*, 2008). Another important activity of Rap1 is preventing excessive resection of telomeres. Rap1-bound protein Rif2 has been shown to oppose the binding of Tel1/MRX complex to telomeres, the latter being a key player of the DBS and telomere resection pathway (Bonetti *et al.*, 2010). In addition, Rif2, as well as Rif1, participate in the counting mechanism of regulation of telomere length (Levy and Blackburn, 2004).

Another prominent telomere-associated protein is Ku. The yeast Ku protein complex consists of two subunits – yKu70 and yKu80. Being a key participant of the NHEJ pathway it is somewhat counterintuitive that the Ku complex is encountered at telomeres. Nevertheless, it plays a pivotal role in telomere biology. As already mentioned, the Ku complex functions in TPE. Additionally it is involved in limiting telomere resection (Bonetti *et al.*, 2010), in telomere tethering to the perinuclear space (Laroche *et al.*, 1998), and telomerase trafficking into the nucleus (Gallardo *et al.*, 2008), which will be considered below in more detail.

The single-stranded G-tail is associated with a different set of proteins of which the proteins of the CST complex are the main constituents. CST is an abbreviation for the protein names Cdc13, Stn1 and Ten1. Being the physical ends of chromosomes, telomeres must be distinguished from double-strand

breaks in order to prevent cells from eliciting DNA damage response and an inappropriate cell-cycle arrest and this important distinction is largely due to the activity of the CST complex (Weinert and Hartwell, 1993; Petreaca, Chiu and Nugent, 2007). This protective effect is called telomere capping and involves preventing excessive resection of telomere C-strand by Exo1 exonuclease and competitive inhibition of RPA binding to ssDNA at telomeres (Zubko, Guillard and Lydall, 2004; Kupiec, 2014). Efficient recruitment of telomerase – the telomere extending enzyme – to telomeres at late S stage of cell cycle depends upon interaction of telomerase subunit Est1 with Cdc13 (Nugent *et al.*, 1996; Evans and Lundblad, 1999; Chan, Boulé and Zakian, 2008).

1.1.4. *S. cerevisiae* telomerase overview

A considerable part of telomerase research has been concentrated on *Saccharomyces cerevisiae*, as this organism is a relatively simple and well-studied model eukaryote (Kupiec, 2014). Yeast telomerase comprises several protein subunits, namely Est1, Est2 and Est3, as well as an RNA-component - TLC1, the latter serving both as a structural element and a template for telomere extension. Est2 is the actual catalytic subunit which elongates 3' telomere overhang using part of TLC1 RNA as a template (Singer and Gottschling, 1994; Counter *et al.*, 1997). Figure 1.3 provides a schematic representation of *S. cerevisiae* telomerase structure.

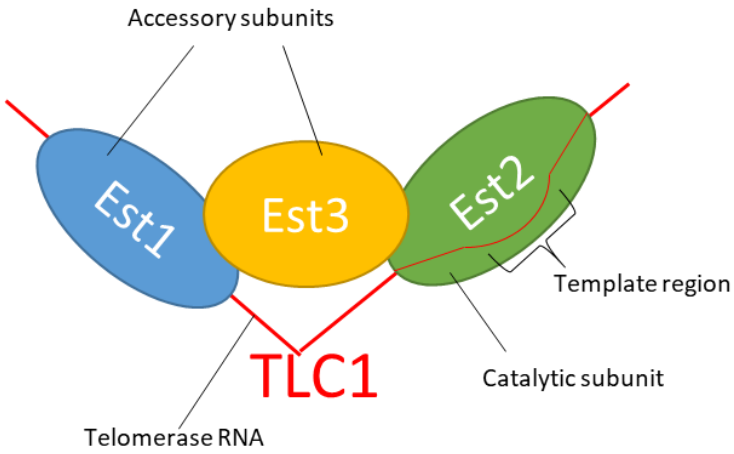

Figure 1.3: Schematic representation of *S. cerevisiae* telomerase

Adapted from Tucey and Lundblad, 2014

The stem-loop structures of the TLC1 RNA provide sites for binding to multiple proteins including the Est1 and Est2 subunits of telomerase as well as the yKu80 protein (Zappulla *et al.*, 2011). *tlc1Δ48* deletion eliminates the interaction between yKu80 and TLC1 (Peterson *et al.*, 2001) but no other impact of *tlc1Δ48* on the rest of protein associations of TLC1 has been reported. Figure 1.4 outlines the model of secondary structure of TLC1 and highlights the stem-loops to which corresponding proteins bind.

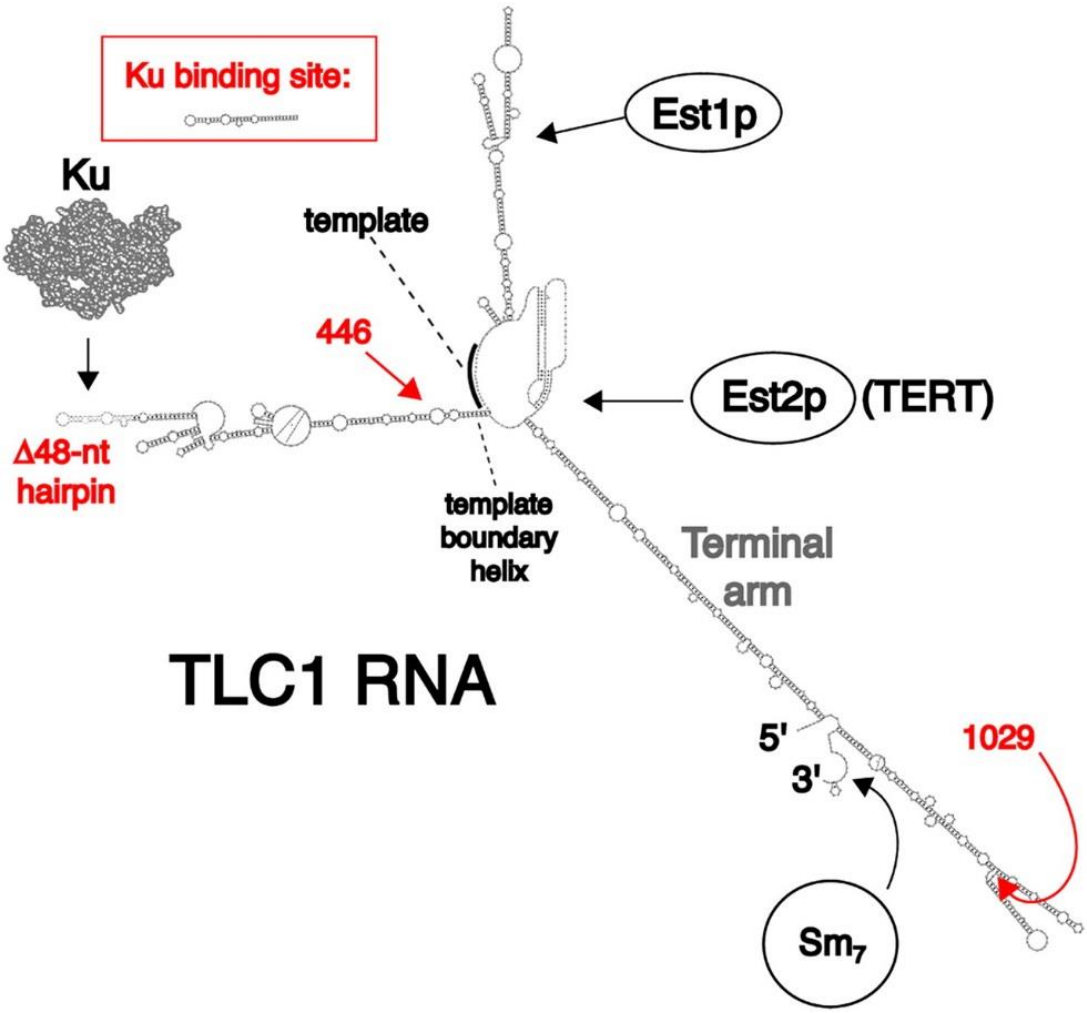

Figure 1.4: Model of stem-loop structures of the TLC1 RNA with the specific locations of its binding partners marked

From Zappulla *et al.*, 2011

1.1.5. *S. cerevisiae* telomerase complex assembly

Recent discoveries have shed light on some stages of the telomerase complex assembly (Tucey and Lundblad, 2014). The established steps are outlined in Figure 1.5.

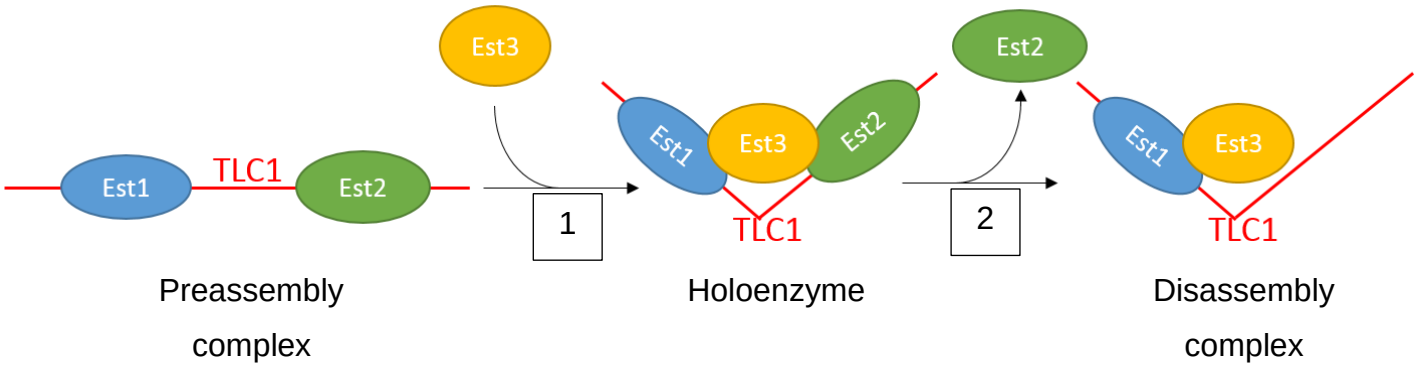

Figure 1.5: Scheme of telomerase quaternary complex assembly (1) and disassembly (2)

See the main text for details. Adapted from Tucey and Lundblad, 2014

It has been proposed that the assembly of the telomerase quaternary complex (holoenzyme) is completed when the Est3 subunit binds to the preassembled complex consisting of Est1 and Est2 associated with TLC1 (Tucey and Lundblad, 2014). Est1 and Est2 have interfaces responsible for the interaction with Est3 and the latter was found to possess a single surface (dubbed “TEL” patch) for binding both (Rao *et al.*, 2014; Tucey and Lundblad, 2014). A toggle switch serine 113 that negatively regulates Est3 inclusion into the preassembly complex is immediately adjacent to the “TEL” patch. This was inferred from the analysis of *est3-S113Y* mutants that demonstrate increased amount of holoenzyme along with slightly extended telomeres (Tucey and Lundblad, 2014). Est3 incorporation is likely accompanied by a conformation change in the preassembly complex (symbolically depicted in Figure 1.5 as a change in the angle between Est1 and Est2), whereby Est3 simultaneously interacts with both Est1 and Est2. In the disassembly pathway Est2 leaves the holoenzyme, whereas Est1 and Est3 remain in the disassembly complex together with

TLC1. Both the assembly and the disassembly processes accelerate towards late S stage, during which chromosomal termini are extended. The holoenzyme seems to be a transient stage that is linked by a dynamic equilibrium to the more stable and thus more abundant states of the preassembly and disassembly complexes, which raises a possibility, that Est2 protein dissociation might be a way of terminating the enzymatic cycle of telomere elongation (Tucey and Lundblad, 2014).

1.1.6. Yeast telomerase nuclear import and recruitment to telomeres

Despite being active only during the late S stage, the telomerase Est2 subunit appears to have a constant cell concentration and is found at telomeres throughout the cell cycle, with two distinct peaks of telomere association: in G1 stage and in late S stage (Fisher, Taggart and Zakian, 2004). The G1 recruitment peak disappears completely in TLC1- and Ku-deficient strains and also in strains where TLC1-Ku interaction is abolished, whereas the S phase peak is diminished to ~50 % of the WT level in these strains (Taggart, Teng and Zakian, 2002; Fisher, Taggart and Zakian, 2004). The second peak also decreases two-fold upon disruption of the interaction between TLC1 and Est1 or between Est1 and Cdc13. Interestingly, among the mutations affecting the second peak of Est2 telomere recruitment, only those disrupting Est1 association with either TLC1 or Cdc13 abrogate telomere length homeostasis. The disruption of telomere length maintenance in these mutants cannot be attributed to a more severe Est2 recruitment defect, since the level of S-phase Est2 recruitment in them is comparable to some mutants with stable telomeres. One solution to this apparent paradox is that Est1 plays an additional role in telomere maintenance distinct from Est2 recruitment to telomeres. For instance, it may activate the holoenzyme by recruiting the Est3 subunit to it (Osterhage, Talley and Friedman, 2006).

Est1 has a single peak of telomere association in late S phase of the cell cycle which also corresponds to the increase of Est1 concentration in the cell during this period (Taggart, Teng and Zakian, 2002; Fisher, Taggart and Zakian,

2004; Chan, Boulé and Zakian, 2008). This association is decreased ~3-fold in *yku70*Δ and *tlc*Δ*48* strains (Fisher, Taggart and Zakian, 2004) and ~4-fold in *cdc13-2* (a mutant defective in Cdc13-Est1 interaction) strains and, intriguingly, is completely lost in *est2*Δ strains (Chan, Boulé and Zakian, 2008). The latter notion indicates that Est1 probably interacts with Cdc13 only as part of the holoenzyme and not on its own (Chan, Boulé and Zakian, 2008).

FISH-experiments probing for endogenous TLC1 showed that the interaction between TLC1 48nt stem-loop region and the Ku protein are necessary for nuclear retention of TLC1 (Gallardo *et al.*, 2008). These results are in accordance with previous reports of the Ku protein-dependent nuclear localization of overexpressed TLC1 (Teixeira *et al.*, 2002). The Est1/2/3 proteins have been also demonstrated to take part in TLC1 nuclear trafficking as deletion of any of the three proteins resulted in localization of TLC1 in the cytoplasm (Gallardo *et al.*, 2008). Since cytoplasmic TLC1 was still able to bind Est1 and Est2 proteins it has been proposed that after being transcribed in the nucleus TLC1 moves to the cytoplasm to undergo some important maturation steps involving binding to Est1 and Est2 proteins. The retention of TLC1 in the cytoplasm upon failing to associate with Est1 or Est2 might represent a safe-guard mechanism that prevents accumulation of incomplete dominant-negative telomerase complexes in the nucleoplasm (Osterhage, Talley and Friedman, 2006; Gallardo and Chartrand, 2008; Gallardo *et al.*, 2008). However, some data indicate, that Est1 facilitates TLC1 distribution to the nucleus by keeping it inside nucleoplasm rather than by driving its import (Hawkins and Friedman, 2014). TLC1 nuclear localization could be also promoted by its association with telomeres, given that the deletion of *TEL1* and of components of MRX complex, known to recruit telomerase to telomeres, also results in a decrease (albeit less pronounced) of TLC1 nuclear compartmentalization (Gallardo *et al.*, 2008). Finally, TLC1 WT steady-state levels were shown to require direct interaction of TLC1 with Ku (Mozdy, Cech and Podell, 2008; Zappulla *et al.*, 2011).

Obviously, there should exist a way for the protein subunits of telomerase to be transferred to the nucleus as well. Consistent with the previously mentioned

holoenzyme incorporation-dependent TLC1 mode of nuclear import, Gallardo and Chartrand postulate a model, whereby the Est1/2/3 proteins are carried along with TLC1 into the nucleus (Gallardo and Chartrand, 2008). This mechanism was later questioned when Hawkins and Friedman demonstrated the existence of non-overlapping pathways for Est1 and TLC1 nuclear import (Hawkins and Friedman, 2014).

Little is currently known about how Est2 and Est3 reach the nuclear compartment. The Small size (20.5 kDa) of Est3 suggests it could passively diffuse through the nuclear pores (Wang and Brattain, 2007). Although no nuclear localization motif has been conclusively identified in Est2 so far, a bipartite NLS has been recently found in the human ortholog of the telomerase catalytic subunit hTERT (Chung, Khadka and Chung, 2012). An equivalent sequence might exist in the yeast enzyme.

Despite its importance for telomerase recruitment to telomeres and TLC1 nuclear retention, Ku (along with Ku-mediated G1-recruitment of Est2 to telomeres) is dispensable for telomere length maintenance, since strains lacking Ku have stable (though short) telomeres and do not senesce (Boulton and Jackson, 1996). Recently it has been discovered that Ku cannot bind both dsDNA and the TLC1 RNA simultaneously which led to a complete revision of the traditional model of Ku-dependent telomerase recruitment to telomeres, where telomerase is bridged to telomeres via TLC1-Ku interaction (Pfingsten *et al.*, 2012). The mutual exclusion between DNA and RNA binding to Ku explains why overexpression of an RNA containing three TLC1-Ku binding sites affects TPE (Peterson *et al.*, 2001; Zappulla *et al.*, 2011).

The so-called “synapsing model” was proposed in an attempt to reconcile the Ku-mediated telomerase recruitment to telomeres with the fact that Ku cannot bind TLC1 and telomere simultaneously. It made use of the ability of the Ku complex to bring together two ends of a DSB apparently via an interaction between two Ku dimers bound to the two chromosomal ends during NHEJ. However separation-of-function Ku70 mutants were obtained that are

incapable of NHEJ (most likely due to defective Ku-Ku interaction), but are fully proficient in terms of their telomeric functions (Pfingsten *et al.*, 2012).

Alternative models as to how the Ku complex recruits telomerase to telomeres have been suggested, some of them prioritizing its TLC1 nuclear translocating role in bringing telomerase to telomeres (Pfingsten *et al.*, 2012). More to this point, most of the telomere-bound Est2 is localized >100 bp away from the actual G-tail in G1 and therefore is effectively unable to elongate telomeres during this time (Sabourin, Tuzon and Zakian, 2007). The significance of telomerase recruitment to telomeres by Ku is further obscured by the fact that it's neither sufficient nor necessary to maintain stable telomere length (Chan, Boulé and Zakian, 2008). This notion prompted some authors to propose that the function of telomerase bound to telomeres in G1 is to cap them rather than to elongate (Vega *et al.*, 2007; Chan, Boulé and Zakian, 2008). It has been also speculated that Ku-mediated localization of Est2 to telomeres in G1 might contribute to its subsequent S phase recruitment via Est2 dimerization (Fisher, Taggart and Zakian, 2004). Noteworthy, some evidence suggests that human telomerase acts as a dimer during the elongation (Beattie *et al.*, 2001; Wenz *et al.*, 2001; Ly *et al.*, 2003). However, different groups report conflicting data on the matter of *S. cerevisiae* telomerase dimerization (Prescott and Blackburn, 1997; Livengood, Cech and Zaug, 2002; Friedman *et al.*, 2003; Shcherbakova *et al.*, 2009; Bajon, Laterreur and Wellinger, 2015). In any case, the precise mechanism and the role of the Ku complex action in trafficking of the telomerase TLC1 subunit to telomeres awaits further elucidation.

1.1.7. Yeast telomerase-deficiency and telomerase-insufficiency survivors

Telomerase deletion survivors. If any of the four telomerase components is deleted, *S. cerevisiae* cells do not die instantly but rather continue to divide until their telomeres reach a critical length and activate cell cycle arrest (Lundblad and Szostak, 1989; Singer and Gottschling, 1994; Lendvay *et al.*, 1996). Consequently, most cells die but few survive and maintain their telomeres through recombination (Le *et al.*, 1999).

There are two major kinds of telomerase-null survivors, which differ in the structure of their telomeres (Figure 1.6), their growth rates and their genetic requirements.

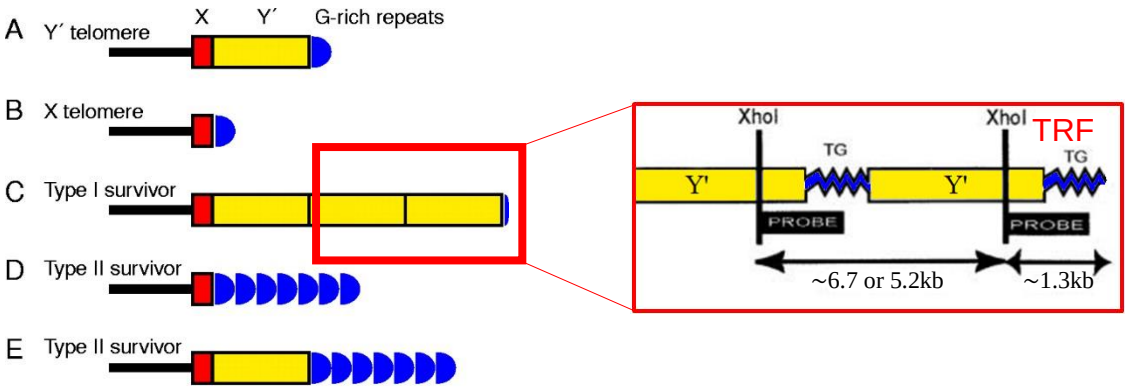

Figure 1.6: Structure of WT X (A) and Y' (B) telomeres, and type I (C) and type II (D,E) survivor telomeres

In the right: a blow-up of type I survivor telomere structure showing XhoI restriction sites and fragments recognized by the probe in terminal restriction fragment (TRF) analysis. Combined and modified from Lydall, 2003; Maringele and Lydall, 2004

Type I survivors are defined by the amplification of Y'-subtelomeric sequences and appearance of Y'-elements on the subset of telomeres that didn't use to have them. Such survivors can be identified in a telomere-specific Southern blot by shorter than wild-type terminal restriction fragments (TRFs, terminal fragments of Y'-telomeres generated by cleavage with XhoI and visualized using a probe for telomeric repeats; see Figures 1.6-1.7) and intense 5.2 and 6.7 kb bands consistent with the amplification of Y'-elements in subtelomeres (Teng and Zakian, 1999). Type II survivors originate via amplification of terminal TG-repeats, rather than subtelomeric sequences. A characteristic feature of this type of survivors is that the pattern of bands observed in telomere-specific Southern blot upon cleavage of their DNA with XhoI is distinct from that of a WT strain (Figure 1.7). Although in some strain backgrounds type II survivors occur less frequently than type I, they grow more rapidly and thus often outcompete the latter kind in liquid media (Teng and Zakian, 1999). Both types of survivors rely on the central recombination gene

RAD52 for their emergence. Type I survivors also require *RAD51, RAD54* and *RAD55/57* genes, whereas type II survivors depend on *SGS1*, *RAD50* and *RAD59* (Teng and Zakian, 1999). These two sets of genes have been shown to participate in *RAD51*-dependent and *RAD51*-independent BIR-pathways, respectively (Signon *et al.*, 2001).

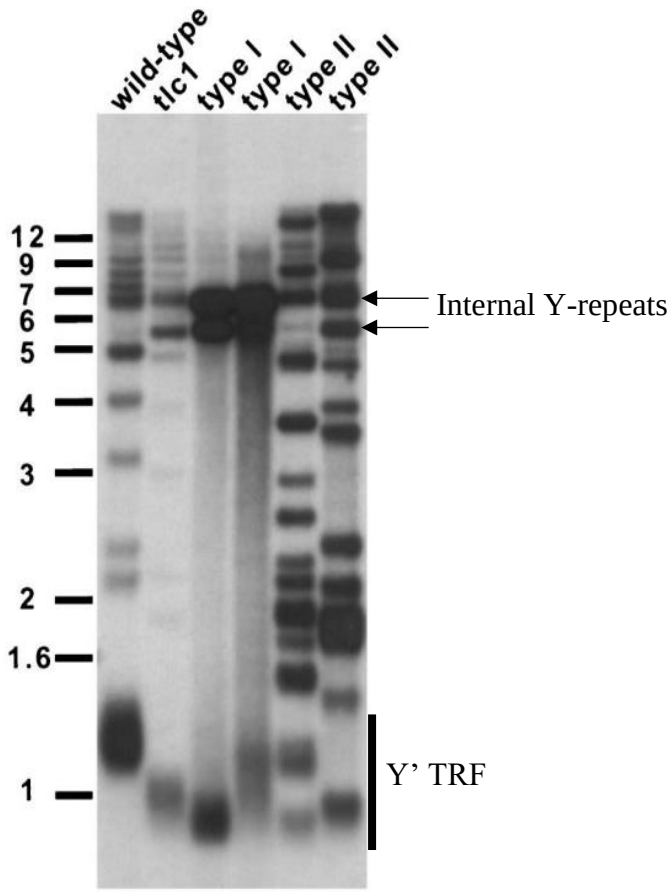

Figure 1.7: Terminal restriction fragment analysis in WT cells and type I and type II survivors

Y' TRF – terminal restriction fragment (~1.3kb in WT) obtained from terminal Y' elements by XhoI cutting. In type I survivors it is shorter and is accompanied by increased intensity of internal Y repeats (~5.2kb and ~6.7 kb), whereas in type II survivors its length is highly heterogeneous. From Teng and Zakian, 1999

Telomerase insufficiency survivors. When propagated at higher temperatures, yeast telomeres equilibrate at shorter length than in normally used conditions of 30°C (Paschini *et al.*, 2012). Yeast cells that grown at 38.5°C undergo a viability crisis after ~80 generations due to critical telomere shortening and form survivors with short and stable telomeres – a morphology different from that seen in previously discussed telomerase-deficient survivors (Figure 1.8, Millet *et al.*, 2015). Telomere shortening at elevated temperatures has been connected to a decrease of telomerase activity (Millet *et al.*, 2015). Est2 subunit seems to be the likely limiting factor at high temperature as its steady-state level is dramatically decreased at 38.5°C, though the level of other telomerase components is hardly changed (Millet *et al.*, 2015).

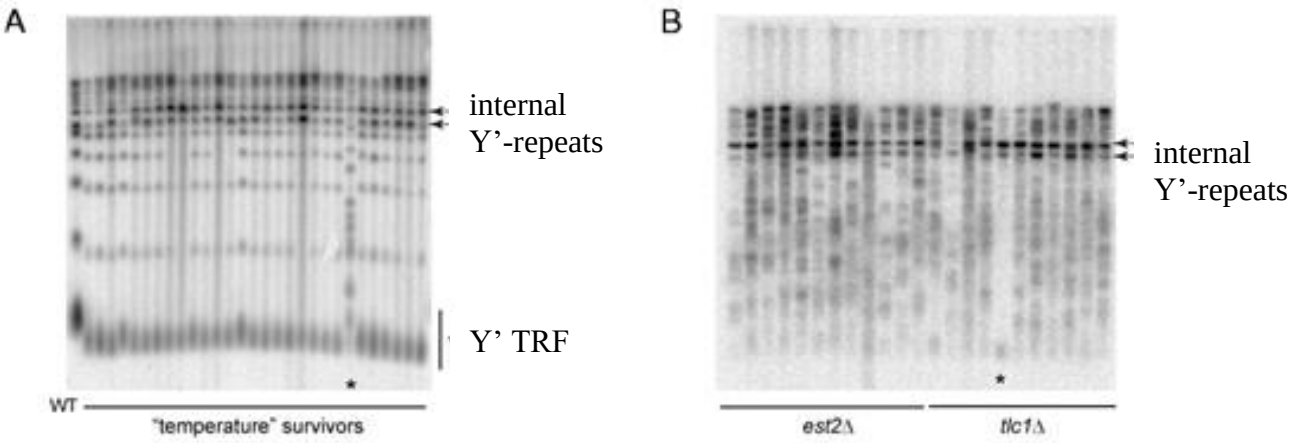

Figure 1.8: Comparison of restriction patterns produced by XhoI cutting between temperature survivors (A) and telomerase-deficient survivors (B)

In A the asterisk denotes type II survivor. In B the asterisk denotes type I survivor, the rest of the survivors in B are type II. Y' TRF – terminal restriction fragment (~1.3kb in WT) that was generated by XhoI cutting. In temperature survivors Y' TRF is shorter than in WT, but there's no amplification of Y'-repeats or change in the telomere band pattern, meaning that temperature survivors have different telomere morphology than either type I or type II survivors. From Millet *et al.*, 2015

Interestingly, temperature survivors were found to be near-diploids and monosomic for chromosome VIII (the strain was initially haploid). Diploidization and loss of chromosome VIII was observed around the time when the cell cycle arrest happened. Genetically engineered aneuploids with one copy of chromosome VIII did not experience a viability crisis at 38.5°C proving chromosome VIII monosomy could compensate for temperature-caused telomerase insufficiency. Detailed deletion analysis of chromosome VIII pointed to 4 genes, namely *PRP8*, *UTP9*, *KOG1* and *SCH9*, simultaneous heterozygosity in which significantly delayed chromosome VIII loss during propagation of yeast at 38.5°C (Millet *et al.*, 2015).

Two of the mentioned genes - *KOG1* and *SCH9* are involved in the TOR pathway that regulates ribosomal protein biogenesis (Broach, 2012). *UTP9* is important for pre-mRNA processing (Dragon *et al.*, 2002) and *PRP8* codes for a splicing factor (Vijayraghavan, Company and Abelson, 1989) (in yeast genome genes with introns predominantly encode ribosomal proteins, Spingola *et al.*, 1999).

These facts considered, it did not come as a surprise that the abundance of many of ribosomal proteins was reduced ≥ 1.5-fold relative to the total cell protein in aneuploid yeast cells compared to diploid cells (Millet *et al.*, 2015). Meanwhile, the quantity of many non-ribosomal proteins was elevated (Millet *et al.*, 2015). The amount of mature 5S and 5.8 rRNA was also decreased in aneuploid yeast relative to wild-type cells. This led the Makovets group to postulate the resource-shift hypothesis, according to which chromosome VIII monosomy leads to underproduction of normally abundant ribosomal proteins and rRNA and redirecting of the thus emancipated resources to production of non-ribosomal proteins and RNAs, including the components of the telomerase complex. The amount of Est3 and Est1 proteins as well as the TLC1 RNA was indeed shown to be 3-4 times higher in the aneuploid cells than in diploid cells at 38.5°C (Millet *et al.*, 2015). Surprisingly the amount of Est2 protein stayed pretty much the same in aneuploids as in diploids at 38.5°C (Millet *et al.*, 2015), which is slightly counterintuitive as Est2 had been shown to be the limiting factor for telomere length maintenance in the conditions of

high temperature and additional copies of either *EST1*, *EST3* or *TLC1* genes introduced in yeast cells had not prevented them from going through viability crisis at 38.5°C (Millet *et al.*, 2015).

So, even though the research conducted by Makovets lab drew a general outline of how yeast cell populations adapt to telomerase insufficiency caused by high temperatures through aneuploidy, some details of the proposed compensation mechanism are still not clear. In my postgraduate research I attempted to gain molecular insights into the mechanism of aneuploidy-dependent bypass of temperature-induced telomerase insufficiency by addressing the following questions:

1. Does the increase of Est1, Est3 and TLC1 steady-state in aneuploids compensate for the shortage of Est2 at elevated growth temperatures and, if yes, how?
2. Why does aneuploidy result in the increase of Est1, Est3 and TLC1 levels, but not of Est2 level?

1.2. DNA double-strand breaks and their physiology

1.2.1. An overview of double-strand break repair

DNA double-strand breaks (DSBs) are among the most detrimental genetic lesions. An unrepaired DSB can lead to a variety of adverse consequences ranging from cellular death to gross chromosomal rearrangements and malignant transformation (Agmon *et al.*, 2009). DSBs can be caused by external factors, such as radiation and chemotherapy drugs, as well as internal factors, including oxidative stress and topoisomerase activity (Hemnani and Parihar, 1998; Symington and Gautier, 2011). DSBs arise routinely during DNA replication (Mehta and Haber, 2014), necessitating efficient DSB detection mechanisms, which would allow DSB recognition and promote repair. Some cells also utilize programmed double-strand breaks for gene rearrangement and meiotic crossing-over (Ramsden and Gellert, 1995; Borde and de Massy, 2013). Cells can fix DNA double-strand breaks using several repair mechanisms (Figure 1.9), namely non-homologous end joining (NHEJ), microhomology-mediated end joining (MMEJ), single-strand annealing and a group of homology-dependent repair pathways (HDR), also known as homologous recombination (HR) (Symington and Gautier, 2011). Alternatively, a broken end can be stabilized by adding a telomere to the centromere-carrying fragment of the broken chromosome (Schulz and Zakian, 1994; Pennaneach, Putnam and Kolodner, 2006).

One of the major determinants of the repair pathway choice is the resection of the 5'-strands of the broken chromosome ends, which is regulated by the cell cycle (Huertas *et al.*, 2008; Chen *et al.*, 2011). Both NHEJ and MMEJ ligate the broken ends, but while NHEJ operates on unprocessed or scarcely processed ends, MMEJ requires a limited extent of 5'-strand resection to reveal microhomologies that would be annealed (Deng *et al.*, 2014; Emerson and Bertuch, 2016; Sinha *et al.*, 2016). Since neither NHEJ or MMEJ can recognize the origin of the chromosome fragments, they often lead to translocations by ligating fragments originating from different chromosomes in

case of multiple DSBs (Yu and Gabriel, 2004; Villarreal *et al.*, 2012). In contrast to NHEJ and MMEJ, efficient homology-dependent repair and single-strand annealing are promoted by long-range 5'-strand resection (Zhu *et al.*, 2008; Deng *et al.*, 2014). Single-strand annealing pairs ssDNA sequences originating from direct repeats surrounding the break, while homologous recombination pathways entail copying of the missing sequence from an intact template (Agmon *et al.*, 2009). Whereas single-strand annealing leads to the deletion of one of the direct repeats being annealed and all the sequences lying between the two repeats and their respective break ends (Bhargava, Onyango and Stark, 2016), homologous recombination can restore the integrity of the broken chromosome making it the least error-prone repair mechanism (Wyman and Kanaar, 2006; Krejci *et al.*, 2012).

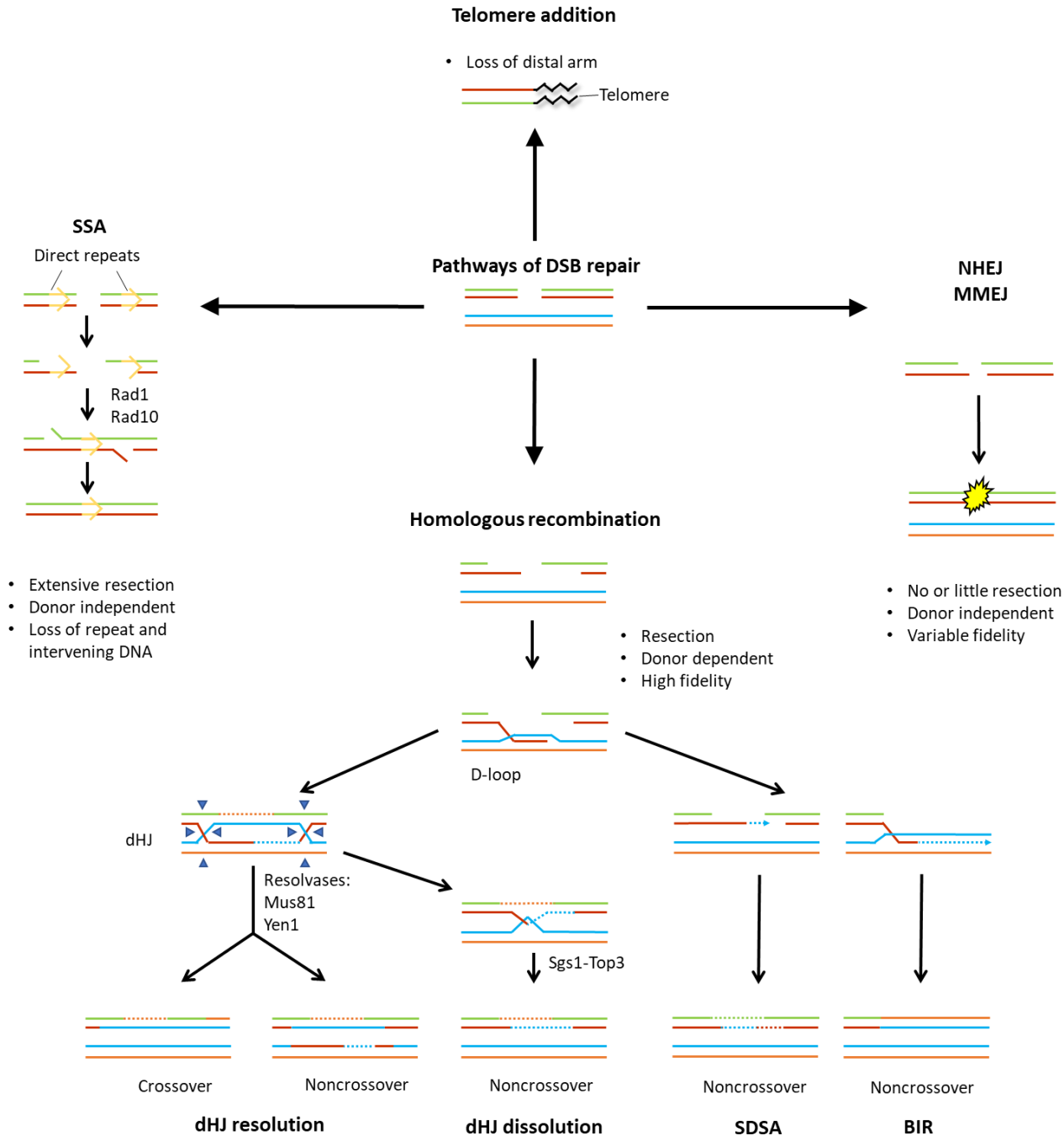

Figure 1.9: Overview of DSB repair pathways

See sections 1.2.3-1.2.5 for details. Adapted from Heyer, 2015

1.2.2. Detection of double-strand breaks and checkpoint activation

Cells are equipped with sentinel proteins, which constantly monitor the integrity of chromosomes and are capable of recognizing DSBs. Upon detection of a DSB these proteins elicit signal cascades called DNA damage checkpoints (DDCs), which serve multiple purposes. One of the most important roles of the DDCs is to arrest cell cycle progression at the pre-anaphase stage in order to provide cells with sufficient time for the break repair before the mitotic separation of chromosomes (Harrison and Haber, 2006).

The execution of DNA damage checkpoints depends on a number of proteins performing a variety of functions (Figure 1.10). In *S. cerevisiae* two apical phosphatidylinositol 3' kinase-like kinases (PIKK) govern DDC initiation in response double-strand breaks: Mec1 and Tel1; their mammalian homologs are kinases ATR and ATM, respectively (Harrison and Haber, 2006). Mec1 is the primary checkpoint regulator in budding yeast, with Tel1 playing a less prominent role, whereas in mammalian cells the contributions of ATR and ATM to the checkpoint signalling are more equal, by comparison (Harrison and Haber, 2006; Mantiero *et al.*, 2007).

Ddc2 is the binding partner of Mec1 that recruits Mec1 to and stimulates its kinase activity at RPA-coated ssDNA (Paciotti *et al.*, 2000; Rouse and Jackson, 2002; Zou and Elledge, 2003; Biswas *et al.*, 2019). RPA-ssDNA tracts can arise as a result of the resection of a broken end (see section 1.2.3) or as a consequence of fork stalling during replication (Lanz, Dibitetto and Smolka, 2019). Although, both resected broken ends and stalled replication forks elicit Mec1-dependent signalling cascades, the cascade initiated by arrested forks is distinct from the DNA damage checkpoints and is called DNA replication checkpoint (DRC).

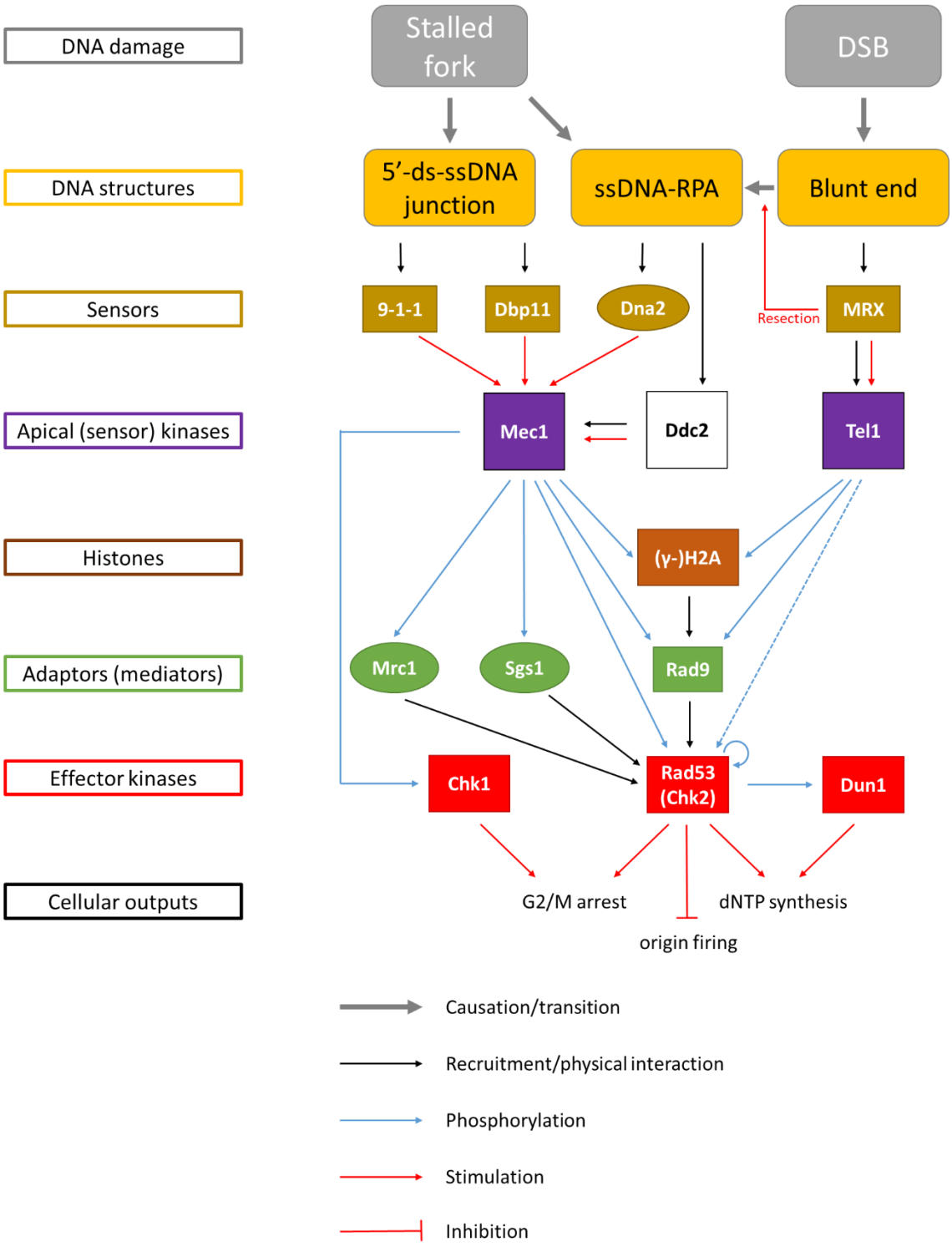

Figure 1.10: Simplified schematic of DNA damage signalling pathways in *S. cerevisiae*

Oval shapes denote proteins that act specifically in the S-checkpoint. Adapted from Harrison and Haber, 2006 and Lanz *et al*., 2019

During the S-phase DDC and DRC comprise two branches of the S-checkpoint, but while the DRC operates only during S-phase, DNA damage checkpoints can be activated throughout the cell cycle (Pardo, Crabbé and Pasero, 2017). Furthermore, even though both types of pathways converge on the same effector kinase Rad53, the dynamics of Rad53 phosphorylation is different in these two cascades, with DRC producing a more rapid but less prolonged accumulation of Rad53-P than DDC (Pardo, Crabbé and Pasero, 2017).

Mere interaction between Mec1-Ddc2 complex is not sufficient for Mec1 activation, which requires an additional input from other sensor proteins, such as 9-1-1 complex, Dpb11 and Dna2 (Mordes, Nam and Cortez, 2008; Navadgi-Patil and Burgers, 2009; Kumar and Burgers, 2013). The 9-1-1 clamp (consisting of Rad17-Mec3-Ddc1), which resembles structurally the PCNA replication clamp, is loaded by a modified version of the RFC clamp loader (RFC^{Rad24}) on the 5'-ds-ssDNA junctions located in the proximity of a DNA lesion site (Venclovas and Thelen, 2000; Melo, Cohen and Toczyski, 2001; Majka and Burgers, 2003; Zou, Liu and Elledge, 2003). Upon the recruitment of Mec1, Ddc1 activates Mec1, which in turn phosphorylates Ddc1 allowing it to recruit Dpb11, thus Ddc1 and Dpb11 appear to be recruited to the same DNA structures (Puddu *et al.*, 2008). As mentioned above, Dna2 also participates in Mec1 activation (Kumar and Burgers, 2013). Given the affinity of Dna2 to 5'-flaps covered with the RPA complex, secondary structures and G-quadruplexes, it could be speculated, that Dna2 activates checkpoint in response to detecting persistent structures of these kinds (Wanrooij and Burgers, 2015). During the S-checkpoint Ddc1, Dpb11 and Dna2 activate Mec1 in a partially redundant manner (Wanrooij and Burgers, 2015).

Unprocessed DSBs are bound by the MRX complex which in turn recruits and activates Tel1 (Nakada, Matsumoto and Sugimoto, 2003; Lisby *et al.*, 2004). MRX complex can also be recruited to stalled replication forks (Tittel-Elmer *et al.*, 2009), indicating a possible role for Tel1 in the DNA replication checkpoint. The MRX complex together with the Sae2 nuclease participates in the initial resection (see next section), upon which the MRX complex dissociates from

the processed end along with Tel1 (Gobbini *et al.*, 2013; Symington, 2014). Once the free 3'-strand of the broken end associates with the RPA complex, it becomes a suitable substrate for Mec1-Ddc2 recruitment, thus providing a switch from Tel1- to Mec1-dependent checkpoint signalling (Gobbini *et al.*, 2013).

The apical checkpoint kinases Mec1 and Tel1 pass their signal through effector kinases Rad53 and Chk1 (Harrison and Haber, 2006). In budding yeast, Rad53 serves as the major effector kinase in the DNA damage checkpoint, while another checkpoint kinase Chk1 plays a relatively minor role (Sanchez *et al.*, 1999). Despite *S. cerevisiae* Rad53 being homologous to the human CHK2 effector kinase (Matsuoka, Huang and Elledge, 1998), in terms of its function in the DNA damage signalling Rad53 is more equivalent to the mammalian CHK1 (Stracker, Usui and Petrini, 2009; Gobbini *et al.*, 2013), although Rad53 and CHK1 share little sequence similarity.

Both Mec1 and Tel1 phosphorylate histone H2A on serine 129 (Downs, Lowndes and Jackson, 2000; Lee *et al.*, 2014). The phosphorylated form of this histone (γ-H2A) recruits the adaptor protein Rad9 to the damage site (Toh *et al.*, 2006), where it is phosphorylated by Mec1 or Tel1 (Emili, 1998; Vialard *et al.*, 1998), allowing Rad9 oligomerize (Soulier and Lowndes, 1999; Usui, Foster and Petrini, 2009) and to mediate the interaction between Mec1 and Rad53 (Sun *et al.*, 1998; Gilbert, Green and Lowndes, 2001; Schwartz *et al.*, 2002). Rad9 also serves as a scaffold for Rad53 autophosphorylation, allowing Rad53 to amplify the checkpoint signal (Gilbert, Green and Lowndes, 2001).

Phosphorylated Rad53 and Chk1 kinases spread the checkpoint signal over multiple targets. Chk1-dependent phosphorylation of anaphase inhibitor Pds1 (securin) leads to Pds1 stabilization. Consequently, Pds1 prevents separase from degrading cohesin and separating the sister chromatids into anaphase (Sanchez *et al.*, 1999; Wang *et al.*, 2001). At the same time Chk1, Dun1 and Rad53 have been reported to prevent mitotic entry in yeast, thus promoting DNA damage-induced cell cycle arrest (Liang and Wang, 2007). Both Rad53 itself and Rad53-phosphorylated Dun1 upregulate the transcription of

ribonucleotide reductase (RNR) subunits (Huang, Zhou and Elledge, 1998; Tsaponina *et al.*, 2011), thus resulting in an increase of cellular dNTP pool, necessary for the survival of DNA damage (Chabes *et al.*, 2003), stimulating replication of damaged templates (Poli *et al.*, 2012) and promoting fork restart upon replicative damage (Morafraile *et al.*, 2015).

Upon the completion of DNA damage repair, yeast cells extinguish DNA damage signalling and restart the progression of the cell cycle via a process of checkpoint recovery (Clémenson and Marsolier-Kergoat, 2009). In case of failure to repair the damage after 12-14 hours of constitutive damage signalling yeast cells invoke the adaptation mechanism, whereby the checkpoint signalling is turned off and cells re-enter the cell cycle (Harrison and Haber, 2006). Adaptation to DNA damage signalling has been also observed in mammals (Van Vugt, Brás and Medema, 2004).

1.2.3. End resection and DSB repair pathway choice

The search for homology and the invasion of the homologous sequence followed by strand exchange and the creation of a D-loop are all crucial steps in homologous repair of a double-strand break (Haber, 2018). All of these steps necessitate the resection of the 5'-strand of the broken end releasing the 3'-ssDNA tail which initially associates with RPA and later with recombinase proteins, such as Rad51 or Dmc1, to form a nucleoprotein filament capable of homology search, pairing and strand displacement (, Symington and Gautier, 2011; Andriuskevicius, Kotenko and Makovets, 2018). At the same time, end resection inhibits non-homologous end joining, and therefore represents a major decision-making point in the selection of the DSB repair pathway (Symington and Gautier, 2011). The resection is regulated by various inputs, such as cell cycle stage and DNA damage checkpoint, thus allowing for coordination between double-strand break repair and other cellular processes (Symington, 2014, 2016). Several protein complexes and enzymes, that participate in end resection, play partially redundant roles and constitute a functional network, regulated by multiple physical interactions, post-translational modifications and chromatin states.

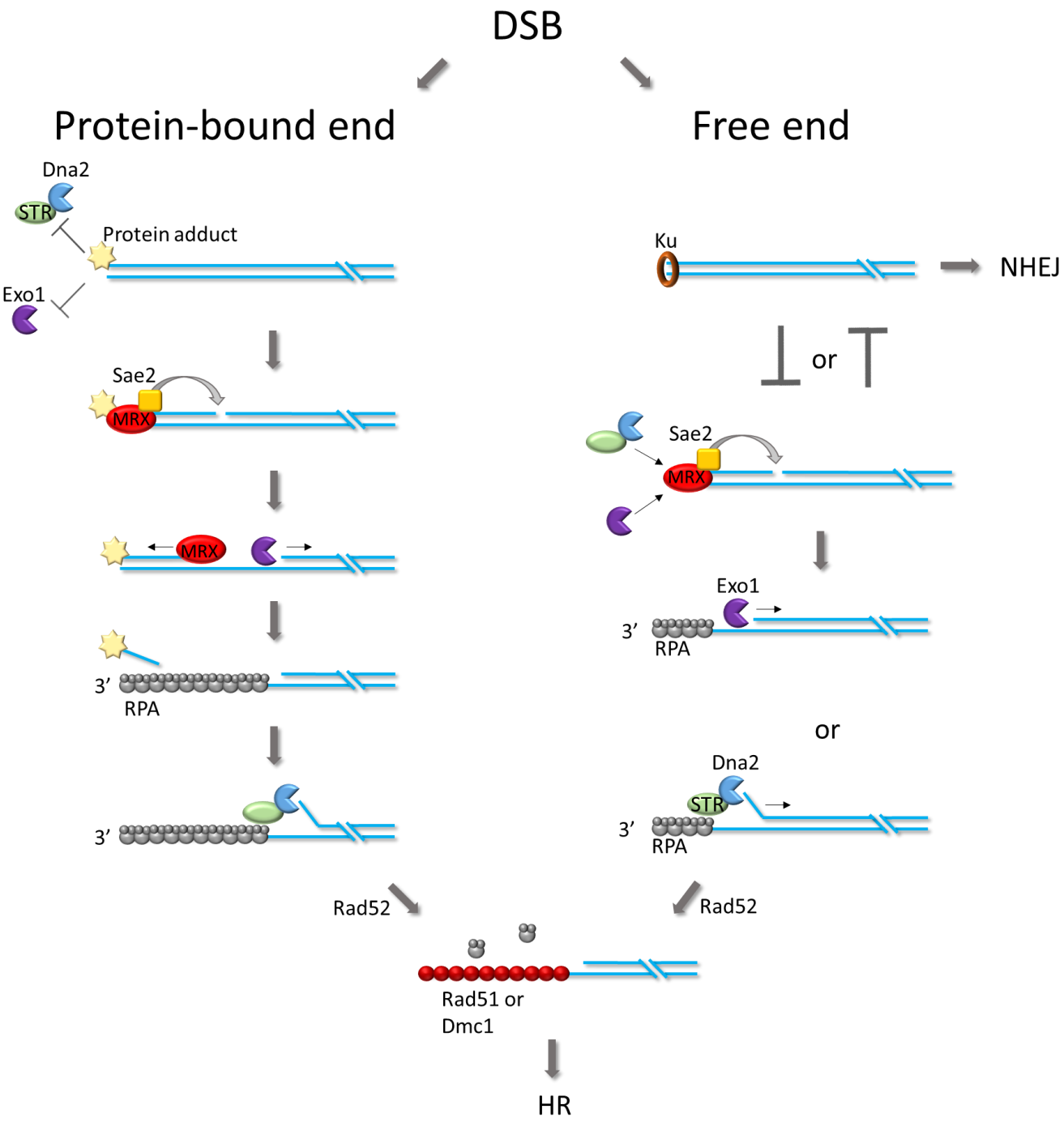

Figure 1.11: Overview of DSB resection and repair pathways choice

Adapted from Symington, 2014. See main text for details

According to the current understanding in the field, the resection in eukaryotes occurs as a two-step process, consisting of initial resection and extensive resection, performed by distinct sets of nucleases (Mimitou and Symington, 2008). In budding yeast initial resection is performed by the MRX complex, which consists of two copies of proteins Mre11, Rad50 and Xrs2 (Hopfner *et al.*, 2001; Mimitou and Symington, 2008). Mre11 is a nuclease, which is conserved across all three domains of life and possess endonuclease and 3'-5' exonuclease activities (Sharples and Leach, 1995; Furuse *et al.*, 1998; Paull and Gellert, 1998; Usui *et al.*, 1998; K. P. Hopfner *et al.*, 2000). Rad50, which is also a conserved protein, is a member of the structural maintenance of chromosomes (SMC) family of proteins (Karl Peter Hopfner *et al.*, 2000). Rad50 contains coiled-coil domains created by intramolecular folding, as well as a nucleotide-binding domain on one end and a dimerization domain on the other end of the protein (Hopfner *et al.*, 2002). Mre11 is associated with the nucleotide-biding domain of Rad50 (Hopfner *et al.*, 2001). Dimerization of the MRX complex through the dimerization domain of its Rad50 subunit is believed to play an important role in NHEJ, by virtue of tethering the two broken ends together via an MRX dimer bridge (Bressan, Baxter and Petrini, 1999; Lobachev *et al.*, 2004; Wiltzius *et al.*, 2005).The Xrs2 subunit of the MRX complex binds to the Mre11 subunit and is responsible for the interaction with Tel1 (Nakada, Matsumoto and Sugimoto, 2003).

The function of the MRX complex depends greatly on an additional factor Sae2 (Clerici *et al.*, 2006; Mimitou and Symington, 2008). Sae2 is a poorly conserved protein, that associates with the MRX complex and stimulates its endonuclease activity (Sartori *et al.*, 2007; Wang *et al.*, 2012; Cannavo and Cejka, 2014). The phosphorylation of Sae2 by CDK stimulates end resection and provides a regulatory mechanism which restricts the resection to the S/G2 phase, when the CDK is active (Huertas *et al.*, 2008). Given that resection channels repair towards HDR-dependent pathways, such regulation ensures that the HR is coordinated with the availability of sister chromatids, which serve as templates for HR (Symington and Gautier, 2011).

Despite possessing 3'-5' exonuclease activity, the MRX complex cleaves the 5'-strand of a broken end, rather than the 3'-strand (Paull and Gellert, 1998; Nicolette *et al.*, 2010; Garcia *et al.*, 2011). According to the current understanding, to achieve the 5'-strand resection, the MRX complex introduces a nick on the 5'-strand a short distance away from the breakpoint and then proceeds to degrade the 5'-strand, moving towards the broken end (Neale, Pan and Keeney, 2005; Garcia *et al.*, 2011).

In yeast cells double-strand breaks are immediately and independently bound by MRX and another protein complex – Yku70-Yku80 (Wu, Topper and Wilson, 2008). The initial resection by the MRX complex is believed to trigger the dissociation of the Ku heterodimer from the broken end by creating a poor substrate for binding by the Ku complex (Mimitou and Symington, 2010). The Ku heterodimer plays an important role in NHEJ (Boulton and Jackson, 1996). Thus, cell-cycle controlled resection by MRX lies at the heart of the choice between NHEJ and other modes of repair.

After the initial resection by the MRX complex two nucleases possessing 5'-3' exonuclease activity, namely Exo1 and Dna2, take over the resection in a partially redundant manner (Zhu *et al.*, 2008). The nicks introduced by the endonuclease activity of Mre11 may also provide a substrate for Exo1-dependent 5'-3' exonucleolytic degradation (Garcia *et al.*, 2011). In addition, MRX physically recruits Dna2 to the break site, even in the absence of Sae2 or Mre11 nuclease activity (Shim *et al.*, 2010). Moreover, the initial resection releases a ssDNA tail, which associates with the RPA complex facilitating the recruitment of Sgs1 and stimulating Dna2 5'-3' exonuclease activity (Cejka, Cannavo, *et al.*, 2010; Niu *et al.*, 2010).

Although the initial resection at the DSBs created by HO-nuclease is delayed significantly in *mre11Δ*, *rad50Δ* and *xrs2Δ* cells, they are capable of commencing the resection later on, suggesting that chemically unmodified ends can in principle be processed in the absence of the MRX complex (Ivanov *et al.*, 1994; Tsubouchi and Ogawa, 2000). In contrast, the ends which are covalently bound to proteins, such as those created during meiosis, can be

processed only in the presence of the MRX complex. MRX is the only resection nuclease with endonucleolytic activity, which can create a nick in the DNA strand conjugated to a protein, allowing removal of the protein along with a covalently-bound short oligonucleotide (Keeney and Kleckner, 1995; Moreau, Ferguson and Symington, 1999; Neale, Pan and Keeney, 2005).

Dna2 is an essential nuclease/helicase with versatile cellular functions (Wanrooij and Burgers, 2015). In resection Dna2 acts in concert with the Sgs1-Top3-Rmi1 complex (STR) (Cejka, Cannavo, *et al.*, 2010). Sgs1 is a RecQ family helicase, that unwinds DNA, generating ssDNA suitable for Dna2-dependent degradation (Cejka, Cannavo, *et al.*, 2010).

Similarly to the MRX complex, the nucleases participating in the long-range resection are also regulated by various cellular inputs. In the G1 phase the Ku complex inhibits the Exo1-dependent resection (Clerici *et al.*, 2008; Mimitou and Symington, 2010). Dna2 is phosphorylated in a CDK-dependent manner, which regulates its nuclear import and localization to DSBs (Chen *et al.*, 2011).

Excessive resection is dangerous for cells, which thus evolved mechanisms that limit long-range resection. Rad53-dependent phosphorylation inhibits Exo1 activity (Morin *et al.*, 2008), whereas Rad9, which associates with γ-H2A, is proposed to physically hinder the progression of Exo1 and Dna2 nucleases along the chromosome fragment (Ngo and Lydall, 2015).

1.2.4. An overview of homology-dependent repair pathways

Once resection is initiated cells commit to the repair either by MMEJ or by an HDR mechanism (Daley *et al.*, 2005; Geuting, Reul and Löbrich, 2013; Deng *et al.*, 2014; Shibata *et al.*, 2014). The group of resection-dependent pathways includes several distinct mechanism with varying degrees of repair accuracy (see Figure 1.9). Within this group the single-strand annealing (SSA) pathway is traditionally regarded separately from the remaining repair mechanisms, collectively referred to as homologous recombination (HR) pathways (Heyer, 2015), although some authors include SSA into the HR group (Agmon *et al.*,

2009; Morrical, 2015). As implied by its name, SSA operates by annealing ssDNA strands, which distinguishes it from the HR pathways relying on the invasion of a homologous duplex by a recombinase-ssDNA nucleoprotein filament (Fishman-Lobell, Rudin and Haber, 1992; Haber, 1992; Ivanov *et al.*, 1996; Morrical, 2015). In buddying yeast during mitotic recombination such a filament is composed of a 3'-ssDNA tail covered by a stretch of Rad51 protein (Shinohara, Ogawa and Ogawa, 1992; Sung, 1994; Sung and Robberson, 1995; Sugawara, Wang and Haber, 2003; Conway *et al.*, 2004), while Dmc1 has been identified as a meiosis-specific homolog of Rad51 (Bishop *et al.*, 1992). The requirement for Rad51 to perform the strand exchange reaction between the resected end and the homologous duplex explains why Rad51 promotes HR, but appears to be dispensable for SSA (Ivanov *et al.*, 1996; Malkova, Ivanov and Haber, 1996). The complementary ssDNA sequences that are annealed by SSA are exposed by resection of direct repeats surrounding the breaks (Mimitou and Symington, 2008), while the non-homologous overhangs are clipped off (Bardwell *et al.*, 1994) and the resulting gaps are filled in. SSA is inherently mutagenic, since the sequences that lie between the repeats are inevitably deleted in the process, along with one of the repeats (Fishman-Lobell, Rudin and Haber, 1992; Davis and Symington, 2001). Moreover, in case of several DSBs SSA can give rise to chromosomal translocations, when the direct repeats belong to fragments originating from different chromosomes (Haber and Leung, 1996; Richardson and Jasin, 2000).

As mentioned above, HR is stimulated by the assembly of a nucleoprotein filament, which facilitates homology search and strand exchange reaction (Sung and Robberson, 1995; Danilowicz *et al.*, 2014) resulting in formation of a D-loop structure (Petukhova, Sung and Klein, 2000). The 3'-ssDNA tail, that is released upon end resection, initially associates with the RPA complex (Wang and Haber, 2004), which serves multiple purposes, such as protecting ssDNA from degradation and folding into secondary structures (Sugiyama, Zaitseva and Kowalczykowski, 1997; Sugiyama, New and Kowalczykowski, 1998; Chen, Lisby and Symington, 2013). However, RPA competes with Rad51 for binding to ssDNA, creating a requirement for additional proteins to

assist Rad51 filament assembly. One such protein is Rad52, which promotes the nucleation of Rad51 filament at RPA-coated ssDNA tails followed by cooperative displacement of RPA by the growing Rad51 filament (Sugiyama and Kowalczykowski, 2002). The displacement of Rad51 from ssDNA is inhibited by the Rad55-Rad57 complex, which is incorporated into the filament as a minor constituent (Liu *et al.*, 2011).

Once the Rad51-filament is created, HR can proceed in one of several ways. If homology can be found only with one of DSB ends, the repair is carried out by break-induced replication (Malkova *et al.*, 2005), wherein the broken end invades into a sister chromatid, a homologous chromosome or an ectopic homology and then primes a long-range copying of the template often all the way to the telomere (see Figure 1.12, Davis and Symington, 2004; Rosen *et al.*, 2013; Mayle *et al.*, 2015). Such a process often leads to extensive loss of heterozygosity (LOH) and occasionally may produce non-reciprocal translocations, when an ectopic homology is used as a template (VanHulle *et al.*, 2007; Rosen *et al.*, 2013). In addition, since in BIR the polymerization of the leading strand is accompanied by bubble(D-loop)-migration and is uncoupled from the lagging strand synthesis, long stretches of ssDNA are exposed and become vulnerable to mutagenic factors, resulting in frameshifts and base substitutions (Deem *et al.*, 2011; Saini *et al.*, 2013; Sakofsky *et al.*, 2014).

When two ends are available for repair with their respective homologies located on the same duplex within the vicinity of each other, the repair is predominantly executed by one of the two gene conversion (GC) mechanisms: synthesis-dependent strand annealing (SDSA) or double-Holliday junction pathway (dHJ), sometimes termed double-strand break repair pathway (DSBR) for historical reasons (Szostak *et al.*, 1983; Malkova *et al.*, 2005). The model holds that both these pathways start by strand exchange between one of the two resected ends and the homologous duplex (Symington, Rothstein and Lisby, 2014). In the SDSA pathway once a stretch of DNA long enough to span the distance between the two resected ends is copied from the template, the D-loop is dismantled with the help of Srs2 helicase, followed by annealing

of the extended 3'-tail to the ssDNA-tail of the second DSB end (Ira *et al.*, 2003; Liu *et al.*, 2017). The repair finalizes by filling in the gaps on the damaged chromosome left by end resection. SDSA produces exclusively non-crossover outcomes, since the template remains intact after the completion of the repair (Ira *et al.*, 2003). Instead, in the dHJ pathway the ssDNA tail of the second chromosome end is captured by the D-loop strand (Nimonkar, Sica and Kowalczykowski, 2009; Shi *et al.*, 2009). Branch migration converts this configuration into a structure with two Holliday junctions. The two chromosomes connected in such a way can be disentangled by the process of dissolution, which requires the activities of Sgs1 and Top3 and yields exclusively non-crossover outcomes (Cejka, Plank, *et al.*, 2010). Alternatively the Holliday junctions can be cut by resolvases (Mus81, Yen1) resulting in either crossover or non-crossover configurations depending on the positions of cuts (Ip *et al.*, 2008). Given that the repair by GC requires only a limited DNA-synthesis and is far less mutagenic compared to BIR, it is understandable why the initiation of BIR is delayed by Sgs1 and Mph1 helicases, and GC pathways are favoured (Jain *et al.*, 2016).

1.2.5. BIR as a mechanism for repair of single-ended double-strand breaks

When only one DSB end is present, cells are left with little choice as to the means of DSB repair, since NHEJ, MMEJ and GC are precluded by the lack of the appropriate substrate. Addition of a telomere to a single DSB end may lead to a terminal deletion potentially causing cell death or, in case of a multicellular organism, malignant transformation, making *de novo* telomere addition (DNTA) an undesirable choice for repair (Pennaneach, Putnam and Kolodner, 2006). Broken replication forks are a major source of single-ended DSBs (Vilenchik and Knudson, 2003), producing a demand for a mechanism capable of restoring the sequence missing from the broken chromosome. Repair of broken forks is particularly relevant for organisms with large genomes, which run a higher risk of fork collapse. BIR occurs by conservative DNA synthesis (Donnianni and Symington, 2013) coupled with D-loop

migration (Figure 1.12, Saini *et al.*, 2013) and provides means for the repair of single-ended DSBs in eukaryotes (Davis and Symington, 2004) and prokaryotes (Motamedi, Szigety and Rosenberg, 1999). During S-phase, BIR initiates invasion into the sister chromatid and initial elongation of the broken end, but is soon terminated by an approaching replication fork or is itself converted into a conventional replication fork by Mus81-dependent D-loop digestion, limiting the extent of BIR-dependent mutagenesis (Mayle *et al.*, 2015). Conversely, in G2 phase BIR may proceed to the very end of the template, leading to an expansive LOH when a homologous chromosome serves as the template (Saini *et al.*, 2013).

BIR has a propensity to switch templates which may result in non-reciprocal translocations and other kinds of permutations (Mayle *et al.*, 2015). A sequence of prematurely terminated BIR-events may lead to a cascade of half-crossovers, causing continuous genome instability (Vasan *et al.*, 2014).

Noteworthy, BIR underlies alternative telomere lengthening (Dilley *et al.*, 2016), making it a promising target for cancer therapy research.

The genetic requirements for BIR and the conventional replication do not fully overlap. For example, the Pol32 subunit of the lagging strand polymerase δ is required for BIR, but not normal replication (Lydeard *et al.*, 2007). Obviously, components of the resection machinery as well as the proteins participating in the nucleoprotein filament assembly and strand exchange are more important for BIR (Ivanov *et al.*, 1996; Chung *et al.*, 2010), than for replication, at least in budding yeast, which have a relatively small genome by eukaryotic standards, making their DNA replication less eventful and reliant on recombinational repair compared to mammals. Interestingly, BIR can operate both by Rad51-dependent and independent mechanisms (Ira and Haber, 2002; Davis and Symington, 2004).

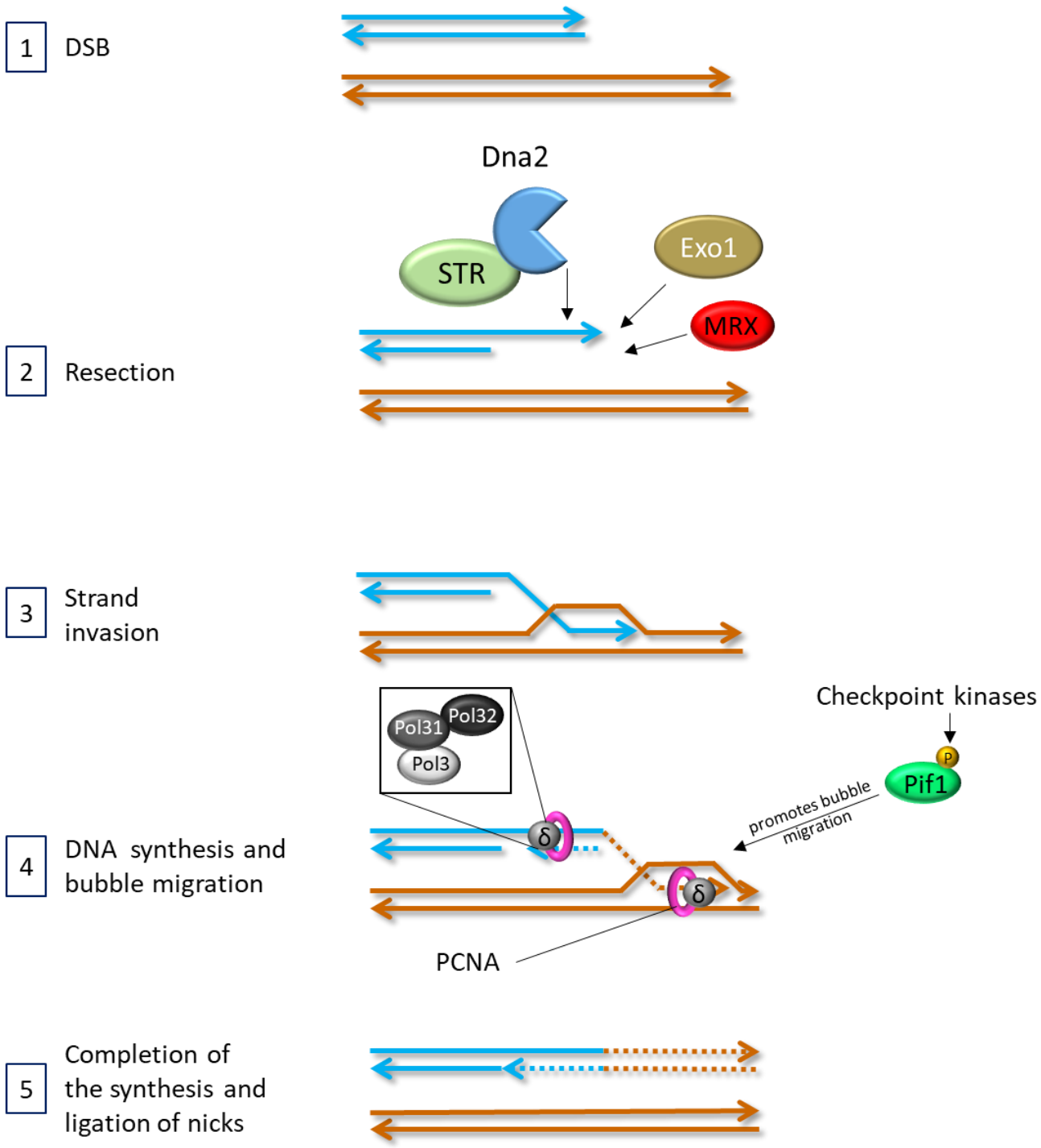

Figure 1.12: Overview of BIR

See main text for details. Adapted from Symington, 2014

Another key protein for BIR is Pif1. Pif1 is a 5'-3' helicase, that is involved in many processes relevant to DNA metabolism. Pif1 functions include unwinding of G-quadruplexes, facilitating the bypass of hard-to-replicate regions, Okazaki fragment maturation, maintenance of mitochondrial DNA, inhibition of telomerase at DSBs and telomeres (Schulz and Zakian, 1994; Budd *et al.*, 2006; Cheng, Dunaway and Ivessa, 2007; Ribeyre *et al.*, 2009; Dahan *et al.*, 2018). The precise role of Pif1 in BIR is still undetermined, although some models accounting for the function of Pif1 in BIR have been put forward. For example Wilson *et al.* have proposed that Pif1 might facilitate BIR by displacing the newly synthesized strand from the D-loop or by stimulating Pol δ-dependent DNA synthesis (Wilson *et al.*, 2013). Phosphorylation of Pif1 by Rad53 promotes BIR by an unknown mechanism as well as Pif1-dependent inhibition of telomerase at DSBs, but not at telomeres (Makovets and Blackburn, 2009; Vasianovich, Harrington and Makovets, 2014). Thus, Pif1 is another component of the regulatory network, governing the fate of chromosome ends.

CHAPTER 2

Materials and Methods

2.1. Yeast strains

Yeast strains used in the study are listed in Table 2.1.

2.2. Growth media

Yeast and bacterial growth media used in the study are listed in Table 2.2. The concentrations of the media components are shown as weight/volume (w/v). The media were sterilised by autoclaving before use.

2.3. Plasmids

The plasmids used in the study are listed in Table 2.3.

2.4. Primers

Primers were designed using the Serial Cloner software and manufactured by Integrated DNA Technologies (IDT). 100 µM stocks were made by dissolving the primers in Milli-Q H_2O and stored at -20°C. The primers used in the study are listed in Table 2.4.

2.5. Restriction enzymes

All the restriction enzymes and buffers were purchased from New England Biolabs (NEB) and used according to the manufacturer's instructions.

Table 2.1: Strains used in this study

Strain	Relevant genotype	Source/construction notes
	Saccharomyces cerevisiae A364a	
NK1	*MATa bar1::LEU2 trp1-289 ura3-52 leu2-3,112*	Makovets & Blackburn, 2009
NK219	*MATα ura3-52 trp1-289 leu2-3,112 bar1::LEU2*	Makovets & Blackburn, 2009
NK500	*MATa tlc1Δ48*	Makovets lab yeast strain collection
NK543	*MATa ura3-52 trp1-289 leu2-3,112 bar1::LEU2 est2::EST2-MYC13-KAN*	Millet *et. al.*, 2015
NK828	*MATa ura3-52 trp1-289 leu2-3,112 bar1::LEU2 pif1-m2*	Makovets & Blackburn, 2009
NK1979	*matΔ::KAN/MATα bar1::LEU2/bar1::LEU2 trp1-289/trp1-289 ura3-5/ura3-52 leu2-3,112/leu2-3,112*	Millet et. al., 2015
NK2442	*matΔ::KAN/MATa bar1::LEU2/bar1::LEU2 trp1-289/trp1-289 ura3-5/ura3-52 leu2-3,112/leu2-3,112*	Millet *et. al.*, 2015
NK2910	*matΔ::KAN/MATα, CHRVIII/chrVIIIΔ (aneuploid for CHRVIII) bar1::LEU2/bar1::LEU2 trp1-289/trp1-289 ura3-5/ura3-52 leu2-3,112/leu2-3,112*	Millet *et. al.*, 2015
NK2914	*matΔ::KAN/MATα, CHRVIII/chrVIIIΔ (aneuploid for CHRVIII) bar1::LEU2/bar1::LEU2 trp1-289/trp1-289 ura3-5/ura3-52 leu2-3,112/leu2-3,112*	Millet *et. al.*, 2015
NK2917	*matΔ::KAN/MATα, CHRVIII/chrVIIIΔ (aneuploid for CHRVIII) bar1::LEU2/bar1::LEU2 trp1-289/trp1-289 ura3-5/ura3-52 leu2-3,112/leu2-3,112*	Millet *et. al.*, 2015
NK3003	*matΔ::KAN bar1::LEU2 trp1-289 ura3-52 leu2-3,112 est3::EST3-MYC13-TRP1*	Millet *et. al.*, 2015
NK3161	*matΔ::KAN/MATα EST3/est3::EST3-MYC13-TRP1, aneuploid for CHR VIII*	Millet *et. al.*, 2015
NK3292	*MATa-inc ura3::NAT leu2::LEU2-P_{GAL1}-HO pif1-m2 trp1::HYG mnt2::HOsite-URA3-STAR-TEL*	Vasianovich thesis 2015
NK3725 $G418^R$ Ura^- derivative clone 1-5	*MATa-inc trp1-289 ura3::NAT leu2::LEU2-P_{GAL1}-HO MNT2::kan::right arm of chrII (from ARO4 to telomere) HIS7::kan*	$G418^R$ Ura^- survivor of NK3725 after DSB induction
NK3725, NK3726	*MATa-inc trp1-289 ura3::NAT leu2::LEU2-P_{GAL1}-HO MNT2::kan::HOsite-URA3-STAR-TEL HIS7::kan*	Vasianovich *et al*., 2014
NK3726 $G418^R$ Ura^- derivative clone 1-5	*MATa-inc trp1-289 ura3::NAT leu2::LEU2-P_{GAL1}-HO MNT2::kan::right arm of chrII (from ARO4 to telomere) HIS7::kan*	$G418^R$ Ura^- survivor of NK3726 after DSB induction
NK3728 $G418^R$ Ura^- derivative clone 1-4	*MATa-inc trp1-289 ura3::NAT leu2::LEU2-P_{GAL1}-HO MNT2::kan::right arm of chrII (from ARO4 to telomere) HIS7::kan pif1-m2*	$G418^R$ Ura^- survivor of NK3728 after DSB induction

NK3728, NK3729	*MATa-inc trp1-289 ura3::NAT leu2::LEU2-P_{GAL1}-HO MNT2::kan::HOsite-URA3-STAR-TEL HIS7::kan pif1-m2*	Vasianovich *et al*., 2014
NK3729 G418^R Ura$^-$ derivative clone 1-3,5	*MATa-inc trp1-289 ura3::NAT leu2::LEU2-P_{GAL1}-HO MNT2::kan::right arm of chrII (from ARO4 to telomere) HIS7::kan pif1-m2*	G418^R Ura$^-$ survivor of NK3729 after DSB induction
NK3731 G418^R Ura$^-$ derivative clone 2-5	*MATa-inc trp1-289 ura3::NAT leu2::LEU2-P_{GAL1}-HO MNT2::kan::right arm of chrII (from ARO4 to telomere) HIS7::kan pif1-m2::pif1-m1-4A*	G418^R Ura$^-$ survivor of NK3731 after DSB induction
NK3731, NK3733	*MATa-inc trp1-289 ura3::NAT leu2::LEU2-P_{GAL1}-HO MNT2::kan::HOsite-URA3-STAR-TEL HIS7::kan pif1-m2::pif1-m1-4A-TRP*	Vasianovich *et al*., 2014
NK3733 G418^R Ura$^-$ derivative clone 1-5	*MATa-inc trp1-289 ura3::NAT leu2::LEU2-P_{GAL1}-HO MNT2::kan::right arm of chrII (from ARO4 to telomere) HIS7::kan pif1-m2::pif1-m1-4A*	G418^R Ura$^-$ survivor of NK3733 after DSB induction
NK3840, NK3841	*MATa-inc trp1-289 ura3::NAT leu2::LEU2-P_{GAL1}-HO MNT2::kan::HOsite-URA3-STAR-TEL HIS7::kan pif1-m2 dna2Δ::HYG*	Makovets lab yeast strain collection
NK3848,3849	*MATa-inc trp1-289 ura3::NAT leu2::LEU2-P_{GAL1}-HO MNT2::kan::HOsite-URA3-STAR-TEL HIS7::kan pif1-m2 exo1Δ::HYG*	Makovets lab yeast strain collection
NK3856, NK3857	*MATa-inc trp1-289 ura3::NAT leu2::LEU2-P_{GAL1}-HO MNT2::kan::HOsite-URA3-STAR-TEL HIS7::kan pol32::HYG*	Vasianovich *et al*., 2014
NK3858, NK3859	*MATa-inc trp1-289 ura3::NAT leu2::LEU2-P_{GAL1}-HO MNT2::kan::HOsite-URA3-STAR-TEL HIS7::kan pol32::HYG*	Vasianovich *et al*., 2014
NK3864 G418^R Ura$^-$ derivative clone 1-5	*MATa-inc trp1-289 ura3::NAT leu2::LEU2-P_{GAL1}-HO MNT2::kan::right arm of chrII (from ARO4 to telomere) HIS7::kan rad27Δ::HYG*	G418^R Ura$^-$ survivor of NK3864 after DSB induction
NK3864 G418^R Ura$^-$ derivative clone 1-5	*MATa-inc trp1-289 ura3::NAT leu2::LEU2-P_{GAL1}-HO MNT2::kan::right arm of chrII (from ARO4 to telomere) HIS7::kan pif1-m2 rad27Δ::HYG*	G418^R Ura$^-$ survivor of NK3869 after DSB induction
NK3864, NK3865	*MATa-inc trp1-289 ura3::NAT leu2::LEU2-P_{GAL1}-HO MNT2::kan::HOsite-URA3-STAR-TEL HIS7::kan rad27Δ::HYG*	Makovets lab yeast strain collection
NK3865 G418^R Ura$^-$ derivative clone 1-4	*MATa-inc trp1-289 ura3::NAT leu2::LEU2-P_{GAL1}-HO MNT2::kan::right arm of chrII (from ARO4 to telomere) HIS7::kan rad27Δ::HYG*	G418^R Ura$^-$ survivor of NK3865 after DSB induction
NK3865 G418^R Ura$^-$ derivative clone 1-4	*MATa-inc trp1-289 ura3::NAT leu2::LEU2-P_{GAL1}-HO MNT2::kan::right arm of chrII (from ARO4 to telomere) HIS7::kan pif1-m2 rad27Δ::HYG*	G418^R Ura$^-$ survivor of NK3871 after DSB induction
NK3869, NK3871	*MATa-inc trp1-289 ura3::NAT leu2::LEU2-P_{GAL1}-HO MNT2::kan::HOsite-URA3-STAR-TEL HIS7::kan pif1-m2 rad27Δ::HYG*	Makovets lab yeast strain collection
NK3980, NK3891	*MATa-inc trp1-289 ura3::NAT leu2::LEU2-P_{GAL1}-HO MNT2::kan::right arm of chrII (from ARO4 to telomere) HIS7::kan*	G418^R Ura$^-$ survivor of NK3725 after DSB induction/Makovets lab yeast strain collection

NK4079	*MATa-inc trp1-289 ura3::NAT leu2::LEU2-P_{GAL1}-HO MNT2::KAN-(ARO4-SPO23)::HOsite-URA3-STAR-TEL HIS7::kan*	Makovets lab yeast strain collection
NK5456-NK5459	*matΔ::KAN/MATα EST3/est3::EST3-MYC13-TRP1 EST2/est2::FLAG3-MYC12-Gly6-EST2-URA3 bar1::LEU2/bar1::LEU2 trp1-289/trp1-289 ura3-5/ura3-52 leu2-3,112/leu2-3,112, aneuploid for CHR VIII*	NK3003::*pVL5273/HpaI*
NK5460-5461	*MATα bar1::LEU2 trp1-289 ura3-52 leu2-3,112 est2::URA3-FLAG3-MYC12-Gly6-EST2*	This study
NK5461 *tlc1Δ* clone 10	*MATα bar1::LEU2 trp1-289 ura3-52 leu2-3,112 est2::FLAG3-MYC12-Gly6-EST2-URA3 tlc1Δ::TRP1*	NK5461 *tlc1Δ::TRP1*
NK5461 *tlc1Δ* clone 17	*MATα bar1::LEU2 trp1-289 ura3-52 leu2-3,112 est2::FLAG3-MYC12-Gly6-EST2-URA3 tlc1Δ::TRP1*	NK5461 *tlc1Δ::TRP1*
NK5461 *tlc1Δ* clone 18	*MATα bar1::LEU2 trp1-289 ura3-52 leu2-3,112 est2::FLAG3-MYC12-Gly6-EST2-URA3 tlc1Δ::TRP1*	NK5461 *tlc1Δ::TRP1*
NK5461 *tlc1Δ* clone 4	*MATα bar1::LEU2 trp1-289 ura3-52 leu2-3,112 est2::FLAG3-MYC12-Gly6-EST2-URA3 tlc1Δ::TRP1*	NK5461 *tlc1Δ::TRP1*
NK5462, 5463	*matΔ::KAN/MATα bar1::LEU2/bar1::LEU2 trp1-289/trp1-289 ura3-5/ura3-52 leu2-3,112/leu2-3,112 EST3/est3::EST3-MYC13-TRP1 EST2/est2::FLAG3-MYC12-Gly6-EST2-URA3*	NK3003 × NK5460, diploidy confirmed by FACS
NK5464, 5465	*matΔ::KAN/MATα bar1::LEU2/bar1::LEU2 trp1-289/trp1-289 ura3-5/ura3-52 leu2-3,112/leu2-3,112 EST3/est3::EST3-MYC13-TRP1 EST2/est2::FLAG3-MYC12-Gly6-EST2-URA3*	NK3003 × NK5461, diploidy confirmed by FACS
NK5549	*MATα bar1::LEU2 trp1-289 ura3-52 leu2-3,112 est3::EST3-MYC13-KAN*	NK1 *est3::EST3-MYC13-KAN* (PCR cassette amplified with OSM966 + OSM967 from *pFA6a-kanMX6-MYC13*)
NK5550-NK5552	*MATα bar1::LEU2 trp1-289 ura3-52 leu2-3,112 est3::EST3-MYC13-KAN*	NK219 *est3::EST3-MYC13-KAN* (PCR cassette OSM966 + OSM967 on *pFA6a-kanMX6-MYC13*)
NK5554	*MATα bar1::LEU2 trp1-289 ura3-52 leu2-3,112 est3::EST3-MYC13-KAN est2::FLAG3-Gly6-EST2-TRP1*	NK5548::*pYT401/HpaI*
NK5557	*MATα bar1::LEU2 trp1-289 ura3-52 leu2-3,112 est3::EST3-MYC13-KAN est2::FLAG3-Gly6-EST2-URA3*	NK5550::*pVL5273/HpaI*
NK5585, NK5586	*MATα bar1::LEU2 trp1-289 ura3-52 leu2-3,112 est2::FLAG3-MYC12-Gly6-EST2-TRP1 tlc1Δ48*	NK500::*pYT401/HpaI*
NK5587, NK5588	*MATα ura3-52 trp1-289 leu2-3,112 bar1::LEU2 yku80Δ::TRP1*	NK5461 *yku80Δ::TRP1* (PCR cassette amplified with OSM195 + OSM 196 from *pFA6a-TRP1*)
NK5658	*MATa/MATα bar1::LEU2/bar1::LEU2 trp1-289/trp1-289 ura3-52 leu2-3,112/leu2-3,112 est3::EST3-MYC13-KAN/est3::EST3-*	NK5554 × NK5557

	MYC13-KAN est2::FLAG3-Gly6-EST2-TRP1/est2::FLAG3-Gly6-EST2-URA3	
NK5668	*MATa/MATΔ bar1::LEU2/bar1::LEU2 trp1-289/trp1-289 ura3-52 leu2-3,112/leu2-3,112 est3::EST3-MYC13-KAN/est3::EST3-MYC13-KAN est2::FLAG3-Gly6-EST2-TRP1/est2::FLAG3-Gly6-EST2-URA3*	NK5658 *MATα::HYG*
NK5812-NK5814	*MATα bar1::LEU2 trp1-289 ura3-52 leu2-3,112 est2::FLAG3-Gly6-EST2-URA3*	NK219::*pYT413/HpaI*
NK5815-NK5817	*MATα bar1::LEU2 trp1-289 ura3-52 leu2-3,112 est2::FLAG3-Gly6-EST2-URA3 est3::EST3-MYC13-KAN*	NK5550::*pYT413/HpaI*
NK5818, NK5821	*MATa bar1::LEU2 trp1-289 ura3-52 leu2-3,112 est3::EST3-MYC13-FLAG3-URA3*	NK1::*pYT414/MfeI*
NK5826-NK5828	*MATa bar1::LEU2 trp1-289 ura3-52 leu2-3,112 est3::EST3-FLAG3-NAT*	NK1 *est3::EST3-MYC13-KAN* (PCR cassette amplified with OSM966 + OSM967 from *pFA6a-FLAG3-natMX6*)
NK5830-NK5832	*MATa bar1::LEU2 trp1-289 ura3-52 leu2-3,112 est2::EST2-MYC13-KAN est3::EST3-MYC13-FLAG3-URA3*	NK543::*pYT414/MfeI*
NK5833-NK5835	*MATa ura3-52 trp1-289 leu2-3,112 bar1::LEU2 est2::EST2-MYC13-KAN est3::EST3-FLAG3-NAT*	NK543 *est3::EST3-MYC13-KAN* (PCR cassette amplified with OSM966 + OSM967 from *pFA6a-FLAG3-natMX6*)
NK5837-NK5839	*MATa bar1::LEU2 trp1-289 ura3-52 leu2-3,112 est2::FLAG3-HA9-Gly6-EST2-URA3*	NK1::*pyt420/HpaI*
NK5875-NK5877	*MATa bar1::LEU2 trp1-289 ura3-52 leu2-3,112 est2::MYC12-Gly6-EST2 est3::EST3-FLAG3-NAT*	NK5826::*pYT416/HpaI*
NK5878-NK5880	*MATa bar1::LEU2 trp1-289 ura3-52 leu2-3,112 est2::FLAG3-HA6-Gly6-EST2-URA3*	NK1::*pyt419/HpaI*
NK5881 $G418^R$ Ura^- derivative clone 1-5	*MATa-inc trp1-289 ura3::NAT leu2::LEU2-P_{GAL1}-HO MNT2::kan::right arm of chrII (from ARO4 to telomere) HIS7::kan dna2::dna2ΔN248-TRP1*	$G418^R$ Ura^- survivor of NK5881 after DSB induction
NK5881, 5882	*MATa-inc trp1-289 ura3::NAT leu2::LEU2-P_{GAL1}-HO MNT2::kan::HOsite-URA3-STAR-TEL HIS7::kan dna2::dna2ΔN248-TRP1*	Makovets lab yeast strain collection
NK5882 $G418^R$ Ura^- derivative clone 1-5	*MATa-inc trp1-289 ura3::NAT leu2::LEU2-P_{GAL1}-HO MNT2::kan::right arm of chrII (from ARO4 to telomere) HIS7::kan dna2::dna2ΔN248-TRP1*	$G418^R$ Ura^- survivor of NK5882 after DSB induction
NK5883 $G418^R$ Ura^- derivative clone 1-5	*MATa-inc trp1-289 ura3::NAT leu2::LEU2-P_{GAL1}-HO MNT2::kan::right arm of chrII (from ARO4 to telomere) HIS7::kan pif1-m2 dna2::dna2ΔN248-TRP1*	$G418^R$ Ura^- survivor of NK5883 after DSB induction
NK5883, 5884	*MATa-inc trp1-289 ura3::NAT leu2::LEU2-P_{GAL1}-HO MNT2::kan::HOsite-URA3-STAR-TEL HIS7::kan pif1-m2 dna2::dna2ΔN248-TRP1*	Makovets lab yeast strain collection
NK5884 $G418^R$ Ura^- derivative clone 1-4	*MATa-inc trp1-289 ura3::NAT leu2::LEU2-P_{GAL1}-HO MNT2::kan::right arm of chrII (from ARO4 to telomere) HIS7::kan pif1-m2 dna2::dna2ΔN248-TRP1*	$G418^R$ Ura^- survivor of NK5884 after DSB induction

NK6380	*MATa-inc trp1-289 ura3::NAT leu2::LEU2-P_{GAL1}-HO MNT2::kan::HOsite-URA3-STAR-TEL HIS7::kan pif1-m2::pif1-m1-4A-HYG*	NK3731 *trp1Δ::HYG* (PCR cassette amplified with OSM910 + OSM911 from *pFA6a-hphMX6*)
NK6381	*MATa-inc trp1-289 ura3::NAT leu2::LEU2-P_{GAL1}-HO MNT2::kan::HOsite-URA3-STAR-TEL HIS7::kan pif1-m2::pif1-m1-4A-HYG*	NK3733 *trp1Δ::HYG* (PCR cassette amplified with OSM910 + OSM911 from *pFA6a-hphMX6*)
NK6382, NK6383	*MATa-inc trp1-289 ura3::NAT leu2::LEU2-P_{GAL1}-HO MNT2::kan::HOsite-URA3-STAR-TEL HIS7::kan pif1-m2::pif1-m1-4A-HYG dna2::dna2ΔN248-TRP1*	NK6380::*pYT394/BseRI*
NK6384, NK6385	*MATa-inc trp1-289 ura3::NAT leu2::LEU2-P_{GAL1}-HO MNT2::kan::HOsite-URA3-STAR-TEL HIS7::kan pif1-m2::pif1-m1-4A-HYG dna2::dna2ΔN248-TRP1*	NK6381::*pYT394/BseRI*
NK6386	*MATa-inc trp1-289 ura3::NAT leu2::LEU2-P_{GAL1}-HO MNT2::kan::HOsite-URA3-STAR-TEL HIS7::kan dna2::dna2ΔN248-HYG*	NK5881 *trp1Δ::HYG* (PCR cassette amplified with OSM910 + OSM911 from *pFA6a-hphMX6*)
NK6387	*MATa-inc trp1-289 ura3::NAT leu2::LEU2-P_{GAL1}-HO MNT2::kan::HOsite-URA3-STAR-TEL HIS7::kan dna2::dna2ΔN248-HYG*	NK5882 *trp1Δ::HYG* (PCR cassette amplified with OSM910 + OSM911 from *pFA6a-hphMX6*)
NK6388	*MATa-inc trp1-289 ura3::NAT leu2::LEU2-P_{GAL1}-HO MNT2::kan::HOsite-URA3-STAR-TEL HIS7::kan pif1-m2 dna2::dna2ΔN248-HYG*	NK5883 *trp1Δ::HYG* (PCR cassette amplified with OSM910 + OSM911 from *pFA6a-hphMX6*)
NK6389	*MATa-inc trp1-289 ura3::NAT leu2::LEU2-P_{GAL1}-HO MNT2::kan::HOsite-URA3-STAR-TEL HIS7::kan pif1-m2 dna2::dna2ΔN248-HYG*	NK5884 *trp1Δ::HYG* (PCR cassette amplified with OSM910 + OSM911 from *pFA6a-hphMX6*)
NK6501	*MATa-inc trp1-289 ura3::NAT leu2::LEU2-P_{GAL1}-HO HEM13::HOsite-URA3 pif1-m2 RAD27-10MYC-TRP*	Makovets lab yeast strain collection
NK6546	*MATa-inc trp1-289 ura3::NAT leu2::LEU2-P_{GAL1}-HO MNT2::kan::HOsite-URA3-STAR-TEL HIS7::kan pif1-m2::pif1-m1-4D-TRP dna2::dna2ΔN248-HYG*	NK6388::*pYT200/BglII*
NK6548	*MATa-inc trp1-289 ura3::NAT leu2::LEU2-P_{GAL1}-HO MNT2::kan::HOsite-URA3-STAR-TEL HIS7::kan pif1-m2::pif1-m1-4D-TRP dna2::dna2ΔN248-HYG*	NK6389::*pYT200/BglII*
NK6550	*MATa-inc trp1-289 ura3::NAT leu2::LEU2-P_{GAL1}-HO MNT2::kan::HOsite-URA3-STAR-TEL HIS7::kan pif1-m2::pif1-m1-4A,R3E-TRP dna2::dna2ΔN248-HYG*	NK6388::*pYT542/BglII*
NK6552, NK6553	*MATa-inc trp1-289 ura3::NAT leu2::LEU2-P_{GAL1}-HO MNT2::kan::HOsite-URA3-STAR-TEL HIS7::kan pif1-m2::pif1-m1-4A,R3E-TRP dna2::dna2ΔN248-HYG*	NK6389::*pYT542/BglII*
NK6556, NK6557	*MATa-inc trp1-289 ura3::NAT leu2::LEU2-P_{GAL1}-HO MNT2::kan::HOsite-URA3-STAR-TEL HIS7::kan pif1-m2::pif1-m1-R3E-TRP dna2::dna2ΔN248-HYG*	NK6388::*pYT540/BglII*
NK6563, NK6564	*MATa-inc trp1-289 ura3::NAT leu2::LEU2-P_{GAL1}-HO MNT2::kan::HOsite-URA3-STAR-*	NK6388::*pYT544/BglII*

	TEL HIS7::kan pif1-m2::pif1-m1-4D,R3E-TRP dna2::dna2ΔN248-HYG	
NK6569	*MATa-inc trp1-289 ura3::NAT leu2::LEU2-P_{GAL1}-HO MNT2::kan::HOsite-URA3-STAR-TEL HIS7::kan pif1-m2::pif1-m1-4D,R3E-TRP dna2::dna2ΔN248-HYG*	NK6389::*pYT544/BglII*
NK6571	*MATa-inc trp1-289 ura3::NAT leu2::LEU2-P_{GAL1}-HO MNT2::kan::HOsite-URA3-STAR-TEL HIS7::kan dna2::dna2ΔN248-TRP1 pol32::HYG*	NK5881 *pol32Δ::HYG* (PCR cassette amplified with OSM1497 + OSM1498 from pFA6a-hphMX6)
NK6573	*MATa-inc trp1-289 ura3::NAT leu2::LEU2-P_{GAL1}-HO MNT2::kan::HOsite-URA3-STAR-TEL HIS7::kan dna2::dna2ΔN248-TRP1 pol32::HYG*	NK5882 *pol32Δ::HYG* (PCR cassette amplified with OSM1497 + OSM1498 from pFA6a-hphMX6)
NK6574	*MATa-inc trp1-289 ura3::NAT leu2::LEU2-P_{GAL1}-HO MNT2::kan::HOsite-URA3-STAR-TEL HIS7::kan pif1-m2 dna2::dna2ΔN248-TRP1 pol32::HYG*	NK5883 *pol32Δ::HYG* (PCR cassette amplified with OSM1497 + OSM1498 from pFA6a-hphMX6)
NK6576	*MATa-inc trp1-289 ura3::NAT leu2::LEU2-P_{GAL1}-HO MNT2::kan::HOsite-URA3-STAR-TEL HIS7::kan pif1-m2 dna2::dna2ΔN248-TRP1 pol32::HYG*	NK5884 *pol32Δ::HYG* (PCR cassette amplified with OSM1497 + OSM1498 from pFA6a-hphMX6)
NK6577	*MATa-inc trp1-289 ura3::NAT leu2::LEU2-P_{GAL1}-HO MNT2::kan::HOsite-URA3-STAR-TEL HIS7::kan pif1-m2 pol32::HYG*	NK3728 *pol32Δ::HYG* (PCR cassette amplified with OSM1497 + OSM1498 from pFA6a-hphMX6)
NK6578	*MATa-inc trp1-289 ura3::NAT leu2::LEU2-P_{GAL1}-HO MNT2::kan::HOsite-URA3-STAR-TEL HIS7::kan pif1-m2 pol32::HYG*	NK3728 *pol32Δ::HYG* (PCR cassette amplified with OSM1497 + OSM1498 from pFA6a-hphMX6)
NK6607, NK6608	*MATa-inc ura3::NAT leu2::LEU2-P_{GAL1}-HO MNT2::kan::HOsite-URA3-STAR-TEL HIS7::kan trp1-289::P_{GAL1}-FLAG3-MYC12-HA-DNA2-6HIS-TRP1*	NK3725::*pYT564/MfeI*
NK6609	*MATa-inc ura3::NAT leu2::LEU2-P_{GAL1}-HO MNT2::kan::HOsite-URA3-STAR-TEL HIS7::kan trp1-289::P_{GAL1}-FLAG3-MYC12-HA-DNA2-6HIS-TRP1*	NK3726::*pYT564/MfeI*
NK6610, NK6611	*MATa-inc ura3::NAT leu2::LEU2-P_{GAL1}-HO MNT2::kan::HOsite-URA3-STAR-TEL HIS7::kan pif1-m2 trp1-289::P_{GAL1}-FLAG3-MYC12-Gly6-HA-DNA2-6HIS-TRP1*	NK3728::*pYT564/MfeI*
NK6616	*MATa-inc ura3::NAT leu2::LEU2-P_{GAL1}-HO MNT2::kan::HOsite-URA3-STAR-TEL HIS7::kan pif1-m2 trp1-289::P_{GAL1}-FLAG3-MYC12-Gly6-HA-dna2-E657A-6HIS-TRP1*	NK3728::*pYT565/MfeI*
NK6618	*MATa-inc ura3::NAT leu2::LEU2-P_{GAL1}-HO MNT2::kan::HOsite-URA3-STAR-TEL HIS7::kan pif1-m2 trp1-289::P_{GAL1}-FLAG3-MYC12-Gly6-HA-dna2-E657A-6HIS-TRP1*	NK3729::*pYT565/MfeI*
NK6770, NK6771	*MATa-inc ura3::NAT leu2::LEU2-P_{GAL1}-HO MNT2::kan::HOsite-URA3-STAR-TEL HIS7::kan trp1-289::P_{GAL1}-RAD27-MYC13-TRP1*	NK3725::*pYT581/MfeI*
NK6772	*MATa-inc ura3::NAT leu2::LEU2-P_{GAL1}-HO MNT2::kan::HOsite-URA3-STAR-TEL*	NK3726::*pYT581/MfeI*

	HIS7::kan trp1-289::P_{GAL1}-RAD27-MYC13-TRP1	
NK6773, NK6774	*MATa-inc ura3::NAT leu2::LEU2-P_{GAL1}-HO MNT2::kan::HOsite-URA3-STAR-TEL HIS7::kan pif1-m2 trp1-289::P_{GAL1}-RAD27-MYC13-TRP1*	NK3728::*pYT581/MfeI*
NK6775	*MATa-inc ura3::NAT leu2::LEU2-P_{GAL1}-HO MNT2::kan::HOsite-URA3-STAR-TEL HIS7::kan pif1-m2 trp1-289::P_{GAL1}-RAD27-MYC13-TRP1*	NK3729::*pYT581/MfeI*
NK6786	*MATa-inc trp1-289 ura3::NAT leu2::LEU2-P_{GAL1}-HO MNT2::kan::HOsite-URA3-STAR-TEL HIS7::kan pif1-m2 dna2::HYG PDNA2::dna2ΔN248-6HIS-TRP1*	NK3840::*pYT576/BsaBI*
NK6793, NK6794	*MATa-inc trp1-289 ura3::NAT leu2::LEU2-P_{GAL1}-HO MNT2::kan::HOsite-URA3-STAR-TEL HIS7::kan pif1-m2 dna2::HYG PDNA2::dna2ΔN248-K1080E-6HIS-TRP1*	NK3840::*pYT578/BsaBI*
NK6796, NK6797	*MATa-inc trp1-289 ura3::NAT leu2::LEU2-P_{GAL1}-HO MNT2::kan::HOsite-URA3-STAR-TEL HIS7::kan pif1-m2 dna2::HYG PDNA2::dna2ΔN248-E657A,K1080E-6HIS-TRP1*	NK3840::*pYT579/BsaBI*
NK6798	*MATa-inc trp1-289 ura3::NAT leu2::LEU2-P_{GAL1}-HO MNT2::kan::HOsite-URA3-STAR-TEL HIS7::kan pif1-m2 dna2::HYG PDNA2::dna2ΔN248-E657A,K1080E-6HIS-TRP1*	NK3841::*pYT579/BsaBI*
NK6887, NK6888	*MATa-inc ura3::NAT leu2::LEU2-P_{GAL1}-HO MNT2::kan::HOsite-URA3-STAR-TEL HIS7::kan trp1-289::P_{GAL1}-FLAG3-MYC12-Gly6-dna2ΔN248 -6HIS-TRP1*	NK3725::*pYT573/MfeI*
NK6889	*MATa-inc ura3::NAT leu2::LEU2-P_{GAL1}-HO MNT2::kan::HOsite-URA3-STAR-TEL HIS7::kan trp1-289::P_{GAL1}-FLAG3-MYC12-Gly6-dna2ΔN248 -6HIS-TRP1*	NK3726::*pYT573/MfeI*
NK6891, NK6892	*MATa-inc ura3::NAT leu2::LEU2-P_{GAL1}-HO MNT2::kan::HOsite-URA3-STAR-TEL HIS7::kan pif1-m2 trp1-289::P_{GAL1}-FLAG3-MYC12-Gly6-dna2ΔN248 -6HIS-TRP1*	NK3728::*pYT573/MfeI*
NK6893, NK6894	*MATa-inc ura3::NAT leu2::LEU2-P_{GAL1}-HO MNT2::kan::HOsite-URA3-STAR-TEL HIS7::kan pif1-m2 trp1-289::P_{GAL1}-FLAG3-MYC12-Gly6-dna2ΔN248 -6HIS-TRP1*	NK3729::*pYT573/MfeI*
NK6895, NK6896	*MATa-inc ura3::NAT leu2::LEU2-P_{GAL1}-HO MNT2::kan::HOsite-URA3-STAR-TEL HIS7::kan dna2::dna2ΔN248-HYG trp1-289::P_{GAL1}-FLAG3-MYC12-Gly6-dna2ΔN248-6HIS-TRP1*	NK6386::*pYT573/MfeI*
NK6897, NK6898	*MATa-inc ura3::NAT leu2::LEU2-P_{GAL1}-HO MNT2::kan::HOsite-URA3-STAR-TEL HIS7::kan dna2::dna2ΔN248-HYG trp1-289::P_{GAL1}-FLAG3-MYC12-Gly6-dna2ΔN248-6HIS-TRP1*	NK6387::*pYT573/MfeI*
NK6899, NK6900	*MATa-inc ura3::NAT leu2::LEU2-P_{GAL1}-HO MNT2::kan::HOsite-URA3-STAR-TEL*	NK6388::*pYT573/MfeI*

	HIS7::kan pif1-m2 dna2::dna2ΔN248-HYG trp1-289::P_{GAL1}-FLAG3-MYC12-Gly6-dna2ΔN248 -6HIS-TRP1	
NK6901, NK6902	*MATa-inc ura3::NAT leu2::LEU2-P_{GAL1}-HO MNT2::kan::HOsite-URA3-STAR-TEL HIS7::kan pif1-m2 dna2::dna2ΔN248-HYG trp1-289::P_{GAL1}-FLAG3-MYC12-Gly6-dna2ΔN248-6HIS-TRP1*	NK6389::*pYT573/MfeI*
NK6903, NK6904	*MATa-inc ura3::NAT leu2::LEU2-P_{GAL1}-HO MNT2::kan::HOsite-URA3-STAR-TEL HIS7::kan trp1-289::P_{GAL1}-FLAG3-MYC12-Gly6-HA-dna2N(1-405)*	NK3725::*pYT574*
NK6905, NK6906	*MATa-inc ura3::NAT leu2::LEU2-P_{GAL1}-HO MNT2::kan::HOsite-URA3-STAR-TEL HIS7::kan trp1-289::P_{GAL1}-FLAG3-MYC12-Gly6-HA-dna2N(1-405)*	NK3726::*pYT574*
NK6907, NK6908	*MATa-inc ura3::NAT leu2::LEU2-P_{GAL1}-HO MNT2::kan::HOsite-URA3-STAR-TEL HIS7::kan pif1-m2 trp1-289::P_{GAL1}-FLAG3-MYC12-Gly6-HA-dna2N(1-405)*	NK3728::*pYT574*
NK6909, NK69010	*MATa-inc ura3::NAT leu2::LEU2-P_{GAL1}-HO MNT2::kan::HOsite-URA3-STAR-TEL HIS7::kan trp1-289::P_{GAL1}-FLAG3-MYC12-Gly6-HA-dna2N(1-405)*	NK3729::*pYT574*
NK7064-NK7066	*MATa bar1::LEU2 ura3-52 leu2-3,112 trp1-289::P_{GAL1}-FLAG3-MYC12-Gly6-HA-DNA2-6HIS-TRP1*	NK1::*pYT564/MfeI*
NK7067-NK7069	*MATa bar1::LEU2 ura3-52 leu2-3,112 pif1-m2 trp1-289::P_{GAL1}-FLAG3-MYC12-Gly6-HA-DNA2-6HIS-TRP1*	NK828::*pYT564/MfeI*
NK7075	*MATa bar1::LEU2 ura3-52 leu2-3,112 trp1-289::P_{GAL1}-FLAG3-MYC12-Gly6-HA-dna2-E657A-6HIS-TRP1*	NK1::*pYT565/MfeI*
NK7077, NK7078	*MATa bar1::LEU2 ura3-52 leu2-3,112 pif1-m2 trp1-289::P_{GAL1}-FLAG3-MYC12-Gly6-HA-dna2-E657A-6HIS-TRP1*	NK828::*pYT565/MfeI*
NK7080	*MATa bar1::LEU2 ura3-52 leu2-3,112 trp1-289::P_{GAL1}-FLAG3-MYC12-Gly6-HA-dna2-K1080E-6HIS-TRP1*	NK1::*pYT566/MfeI*
NK7084	*MATa bar1::LEU2 ura3-52 leu2-3,112 pif1-m2 trp1-289::P_{GAL1}-FLAG3-MYC12-Gly6-HA-dna2-K1080E-6HIS-TRP1*	NK828::*pYT566/MfeI*
NK7086	*MATa bar1::LEU2 ura3-52 leu2-3,112 trp1-289::P_{GAL1}-FLAG3-MYC12-Gly6-HA-dna2-E657A,K1080E-6HIS-TRP1*	NK1::*pYT567/MfeI*
NK7088-NK7090	*MATa bar1::LEU2 ura3-52 leu2-3,112 pif1-m2 trp1-289::P_{GAL1}-FLAG3-MYC12-Gly6-HA-dna2-E657A,K1080E-6HIS-TRP1*	NK828::*pYT567/MfeI*
NK7092	*MATa bar1::LEU2 ura3-52 leu2-3,112 trp1-289::P_{GAL1}-FLAG3-MYC12-Gly6-dna2ΔN248-6HIS-TRP1*	NK1::*pYT573/MfeI*
NK7095	*MATa bar1::LEU2 ura3-52 leu2-3,112 pif1-m2 trp1-289:P_{GAL1}-FLAG3-MYC12-Gly6-dna2ΔN248-6HIS-TRP1*	NK828::*pYT573/MfeI*
NK7098	*MATa bar1::LEU2 ura3-52 leu2-3,112 trp1-289::P_{GAL1}-FLAG3-MYC12-Gly6-HA-dna-2N(2-405)*	NK1::*pYT574/MfeI*

NK7101	*MATa bar1::LEU2 ura3-52 leu2-3,112 pif1-m2 trp1-289:P_{GAL1}-FLAG3-MYC12-Gly6-HA-dna2-N(2-405)*	NK828::*pYT574/MfeI*
NK8066, NK8067	*MATa-inc trp1-289 ura3::NAT leu2::LEU2-P_{GAL1}-HO MNT2::kan::HOsite-URA3-STAR-TEL HIS7::kan pif1-m2 exo1Δ::HYG trp1-289::FLAG3-Gly6-HA-dna2-N(2-282)*	3848::*pYT676/MfeI*
NK8068	*MATa-inc trp1-289 ura3::NAT leu2::LEU2-P_{GAL1}-HO MNT2::kan::HOsite-URA3-STAR-TEL HIS7::kan pif1-m2 exo1Δ::HYG trp1-289::FLAG3-Gly6-HA-dna2-N(2-282)*	3849::*pYT676/MfeI*
NK8070, NK8071	*MATa-inc trp1-289 ura3::NAT leu2::LEU2-P_{GAL1}-HO MNT2::kan::HOsite-URA3-STAR-TEL HIS7::kan pif1-m2 exo1Δ::HYG trp1-289::FLAG3-Gly6-HA-dna2-N(2-309)*	3848::*pYT677/MfeI*
NK8072	*MATa-inc trp1-289 ura3::NAT leu2::LEU2-P_{GAL1}-HO MNT2::kan::HOsite-URA3-STAR-TEL HIS7::kan pif1-m2 exo1Δ::HYG trp1-289::FLAG3-Gly6-HA-dna2-N(2-309)*	3849::*pYT677/MfeI*
NK8074, NK8075	*MATa-inc trp1-289 ura3::NAT leu2::LEU2-P_{GAL1}-HO MNT2::kan::HOsite-URA3-STAR-TEL HIS7::kan pif1-m2 exo1Δ::HYG trp1-289::FLAG3-Gly6-HA-dna2-N(2-370)*	3848::*pYT679/MfeI*

Table 2.2: Media used in this study

Yeast rich media	
YPD	1% bacto-yeast extract, 2% bacto-peptone, 2% dextrose (D-glucose)
YPD Agar	1% bacto-yeast extract, 2% bacto-peptone, 2% bacto-agar, 2% D-glucose, 0.01% adenine sulphate, 0.01% L-tryptophan, 0.002% uracil
YPGal	1% bacto-yeast extract, 2% bacto-peptone, 2% D-galactose
YPGal Agar	1% bacto-yeast extract, 2% bacto-peptone, 2% bacto-agar, 2% D-galactose, 0.01% adenine sulphate, 0.01% L-tryptophan, 0.002% uracil
YPRaf	1% bacto-yeast extract, 2% bacto-peptone, 2% D-raffinose
YPRaf Agar	1% bacto-yeast extract, 2% bacto-peptone, 2% bacto-agar, 2% D-raffinose, 0.01% adenine sulphate, 0.01% L-tryptophan, 0.002% uracil
Yeast rich media with drugs *	
YPD Agar + G418	YPD Agar containing 200 µg/ml G418 disulphate (Formedium, G4185)
YPD Agar + HYG	YPD Agar containing 300 µg/ml Hygromycin B (Toku-E, H010)
YPD Agar + NAT	YPD Agar containing 100 µg/ml Nourseothricin (Jena Bioscience, AB-102)
Synthetic defined (SD) drop-out media	
SD –URA	0.69% yeast nitrogen base without amino acids, 2% D-glucose, 2% bacto-agar supplemented with –URA complete supplement mixture (CSM) drop-out **
SD –TRP	0.69% yeast nitrogen base without amino acids, 2% D-glucose, 2% bacto-agar supplemented with –TRP complete supplement mixture (CSM) drop-out **
SD –TRP–URA	0.69% yeast nitrogen base without amino acids, 2% D-glucose, 2% bacto-agar supplemented with –TRP–URA synthetic complete (Kaiser) drop-out **
SD –LEU	0.69% yeast nitrogen base without amino acids, 2% D-glucose, 2% bacto-agar supplemented with –LEU synthetic complete (Kaiser) drop-out **
Bacterial media	
LB	1% bacto-tryptone, 0.5% bacto-yeast extract, 1% NaCl, pH adjusted to 7.0 with 1 M NaOH
LB + Amp	1% bacto-tryptone, 0.5% bacto-yeast extract, 1% NaCl, 100 µg/ml ampicillin sodium salt (Sigma, A0166), pH adjusted to 7.0 with 1 M NaOH

* drugs were dissolved in dH_20, filter-sterilized and mixed with autoclaved media;

** yeast nitrogen base and drop-out supplements were purchased from Formedium and used according to the manufacturer's guidance.

Table 2.3: Plasmids used in this study

Plasmid	Description	Source/construction notes
pEHB12009	*pMPY-FLAG3-URA-FLAG3*	E. Blackburn lab plasmid collection
pFA6a-FLAG3-natMX6		(Longtine *et al*., 1998)
pFA6a-HA3-TRP1		(Longtine *et al*., 1998)
pFA6a-hphMX6		(Longtine *et al*., 1998)
pFA6a-kanMX6		(Longtine *et al*., 1998)
pFA6a-kanMX6-MYC13		(Longtine *et al*., 1998)
pFA6a-TRP1		(Longtine *et al*., 1998)
pFA6a-TRP1-MYC13		(Longtine *et al*., 1998)
pRS314-HA-DNA2-6HIS		J. Campbell lab plasmid collection
pRS314-HA-dna2-E657A-6HIS		J. Campbell lab plasmid collection
pRS314-HA-dna2-E657A,K1080E-6HIS		J. Campbell lab plasmid collection
pRS314-HA-dna2-K1080E-6HIS		J. Campbell lab plasmid collection
pVL5723	*YIplac211-URA3 EST2(5'UTR)-FLAG3-MYC12-Gly6-EST2(5'end)*	Tucey, *et. al.*, 2014
pYT200	*pRS404-pif1-m1-4D*	Makovets lab plasmid collection
pYT356	*pFA6a-EST3(3'-end)-MYC13 URA3*	Makovets plasmid lab collection
pYT394	*pRS404-dna2(249-413)*	Makovets plasmid lab collection
pYT401	*pRS404-EST2(5'UTR)-FLAG3-MYC12-Gly6-EST2(5'end)*	
pYT413	*YIplac211-URA3 FLAG3-Gly6-EST2(5'end)*	PCR product amplified with OSM2492 + OSM2494 from *pVL5273* was digested with Sal +PstI and inserted into *pVL5273* digested with SalI and PstI
pYT413::HA3	*YIplac211-URA3 EST2(5'UTR)-FLAG3-HA3-Gly6-EST2(5'end)*	HA3 sequence was amplified from *pFA6a-HA3-TRP1* with OSM2495 + OSM2502, digested with SalI + XhoI and ligated into *pYT413* digested with SalI
pYT414	*pFA6a-EST3(3'-end)-MYC13-FLAG3 URA3*	1) Oligos OSM2497 and 2948 were annealed 2) The resulting double-tailed duplex was amplified with OSM163 + OSM164 to generate FLAG3 sequence 3) The FLAG3 PCR product was digested with EcoRI and EcoRV and ligated into pYT365 digested with SpeI then blunted with Mung bean nuclease and digested with EcoRI
pYT415	*pRS404-EST2(5'UTR)-FLAG3-HA3-Gly6-EST2(5'end)*	*HA3* sequence was amplified from *pFA6a-HA3-TRP1* with OSM2495 + OSM2496, digested with SalI and ligated into *pVL5273* digested with SalI

pYT416	*pRS404-EST2(5'UTR)-MYC12-Gly6-EST2(5'end)*	*EST2(5'UTR)* sequence was amplified from *pYT401* with OSM2499 + OSM2500, digested with SalI and ligated into *pYT401* digested with SalI
pYT419	*YIplac211-URA3 EST2(5'UTR)-FLAG3-HA6-Gly6-EST2(5'end)*	*HA3* sequence was amplified from *pFA6a-HA3-TRP1* with OSM2495 + OSM2502, digested with SalI + XhoI and ligated into *pYT413::HA3* digested with SalI
pYT420	*YIplac211-URA3 EST2(5'UTR)-FLAG3-HA9-Gly6-EST2(5'end)*	*HA3* sequence was amplified from *pFA6a-HA3-TRP1* with OSM2495 + OSM2502, digested with SalI + XhoI and ligated as a tandem of two HA3 repeats into *pYT413::HA3* digested with SalI
pYT445	*YIplac211-URA3-P_{GAL1}-FLAG3-MYC12-Gly6-EST2*	Makovets lab plasmid collection
pYT540	*pRS404-pif1-m1-R3E*	Makovets lab plasmid collection
pYT542	*pRS404-pif1-m1-4A,R3E*	Makovets lab plasmid collection
pYT544	*pRS404-pif1-m1-4D,R3E*	Makovets lab plasmid collection
pYT563	*pRS404-P_{GAL1}-FLAG3-MYC12-Gly6*	*P_{GAL1}-FLAG3-MYC12-Gly6* sequence was amplified from *pYT445* with OSM2940 + OSM2941, digested with EagI + EcoRI and ligated into *pRS404* digested with EagI + EcoRI
pYT564	*pRS404-P_{GAL1}-FLAG3-MYC12-Gly6-HA-DNA2-6HIS*	MfeI-fragment of *pRS314-HA-DNA2* containing *HA-DNA2* was subcloned into *pYT563* digested with EcoRI
pYT565	*pRS404-P_{GAL1}-FLAG3-MYC12-Gly6-HA-dna2-E657A-6HIS*	MfeI-fragment of *pRS314-HA-dna2-E657A* containing *HA-dna2-E657A* was subcloned into *pYT563* digested with EcoRI
pYT566	*pRS404-P_{GAL1}-FLAG3-MYC12-Gly6-HA-dna2-K1080E-6HIS*	MfeI-fragment of *pRS314-HA-dna2-K1080E* containing *HA-dna2-K1080E* was subcloned into *pYT563* digested with EcoRI
pYT567	*pRS404-P_{GAL1}-FLAG3-MYC12-Gly6-HA-dna2-E657A,K1080E-6HIS*	MfeI-fragment of *pRS314-HA-dna2-E657A,K1080E* containing *HA-dna2-E657A,K1080E* was subcloned into *pYT563* digested with EcoRI
pYT568	*pFA6a-TRP1-P_{GAL1}-FLAG3-MYC12-Gly6*	1)*P_{GAL1}* sequence was amplified from *pYT445* using OSM2965 + OSM2966, with OSM2966 introducing a mismatch to create XmaI site a the 5'end of the sequence 2) *FLAG3-MYC12-Gly6* sequence was amplified from *pYT445* using OSM 2967 + OSM2968, with OSM2967 introducing a mismatch to create a XmaI site on the 5'end of the

		sequence 3) The two PCR products were fused by recombinant PCR to create *P_{GAL1}-FLAG3-MYC12-Gly6* sequence with XmaI site between *P_{GAL1}* and *FLAG3* 4) The recombinant PCR product was digested with BglII + PstI and subcloned into *pFA6a-TRP1* digested with BglII + PstI
pYT573	*pRS404-P_{GAL1}-FLAG3-MYC12-Gly6-dna2ΔN248*	1) *P_{GAL1}-FLAG3-MYC12-Gly6* fragment was amplified from *pYT564* using OSM2940 + OSM2993 2) *DNA2* fragment containing codons 248-405 was amplified using oligos OSM2994 + OSM2193 3) The two sequences were fused by recombinant PCR using OSM2940
pYT574	*pRS404-P_{GAL1}-FLAG3-MYC12-Gly6-HA-dna2-N(2-405)*	*DNA2* terminator was amplified from *pYT564* using OSM2997 + OSM2998 and then subcloned as a XhoI-MseI fragment into *pYT564* digested with NdeI + XhoI
pYT576	*pRS404-dna2ΔN248-6HIS*	NdeI-XhoI fragment of *pYT564* subcloned into *pYT394*
pYT578	*pRS404-dna2ΔN248-K1080E-6HIS*	NdeI-XhoI fragment of *pYT566* subcloned into *pYT394*
pYT579	*pRS404-dna2ΔN248-E657A,K1080E-6HIS*	NdeI-XhoI fragment of *pYT567* subcloned into *pYT394*
pYT581	*pRS404-P_{GAL1}-RAD27-MYC13-TRP1*	1) *P_{GAL1}* was amplified from *pFA6a-P_{GAL1}-TRP1* plasmid using OSM3092 + OSM3093 2) *RAD27* ORF was amplified from genomic DNA of NK6501 using OSM3093 + OSM631 3) *13-myc-ADH1* terminator sequence was amplified from *pFA6a-MYC13-TRP1* using OSM2995 + OSM3095 4) *P_{GAL1}-RAD27-MYC13-T_{ADH1}* fragment was obtained by recombinant PCR using the PCR products from steps 1-3 and OSM3092 + OSM3095 5) *P_{GAL1}-RAD27- T_{ADH1}* sequence was subcloned as a PstI-SalI fragment into *pRS404*
pYT605	*pRS404-P_{GAL1}-FLAG3-Gly6-HA-DNA2*	*Gly6-HA-DNA2(5'end)* fragment was amplified from *pYT564* from *pYT564* using OSM2492 + OSM2194 and then was subcloned as a NdeI-SalI fragment into *pYT564*
pYT610	*pRS404-P_{GAL1}-FLAG3-Gly6-HA-dna-2N(2-405)*	*DNA2* terminator was amplified from *pYT564* using OSM2997 + OSM2998 and then subcloned as a

		XhoI-MseI fragment into *pYT605* digested with NdeI + XhoI
pYT676	*pRS404-P_{GAL1}-FLAG3-Gly6-HA-dna2-N(2-282)*	1)*DNA2* ORF fragment was amplified from *pYT610* using OSM3410 + OSM3412 2)*DNA2* terminator was amplified from *pYT610* using OSM3416 + OSM2997 3) the products from steps 1 and 2 were fused using recombinant PCR with OSM3410 + OSM 2997 and the resulting sequence was subcloned as a NcoI XhoI fragment into *pYT610*
pYT677	*pRS404-P_{GAL1}-FLAG3-Gly6-HA-dna-N(2-309)*	1) *DNA2* ORF fragment was amplified from *pYT610* using OSM3410 + OSM3413 2) *DNA2* terminator was amplified from *pYT610* using OSM3416 + OSM2997 3)the products from steps 1 and 2 were fused using recombinant PCR with OSM3410 + OSM 2997 and the resulting sequence was subcloned as a NcoI XhoI fragment into pYT610
pYT679	*pRS404-P_{GAL1}-FLAG3-Gly6-HA-dna-2N(2-376)*	1) *DNA2* ORF fragment was amplified from *pYT610* using OSM3410 + OSM3415 2) *DNA2* terminator was amplified from *pYT610* using OSM3416 + OSM2997 3) the products from steps 1 and 2 were fused using recombinant PCR with OSM3410 + OSM2997 and the resulting sequence was subcloned as a NcoI XhoI fragment into *pYT610*

Table 2.4: Oligos used in this study

Primer	Sequence	Purpose	Source
OSM32	*CACCCACACCCACACCCACACCCA*	Telomere-specific probe	Makovets lab primer collection
OSM60	*CCCACACTTTTCACATCTACCTCTACTCTCGCTGTCACTCCTTACCCGGC*	To amplify KL1 hybridization probe	Makovets *et. al.*, 2004
OSM106	*CCCCGAATTCCGGCATTCCTGTCGATGCTGATAGGG*		
OSM163	*CGGATCCCCGGGTTAATTAA*	To construct *pYT414*	Makovets lab primer collection
OSM164	*AATTCGAGCTCGTTTAAAC*	To construct *pYT414*	
OSM169	*AGACCTTCTTTGTAGCTTTTAGTGTGATTTTTCTGGTTTGAGAATCGGATCCCCGGGTTAATTAA*	To knock out *TLC1* with *KAN*/*TRP1*/*HIS*	
OSM170	*TGTATATTGTATATTCTAAAAAGAAGAAGCCATTTGGTGGGCTTTATTATGAATTCGAGCTCGTTTAAAC*	To knock out *TLC1* with *KAN*/*TRP1*/*HIS*	
OSM171	*TGGTGAAAAGGAAGAGCAATCCTGC*	To screen *TLC1* knockouts from F-end	
OSM194	*TAACGAGAGTGCAGGACATATGCACAAATAATATATCTCACACCATAATACGGATCCCCGGGTTAATTAA*	To make *yku80Δ*::*KAN*/*TRP1*/*HIS*	
OSM195	*TTAATTATTGCTATTGTTTGGACTTCCCCTACTGTGTTGTTCACCGCGCTGAATTCGAGCTCGTTTAAAC*	To make *yku80Δ*::*KAN*/*TRP1*/*HIS*	
OSM196	*ACTAGATTACCGCATGTCCGTCAGG*	To screen *YKU80* knockouts from the F side	
OSM205	*TTAATTAACCCGGGGATCC*	To screen for *pol32Δ*::*HYG*	
OSM631	*TTAATTAACCCGGGGATCCG*	To screen for integration of Pringle cassettes at the F-end	
OSM801	*GTTTAAACGAGCTCGAATTC*	To screen for integration of Pringle cassettes at the R-end	
OSM910	*TATTGAGCACGTGAGTATACGTGATTAAGCACACAAAGGCAGCTTGGAGTcggatccccgggttaattaa*	To knock out *TRP1*	
OSM911	*TGCAGGCAAGTGCACAAACAATACTTAAATAAATACTACTCAGTAATAACgaattcgagctcgtttaaac*		
OSM966	*GATCAAGTCGGATCGTTAAGTACTTTCCCATTTGTATATAAATATTTACGGATCCCCGGGTTAATT*	To tag *EST3* at the C-terminus	
OSM967	*TCCCTTTATATATGTAGATAAACGAAGATATTCTAACTCTCTCACACTTAGAATTCGAGCTCGTTTAAAC*		
OSM970	*TTTTGTTTATCATATCTTGAGTTACCACATTAAATACCAACCCATCCGCCcggatccccgggttaattaa*	To delete *MATα*	

OSM971	*TATAGATGTCTTATTGAACTGTCGAAACTGAGTATTTTGACTTCCAGACGgaattcgagctcgtttaaac*		
OSM1497	*ATAATATTTCACATTAACTAACAACCAGAAATAGGCTTTAGTTAACTCAATCGGTAATTAggatccccgggttaattaa*	To knock out *POL32*	
OSM1498	*CATTTGTATTATACATTACATCACAATTAGTAATGGAAAGTGTTTGGAAAAAAAAGAAGAgaattcgagctcgtttaaac*		
OSM1499	*ACGAATAGGTCTATTTTCCACTAC*	To screen for *pol32Δ*::*HYG*	
OSM2194	*Cttactattactaatcgtactacgcc*	To test plasmid integration into *DNA2* locus	
OSM2408	*GGTGACGAAAACATAACTCAAAGG*	To screen *YKU80* knockouts from the R side	
OSM2492	*AaaagtcgacGGTGGAGGCAATGGAGGCG*	To amplify *(Gly)$_6$-EST2* (first 1.5 kb) region of *pVL5273* with a SalI site on R-end and create a SalI-site on F-end	This study
OSM2494	*atgcctgcaggtttACTCTAGAGGATCCCCGG*	To mutate SalI site and add a PstI site on R-end of *(Gly)$_6$-EST2* (first 1.5 kb) amplification product of *pVL5273* (PCR with OSM2492)	
OSM2495	*GCAGGTCGACGGtATCCCCGGGTTAATTAAC*	To amplify *HA3*-tag sequence from *pFA6a-HA3-TRP1* with adjacent aminoacids on both ends and SalI site on F-end, to mutate Cys to Ser and stop codon to Gly on R-end and to create SalI site on R-end.	
OSM2496	*aaaaGTCGACCGCGCCTCcGgACTGAGCAGCGTAATCT*		
OSM2497	*cggatccccgggttaattaaGATATCCGGTGGAGGCAATGGAGGCGGTGATTATAAAGACGACGACGACAAGGACTACAAG*	To synthesize *(Gly)$_6$-FLAG3*-tag sequence (for C-tagging of *EST3* in *pYT356*) with stop-codon and EcoRI site on R-end, EcoRV site on F-end and flanking sequences on both ends to amplify the product with OSM163+OSM164	
OSM2498	*aattcgagctcgtttaaacGAATTCTTATTTATCATCATCATCTTTATAATCTTTATCATCATCATCCTTGTAGTCCTTGTCGTCGTCG*		
OSM2499	*TCGAGGTCGACGGTATCGATAAGC*	To amplify *EST2*-promotor containing region of *pYT401* and to create a SalI site on	
OSM2500	*AGTCgTCGACCATATGTATAAATCAG*		

		R-end (for subsequent removal of *FLAG3*-tag sequence from *pYT401* using SalI digest)
OSM2502	*aaaaCTCGAGCGCGCCTCcGgACTGAGCAGC GTAATCT*	To amplify *HA3*-tag sequence from *pFA6a-HA3-TRP1* with adjacent aminoacids on both ends, to mutate SalI site into XhoI site on F-end, to mutate Cys to Ser and stop codon to Gly on R-end and to create XhoI site on R-end
OSM2940	*cccccggccgAGTACGGATTAGAAGCCGCCGA GC*	To amplify P_{GAL1}-*FLAG3-MYC12-Gly6* from *pYT445* and add EagI site to the 5'-side and EcoRI site to the 3'-side of the PCR product for subsequent three-piece ligation of this product together with *DNA2* gene (cut by MfeI) into *pRS404*
OSM2941	*ccccgaattcTACCGCCTCCATTGCCTCCAC*	To amplify P_{GAL1}-*FLAG3-MYC12-Gly6* from *pYT445* and add EagI site to the 5'-side and EcoRI site to the 3'-side of the PCR product for subsequent three-piece ligation of this product together with *DNA2* gene (cut by MfeI) into *pRS404*
OSM2965	*ccccagatctAGTACGGATTAGAAGCCGCCGA GC*	To amplify P_{GAL1}-*FLAG3-MYC12* from *pYT445*, introduce a mutation in the P_{GAL1}-*FLAG3* junction creating an XmaI site between P_{GAL1} and *FLAG3* and add BglII site to the 5' end and SalI site to the 3' end of the PCR product for subsequent subcloning into *pFA6a-TRP1*
OSM2966	*CGACCATTTTGAGAcCCGGGTTTTTTCTCC*	
OSM2967	*GGAGAAAAAACCCGGgTCTCAAAATGGTCG*	
OSM2968	*ccccctgcagACCGCCTCCATTGCCTCCAC*	

OSM2993	*ACCACACCTCTACCGGCAGATCCGCTAGGGATAACAGGGTAATATAGATCcggatccccgggttaattaa*	*pYT573* construction
OSM2995	*AAAATAAAAAATTGAACAAAAATAAGAATAAAGTCACAAAGGGAAGAAGAcggatccccgggttaatt*	To tag Rad27 at the C-terminus
OSM2996	*ATATATGCCAAGGTGAAGGACCAAAAGAAGAAAGTGGAAAAAGAACCCCCgaattcgagctcgtttaaac*	
OSM2997	*ccccctcgagTTCGTTTATGAGGAAGCTTTTGG*	To amplify *DNA2* terminator from *pYT564* and mutate the first MseI site, add MseI site to the 5'-end and XhoI site to the 3'end of the PCR product so as to subclone it into *pYT564* cut with XhoI and MseI thereby creating a construct for overexpression of Dna2 N-terminus
OSM2998	*ccccTTAACAGGGGGAATAAGAAGAGCTTC*	
OSM3092	*ccccctgcagAGTACGGATTAGAAGCCGCCGAGC*	To amplify *RAD27-MYC13-*T_{ADH1} from the genome of NK6501 and fuse it to P_{GAL1} using recombinant PCR and then subclone the construct into *pRS404* using PstI and SalI
OSM3093	*gcattcaaacctttaatacccatGTTTTTTCTCCTTGACGTTAAAG*	
OSM3094	*CTTTAACGTCAAGGAGAAAAAACatgggtattaaaggtttgaatgc*	
OSM3095	*ccccgtcgacCTATACCTGAGAAAGCAACCTG*	
OSM3410	*GGCCCCATGGAAGAAGTAATATGG*	To create a series of C-terminal deletions of Dna2 N-terminus using recombinant PCR on the template of *pYT610* with subsequent subcloning PCR products into *pYT610* with NcoI and XhoI
OSM3412	*tcttcttattccccctgttaCTTTGAGTTAAAATATCTATCAAAG*	
OSM3415	*tcttcttattccccctgttaTTCGTTCAATAGTTCAATTAGTG*	

2.6. Growth and genetic manipulations of yeast and bacteria

2.6.1. Yeast stocks

Materials:

- 25% (w/v) glycerol in 50% YPD

Cells for stocks were taken from purified strains and patched either on YPD plates or selective plates (such as -ura plates for certain types of strains with unstable genotypes) and grown overnight at 30°C. The cells were collected from a plate with a toothpick, resuspended in 2 mL of 25% (w/v) glycerol in 50% YPD in Corning™ Cryogenic Vials by vortexing and frozen at -80°C for indefinite storage and retrieval.

2.6.2. Yeast transformation via cell starvation in lithium acetate

Materials:

- 0.1 M lithium acetate
- 40% (w/v) polyethylene glycol 3350 (Sigma-Aldrich®, P4338) in 0.1 M lithium acetate
- 10 mg/ml (w/v) Salmon Sperm ssDNA solution

For yeast transformations, yeast cells from freshly grown patches were resuspended in YPD at $OD_{600} \leq 0.1$ (5 mL of YPD culture per transformation + 5 mL for no DNA control). The cells were grown at 30°C in a shaking incubator until the OD_{600} reached 0.4-0.6 and harvested by centrifugation in eppendorf® 5810R centrifuge at 3,000 rpm for 3 minutes at room temperature. The medium was decanted and after an additional 12-second round of centrifugation the residual medium was removed with a pipette. The cells were washed two times in 1 mL of 0.1 M lithium acetate and resuspended in N × 100 µL of 0.1 M lithium acetate mixed with N × 10 µL of salmon sperm (or bovine) single-stranded carrier DNA, where N = the number of transformations for a particular strain +

1. Cell suspension was split into 110 µL aliquots, one per each transformation and one for a negative, no DNA, control sample. 3-10 µL of linearized plasmid or PCR product were added into each aliquot, except for the negative control, followed by the addition of 600 µL of freshly-made 40% (w/v) PEG 3.350 in 0.1 M lithium acetate, and vortexed. Cell suspensions were then incubated at 30°C in an aluminium rack (to facilitate heat-transfer) for 30-40 minutes and transferred to a 42°C water-bath for 16-18 minutes to heat-shock. The cells were pelleted in an eppendorf® Centrifuge 5424 for 2 minutes at 5,000 rpm at room temperature, washed with 1 mL of YPD, resuspended in 100 µL of YPD and plated either directly onto selective media (in case of selection for auxotrophic markers) or first on YPD and replica-plated on drug plates the next day (in case of selection for drug-resistance markers).

2.6.3. Yeast matings

For yeast mating, cells from two haploid parental strains of opposite mating types were mixed and spotted on a pre-warmed YPD plate, followed by incubation at 30°C for at least 6 hours. Depending on the availability of selection directed against only one or both of the parental strains, the parents were mixed either in equal proportion (when both parents can be counter-selected) or with a 20-fold excess of one parent over the other (the parent that can be selected against was in excess over the one with no available counter-selection). After the 6 hour incubation, the cells from the centre of the spot were streaked for single colonies on selective media.

Acquisition of the diploid genotype was tested by mating pheromone production assay (Sprague and Herskowitz, 1981). Cells from the putative diploid colonies were spotted onto two plates with freshly inoculated lawns of cells, one plate – with *MATa sst1 (bar1)* cells (the tester strain NK1), sensitive to the α-factor pheromone, and the other – with *MATα sst2* cells (the tester strain NK1542), sensitive to the a-factor pheromone. Haploid cells produce mating pheromones that inhibit growth of the tester strain of the opposite mating type, thus forming an area of arrested growth in the lawn around the

spotted cell mass (a halo). Diploid strains do not produce mating pheromones and therefore do not form halos in the lawns of the tester strains.

2.6.4. Active deletion of chromosome VIII

The 2n-1 strains (CHRVIII) that were used in the experiments on co-immunoprecipitation of the telomerase subunits were constructed is several steps. As a starting point for the strain construction, I used a *MATα* haploid strain (NK2795, Millet *et al.*, 2015) with a modified chromosome VIII (). The *URA3* marker had been introduced near the centromere region of chromosome VIII in this strain, and both arms of the chromosome had been marked with drug resistance markers (*NAT* and *HYG*). The strain was first modified by adding tags to its Est2 and/or Est3 proteins. Next, the strain was mated to a *MATa* haploid expressing the same tagged versions of Est2 and/or Est3 but with a WT chromosome VIII. The diploid clones were selected and verified as described in the previous section. The diploids were transformed with a PCR product that upon recombination with the CHRVIII, induced a deletion spanning the CHRVIII centromere and the adjacent *URA3* marker. Deletion of CHRVIII centromere would lead to mitotic missegregation of chromosome VIII resulting in CHRVIII monosomy or trisomy. Deletion of CHRVIII centromere was selected for on 5-FOA plates. The clones were then screened on NAT and HYG plates for the loss of the marked copy of CHRVIII. The CHRVIII aneuploidy was additionally verified by quantitative pulse-field gel electrophoresis (see section 2.8.14).

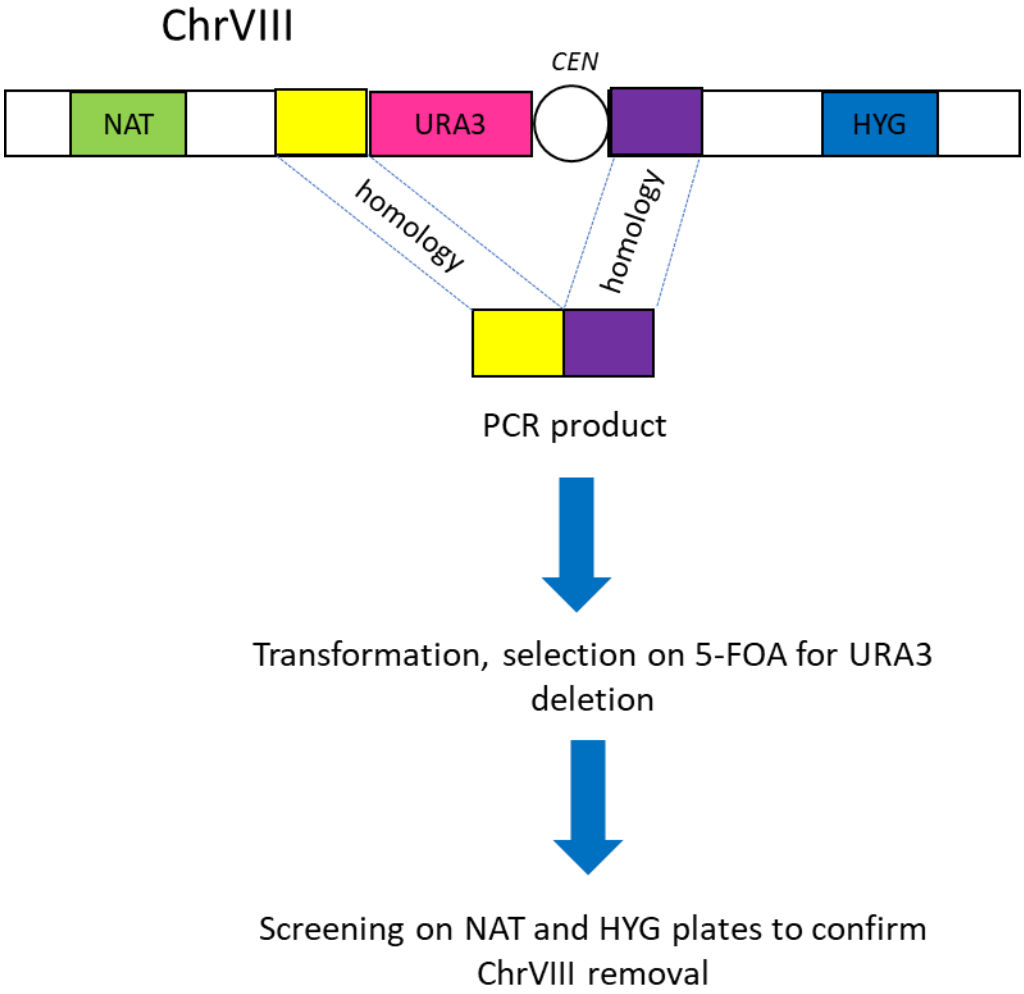

Figure 2.1: The scheme of active deletion of ChrVIII

2.6.5. Preparation of chemically competent *E. coli* cells

Materials:

- 0.1 M $CaCl_2$
- 20% (w/v) glycerol in 0.1 M $CaCl_2$

A colony of a *recA E. coli* K-12 strain (DH5 alpha) was inoculated into 10 mL of LB broth in a 100 mL flask and grown overnight at 37°C on a shaker. In the morning 2 mL of the overnight culture were transferred into a 2 L flask with 200 mL of LB. The culture was grown to OD_{600}=0.4-0.5 and rapidly cooled down in an ice-water bath for 5 minutes. The culture was poured into pre-cooled 50 mL conical plastic tubes and the cells were pelleted in eppendorf® 5810R centrifuge at 4,000 rpm for 10 minutes at 4°C. The supernatant was decanted, cells were gently resuspended in 25 mL of cold 0.1 M $CaCl_2$, added to each tube, and incubated on ice for 1 hour. Upon the incubation, cell suspensions from two tubes were pooled into one tube and the cells were pelleted again under the same conditions. The supernatants were removed and the cells were gently resuspended in 5 mL of cold 20% glycerol in 0.1 M $CaCl_2$ and aliquoted into 1.7 mL tubes pre-cooled at -80°C (100 µL per aliquot). The aliquots were stored at -80°C.

2.6.6. Genetic assay of the efficiency of BIR and DNTA in cells with inducible double-strand breaks

The strains for the assay were derived from the *MATa-inc* strains carrying the *HO* endonuclease gene under the P_{GAL1} promoter and *MNT2::kan::HOsite-URA3-STAR-TEL* construct on their chromosome VII. The 3'-fragment of the *KAN* gene shares 500 bp of homology with a 5' fragment of *KAN* on chromosome II so that BIR can be initiated via the homology. The cells were patched on YPRaf plates and incubated overnight at 30°C to de-repress the P_{GAL1} promoter. Next day, ~1 OD of cells was resuspended in 1 mL of YP and a series of 10-fold dilutions was made in YP going down to 10^{-4}. 100 µL of each dilution were plated on YPGal plates and 100 µL of the dilution 10^{-4} were plated

on a YPD plate to estimate the cell titre. The plates were incubated at 30°C (2 days for YPD plates and 3 days for YPGal plates). Once the colonies have emerged on the YPGal plates, they were replica-plated on SC-ura and G418 plates. The plates were incubated at -30°C overnight. The colonies were scored the next day. The fractions of BIR- and DNTA-survivors were determined as the number of $G418^{R}$ Ura^{-} and $G418^{S}$ Ura^{-} colonies divided by cell titre, respectively.

2.7. Protein methods

2.7.1. Rapid budding yeast protein extraction

Materials:

- Lysis Solution: 1.85 M NaOH, 7.4% (v/v) β-mercaptoethanol
- 50% Trichloroacetic acid (TCA, 4°C cold)
- Acetone (-20°C cold)
- 4x Laemmli Sample Loading buffer: 200 mM Tris-HCl, pH 6.8, 400 mM dithiothreitol (DTT), 8% SDS, 40% (v/v) glycerol, 0.1% (w/v) bromophenol blue
- TCA Sample buffer: 1x Laemmli Sample Loading buffer, 50 mM DTT, 30 mM Tris (pH is not adjusted)

For total protein extraction from *S. cerevisiae,* cells were harvested either upon growing in liquid growth media or from agar plates. When grown in liquid media cell pellets were collected by centrifugation at 1,300-2,350 g, washed with Milli-Q water and either frozen at -80°C or immediately used to prepare protein extracts. Throughout the protein extraction procedure, samples were incubated on ice.

Cells were lysed in 150 µL of 1.85 M NaOH solution with 7.4 % of 2-mercaptoethanol for 10 minutes. 150 µL of cold 50% trichloroacetic acid were added to each sample. Samples were mixed by vortexing and incubated 10 minutes on ice. Following that, total protein was pelleted by centrifugation at 20,200 g for 2 minute

s (room temperature). Pellets were washed with 1 mL of cold acetone (pre-cooled at -20°) and resuspended in the TCA sample buffer by using a pipette tip for mechanical breaking of the pellet followed by hard vortexing.

Samples were incubated for 5 minutes either in a heat-block at 100°C or in boiling water, centrifuged briefly to collect the condensate, mixed by vortexing

and centrifuged for 2 minutes at 20,200 g to separate cell debris from the solubilized proteins. The supernatant was transferred into new tubes and either preserved at -80°C or loaded immediately on polyacrylamide gel.

2.7.2. SDS polyacrylamide gel electrophoresis (SDS-PAGE)

Materials:

- 30% acrylamide:bis-acrylamide solution (37.5:1) (Severn Biotech Ltd.)
- 1.5 M Tris-HCl, pH 8.8
- 0.5 M Tris-HCl, pH 6.8
- 10% (w/v) SDS
- 10% ammonium persulfate (APS)
- Tetramethylethylenediamine (TEMED, UltraPure™, Invitrogen)
- 4x Laemmli Sample Loading buffer: 200 mM Tris-HCl, pH 6.8, 400 mM DTT, 8% SDS, 40% (v/v) glycerol, 0.1% (w/v) bromophenol blue
- TCA Sample buffer: 1x Laemmli Sample Loading buffer, 50 mM DTT, 30 mM Tris (pH is not adjusted)
- 10x SDS-PAGE Running Buffer: 250 mM Tris-HCl, pH 8.3, 1.92 M glycine, 1% (w/v) SDS
- Amersham™ ECL™ Rainbow™ molecular weight marker (#RPN800E)

Polyacrylamide mini-gels were cast using vertically positioned gel-casting mini-plates fixed in a casting stand (Bio-Rad Mini-PROTEAN™3 Cell system). 1.5 mm spacer plates were used for gel-casting, unless specified otherwise. Each mini-gel consisted of two layers, a stacking (top layer) and a resolving (bottom layer) one. For the resolving gel, the following reagents and concentrations were used:

Table 2.5: Recipe for resolving gel

Reagent	Final concentration
1.5 M Tris-HCl (pH 8.8)	0.375 M
30% acrylamide:bis-acrylamide, ratio 37.5:1	5-15%
10 % SDS	0.1%
10% APS (added just before pouring)	0.1%
TEMED (added just before pouring)	0.1%

For the stacking gel, the following reagents and concentrations were used:

Table 2.6: Recipe for stacking gel

Reagent	Final concentration
Tris-HCl (pH 6.8)	0.125 M
30% acrylamide:bis-acrylamide, ratio 37.5:1	4-4.5%
10 % SDS	0.1%
10% APS (added just before pouring)	0.125%
TEMED (added just before pouring)	0.13%

10 mL of the resolving gel mixture and 5 mL of the stacking gel mixture were routinely made per single 10 mL mini-gel. The concentration of acrylamide/bis-acrylamide in the gel mixtures was adjusted according to the molecular weight of the target protein/proteins. In case of several target proteins with starkly different molecular weights, two layers of the resolving gel with the appropriate acrylamide concentrations were cast sequentially.

The ingredients for the resolving gel were added to a 15 mL conical plastic tube and mixed by inverting the tube gently. 1 mL of the mixture was transferred into a separate tube, mixed with 2 µL of TEMED and 20 µL of 10% APS and used for sealing the bottom of the gel. After 5 minutes, the excess of the un-polymerized acrylamide was removed. 10 mL of the resolving gel were mixed with 10 µL of TEMED and 100 µL of 10% APS and the mixture was poured between the glass plates while leaving some space for the stacking gel to be cast later. The resolving gel was covered with 3 mL of 100% ethanol and left to polymerize for 20 minutes. The ethanol was removed and 5 mL of the stacking gel were mixed with 6.5 µL of TEMED and 62.5 µL of 10% APS, poured over the resolving gel and covered with a comb to shape wells. The stacking gel was left to polymerize for 20 minutes upon which the gel was either used immediately or preserved in 1x SDS-PAGE Running Buffer at 4°C overnight.

Before sample loading, the gel was placed into a vertical electrophoresis apparatus (Bio-Rad) tank filled with 1x SDS-PAGE Running Buffer. Protein samples were loaded into the wells along with 3-5 µL of the molecular weight marker. The gel was run at 150 V until the samples entered resolving gel and at 200V afterwards, until the dye front reached the bottom of the gel. The SDS-PAGE was performed at room temperature, unless specified otherwise.

2.7.3. Western blotting using fluorophore-conjugated secondary antibodies

Materials:

- 1x western blotting Transfer buffer: 25 mM Tris, 192 mM glycine
- 10x TBST: 0.5 M Tris-HCl, pH 7.6, 1.5 M NaCl, 1% (v/v) Tween 20
- Blocking solution: 5% (w/v) non-fat dry milk diluted in 1x TBST
- Whatman® 3MM CHR paper (GE Healthcare)
- Immobilon®-FL Transfer Membrane with 0.45 µm pores (Merck Millipore Ltd., #IPFL00010)
- Methanol (Fisher Chemical)
- Skimmed milk powder (Oxoid™, Thermo Fisher Scientific)

Proteins resolved in a polyacrylamide gel were transferred onto a PVDF membrane. For the transfer the gel was separated from the glass plates and the stacking gel as well as the bottom part of the resolving gel were cut off. The PVDF membrane cut to the size of the trimmed gel was activated by incubation in methanol for at least 20 seconds. A gel sandwich was assembled, with the resolving gel covered with the membrane and three layers of Whatman® 3MM filter paper on one side and three sheets of the filter paper on the other side (see Figure 2.2). The sandwich was placed between two fiber pads and encased in a plastic transfer cassette while fully submerged in the transfer buffer (to avoid trapping bubbles between the layers of the sandwich). The transfer was performed in the western blotting transfer buffer in a Mini Trans-Blot® Electrophoretic Transfer Cell (Bio-Rad) for 1 hour (unless otherwise specified) at constant current (250 mA).

Upon the completion of the transfer, the sandwich was disassembled and the membrane was blocked in 10 mL of 5% skimmed milk in 1xTBST by incubation with gentle rocking. Following the blocking, the membrane was incubated in a 50 mL plastic tube with 4 mL of primary antibody diluted in 1xTBST (unless specified otherwise, the dilution was 1:1,000) either for 1 hour at room temperature or overnight at 4°C. The antibody was removed and the membrane was briefly rinsed with 1xTBST, washed 3 times in 1xTBST, 10-minute per wash using an orbital shaker. Subsequently, the membrane was incubated in a plastic box with 7.5 mL of fluorophore-conjugated secondary antibody diluted 1:12,500 in 1xTBST for 1 hour on a rocker at room temperature. During the final steps of the procedure, the membrane was briefly rinsed in 1xTBST and then washed in TBST on an orbital shaker first for 15 and then for 10 minutes. The membrane was scanned using Odyssey® CLx fluorescent scanner (LI-COR®) either in the 700 or 800 nm channel, depending on the fluorophore borne by the secondary antibody. Image analysis and protein band intensity quantifications were performed using the Image Studio™ Lite software.

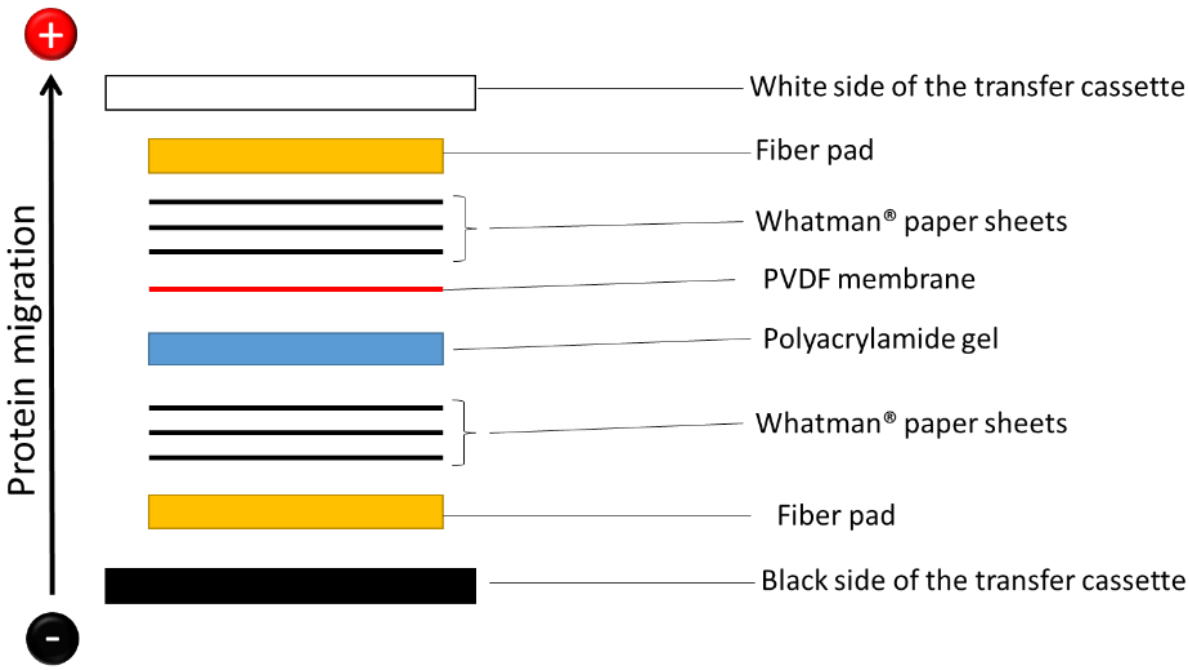

Figure 2.2: The structure of the protein transfer sandwich

2.7.4. Assessment of the DNA damage checkpoint activation upon overexpression of Dna2 or its mutant versions by Rad53 western blot analysis (ECL-based)

Materials:

- 30% acrylamide:bis-acrylamide solution (37.5:1) (Severn Biotech Ltd.)
- 1.5 M Tris-HCl, pH 8.8
- 0.5 M Tris-HCl, pH 6.8
- 10% (w/v) SDS
- 10% APS
- TEMED (UltraPure™, Invitrogen)
- 4x Laemmli Sample Loading buffer: 200 mM Tris-HCl, pH 6.8, 400 mM DTT, 8% SDS, 40% (v/v) glycerol, 0.1% (w/v) bromophenol blue
- TCA Sample buffer: 1x Laemmli Sample Loading buffer, 50 mM DTT, 30 mM Tris (pH is not adjusted)
- 10x SDS-PAGE Running Buffer: 250 mM Tris-HCl, pH 8.3, 1.92 M glycine, 1% (w/v) SDS
- PVDF blotting membrane (Amersham™ Hybond® P 0.45, GE Healthcare, #RPN303F)
- Pierce™ ECL2 Western Blotting Substrate (Thermo Scientific, #80196)
- Immobilon®-FL Transfer Membrane with 0.45 µm pores (Merck Millipore Ltd., #IPFL00010)
- 1x western blotting Transfer buffer: 25 mM Tris, 192 mM glycine
- 10x TBST: 0.5 M Tris, pH 7.6, 1.5 M NaCl, 1% (v/v) Tween 20

- Blocking solution: 5% (w/v) non-fat dry milk diluted in 1x TBST
- Whatman® 3MM CHR paper (GE Healthcare)
- Methanol (Fisher Chemical)
- Skimmed milk powder (Oxoid™, Thermo Fisher Scientific)
- Amersham™ ECL™ Rainbow™ molecular weight marker (#RPN800E)

In yeast cells, the DNA damage checkpoint activation leads to the phosphorylation of Rad53 protein resulting in a slower Rad53 SDS-PAGE mobility readily detected by western blotting. Successful detection of the mobility shift requires sufficient level of protein mobility resolution during SDS-PAGE. Therefore, I used a larger polyacrylamide gel to resolve protein samples for Rad53 ECL western blotting. ECL-based western blot visualisation was chosen for the detection of Rad53-P species since it allows for higher sensitivity of Rad53 signal detection.

The gel was cast using glass plates, 1.5 mm spacers, and a comb from Biometra Model V15·17 Gel Electrophoresis system (Analytik Jena AG). The resolving and stacking layers were prepared using 6.5% and 4.5% acrylamide/bis-acrylamide (37.5:1) final concentrations, respectively. The stacking/resolving gel separation line was approximately 1 cm below the bottom of the wells. Upon the installation of the gel into the gel-running tank filled with 1x running buffer, the air bubbles trapped at the bottom of the gel were removed using a syringe with a 16G bent needle.

The protein samples were prepared from liquid yeast cultures, grown as specified in the Results section of this work. Cells were centrifuged at 4°C, washed with cold water and either stored at -80°C or used immediately for protein extraction using the TCA-based protocol (see section 2.7.1). For each OD unit of cells, 16.7 µL of the TCA sample buffer were added to the protein pellets before boiling. Upon boiling, the samples were immediately used for

SDS-PAGE to avoid dephosphorylation of the Rad53-P species by repeated re-heating of the samples.

10 µL of the protein samples (corresponding to 0.6 ODs of cells) were loaded per gel well and 10 µL of the molecular weight marker was loaded into a spare well. The samples were run through the stacking gel at 150 V (for approximately 50 minutes) and through the resolving gel at 200 V (for approximately 3 hours) allowing for a slight overrunning of the dye front, thus improving protein resolution.

Two 9×7 cm gel slices containing the proteins running between the yellow (76 kDa) and the green (102 kDa) dye markers were cut out and transferred onto Amersham™ Hybond® P 0.45 PVDF blotting membrane (GE Healthcare) optimized for ECL-western blot. The 9×5 cm gel slices immediately above the 102 kDa marker band were transferred onto Immobilon® PVDF membrane which was processed according to the fluorescence-based western blot protocol (see section 2.7.3) in order to assay the expression of Dna2 and its variants. Both transfers were performed under identical conditions (250 A constant current for 1 hour at room temperature in transfer buffer in a Bio-Rad Mini Trans-Blot® Cell).

All the following steps are specific to the ECL-western blot protocol.

The membranes were blocked in 15 mL of 5% skimmed milk in 1xTBST for 1 hour at room temperature and then incubated in 4 mL of 500-fold dilution of α-Rad53 antibody (Goat polyclonal, yC-19, Santa Cruz Biotechnology, Inc.) in 2% milk in 1xTBST overnight at 4°C. The membrane was rinsed and then washed three times in 1xTBST (each wash 10 minutes) and incubated for 1 hour at room temperature with HRP-conjugated Donkey anti-Goat secondary antibody (Thermo Fisher), diluted in 2% milk in 1xTBST to 1:15,000. The membrane was rinsed and washed as after the incubation with the primary antibody.

Rad53 was detected based on the chemiluminescence produced by the chemical reaction catalysed by HRP conjugated to the secondary antibody.

Pierce ECL Western Blotting Substrate (Thermo Fisher) was used to prepare the substrate for the reaction, according to the manufacturer's recommendations. The membrane was incubated in the substrate mix for 5 minutes immediately upon the substrate preparation. It was covered with Saran wrap and the excess of the substrate was blotted away by clean absorbent paper tissue. The membrane was immediately scanned by C-DiGit Blot Scanner (LI-COR) for 12 minutes. The image was analysed using Image Studio™ Lite software.

2.7.5. Co-immunoprecipitation of Est2-myc$_{13}$ with Est3-FLAG$_3$

Materials:

- Basic TMG buffer: 10 mM Tris-HCl (pH 8.0), 1 mM $MgCl_2$, 5% (v/v) glycerol, 300 mM NaCl, 0.5% Tween 20
- TMG buffer: basic TMG buffer, 100 µM DTT, 12 U/mL RNAsin® + cOmplete™ EDTA-free Protease Inhibitor Cocktail (1 mini-tablet/5 mL)
- 4x Laemmli Sample Loading buffer: 200 mM Tris-HCl, pH 6.8, 400 mM DTT, 8% SDS, 40% (v/v) glycerol, 0.1% (w/v) bromophenol blue

The protocol is based on Hughes *et al.*, 2000; Tucey and Lundblad, 2014. See Figure 3.15 for the outline of the co-immunoprecipitation protocol.

Cell cultures were grown either at 30°C or at 38.5 °C in 250 mL of YPD media up to OD_{600} = 0.8. The cells were harvested by centrifugation in a floor-top Avanti J-30I centrifuge (Beckman Coulter) at 2,300 g for 5 minutes at 4°C and then washed with 10 mL of cold water. The cell suspensions were transferred into 15 mL conical tubes, washed with 1 mL of basic TMG buffer, resuspended

in 1 mL of TMG and stored at -80°C. From this point onward, gloves were worn at all steps to avoid RNase contamination and prevent TLC1 degradation and the samples were incubated on ice whenever possible.

The samples were defrosted on ice and 1 volume of 0.5 mm glass beads was added to each sample. Cells were lysed by bead-beating using high power vortexing in alternating cycles of 30 second vortexing followed by a minimum of 30 seconds incubation on ice to avoid sample overheating and protein degradation. The cycles were repeated until over 90% of the cells were lysed as assayed by light microscopy (normally, 10-20 cycles of bead-beating per sample).

The 15 mL tubes were pierced at the bottom with 21G needles and inserted into a set of fresh 15 mL tubes (pre-cooled on ice). The lysates were separated from the beads by briefly centrifuging the lysates through the pierced tubes into the new ones in a tabletop centrifuge at ~1,200 rpm. A 20 µl aliquot of each sample was transferred into a new microcentrifuge tube for further analysis of the **total lysate**.

The rest of the lysates were transferred into fresh microcentrifuge tubes and centrifuged in an eppendorf® 5417R microcentrifuge at 4,700 rpm for 10 minutes at 4°C to remove cell debris and unbroken cells from the lysates (pellet 1). The supernatants were transferred into fresh microcentrifuge tubes while measuring their volumes (V_1). Pellet 1 was washed in 1 mL of the basic TMG buffer, centrifuged for 10 minutes at 4°C and 4,700 rpm one more time and resuspended in V_1 of the TMG buffer. A 20 µl aliquot of this suspension was moved to a new tube and constituted the **pellet 1 sample**.

The supernatant from the previous step was centrifuged for 30 minutes at 4°C and 14,000 rpm to separate the lysate from chromatin. During this centrifugation step, anti-FLAG Affinity gel resin (M2, Sigma) was defrosted and resuspended gently (no vortexing). A wide orifice tip was used to transfer the required volume of the slurry (40 µl × number of samples) into a new microcentrifuge tube with 1 mL of the basic TMG buffer already added (pre-cooled on ice). The tip was washed by repeated pipetting of the basic TMG

buffer in the tube to avoid any loss of the resin. The resin was centrifuged 1 minute at 2,500 rpm in the eppendorf® 5424 microcentrifuge at room temperature. The tube was lightly knocked against the bench to allow the resin to settle at the bottom of the tube. The bulk of the supernatant was removed using a 1 mL pipette, whereas the residual liquid was removed using a 200 µL pipette and a gel-loading tip pressed against the bottom of the tube. The resin was washed again with 1 mL of the basic TMG buffer, resuspended in 1 mL of the buffer and aliquoted into fresh tubes equal to the number of the samples being processed in the experiment. The basic TMG buffer was removed from the tubes upon aliquoting.

20 µL of the lysate cleared upon 30 minute centrifugation were transferred into new tubes as **cleared lysate samples** (or **input**). The total volume of the cleared lysate was measured for each sample (V_2). Equal volumes of the rest of the lysates were transferred into the tubes with the affinity resin (leaving cloudy dark pellet behind - pellet 2) and incubated on a rotator for 3 hours at 4°C to allow binding of the target protein (Est3-FLAG$_3$) to the resin. The pellet 2 samples were washed with 1 mL of the basic TMG buffer, centrifuged for 30 minutes at 4°C and 14,000 rpm and resuspended in volume 2 of the TMG buffer. 20 µL aliquots of these suspension were saved as the **pellet 2 samples**.

The resin was pelleted by centrifugation for 1 minute at 2,500 rpm in a microcentrifuge at 4°C. 20 µl aliquots of the supernatants were drawn as the **depleted lysate samples** (or flow-through), while the rest of the supernatants were discarded. The resin was washed in 1 mL of TMG once and resuspended in volume 2 of TMG buffer. 20 µl aliquots of the suspension were taken as the **IP samples**, while the rest of it was centrifuged once more (same conditions). The supernatant was removed using a 1 mL pipette and a 200 µL pipette with a gel-loading tip.

The Est3-FLAG$_3$ was eluted from the resin by incubating the resin in 30 µL of 1% SDS at 65°C for 10 min, while flicking the tubes every 2 minutes to maximise the elution. The eluate was transferred into a new tube. For sample

preparation, 20 µL of 2x Laemmli was added to total lysate, cleared lysate, depleted lysate, pellet 1, pellet 2 and IP samples and 10 µL of 4x Laemmli were added to the eluate. The samples were boiled in water for 5 minutes and processed further as described in the section for SDS-PAGE (2.7.2). 20 µL of each sample, except the eluate samples (30 µL), were loaded into gel.

2.7.6. Coimmunoprecipitation of Sgs1-myc$_7$ with FLAG$_3$-HA-Dna2

Materials:

- Basic Budd buffer: 50 mM Tris (pH 7.5), 10% (v/v) glycerol, 150 mM NaCl, 0.1 % Tween 20
- Budd buffer: basic Budd buffer + cOmplete™ EDTA-free Protease Inhibitor Cocktail (1 mini-tablet/5 mL)
- Protein LoBind Tubes, 1.5 mL (eppendorf®, #30108116)
- 4x Laemmli Sample Loading buffer: 200 mM Tris-HCl, pH 6.8, 400 mM DTT, 8% SDS, 40% (v/v) glycerol, 0.1% (w/v) bromophenol blue
- 200 mM PMSF in DMSO (200x stock)
- 2.0 ml Graduated Conical Tubes (Starlab, #E1420-2331)
- Dynabeads™ Protein G for Immunoprecipitation (Invitrogen™, #10004D)

The protocol is based on Budd, Choe and Campbell, 1995.

Cell cultures were pre-grown at 30°C in 10 mL of YPRaf media to the log phase, resuspended in 100 mL of YPRaf and grown at 30°C up to OD_{600} = 0.35, at which point 2 g of galactose were added to each culture to induce

overexpression of *SGS1-MYC3* and *FLAG3-HA-DNA2*, both of which were under the *GAL1* promotor. The cultures were incubated at 30°C for two more hours and then transferred into pre-cooled 50 mL conical tubes and centrifuged at 3,000 rpm for 3 minutes at 4°C in an eppendorf® 5810R table-top centrifuge. The media was decanted and the tubes were centrifuged again for 12 seconds to collect residual media at the bottom of the tubes. The cells were washed once in 500 µL of cold water and once in 500 µL of the basic Budd buffer. Cell pellets were transferred into 2 mL screw-cap tubes (Starlab), resuspended in the Budd buffer + 1 mM PMSF (5 µL per 1 OD unit of cells) and combined with an equal volume of 0.5 mm glass beads. Cells were lysed by bead-beating using a Mini-Beadbeater-16 (Biospec Products) at 4°C in cycles of alternating 30-second periods of bead-beating and 1-minute periods of incubation on ice to avoid sample overheating and protein degradation. The cycles were repeated until over 95% of the cells were lysed as assayed by light microscopy (normally, 12 cycles of bead-beating per sample).

Upon bead-beating, the 2 mL tubes were pierced with 21G syringe needles and inserted into 1.7 mL microcentrifuge tubes, the lysate was transferred into the tubes by centrifugation at 2,000 rpm for 1 minute at 4°C in an eppendorf® 5417R microcentrifuge. The lysates were resuspend by pipetting and 20 µL aliquots of the lysates were saved as a set of **total lysate samples**. The rest of the lysates were transferred into new microcentrifuge tubes and centrifuged at 4,700 rpm for 10 minutes at 4°C in the eppendorf® 5417R microcentrifuge to remove cell debris and unbroken cells from the lysates (pellet 1). The supernatants were transferred into fresh microcentrifuge tubes while measuring their volume (V_1). Pellet 1 was washed in 0.5 mL of the basic Budd buffer and resuspended in V_1 of the Budd buffer + 1mM PMSF. A 20 µl aliquot of each suspension was moved to a new tube and saved as a **pellet 1 sample**.

The supernatant from the previous step was centrifuged for 30 minutes at 4°C and 14,000 rpm to separate the lysate from chromatin. During this centrifugation, M2 anti-FLAG antibody (Sigma) was diluted 10-fold in the Budd buffer + 1mM PMSF. 20 µL of the lysate cleared upon 30 minute centrifugation were transferred into new tubes as **cleared lysate samples** (or **input**). The

total volume of the cleared lysate was measured for each sample (V_2) and equal volume aliquots (V_3) of the cleared lysate were transferred into new tubes and mixed with 1/50 V_3 of the 10-fold M2 antibody dilution (resulting in 1/500 final antibody dilution) and incubated on a rotator for 1 hour at 4°C. Dark and cloudy pellet 2 left behind upon the removal of the cleared lysate was washed with 0.5 mL of the basic Budd buffer, centrifuged for 30 minutes at 4°C and 14,000 rpm one more time and resuspended in V_2 of the Budd buffer +1 mM PMSF. 20 µL of this suspension was saved as a **pellet 2 sample**.

During the 1 hour incubation, the required volume of protein G magnetic beads (Invitrogen) (100 µL of slurry per 200 OD units of cells) was transferred into a microcentrifuge tube with 1 mL of the basic Budd buffer. The beads were washed twice in the fresh basic Budd buffer and resuspended in 1 mL of the basic Budd buffer and divided into X equal volume aliquots (X= the number of samples) in the low protein binding 1.5 mL tubes (eppendorf®) to be used later for the M2 antibody pull-down. The buffer was removed from the magnetic beads after 1 hour incubation of the lysate with M2 antibody immediately followed by the transfer of the lysate-antibody mixture into the tubes with magnetic beads. This was followed by 2 hour incubation on a rotator at 4°C.

The beads were separated from the lysate and 20 µL aliquots were saved as **depleted lysates** or flow-through. The rest of the lysates were discarded and the magnetic beads were washed once in 0.5 mL of the basic Budd buffer followed by transfer of the suspension into a new set of low protein binding tubes. During the washing steps, the samples were washed one-by-one to avoid extended periods of drying the beads. The beads were separated one more time and then resuspended in V_3 of the Budd Buffer + 1mM PMSF. 20 µL of this suspension was saved as an **IP sample**, while the rest of the suspension was transferred into a new low protein binding tube. Upon wash removal, 30 µL of 2x Laemmli buffer were added to each IP sample. 20 µL of 2x Laemmli sample buffer were added to each of the rest of the samples. The samples were boiled in water for 5 minutes and processed further as described in the section 2.7.2. 5 µL of each sample, except for eluate samples (30 µL), were loaded per well.

2.8. DNA manipulations

2.8.1. PCR to amplify modules for yeast gene deletion, truncation or addition of tagging sequences

Materials:

- 10x PCR buffer: 500 mM KCl, 100 mM Tris-HCl, pH 9.0, 1% (v/v)Triton X-100
- 25 mM $MgCl_2$
- 10 mg/ml Purified BSA (NEB, #B9001)
- dNTPs mix (10 mM each) from *Taq* PCR Core Kit (Qiagen, #201225)
- *Taq* DNA polymerase (NEB, #M0273)
- *Vent*™ DNA polymerase (NEB, #M0254)

The modules for yeast gene modifications are described in Longtine *et al.*, 1998. For the list of plasmid templates and primers see Tables 2.3-2.4. Mixtures for module PCR amplification were prepared according to the recipe in Table 2.7:

Table 2.7: Recipe for module amplification PCR

Reagent	Volume added, µL	Final concentration
10x PCR Buffer	5	1x
Template DNA (1:10 dilution of a plasmid Miniprep)	1	0.1-0.5 ng/µL
Tris-HCl(1M, pH 9)	0.5	10 mM
$MgCl_2$ (25 mM)	3	1.5 mM
dNTP (10 mM each)	1	0.2 mM
Forward primer (100 µM)	0.25	0.5 µM
Reverse primer (100 µM)	0.25	0.5 µM
BSA (10mg/mL)	0.5	0.1 mg/mL
Vent polymerase (2 U/µL)	0.5	0.02 U/µL
Taq polymerase(2 U/µL)	0.5	0.02 U/µL
H_2O	to 50	

The following program was implemented for module amplification:

Table 2.8: Program for module amplification PCR

Step	Temperature	Length	Number of cycles
Initial denaturation	94°C	2 minutes	1
	80°C	2 minutes	1
Denaturation	94°C	1 minute	30
Annealing	55°C	45 seconds	
Elongation	72°C	2 minutes 50 seconds	
Final elongation	72°C	10 minutes	1

2.8.2. High-fidelity PCR to amplify DNA fragments for cloning

Materials:

- *Pfu* DNA Polymerase 10X Reaction Buffer with $MgSO_4$ (Promega, #M776A)
- *Pfu* DNA Polymerase (Promega, #M7745)
- *Herculase II Fusion* DNA Polymerase (Agilent Technologies, #600675)
- 5× Herculase II Reaction Buffer (Agilent Technologies)
- *Q5*® High-Fidelity DNA Polymerase (#M0491G)
- 5X Q5 Reaction Buffer
- dNTPs mix (10 mM each) from *Taq* PCR Core Kit (Qiagen, #201225)

Three different proofreading DNA polymerases were used to amplify DNA fragments for cloning: *Pfu* DNA polymerase (Promega), *Herculase II Fusion* DNA Polymerase (Agilent Technologies) or *Q5*® High-Fidelity DNA Polymerase (NEB). The reaction mixes were prepared according to the manufacturers' protocols and the amplification programs for these enzymes are described in the tables below. All high-fidelity PCRs were hot-started to avoid primer degradation by the polymerases' proofreading activities.

Table 2.9: Program for *Pfu* PCR

T_m (primer melting temperature) was determined using IDT OligoAnalyser (https://www.idtdna.com/calc/analyzer). The lower T_m of two primers used in a reaction was used to calculate T_a

Pfu			
Step	**Temperature**	**Length**	**# of cycles**
Initial denaturation	95°C	1 min.	1
Denaturation	95°C	30 sec.	20
Annealing	T_a (T_m-2°C)	30 sec.	
Elongation	72°C	1 min./kb	
Final elongation	72°C	5 minutes	1

Table 2.10: Program for *Herculase II Fusion* PCR

T_m (primer melting temperature) was determined using IDT OligoAnalyser (https://www.idtdna.com/calc/analyzer). The lower T_m of two primers used in a reaction was used to calculate T_a

Herculase			
Step	**Temperature**	**Length**	**# of cycles**
Initial denaturation	95°C	2 min.	1
Denaturation	95°C	20 sec.	20
Annealing	T_a (T_m-5°C)	20 sec.	
Elongation	72°C	30 sec/kb	
Final elongation	72°C	3 minutes	1

Table 2.11: Program for *Q5*® PCR

T_a (primer annealing temperature) was determined using NEBTm Calculator (http://tmcalculator.neb.com/#!/main)

Q5			
Step	**Temperature**	**Length**	**# of cycles**
Initial denaturation	98°C	30 sec.	1
Denaturation	98°C	10 sec.	20
Annealing	T_a	30 sec.	
Elongation	72°C	30 sec/kb	
Final elongation	72°C	2 min.	1

Following DNA amplification, the PCR products were purified using QIAquick PCR Purification Kit (Qiagen) according to the manufacturer's protocol and eluted in 100 µL of pre-warmed (~55°C) Milli-Q water. After adding water, the columns were incubated for 15 minutes at room temperature before the final spin. For clonings, 5 µL of the purified PCR product were used per one 30 µL restriction reaction.

2.8.3. Screening yeast recombinants by colony PCR

Materials:

- 20 mM NaOH
- *Taq* PCR Core Kit (Qiagen, #201225)

Colony PCR was used to identify positive clones after yeast transformations. To this end, a small amount of cells was picked from a colony and lysed in 3 µL of 20 mM NaOH by heating at 99°C for 10 minutes in a PCR machine. A PCR reaction mix was prepared using the reagents from *Taq* PCR Core Kit (Qiagen) and added to the cell lysates. The following program was used for amplification:

Table 2.12: Program for yeast colony PCR

T_m (primer melting temperature) was determined using IDT OligoAnalyser (https://www.idtdna.com/calc/analyzer). The lower T_m of two primers used in a reaction was used to calculate T_a

Step	Temperature	Length	# of cycles
Initial denaturation	94°C	2 min.	1
Denaturation	94°C	30 sec.	20
Annealing	T_a (T_m-2°C)	30 seconds	
Elongation	72°C	1 min./kb	
Final elongation	72°C	2 min.	1

2.8.4. Screening *E.coli* transformants by colony PCR

Materials:

- 10X ThermoPol® Reaction Buffer (NEB, #B9004S)
- dNTPs mix (10 mM each)
- *Taq* DNA polymerase (NEB, #M0273)

E. coli colony screen was used for identifying positive clones after bacterial transformation. The PCR mixture for *E. coli* colony screen was prepared as described in Table 2.13:

Table 2.13: Recipe for *E. coli* colony PCR mix

Reagent	Volume added, µL
10X ThermoPol® Reaction Buffer (NEB)	2.5
dNTP (10 mM each)	0.5
Forward primer (100 µM)	0.5
Reverse primer (100 µM)	0.5
Taq (NEB)	0.25
H_2O	to 25

Cells were picked from the colonies using a pipette tip and mixed with the reaction mixture. The amplification was performed using the following program:

Table 2.14: Program for *E. coli* colony-screen PCR

T_m (primer melting temperature) was determined using IDT OligoAnalyser (https://www.idtdna.com/calc/analyzer). The lower T_m of two primers used in a reaction was used to calculate T_a

Step	Temperature	Length	# of cycles
Initial denaturation/disintegration	94°C	10 min.	1
Denaturation	94°C	30 sec.	35
Annealing	T_a (T_m-2°C)	30 sec.	
Elongation	72°C	1 min./kb	
Final elongation	72°C	10 min.	1

2.8.5. Yeast genomic DNA extraction

Materials:

- SE solution: 1 M sorbitol, 0.1 M EDTA
- Zymolyase-100T from Arthrobacter luteus, 100 U/mg (MP Biomedicals, #08320932)
- EDS solution: 50 mM EDTA, 0.2% (w/v) SDS, 2.5 mM NaOH
- 8 M ammonium acetate
- Isopropanol
- 70% (v/v) ethanol (4°C cold)
- 1x TE: 10 mM Tris, pH 8.0, 1 mM EDTA
- Ribonuclease A (RNase A) from bovine pancreas (Sigma, #R4875)

All centrifugation steps were performed at room temperature in the eppendorf® centrifuge 5424. Cells for genomic DNA extraction were either collected from a freshly-grown patch on an agar plate or harvested by centrifugation from liquid culture. ~5 OD units of cells were resuspended in 150 µL of the SE solution with zymolyase-100T (0.1 - 1mg/ml final concentration) and incubated in a water bath at 42°C for 10-20 minutes until spheroplast sedimentation became visible at the bottom of the tubes. The spheroplasts were pelleted by centrifugation at 5,000 rpm for 2 minutes. Most of the SE solution was removed with a pipette, leaving ~20 µL of liquid behind. The pellets were resuspended by brief vortexing. In order to lyse the cells, 150 µL of the EDS solution were added to each sample followed by brief (up to three seconds) vortexing. The samples were incubated in a water bath at 65°C for 15 minutes to inactivate cellular nucleases. 75 µL of 8M ammonium acetate were added to each sample and the samples were incubated on ice for at least 30 minutes to precipitate proteins. The samples were centrifuged for 10 minutes at top speed in a microcentrifuge and the supernatants were transferred into a new set of 1.7 mL tubes. 135 µL of isopropanol were added to each sample and the tubes were inverted 4 times for gentle mixing. Precipitated nucleic acids were pelleted by centrifugation at top speed for 10 minutes and washed with 500 µL of cold 70% (v/v) ethanol. The ethanol was removed in two steps, each following a 5-minute round of centrifugation. The pellets were dried in air for several minutes, dissolved in 20-50 µL of the TE buffer with 20 mg/L of RNase A and incubated at room temperature for 1 hour or at 4°C overnight. The samples were stored at 4°C.

2.8.6. Agarose gel electrophoresis

Materials:

- 10x TBE: 0.89 M Tris, 0.89 M boric acid, 20 mM EDTA
- 6x Gel-Loading buffer: 0.25% (w/v) bromophenol blue, 0.25% (w/v) xylene cyanol FF, 15% (w/v) Ficoll-400
- Agarose, molecular biology grade (Melford, #MB1200)
- 10 mg/mL ethidium bromide (Fisher Scientific, #E/P800/03)
- 100 bp and 1 kb DNA ladder, 500 µg/ml (NEB, #N3231L, #N3232L)

0.5-2% of agarose in 1x TBE were melted in a microwave. Upon complete dissolving of agarose, ethidium bromide was added to the mixture to the final concentration of 0.5 µg/mL. The gel was cast in a horizontal gel tank. Depending on the application, combs with different teeth size were used to shape wells. 1x TBE was used as running buffer.

DNA samples were mixed with 1/5 volume of 6X loading buffer and loaded into wells along with a corresponding DNA molecular weight marker. The samples were resolved at constant electric field strength (1.5-11 V/cm, depending on the application) until a satisfying degree of band separation was achieved. The DNA was visualized using Molecular Imager® Gel Doc™ XR System in the ethidium bromide visualization mode.

2.8.7. Labelling of DNA probes with α-^{32}P-dATP or γ-^{32}P-ATP

Materials:

- Prime-it II Random Primer Labelling Kit (Agilent Technologies, #300385)
- α-^{32}P-dATP, 6,000 Ci/mmol (Perkin Elmer, #BLU012Z)
- γ-^{32}P-ATP, 6,000 Ci/mmol (Perkin Elmer, #BLU002Z)
- T4-polynucleotide kinase, 10 U/µl (NEB, #M0201S)
- 10X ThermoPol® Reaction Buffer (NEB, #B9004S)
- dNTPs mix (10 mM each)
- *Taq* DNA polymerase (NEB, #M0273
- illustra™ Microspin G-25 columns

α-^{32}P-dATP was used to label probes templated by PCR-products. The PCR products used as templates for probe labelling were synthesized using yeast genomic DNA as a template according to the following protocol:

Table 2.15: Recipe for probe template synthesis by PCR

Reagent	Volume added, µL
10X ThermoPol® Reaction Buffer (NEB)	2.5
Template DNA (genomic DNA, dilution 1:10)	1
dNTP (10 mM each)	0.5
Forward primer (100 µM)	0.5
Reverse primer (100 µM)	0.5
Taq (NEB)	0.25
H_2O	to 25

Table 2.16: PCR program to amplify a template for a DNA probe

Step	Temperature	Length	# of cycles
Initial denaturation	94°C	10 min.	1
Denaturation	94°C	30 sec.	35
Annealing	T_m-2°C	30 sec.	
Elongation	72°C	1 min./kb	
Final elongation	72°C	2 min.	1

After the amplification, the PCR product was run in an agarose gel and gel-purified using QIAquick Gel Extraction Kit (Qiagen). The concentration of the purified PCR-product was adjusted to 2.5 ng/µL. The labelling was performed using Prime-it II Random Primer Labelling Kit and α-^{32}P-dATP (6,000 Ci/mmol). During the first step the following components were combined in a PCR tube:

Table 2.17: Mixture for DNA probe labelling

Reagent	Volume added, µL
PCR product (2.5 ng/µL)	2.5
Random 9-mer Primers	2.5
H_2O (Milli-Q)	2

The mixture was heated up in a PCR machine for 5 minutes at 99°C and cooled at room temperature for 2 minutes. 2.5 µL of 5x reaction buffer with dNTPs (except dATP) were added to the mix. 0.5 µL of Exo(–) Klenow DNA polymerase were put on the wall of the tube without contacting the rest of the mix. In the radiation room, 2.5 µL of α-^{32}P-dATP were added to the reaction mix, which was then mixed by pipetting and used to wash the enzyme off the tube wall, followed by more mixing. The tube was immediately transferred to a PCR machine pre-set at 37°C and incubated at 37°C for 35-40 minutes. Subsequently, 60 µL of Milli-Q water were added to the reaction and the probe was purified from unincorporated nucleotides using an illustra™ Microspin G-25 column according to the manufacturer's protocol. The probe was stored at -20°C.

γ-^{32}P-ATP was used to label the oligo OSM32 (see Table 2.4) to probe for yeast telomeric repeats in dot-blots. The labelling was performed using T4-polynucleotide kinase (PNK) (10 U/µl). 2.5 µL of 2 µM oligo were combined with 2 µL of 5x PNK buffer and 5 µL of γ-^{32}P-ATP in a PCR tube. Once the components were mixed, 0.5 µL of T4 PNK were added to the mix and the tube was incubated at 37°C in a PCR machine for 15-30 minutes. The reaction was mixed with 40 µL of Milli-Q water and the labelled oligo was purified from the excess of γ-^{32}P-ATP using illustra™ Microspin G-25 column according to the manufacturer's protocol. The probe was stored at -20°C. No boiling was required before the addition of the probe to hybridization buffer.

2.8.8. Southern blotting

Materials:

- Depurination solution: 0.25 M HCl
- Denaturing solution: 0.5 M NaOH, 1.5 M NaCl
- Neutralizing solution: 1.5 M NaCl, 0.5 M Tris-HCl, 1 mM Na-EDTA, pH 7.2
- 20x SSC: 3 M NaCl, 0.3 M sodium citrate, pH 7.0
- 20x SSPE: 3 M NaCl, 0.2 M NaH_2PO_4, 20 mM EDTA, pH 7.4
- 100x Denhardt's solution: 2% (w/v) bovine serum albumin (BSA), 2% (w/v) polyvinylpyrrolidone (PVP), 2% (w/v) Ficoll-400
- Hybridization buffer: 6x SSPE, 0.5% (w/v) SDS, 5x Denhardt's solution
- Wash buffer: 0.1x SSPE, 0.1% (w/v) SDS
- Positively charged nylon transfer membrane Amersham Hybond®-N+ (GE Healthcare, #RPN303B)

The DNA transfer from agarose gels onto the membranes was performed under neutral conditions, unless otherwise specified. After the completion of the gel run, the DNA was visualized and photographed using Molecular Imager® Gel Doc™ XR System in the ethidium bromide visualization mode, with a fluorescent ruler placed next to the DNA size marker. The unused sides of the gel were cut off and the gel was incubated in 3 volumes of depurination solution for 30 minutes at room temperature with gentle agitation. The gel was rinsed with deionised water and incubated in 3 volumes of denaturation solution for 30 minutes at room temperature with gentle agitation. The gel was rinsed again with deionised water and incubated in 3 volumes of neutralisation buffer for 45 minutes at room temperature with gentle agitation. During the last incubation, a piece of charged nylon membrane and three pieces of Whatman

3MM paper were prepared, with the dimension exceeding the measurements of the gel by 5 mm. The membrane was firstly incubated in deionised water for 1 minute and then equilibrated in 20X SSC for 10 minutes. Once the incubation in the neutralisation buffer was complete, the gel was laid face-down onto a paper wick (3 sheets of 20X SSC-soaked Whatman) covering a plexiglass support positioned in a tray filled with 20X SSC. The gel was covered with the charged nylon membrane and then with the three sheets of Whatman 3MM paper soaked with 20X SSC. A glass pipette was rolled over the surface of the sheet stack to remove any trapped bubbles. The area of the tray surrounding the gel was covered with Saran Wrap. A stack of blotting paper was placed on top of the Whatman sheets and weighed down with a plexiglass plate and glass bottles (see Figure 2.3). The transfer was performed overnight. In the morning, the membrane was retrieved from the transfer system and air-dried for 30 minutes. The DNA was crosslinked to the membrane in a UVP CX-2000 Ultraviolet Crosslinker at 1200 J/cm^2. The membrane was incubated in 15 mL of hybridization buffer for 1 hour at 65°C. The buffer was replaced with 10 mL of fresh pre-warmed (65°C) hybridization buffer. 5 µL of a random-primed labelled probe (see section 2.8.7 for probe preparation) was combined with 50-100 µL of water, melted in a PCR machine at 99°C for 5 minutes and added to the hybridization buffer immediately. The hybridization was performed at 65° for at least 8 hours, in a hybridisation bottle on a rotisserie. After the hybridization, the membrane was rinsed 3 times with the washing solution and incubated with ~30 mL of the washing solution at 65°C for 40 minutes on a rotisserie. The membrane was rinsed again 3 times with the washing solution, wrapped in Saran Wrap and exposed to a phosphor storage screen for up to several days depending on the activity of the probe. Upon the exposure, the screen was scanned with Typhoon FLA 7000 scanner and the image was analysed using the ImageQuant TL Software.

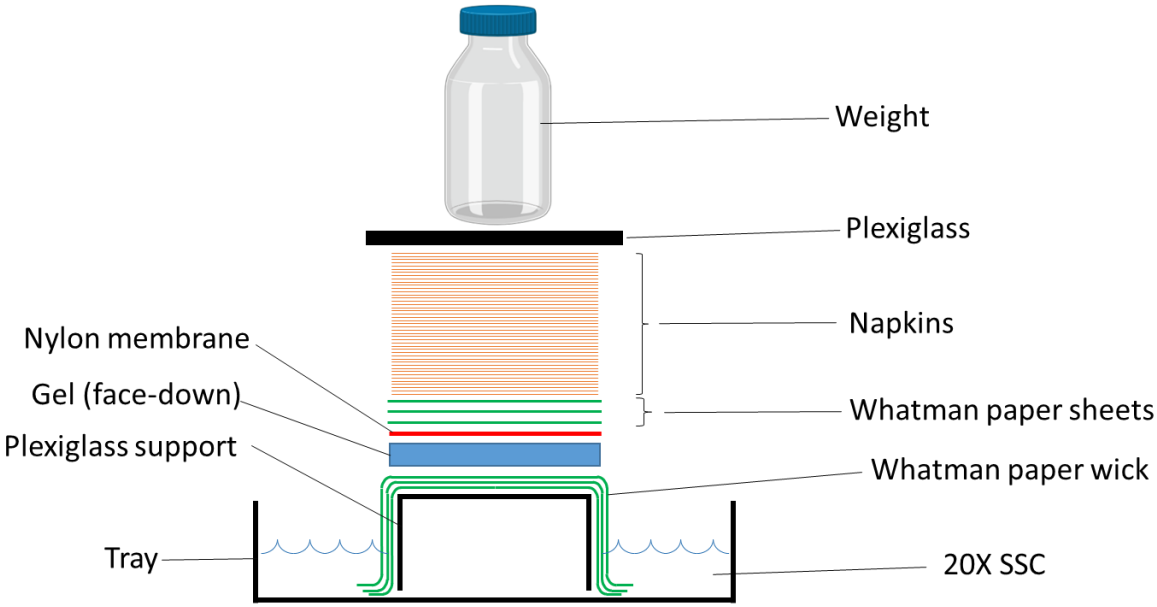

Figure 2.3: Capillary transfer setup for Southern blotting

2.8.9. Stripping of a probe off a Southern blotting membrane

Materials:

- Stripping buffer: 50% (v/v) formamide, 5x SSPE
- Wash buffer: 0.1x SSPE, 0.1% (w/v) SDS

Count reading emitting from the membrane was taken with a Geiger counter before and after stripping to provide a rough estimate of the stripping efficiency. The membrane was stripped in 25 mL of the stripping buffer for 1 hour at 65°C, in a hybridisation bottle on a rotisserie. The membrane was rinsed three times with the wash buffer and incubated in ~30 mL of the wash buffer for 1 hour at 65°C. Subsequently, the membrane was rinsed three more times with the wash buffer and exposed to a phosphor screen for two days to confirm stripping.

2.8.10. Telomere length analysis by Southern blotting

Materials:

- 1x TE: 10 mM Tris-HCl, pH 8.0, 1 mM EDTA
- Ribonuclease A (RNase A) from bovine pancreas (Sigma, #R4875)
- NEBuffer™ 1.1 (NEB, # B7201S)
- KpnI (NEB, #R0142S)
- 6x Gel-Loading buffer: 0.25% (w/v) bromophenol blue, 0.25% (w/v) xylene cyanol FF, 15% (w/v) Ficoll-400
- Agarose, molecular biology grade (Melford, #MB1200)
- 10 mg/mL ethidium bromide (Fisher Scientific, #E/P800/03)
- 1 kb DNA ladder, 500 µg/ml (NEB, #N3232L)

Telomere length was equilibrated by passaging strains at 30°C (unless specified otherwise) for ~80 generations (4 streaks). Genomic DNA was extracted from the cells of the last streak as described in section 2.8.5 and resuspended in 50-100 µL of TE buffer + 20 mg/L of RNAse A. 5 µL of each DNA sample were mixed with 8 µL of Milli-Q water, 1.5 µL of NEB buffer 1.1 and 0.5 µL of KpnI. The digest was performed overnight at 37°C in a PCR machine. In the morning, the samples were mixed with 3 µL of 6X loading buffer, loaded into a 25 cm-long 0.85% agarose gel, along with NEB 1 kb ladder and resolved at 3.4 V/cm for approximately 8.5 hours (until the 0.5 kb band of the ladder migrated 17-17.5 cm away from the wells). The regions of the gel above the 10 kb band and below 0.5 kb band as well as to the left and right of the used lanes were cut off. The subsequent procedures were performed as described in section 2.8.8. The PCR product for the probe (KL1, Makovets, Herskowitz and Blackburn, 2004) annealing to the subtelomeric Y'-element was synthesized using *S. cerevisiae* NK1 genomic DNA and the oligos OSM60 and OSM106 as described in section 2.8.7.

2.8.11. Quantitative DNA analysis using dot-blotting

Materials:

- Basic TMG buffer with 100 mM NaCl: 10 mM Tris-HCl (pH 8.0), 1 mM $MgCl_2$, 5% (v/v) glycerol, 100 mM NaCl, 0.5% Tween 20
- Basic TMG buffer with 300 mM NaCl: 10 mM Tris-HCl (pH 8.0), 1 mM $MgCl_2$, 5% (v/v) glycerol, 300 mM NaCl, 0.5% Tween 20
- TMG-100 buffer: basic TMG buffer with 100 mM NaCl, 100 µM DTT, 12 U/mL RNAsin® + cOmplete™ EDTA-free Protease Inhibitor Cocktail (1 mini-tablet/5 mL)
- TMG-300 buffer: basic TMG buffer with 300 mM NaCl, 100 µM DTT, 12 U/mL RNAsin® + cOmplete™ EDTA-free Protease Inhibitor Cocktail (1 mini-tablet/5 mL)
- NEBuffer™ 3.1 (NEB, #B7203S)
- Benzonase® Nuclease (Sigma-Aldrich®, #E1014)
- 200 mM EDTA (pH 8.2)
- 0.4 M NaOH
- 2x SSC: 0.3 M NaCl, 30 mM sodium citrate, pH 7.0
- 20x SSPE: 3 M NaCl, 0.2 M NaH_2PO_4, 20 mM EDTA, pH 7.4
- 100x Denhardt's solution: 2% (w/v) bovine serum albumin (BSA), 2% (w/v) polyvinylpyrrolidone (PVP), 2% (w/v) Ficoll-400
- Hybridization buffer: 6x SSPE, 0.5% (w/v) SDS, 5x Denhardt's solution
- Low-stringency wash buffer: 1x SSPE, 0.1% (w/v) SDS

- Positively charged nylon transfer membrane Amersham Hybond®-N+ (GE Healthcare, #RPN303B)

Dot-blotting was used to assess the relative efficiency of benzonase-mediated degradation of non-telomeric and telomeric DNA at different salt concentrations in yeast lysate. The dot-blotting protocol is based on Brown, 2001 and involves using a vacuum manifold (DHM-96, Scie-Plas, Figure 2.4) and a vacuum pump (Laboport® N86KN.18).

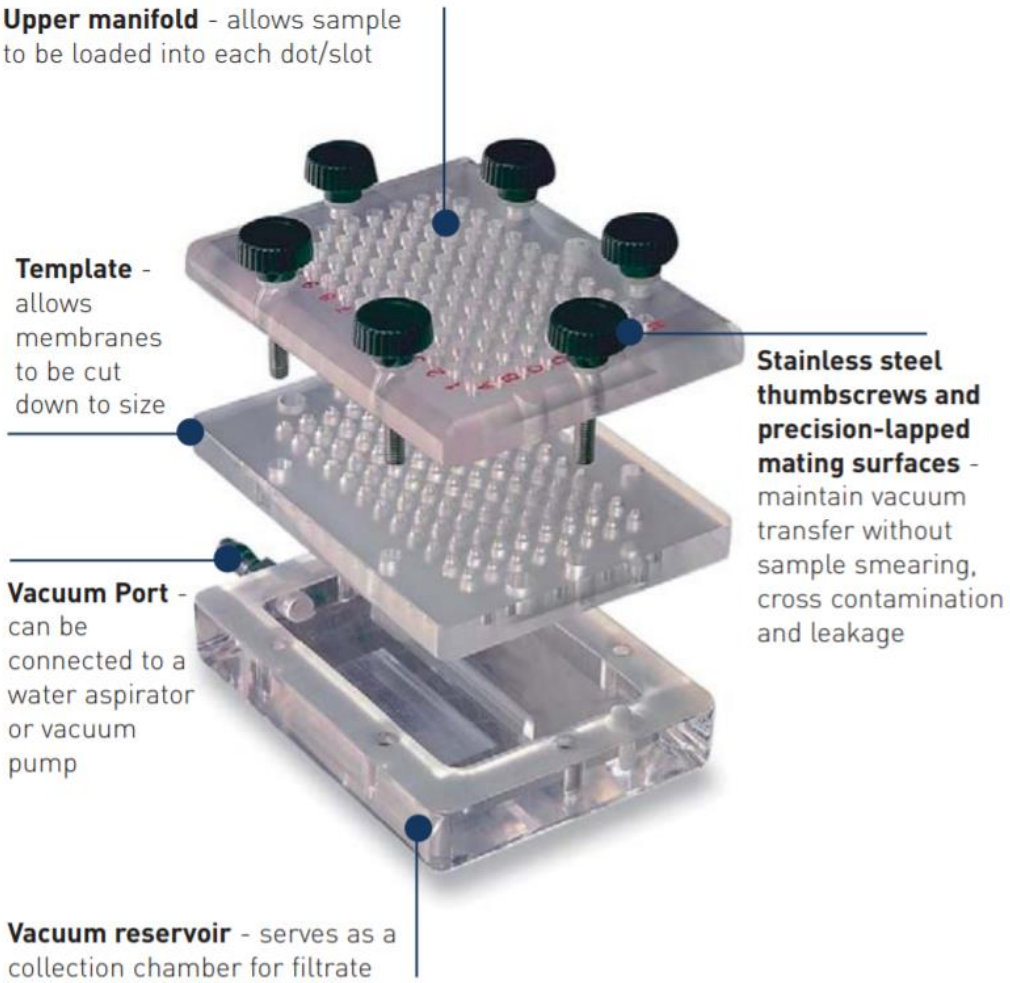

Figure 2.4: Vacuum manifold DHM-96, Scie-Plas

From http://www.scie-plas.com/documents/SCIE-PLAS/distributors/493.pdf

To obtain cell lysate for the experiment the cultures were grown in 200 mL of YPD at 30°C starting from OD_{600} = 0.1. At the OD_{600} = 0.8-0.9 the cultures were poured into pre-cooled 250 mL centrifugation bottles and centrifuged in an Avanti J-30I centrifuge (Beckman Coulter) at 2,300g for 5 minutes at 4°C. The medium was removed and the cells were resuspended in 9 mL of cold water in a 15 mL conical tube. The cell suspension was split into halves and centrifuged in eppendorf® 5810R centrifuge at 3,000 rpm for 3 minutes at 4°C. One half of the cells from each culture was washed in 400 µL of the cold basic TMG buffer with 100 mM NaCl and the other half was washed with 400 µL of the cold basic TMG buffer with 300 mM NaCl. The cells were pelleted again under the same conditions and resuspended in 400 µL of the cold TMG-100 and TMG-300 buffers, respectively. 500 µL of cold 0.5 mm glass beads were added to each tube and the cells were lysed by bead-beating in 30 cycles of alternating 30-second vortexing and 30-second incubation on ice, until >90% of cells lysed (as determined by light microscopy). Two 40 µL aliquots of the total lysate from each sample were transferred into new tubes, one of them was later used for DNA extraction and the other – for western blotting. The rest of the lysate was centrifuged in an eppendorf® 5417R centrifuge at 4,700 rpm for 10 minutes at 4°C. After the centrifugation, two 130 µL aliquots of the supernatant from each tube were transferred into two new tubes. 1.3 µL of 100X benzonase stock (25 U/mL) in TMG-100 or TMG-300 were added to one of the two aliquots of the supernatant originating from a single tube (the buffers of the benzonase stock were chosen to match the buffers in which the cells were lysed). The tubes were then incubated for 10 minutes in an eppendorf® Thermomixer® comfort at 22°C and centrifuged in an eppendorf® 5417R centrifuge at 14,000 rpm for 30 minutes at 4°C to sediment chromatin. 85 µL of the supernatant were removed and 40 µL were saved as a cleared lysate sample to be used in western blotting later. Meanwhile, the pellet was washed with 500 µL of cold TMG-100 or TMG-300, depending on the buffer used during bead-beating. The pellet was centrifuged again under the same conditions, the liquid was removed and the pellet was resuspended in 125 µL of either TMG-100 or TMG-300. Two 40 µL aliquots of resuspended chromatin pellet were

moved to new tubes, one of them was later used in western blotting as a pellet 2 sample, and the other was used for DNA extraction.

The DNA extraction was performed as described in section 2.8.5, starting from the step of adding 150 µL of EDS to the samples. At the final step, the nucleic acids were resuspended in 11 µL of TE + 20 mg/L of RNase A. After 1 hour incubation at room temperature (or overnight at 4°C), 1 µL of the DNA sample was mixed with 4 µL of Milli-Q water, 0.5 µL of NEB buffer 3.1 and 1 µL of 6X loading buffer and resolved in 0.5% agarose gel to assess the benzonase-dependent degradation of genomic DNA at different salt concentrations.

A piece of positively charged nylon membrane and a piece of Whatman 3MM paper were cut to the size of the grid of the manifold template (10.9 cm X 7.2 cm). The membrane was incubated in deionised water for 10 minutes. The paper was submerged in deionised water and placed onto the grid of the manifold template and the membrane was placed on top of the paper.

The 10 µL DNA extracts were mixed in a PCR tube with 0.9 µL of 200 mM EDTA (pH 8.2) and 7.3 µL of 1 M NaOH to the final concentration of 10 mM EDTA 0.4 M NaOH. The mixture was incubated at 99°C in a PCR machine for 10 minutes followed by a brief centrifugation. The pump was turned on and the wells of the manifold were washed with 500 µL of deionised water. The samples were applied to the wells and the wells were rinsed with 500 µL of 0.4 M NaOH. The membrane was removed from the manifold, rinsed briefly with 2X SSC and air-dried.

During the next step, the DNA was cross-linked to the membrane in a UVP CX-2000 Ultraviolet Crosslinker at 1,200 J/cm^2. The membrane was incubated for 1 hour at 50°C in 15 mL of hybridization buffer in a bottle on a rotisserie and the buffer was replaced by fresh pre-warmed (50°C) hybridization buffer with 5 µL of the telomere-specific probe based on the OSM32 oligo. The hybridization was performed at 50°C for 8 hours. Following the hybridization, the membrane was rinsed three times in the low-stringency wash buffer, washed in ~30 mL of the same buffer for 40 minutes at 50°C and again rinsed three times. The membrane was wrapped in Saran Wrap and exposed a

storage phosphor screen overnight. The screen was scanned using a Typhoon FLA 7000 scanner and the image was analysed using the ImageQuant TL Software. After that the membrane was stripped of the telomere-specific probe, as described in section 2.8.9, the membrane was hybridized to either a *URA3* probe or an *ARS1* probe as described in section 2.8.8 and exposed to a storage phosphor screen overnight. The screen was scanned using a Typhoon FLA 7000 scanner and the image was analysed with the ImageQuant TL Software.

2.8.12. Cloning

Materials:

- QIAquick™ Gel Extraction Kit (Qiagen, #28706)
- MinElute PCR Purification Kit (Qiagen, #28006)
- Restriction enzymes (NEB)
- Calf Intestinal Alkaline Phosphatase (NEB, #M0290S)
- T4 DNA Ligase (NEB, #M0202S)

All centrifugation steps throughout the procedure were performed at room temperature.

DNA fragments for cloning were generated either by cutting out an existing fragment from a plasmid or generating such a fragment by high-fidelity PCR, with the desired restriction sites added to the 5'ends of the PCR primers. For the latter option, *Pfu*, *Herculase*, or *Q5*® polymerase was used (see section 2.8.2 on high-fidelity PCR). For the digest of a PCR product, ~ 5% of the column-purified DNA of a single 50 µL PCR reaction were taken into a restriction reaction.

Both vector and insert digests were usually performed in 30 µL reaction volumes. 5-20 U of restriction enzymes were used per 30 µL of the reaction.

The volume of each enzyme to be added was calculated according to the following set of formulas: $\frac{V_A}{V_B} = \frac{N_B \times C_B}{N_A \times C_A}$, $V_A + V_B + V_{CIF} \leq 0.1 \times V_T$, where V_A, V_B are the volumes of stocks of enzymes A and B to be added into the restriction digest, respectively, V_{CIF} is the volume of Calf Intestinal Phosphatase to be added into the restriction digest, V_T is the total volume of the restriction mixture, N_A and N_B are the numbers of restriction sites in the DNA molecule used for activity assay of enzymes A and B, respectively and C_A and C_B are unit stock concentrations of enzymes A and B, respectively. Calf Intestinal Phosphatase was used when only one vector restriction site was used for cloning, or when two restriction sites where too close to each other to resolve fully-digested vector from linearized molecules.

For two-enzyme vector digests, no-enzyme and single-enzyme 10 µL control mixtures were also made, allowing to visualise electrophoretic separation of the target fragment from the undigested and linearized forms of the plasmid and confirm efficient digestion of both target restriction sites.

The restriction mixtures were incubated in a PCR machine at the optimal temperature for 1 hour (plasmid digests) or 3-4 hours (PCR product digests). The plasmid fragments were resolved in agarose gel electrophoresis and gel slices with the desired fragments were cut out from the gel. The DNA fragments were extracted from the gel using QIAquick™ Gel Extraction Kit according to the manufacturer's protocol. Digested PCR products were purified using MinElute PCR Purification Kit according to the manufacturer's protocol.

The elution was performed for 15 minutes. Vector DNA was eluted with 30 µL of warm (~55°C) Milli-Q water and 15 µL of the vector eluate was used to elute the insert. The rest of the vector eluate was used as a vector-only control to assess the background level of non-digested and self-ligated vector upon transformation. Both vector-only and vector+insert eluates were combined with water, T4 DNA Ligase Reaction Buffer and 400 U of T4 ligase (NEB) in 20 µL ligation reaction mixtures which and left at room temperature. 55 minutes into the ligation reaction, competent *E.coli* cell aliquots were transferred from -80°C on ice to defrost: the number of aliquots matched the number of ligation

reaction mixtures. 10 µL of each ligation reaction were added per single *E.coli* aliquot, leaving the remaining 10 µL of the reaction incubating overnight at room temperature. The competent cells were left on ice for 30 minutes, followed by a two minute heat-shock at 42°C and one minute of incubation on ice. 900 µL of LB broth + 1% glucose were added to each aliquot and the tubes with the cells were incubated on a shaker at 37°C for 1 hour. The cells were pelleted at 5,000 rpm in an eppendorf® Centrifuge 5424 for 2 minutes. 900 µL of the media were removed, the cells were resuspended in the remaining LB and plated onto LB plates with an antibiotic (most often – ampicillin at 100 mg/L) to select for transformants. The plates were incubated at 37°C overnight. The colonies were either screened by PCR (in the case of high background on the control plate) and/or inoculated into 5 mL of LB broth with a corresponding antibiotic for subsequent plasmid extraction (at least three colonies per cloning). The cultures were incubated at 37°C on a shaker for at least 8 hours. The plasmids were extracted Wizard® Plus Minipreps DNA Purification System according to the manufacturer's protocol. At the elution step, 50-100 µL of pre-warmed (~55°C) Milli-Q water were added to each column and the columns were incubated for 15 minutes at room temperature before the spin.

Diagnostic digests were performed in 10 µL reaction mixtures and analysed by agarose gel electrophoresis. 2 clones with correct fragment size patterns were additionally verified by sequencing (see next section for Sanger sequencing) if the cloned DNA was generated by PCR.

2.8.13. Sanger sequencing

Materials:

- QIAquick™ PCR Purification Kit (Qiagen, #28106)

To validate sequences of plasmids and PCR products, 300-1,000 ng of plasmid DNA or 2-40 ng (depending on the molecular weight) of a purified PCR product were mixed with 3.33 pmoles of the corresponding primer in 6 µL volume and submitted for Big Dye Reaction Sanger sequencing to the

Edinburgh Genomics facility of the University of Edinburgh. PCR products were purified using QIAquick PCR Purification Kit prior to submission. The sequence reads were analysed in FinchTV software.

2.8.14. Quantitative analysis of yeast chromosomes resolved by Pulse-Field Gel Electrophoresis

Materials:

- Wash buffer: 10 mM Tris-HCl (pH 7.6), 50 mM EDTA
- SeaKem® LE Agarose (Lonza, #50000)
- Certified™ Megabase Agarose (Bio-Rad, #161-3109)
- Lyticase from Arthrobacter luteus (Sigma-Aldrich®, # L2524)
- Lyticase stock: 17,000 U/ml of lyticase in 50% (v/v) glycerol, 10 mM K_2HPO_4, 10 mM KH_2PO_4
- Proteinase K, recombinant, PCR Grade (Sigma-Aldrich®, #3115801001
- Proteinase K Buffer: 100 mM Na-EDTA (pH 8.0), 0.2% sodium deoxycholate, 1% N-lauroylsarcosine sodium
- 1x TBE: 90 mM Tris, 86 mM boric acid, 2 mM Na-EDTA (pH 8.0)
- 0.5x TBE: 45 mM Tris, 43 mM boric acid, 1 mM Na-EDTA (pH 8.0)
- 10 mg/mL ethidium bromide (Fisher Scientific, #E/P800/03)
- 50-Well Disposable Plug Molds (Bio-Rad, #1703713)

For one sample, 1.5-3.0 OD units of cells were harvested from overnight plate patches and resuspended in 1 mL of the wash solution in microcentrifuge tubes. The cells were centrifuged at 5,000 rpm in an eppendorf® Centrifuge 5424 for 2 minutes at room temperature. The cells were washed with 1 mL of the wash solution and resuspended in 100 µL of the wash solution. The tubes were inserted into an eppendorf® Thermomixer® comfort to keep them 50°C warm and shaking at 500 rpm. The samples were mixed with 100 µL of warm (50°C) 1.6-1.8% SeaKem® LE Agarose (in water) and cast into plug molds. The plugs were allowed to solidify at 4°C and then were transferred into 1.7 mL tubes with 500 µL of the wash solution with 340 U/mL of Lyticase. The tubes were incubated at 37°C for 1 hour on a nutator and the wash solution was replaced with 500 µL of the Proteinase K Buffer with 1 mg/ml of proteinase K. The tubes were placed into the Thermomixer again and incubated overnight at 50°C with shaking at 500 rpm. Next day, the plugs were washed four 30-minute rounds with 1 mL of the wash solution by incubating on a nutator at room temperature. The plugs were either used immediately or stored at 4°C in the wash solution.

1.2 g of Certified™ Megabase Agarose were melted in 120 mL of 0.5x TBE buffer to cast a single gel. The plugs were cut into halves and a half of each plug was attached to the comb using molten agarose. The comb was inserted into a Standard Casting Stand (Bio-Rad) and the gel was poured into the Stand at 4°C. After the gel has solidified, the comb was removed, the gel was transferred into an Electrophoresis Cell of CHEF-DR® III System (Bio-Rad) with 3 L of 0.5x TBE buffer pre-cooled to 14°C. Yeast chromosomes were resolved under the following conditions:

- Stage 1: Switch time - 60 seconds, electric field strength - 6 Volts/cm, included angle – 120°, temperature – 14°, length – 15 hours
- Stage 2: Switch time - 90 seconds, electric field strength - 6 Volts/cm, included angle – 120°, temperature – 14°, length – 7.6-10 hours

After the run was finished, the gel was stained in 500 mL of 1x TBE with 600 µg/L of ethidium bromide for 30 minutes on an orbital shaker and then washed

two times with 500 mL of 1x TBE for 15 minutes on an orbital shaker. The DNA was visualized using Molecular Imager® Gel Doc™ XR System in the ethidium bromide visualization mode. The exposure time was adjusted to maximize the intensity while avoiding saturation of the target bands. To assess the number of CHRVIII copies per cell, the ratio of CHRVIII/CHRV band intensity was calculated and normalized to a diploid strain control using the Bio-Rad Image Lab™ Software.

2.8.15. Southern blotting of PFGE-resolved yeast chromosomes

Materials:

- MagnaGraph Nylon Membranes, Tight pore size (0.22µM), 20 cm x 3 m (Osmonics, #NJTHYA0010)
- 10 mg/mL ethidium bromide (Fisher Scientific, #E/P800/03)
- Denaturing solution: 0.5 M NaOH, 1.5 M NaCl
- Neutralizing solution: 1.5 M NaCl, 0.5 M Tris-HCl, 1 mM Na-EDTA, pH 7.2
- 20x SSC: 3 M NaCl, 0.3 M sodium citrate, pH 7.0

The steps for the PFGE part of the protocol are the same as in the previous section, except that during the staining step the concentration of 1mg/L of ethidium bromide was used and the gel washing steps were omitted. After the visualization, the gel was incubated in 3 volumes of the denaturing solution for 30 minutes on a rocker, rinsed with deionised water and incubated in 3 volumes of the neutralization buffer. The gel was transferred onto MagnaGraph Nylon Membrane (0.22 µm pore size) using a capillary transfer system (as in Figure 2.3, but without the bottle) for six hours during the day and then overnight. During the first six hours the napkins were changed every 1.5-2 hours. To avoid gel collapsing, a plexiglass sheet was used as the only weight. The rest of the procedure was performed as described in the section 2.8.8.

CHAPTER 3

Optimization of Co-immunoprecipitation of Est2 and Est3

3.1. Introduction

Previously, Millet *et al.* have demonstrated that elevated growth temperature decreases the steady-state level of Est2, causing senescence in yeast and that chromosome VIII monosomy can compensate for Est2 insufficiency at elevated growth temperature without increasing Est2 amount (Millet *et al.*, 2015). In order to understand the connections between aneuploidy and telomere biology in yeast and the potential relevance of these connections to cancer I set two main investigative aims, which would be detailed below:

1. Gaining molecular insights into the mechanism of aneuploidy-dependent compensation of temperature-induced telomerase insufficiency
2. Understanding how the steady-state level of Est2 is controlled

The **first** aim entails clarifying whether and how the increase in the amount of Est1 and Est3 proteins as well as TLC1 RNA compensates for insufficient Est2 in aneuploids. One of the possible explanations could be that the higher levels of the telomerase components lead to more efficient incorporation of Est2 into telomerase complex, even with the same amount of Est2 present in each cell. This notion is supported by a study, in which two copies of *EST1-MYC12* were introduced in tandem into a *FLAG3-MYC12-EST2* yeast strain, resulting in an excess of Est1-myc$_{12}$ over FLAG$_3$-myc$_{12}$-Est2. This was accompanied by a substantial increase in the amount of Est1-Est2 containing complex in the G1 phase of the cell cycle, when Est1-Est2 interaction is normally hard to detect, despite the apparent parity in the numbers of Est1 and Est2 molecules at this cell cycle stage (Tucey and Lundblad, 2013). In order to test the hypothesis that aneuploid cells overcome temperature-induced telomerase insufficiency through increasing the amount of telomerase complex I was going to perform Est2-Est3 co-immunoprecipitation experiments and compare the amount of Est3 associated with Est2 or vice versa in aneuploid cells versus diploid cells grown at 38.5°C. Choosing Est3 as the co-immunoprecipitation partner of Est2

in the experiment was justified by the fact that Est3 subunit is included last during the full telomerase complex assembly (Tucey and Lundblad, 2014).

The **second** aim concerns understanding the reasons underlying the fact that the amount of Est2 protein remains the same in aneuploids and diploids, despite the increases in all the other telomerase components (Millet *et al.*, 2015). We hypothesized that the steady level of Est2 is maintained through active Est2 degradation. A decrease in the Est2 level similar to the one caused by growth at elevated temperature has also been previously observed upon deletion of the TLC1 stem-loop structure responsible for the association with Est2 (Tucey and Lundblad, 2014). This suggests a possible connection between Est2-TLC1 interaction and the Est2 protein stability. There are known examples in prokaryotes, where an RNA hairpin is disrupted by an increase in temperature (Krajewski and Narberhaus, 2014). It is therefore possible that the stem-loop of TLC1 where Est2 binds could be similarly prone to temperature-dependent destabilization. This hypothesis potentially links the temperature-induced decline in the Est2 level to the loss of the Est2-TLC1 interaction. How exactly the impaired binding between Est2 and TLC1 renders Est2 unstable is not clear; one hypothesis speculates that in the absence of TLC1, the nuclear import of Est2 is decreased, Est2 remains trapped in the cytoplasm where it is recognised and marked for degradation. TLC1 itself is imported into the nucleus by the yKu protein complex (Gallardo *et al.*, 2008) which could potentially carry Est2 into the nucleus along with TLC1.

3.2. Selection of the tagging constructs for Est2 and Est3

3.2.1. Pilot co-immunoprecipitation of Est3-myc$_{13}$ with FLAG$_3$-myc$_{12}$-Est2 from haploid cells grown at 30°C or at 38.5°C

Before performing the bona fide comparative co-immunoprecipitation of Est2 and Est3 in aneuploid and diploid cells, I did pilot experiments in order to establish an optimal protocol for co-immunoprecipitation. The protocol described in Tucey and Lundblad, 2014 was used as a starting point for the optimization of the co-immunoprecipitation experiment and dictated the choice of the tagging constructs for Est2 and Est3 proteins (see section 2.7.5 and Figure 3.15 for the outline of the co-immunoprecipitation protocol). Initially, diploid strains were created with the tags fused to the single copies of *EST2* and *EST3* genes. A FLAG-tag was fused to the Est2 N-terminus allowing to pull down Est2 from cell lysate with anti-FLAG resin, while a myc-tag was added to both the Est2 N-terminus and the Est3 C-terminus in order to quantify the amounts of these proteins by western blotting.

First, I assessed the efficiency of FLAG$_3$-myc$_{12}$-Est2 immunoprecipitation. Cell lysates were obtained from 250 mL of log-phase cultures grown at 30°C to OD_{600}≈0.8 and the Est2 protein was immunoprecipitated using anti-FLAG antibody covalently attached to agarose beads (resin). The IP samples as well as the samples of total lysate, pellet 1, pellet 2 (taken after two subsequent rounds of cell lysate centrifugation, respectively), cleared lysate (after the second centrifugation), depleted lysate (after IP) were taken. An isogenic diploid strain with untagged Est-proteins was used as a negative control for the FLAG$_3$-myc$_{12}$-Est2 and Est3-myc$_{13}$ signals (Figure 3.1). FLAG$_3$-myc$_{12}$-Est2 protein was efficiently depleted from the cleared lysate as evident from the comparison between the cleared and depleted lysate samples (lanes 8 and 10, respectively). An intense band of about 50 kDa was observed in the negative control IP sample (lane 11), but not in the rest of negative control

lanes. I speculate that this band might correspond to the heavy chain of the mouse anti-FLAG antibody that could have detached from the beads present in the IP sample during the boiling step of protein sample preparation and then could have been recognised by the secondary antibody, since the size of the band corresponds to that of an antibody heavy chain.

During the next step of the procedure, I pelleted the beads with the immunoprecipitated proteins, washed them and resuspended in a solution containing FLAG3 peptide for competitive elution of the bound $FLAG_3$-myc_{12}-Est2 protein. The eluate was separated from the beads and both these fractions were mixed with Laemmli buffer and boiled. Equal portions of these samples were resolved in 10% SDS polyacrylamide gel along with total lysate samples in order to assess the efficiency of the elution as well as the Est3-myc_{13} co-immunoprecipitation (Figure 3.2)

The comparison between the amounts of $FLAG_3$-myc_{12}-Est2 protein in the eluate (lane 4) and remaining on the beads (lane 6) indicates that most of $FLAG_3$-myc_{12}-Est2 protein is present in the eluate. Also, I observed a 50 kDa band in the negative control eluate sample (lane 3) similar to the one previously found in the IP sample of the negative control (see Figure 3.1, lane 11). Given that this band overlapped in size with the predicted band for the Est3-myc_{13} protein (as judged from the total lysate sample, Figure 3.2, lane 2), it might obscure the signal coming from the Est3-myc_{13} when in the same lane. The absence of the respective band in the depleted lysate sample of the negative control (Figure 3.1, lane 9) implies that the protein that produces this signal appears in the soluble fraction after the immunoprecipitation step. As noted above, this band may represent the heavy chain of the anti-FLAG antibody that detaches during the boiling step from the beads that contaminate the eluate.

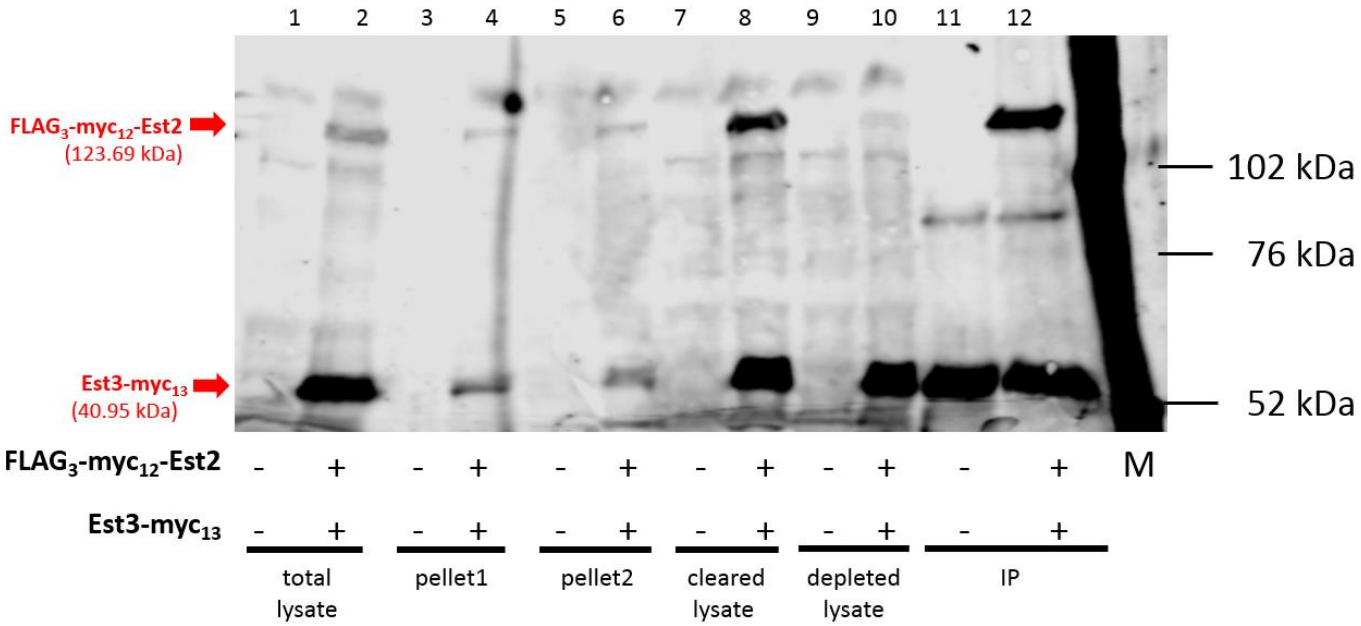

Figure 3.1: Assessment of the efficiency of Est2 immunoprecipitation from *FLAG3-MYC12-EST2/EST2 EST3-MYC13/EST3* cells

IP – immunoprecipitate, M-molecular weight marker. The scale on the right denotes the sizes of the proteins in the marker sample. For a detailed description of samples loaded on the gel see the main text above. An isogenic diploid strain with no tags was used as a negative control for the Est2 and Est3 signals (lanes with odd numbers). Est2 is almost completely depleted from the cleared lysate (compare lanes 8 and 10). Est3-myc13 runs as a 50 kDa band in total lysate, despite the calculated size of 40.95 kDa. The band of the corresponding size appears in the IP sample (lane 11) of the negative control but is absent from the rest of the negative control samples

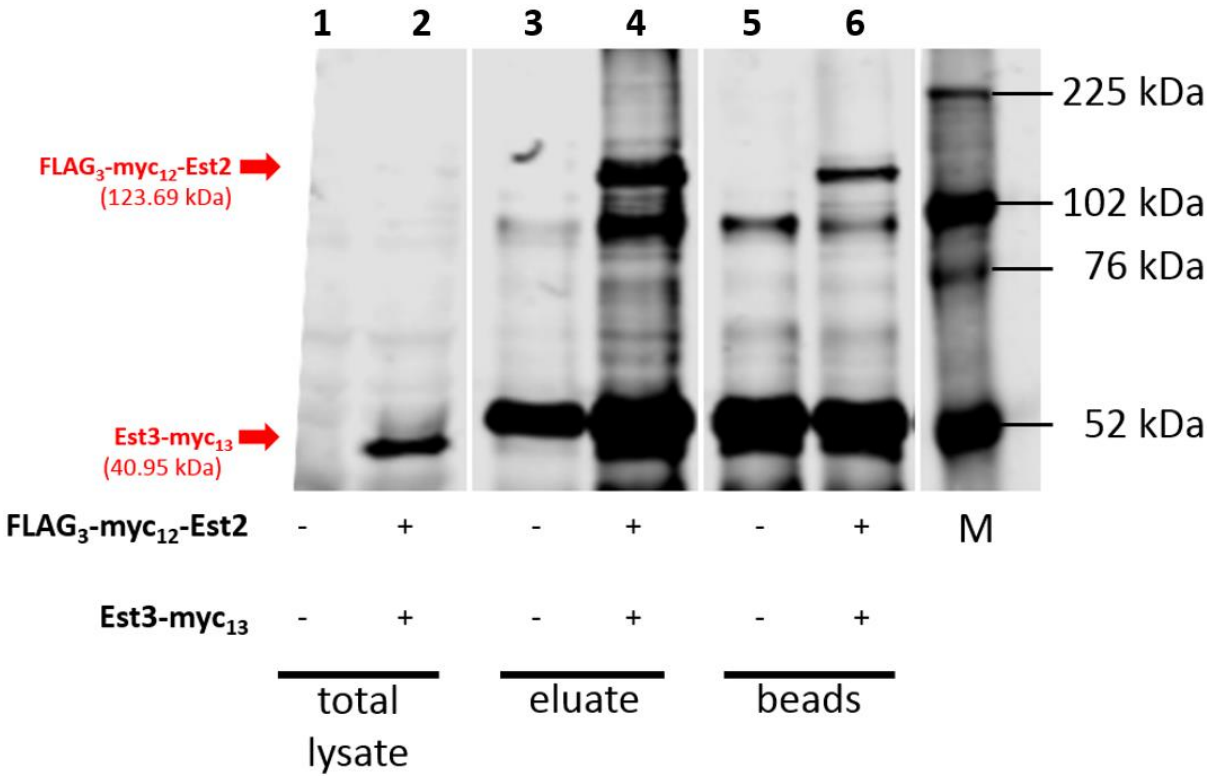

Figure 3.2: Pilot co-immunoprecipitation of Est3-myc$_{13}$ with FLAG$_3$-myc$_{12}$-Est2 from *FLAG3-MYC12-EST2/EST2 EST3-MYC13/EST3* cells grown at 30°C

The legend is as in Figure 3.1. White stripes denote the places where irrelevant lanes were cut out. An isogenic diploid strain with untagged Est-proteins was used as a negative control for the FLAG$_3$-myc$_{12}$-Est2 and Est3-myc$_{13}$-tag signals (lanes 1, 3, 5)

In order to prevent the resin contamination (which is the likely source of the heavy antibody chain) in the eluate I filtered it through 0.65 µm Durapore® filters before boiling. The 50 kDa band was not observed in the filtered eluate samples from the strain with untagged proteins upon elution with FLAG3 (see Figure 3.3, lanes 5 and 7). Considering that the elution by heating in SDS solution was previously found to be more efficient compared to FLAG-peptide elution (data not shown), I also tested, whether the 50 kDa band would still be recovered in the filtered eluate from the strain with no tags in case of elution with SDS at 65°C. I found the filters did not prevent the appearance of the 50 kDa band in the eluate when SDS elution was used (data not shown) and therefore decided to adhere to using FLAG-peptide elution.

Since it has been shown that at 38.5°C the amount of Est2 protein is drastically decreased in yeast cells (Millet *et al.*, 2015), it would be reasonable to expect that for cells grown at this temperature the yield of both $FLAG_3$-myc_{12}-Est2 and Est3-myc_{13} in the immunoprecipitate would be lower than for the same yeast grown at 30°C. Therefore, I performed a side-by-side co-immunoprecipitation of Est3-myc_{13} with $FLAG_3$-myc_{12}-Est2 from the cells grown at 30°C and at 38.5°C in order to test whether the amount of Est3-myc_{13} co-immunoprecipitated with $FLAG_3$-myc_{12}-Est2 would be sufficient for a reliable quantification (Figure 3.3). In the samples obtained from the cells grown at 38.5°C, I could not see a clear band in the gel region corresponding to the 50 kDa protein weight (Figure 3.3, lane 8). Also, in the samples from the same strain grown at 30°C, two closely running bands were discovered in the area of the expected Est3-myc_{13} mobility (Figure 3.3, lane 6). As discussed later, I introduced an additional negative control for the Est3-myc_{13} signal to determine which (if any) of these two bands represents the Est3-myc_{13} protein (see Figure 3.5).

To increase the yield of Est3 protein in the immunoprecipitate, I constructed diploid strains with both copies of the *EST2* and *EST3* genes fused to the tag sequences, with the expectation of a 4-fold increase in the co-IPed Est3-myc_{13} signal. This time I managed to see a distinct band corresponding in size to the Est3-myc_{13} protein in the samples from the cells grown at the elevated temperature (Figure 3.4, lane 7).

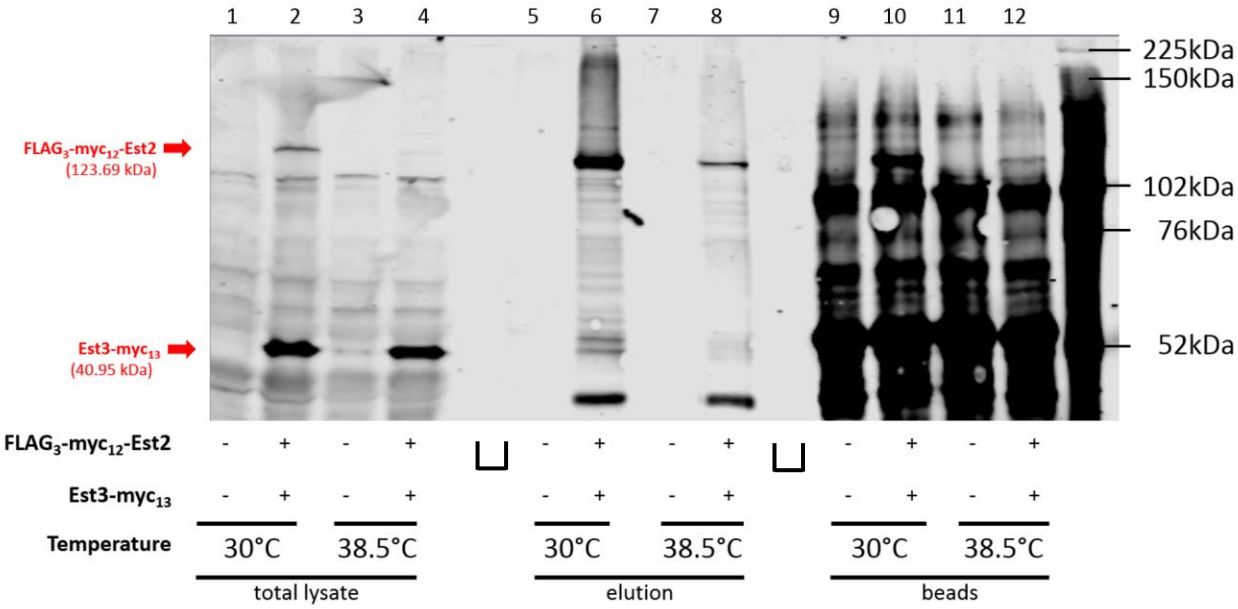

Figure 3.3: Comparison of the yield of Est3 co-immunoprecipitated with Est2 from *FLAG3-MYC12-EST2/EST2 EST3-MYC13/EST3* cells grown at 30°C or at 38.5°C upon sifting samples through particle filters

␣ - empty lanes; legend as in Figure 3.1. The eluates were centrifuged through 0.65 µm filters which captured the agarose beads and thus the band of 50 kDa size was no longer observed in the samples from the strain with untagged proteins (lanes 5 and 7). Two closely running bands are seen in the region corresponding to the expected Est3 protein band in the sample from the tagged strain grown at 30°C (lane 6). No clear band can be seen in case the same strain is grown at 38.5°C (lane 8)

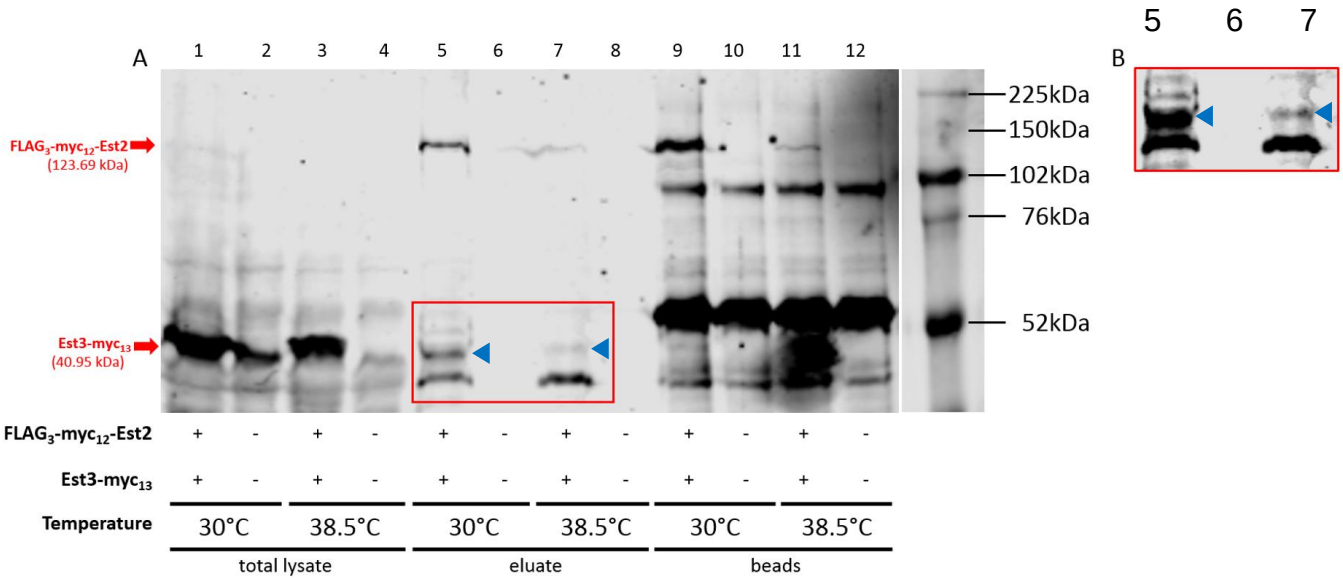

Figure 3.4: Comparison of the yield of Est3 co-immunoprecipitated with Est2 from *FLAG3-MYC12-EST2/FLAG3-MYC12-EST2 EST3-MYC13/EST3-MYC13* cells grown at 30°C or at 38.5°C

Legend as in Figure 3.1. A - western blot of total lysate, eluate and beads samples from the strains with or without FLAG$_3$-myc$_{12}$-Est2 and Est3-myc$_{13}$ grown at 30°C and 38.5°C. The white stripe to the left of the marker indicates where a lane was cut off. The red rectangle highlights the area of the expected Est3 band. Note that the 50 kDa band can now be seen at both growth temperatures (blue arrowheads). B - area within the rectangle from the image in A shown at lower intensity threshold settings

To verify that the 50 kDa band seen in the strain with the tagged proteins represents the Est3-myc$_{13}$ protein I performed an experiment similar to the one shown in Figure 3.2, using a strain with the tag only on Est2 protein (FLAG$_3$-myc$_{12}$-Est2), as a negative control for Est3-myc$_{13}$ signal (Figure 3.5). A band of the same size as the aforementioned 50 kDa band, albeit less intense, was discovered in the negative control eluate sample (lane 6; compare to lane 5). Therefore, in the strain carrying tags on both proteins, the Est3-myc$_{13}$ band might overlap with the corresponding band revealed in the negative control. There are two explanations for the origin of the latter band: the first attributes it to a degradation product of the tagged Est2 protein, the second – to some protein binding to FLAG$_3$-myc$_{12}$-Est2 and cross-reacting with anti-myc antibody. In order to distinguish between these two possibilities I performed an

additional immunoprecipitation experiment with the same strains: two western blots were done in parallel with the same set of samples using two different primary mouse antibodies: anti-myc and anti-FLAG (Figure 3.6). The band previously seen in the 50 kDa region of the sample coming from the Est2-only tagged haploid strain was again observed in anti-myc WB (Figure 3.6A,C lane 5). A band with a matching mobility was also discovered in anti-FLAG WB in the corresponding lane (Figure 3.6B,D, lane 5) as well as in the lane with the sample from the double-tagged strain (Figure 3.6B and D, lane 6). I concluded that the band in question is most likely a degradation product of Est2 rather than its binding partner (although, it's still possible that a secondary antibody has a cross-reactivity with an $FLAG_3$-myc_{12}-Est2 binding partner). I tried to use PMSF in addition to cOmplete™ protease inhibitor cocktail to slow down possible degradation of $FLAG_3$-myc_{12}-Est2 in samples in vitro. However, the addition of PMSF did not produce any significant difference in the band pattern of the *FLAG3-MYC12-EST2* strain (data not shown).

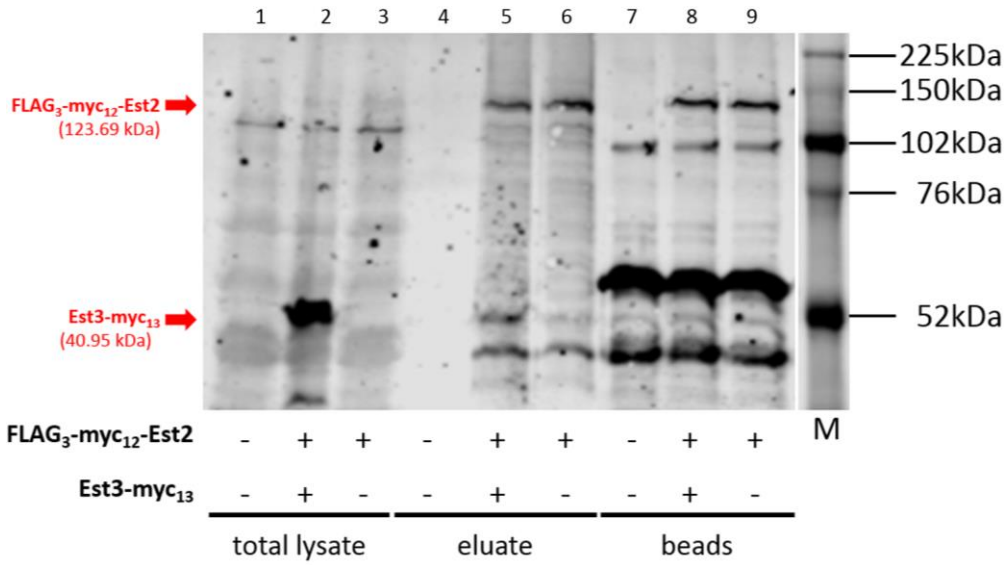

Figure 3.5: Est3-myc_{13} band might overlap with a non-specific band in western blot of samples from *FLAG3-MYC12-EST2 EST3-MYC13* cells

Legend as in Figure 3.1. Haploid strains were used in this experiment. The western blot shows that the band in the Est3-region of the sample from *FLAG3-MYC12-EST2 EST3-MYC13* strain has a counterpart in *FLAG3-MYC12-EST2* strain, although the latter band is less intense. This might indicate that the Est3 band overlaps with one of the bands resulting from Est2 degradation or some cross-specific Est2-binding protein

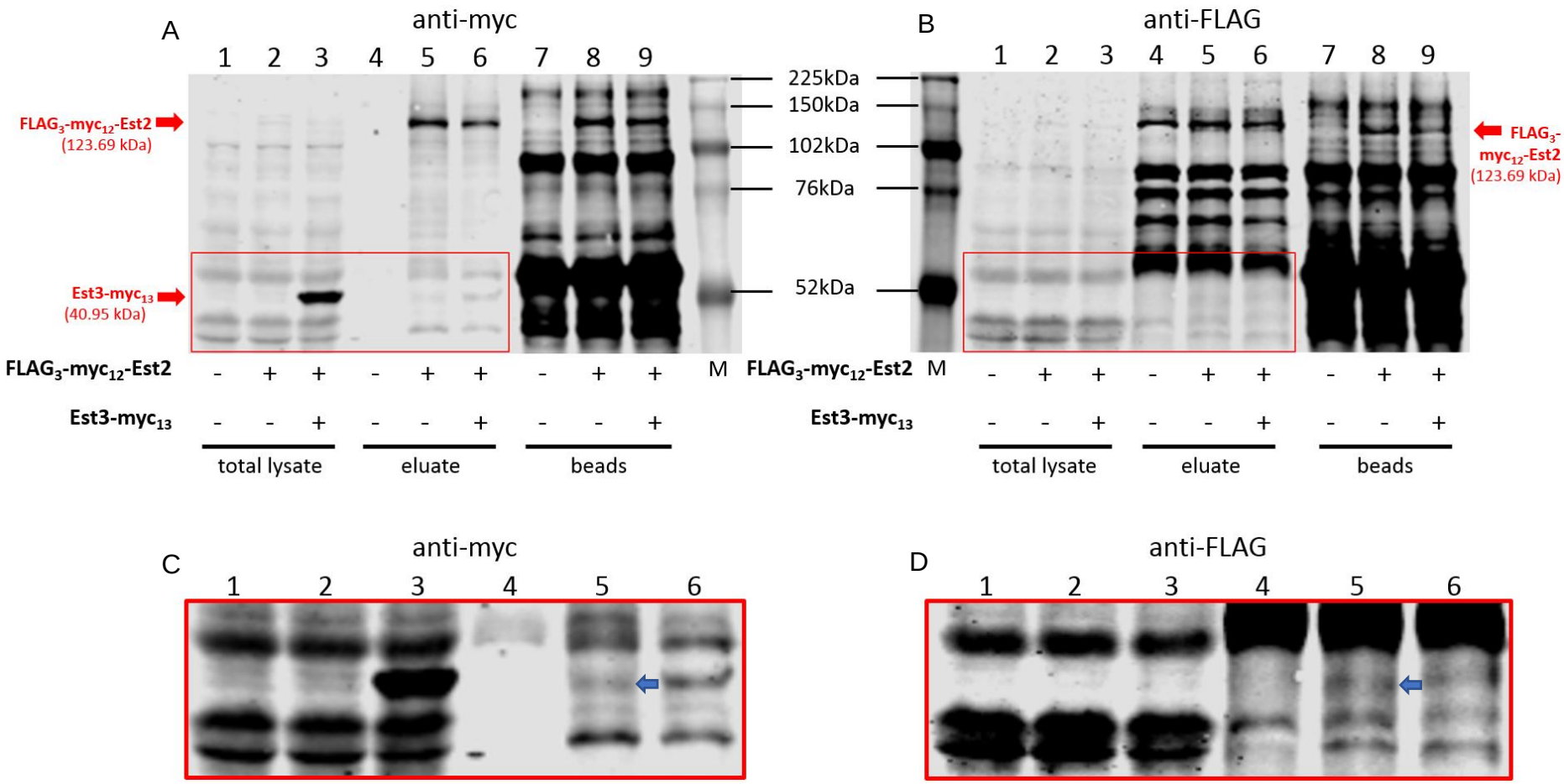

Figure 3.6: $FLAG_3$-myc_{12}-Est2 degradation product band overlaps with Est3-myc_{13} band

Legend as in Figure 3.1. The same strains were used as in Figure 3.5. A and B – full images of the western blots. C and D – close-up views of the areas within the red rectangles in A and B, respectively. The two bands marked by the two blue arrows in C and D have matching locations on the blots. They are likely to represent a degradation product of Est2 since Est2 is the only protein with both a myc and a FLAG tag in these strains and it is quite unlikely that an unspecific protein would react with both antibodies

3.2.2. Qualitative western blot analysis of signal intensity of Est2 and Est3 with various tags

In order to tackle the problem of overlapping signal between the bands of Est3-myc$_{13}$ and the degradation product of FLAG$_3$-myc$_{12}$-Est2 I decided to try alternative tagging constructs for both Est2 and Est3 proteins (Table 3.1). The constructs were introduced into the genome either by a linearized plasmid or by a selective PCR product insertion (see Table 3.1). I assayed these constructs in pilot western blot experiments to determine, whether the epitope signal/background ratio was sufficient for reliable quantitative analysis in subsequent co-immunoprecipitation experiments (Figures 3.7-3.8). For the western blotting analysis of each construct, at least three clones were purified from a selective plate upon transformation. Clones resulting from a PCR cassette insertion were additionally pre-screened by colony-PCR before the purification (see Figure 3.8E).

Table 3.1: Tagging constructs for Est2 and Est3 proteins analysed in this study

Target protein	Tagging construct	Vehicle for gene modification
Est2	N-FLAG$_3$-myc$_{12}$-Gly$_6$-Est2	Plasmid (*pVL5273*/HpaI)
	N-FLAG$_3$-Gly$_6$-Est2	Plasmid (*pYT413*/HpaI)
	N-FLAG$_3$-Gly$_6$-HA$_3$-Est2	Plasmid (*pYT415*/HpaI)
	N-FLAG$_3$-Gly$_6$-HA$_6$-Est2	Plasmid (*pYT419*/HpaI)
	N-FLAG$_3$-Gly$_6$-HA$_9$-Est2	Plasmid (*pYT420*/HpaI)
	N-myc$_{12}$-Gly$_6$-Est2	Plasmid (*pYT416*/HpaI)
	Est2-myc$_{13}$-C	PCR cassette amplified from *pFA6a-kanMX6-MYC13*
Est3	Est3-myc$_{13}$-C	PCR cassette amplified from *pFA6a-MYC13-kanMX6*
	Est3-myc$_{13}$-Gly$_6$-FLAG$_3$-C	Plasmid (*pYT414*/MfeI)
	Est3-HA$_3$-C	PCR cassette amplified from *pFA6a-HA3-TRP1*
	Est3-FLAG$_3$-C	PCR cassette amplified from *pFA6a-FLAG3-TRP1*
	N-FLAG$_3$-Est3	*FLAG3-URA3-FLAG3* PCR cassette amplified from *pEHB12009* with subsequent -*URA3* loop-out on 5-FOA

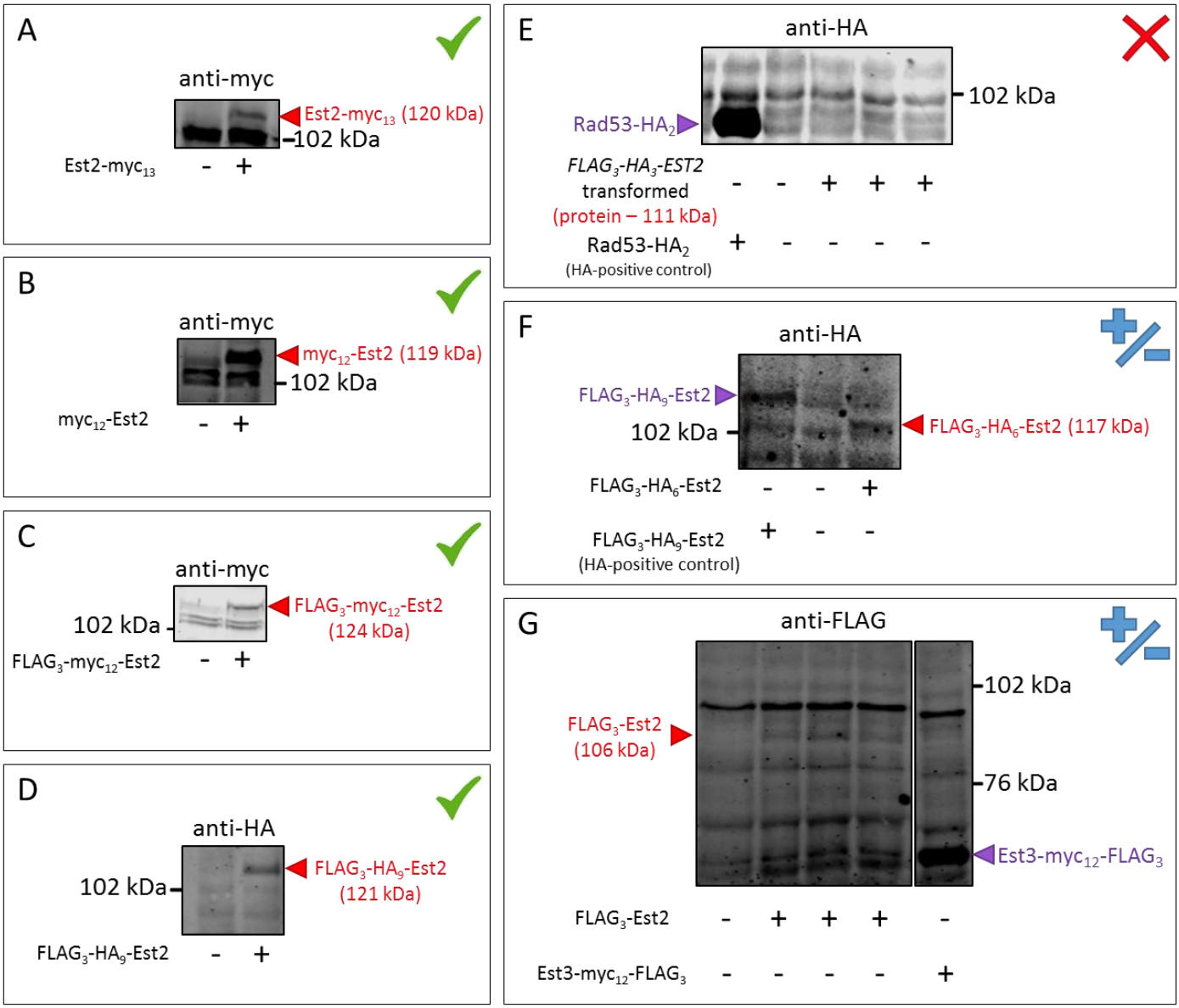

Figure 3.7: Qualitative western blot analysis of Est2 with different epitopes

Red arrowheads point to the bands corresponding to the proteins of interest. Purple arrowheads point to the bands corresponding to proteins serving as positive controls of protein detection by western blotting. Green tick marks denote constructs encoding proteins whose expression results in high signal/background ratio, +/- sign denotes constructs with marginally detectable signal and red “X” sign denotes constructs with signal below detection limit. In cases where the target protein signal is below or at the margin of detection threshold (E-G), three independently isolated clones are shown

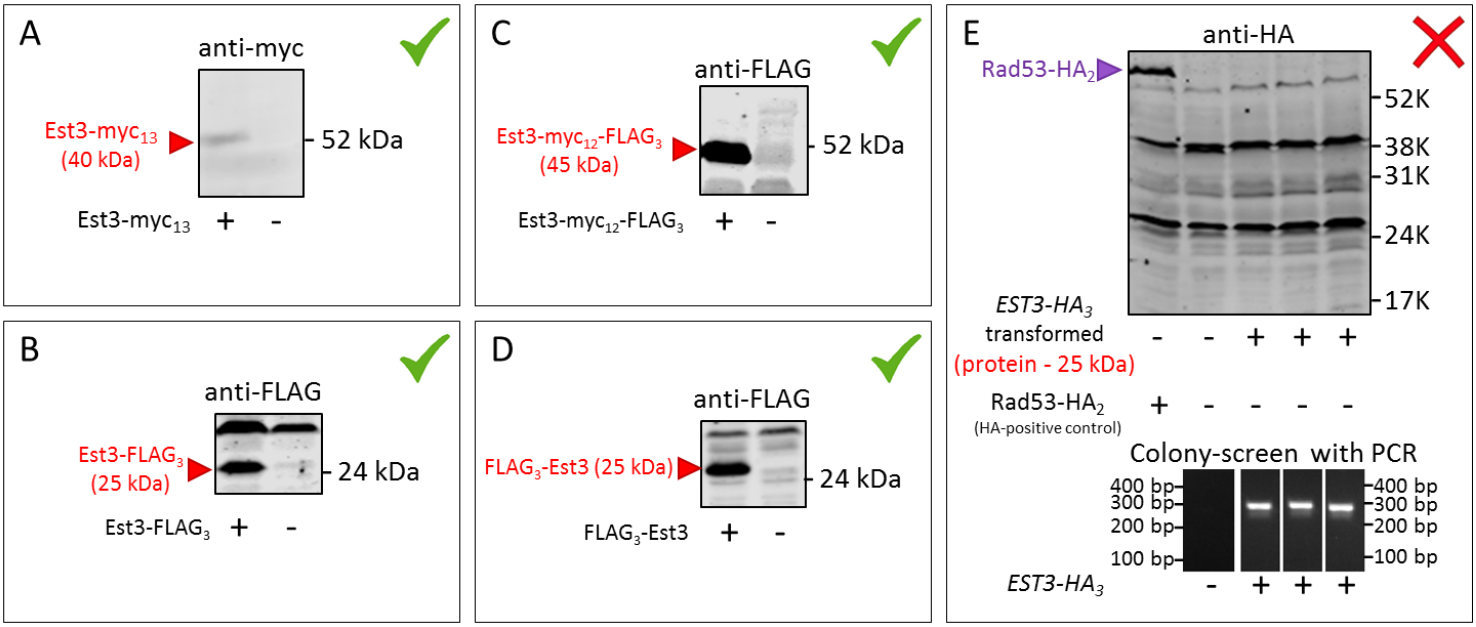

Figure 3.8: Qualitative western blot analysis of Est3 with different epitopes

Red triangles point to the bands corresponding to the proteins of interest. Purple triangles point to the bands corresponding to proteins serving as positive control of western blotting. Green tick marks denote constructs with high signal/background ratio, red "X" sign denotes constructs below detection limit. In case where target protein signal is below detection threshold (E), three separate clones are shown

The constructs that demonstrated high signal/background ratio in the western blotting experiments were selected for further analysis, while the rest of the constructs (namely Est3-HA_3 and $FLAG_3$-HA_3-Gly_6-Est2) were discarded.

3.2.3. Temperature-sensitivity assay of the strains with tagged Est2 and Est3 proteins

It has been reported in Tucey & Lundblad, 2014 that cells with Est3-myc$_{13}$ have somewhat shorter telomeres than the cells with no tag on Est3. Shortened telomeres indicate that the telomerase function in the cells with Est3-myc$_{13}$ is suboptimal, potentially due to the tag interfering with the binding of Est3 to the other telomerase subunits. If Est3-myc$_{13}$ binding to the telomerase complex is significantly less efficient than that of the untagged Est3, then the quantitative output of the co-immunoprecipitation of Est2 with Est3 (or *vice versa*) might not be reflective of the amount of telomerase complex and therefore might fail to detect the difference in the telomerase complex levels between aneuploids and diploids. Thus, I decided to test whether the tagged versions of Est2 and Est3 or their combinations affect telomerase function, to eliminate the tags with the potential to significantly impact telomerase complex assembly. Since the design of the co-immunoprecipitation experiment entails using anti-FLAG affinity resin to pull down one of the two proteins, the strains were constructed in such a way that only one of the two proteins bore FLAG$_3$-epitope in any given strain.

Initially I performed an indirect preliminary assessment of the telomerase function by a temperature-sensitivity assay. This method takes advantage of the fact that the equilibrium length of *S. cerevisiae* telomeres decreases progressively as the growth temperature increases, with cells undergoing senescence after several passages when grown at temperature as high as 38.5°C, but not at 37°C (Millet *et al.*, 2015). Assuming that the tags affect telomerase performance independently of the temperature-related decrease in telomerase function, telomerase-inhibiting tags and growth temperature should have an additive effect on telomerase activity (see Figure 3.9). Consequently, tags that decrease telomerase function should lower the temperature threshold for senescence and thus can be identified by passaging strains carrying such tags at subsenescent temperatures.

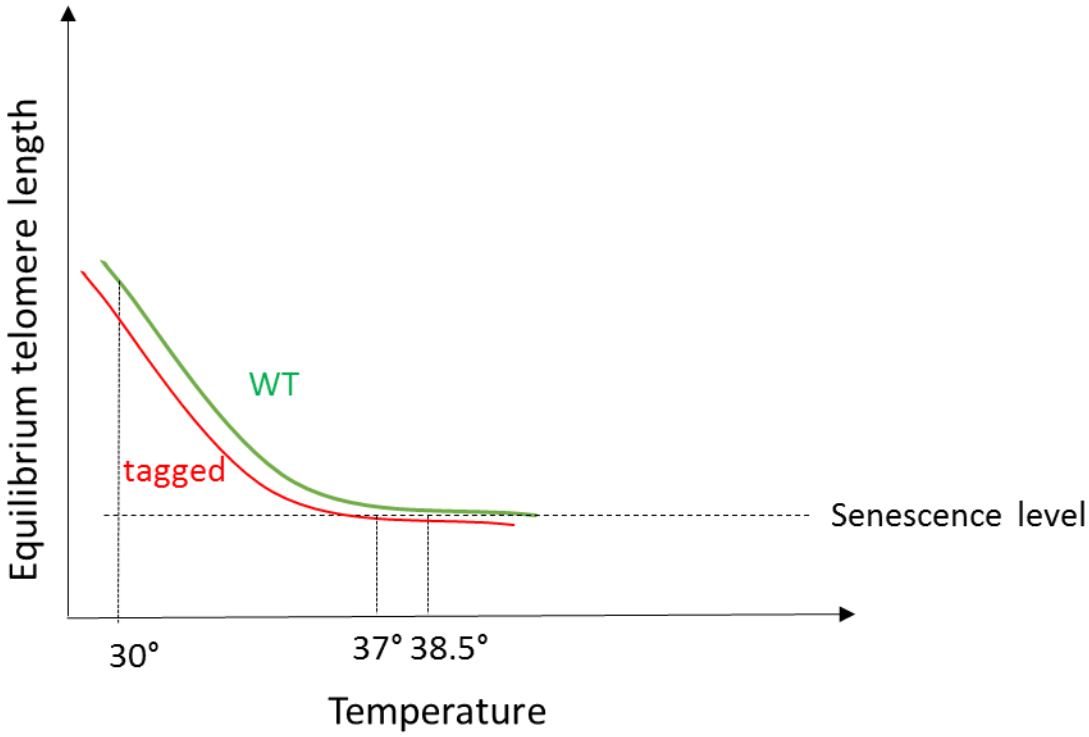

Figure 3.9: Schematic illustrating the hypothetical additive effect of growth temperature and hypomorphic alleles of *EST2* or *EST3* affecting telomerase complex assembly on telomere length equilibrium

Strains with tagged Est2, Est3 or both proteins were continually grown at 37°C for 3 or 4 passages (1 passage every two days) along with the isogenic WT control strain and a temperature-sensitive strain (*yku80Δ*) to reach telomere length equilibrium. As seen in Figures 3.10-3.12, the only three constructs that did not lead to senescence at 37°C either separately or in combination were Est2-myc$_{13}$, myc$_{12}$-Est2 and Est3-FLAG$_3$ (note, that Est3-myc$_{13}$-Gly$_6$-FLAG$_3$ was not tested in this assay, but was tested in a different assay below).

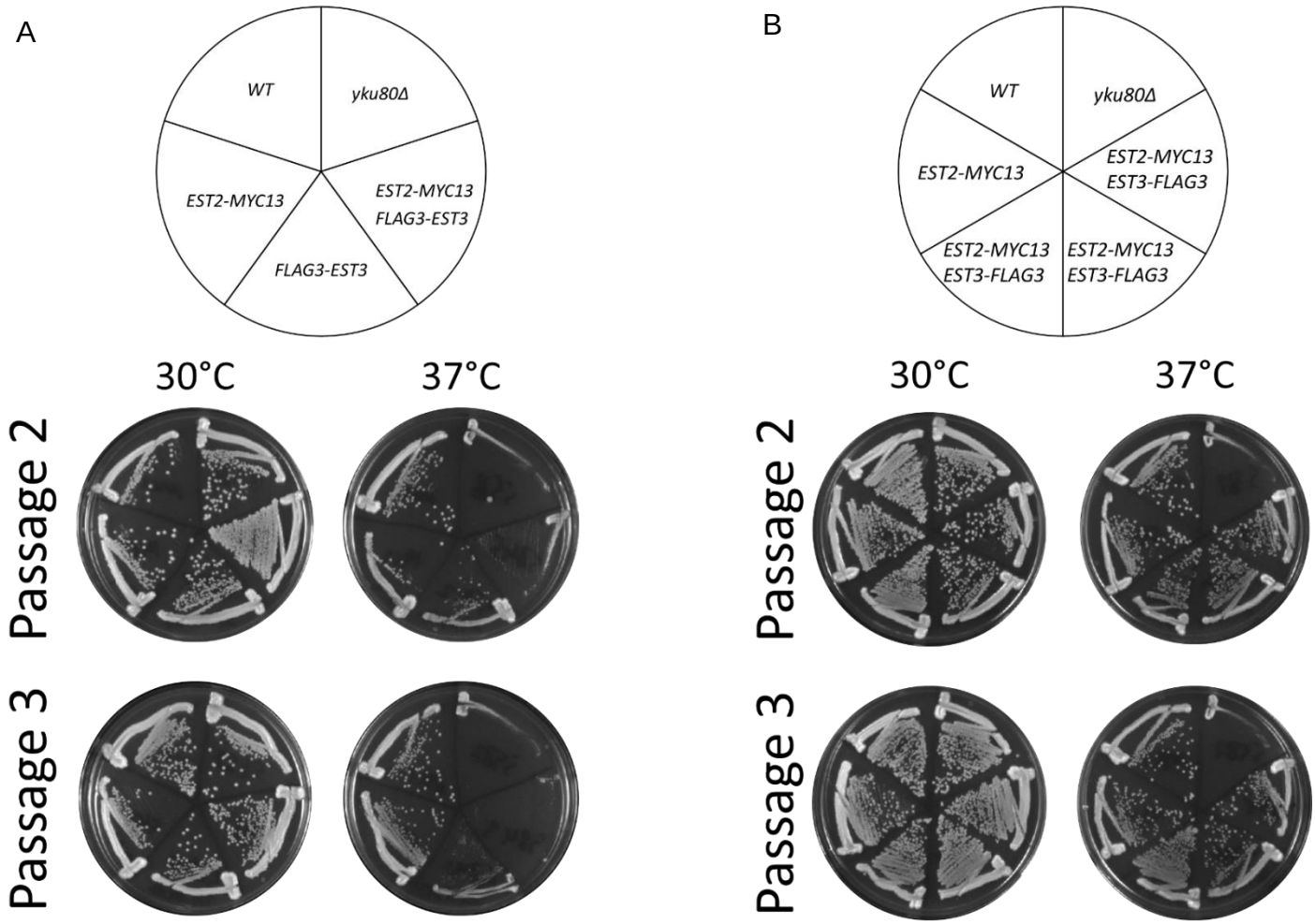

Figure 3.10: Temperature-sensitivity assay of haploid strains with Est2-myc$_{13}$ and/or either FLAG$_3$-Est3 (A) or Est3-FLAG$_3$ (B)

Second and third passages are shown. *FLAG3-EST3* alone causes senescence by the third passage at 37°C and by the second passage when combined with *EST2-MYC13*. *EST2-MYC13* and *EST3-FLAG3* do not cause senescence either separately or in combination by passage 3 at 37°C. *yku80Δ* – strain non-viable at 37°C

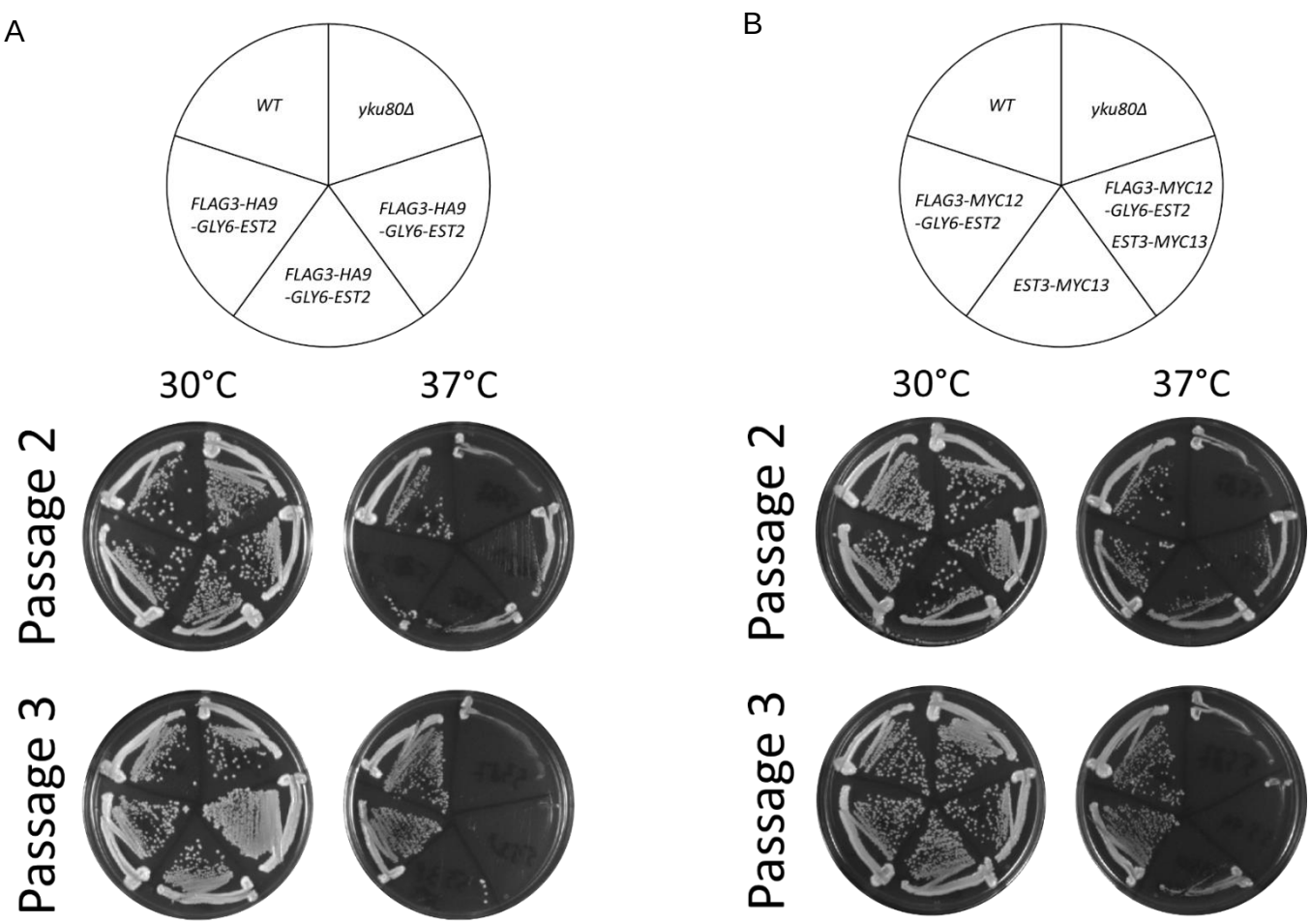

Figure 3.11: Temperature-sensitivity assay of haploid strains with $FLAG_3$-HA_9-Gly_6-Est2 (A), $FLAG_3$-myc_{12}-Gly_6-Est2 (B) or $FLAG_3$-myc_{12}-Gly_6-Est2 combined with Est3-myc_{13} (B)

Second and third passages are shown. *FLAG3-HA9-GLY6-EST2* causes senescence by passage 2 at 37°C, while *EST3-MYC13* alone or in combination with *FLAG3-MYC12-GLY6-EST2* causes senescence by passage 3 at 37°C. Senescence was not observed in *FLAG3-MYC12-GLY6-EST2* by passage 3 at 37°C

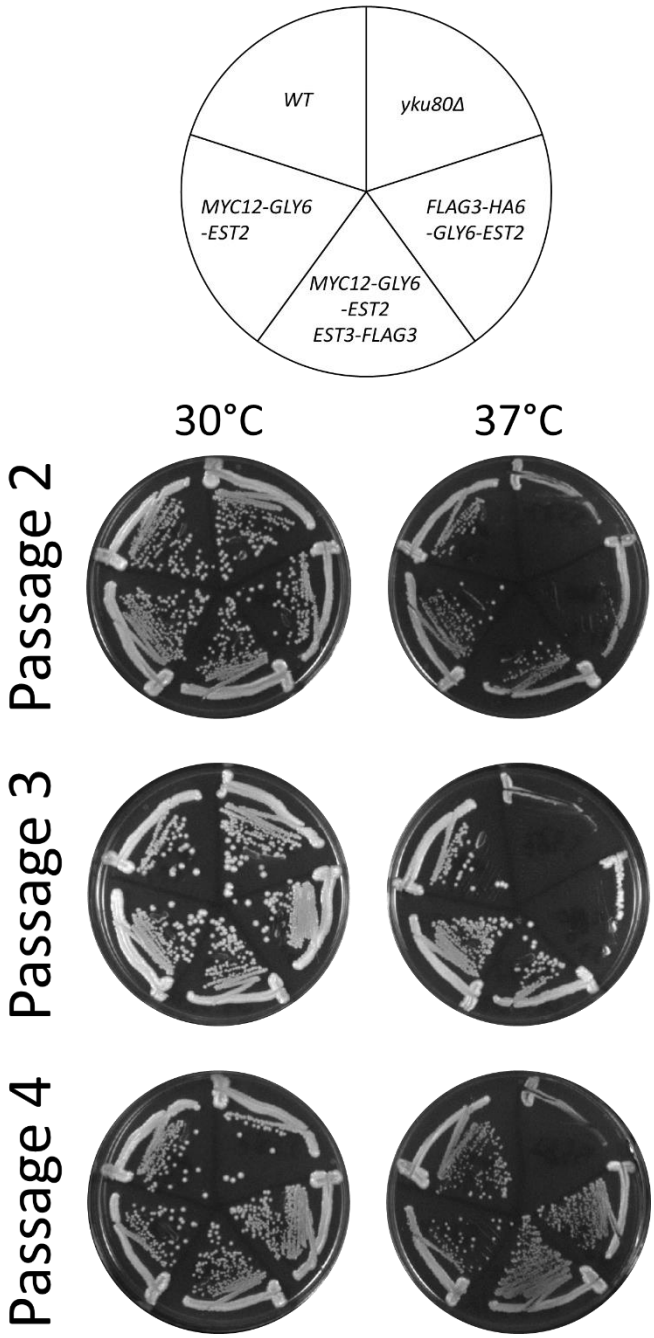

Figure 3.12: Temperature-sensitivity assay of haploid strains with $FLAG_3$-HA_6-Gly_6-Est2, myc_{12}-Gly_6-Est2 or myc_{12}-Gly_6-Est2 combined with Est3-$FLAG_3$

Passages 2-4 shown. *FLAG3-HA6-GLY6-EST2* causes senescence by passage 2 at 37°C, while *MYC12-GLY6-EST2* and *EST3-FLAG3* do not cause senescence either separately or in combination by passage 4 at 37°. Note that *FLAG3-HA6-GLY6-EST2* strain managed to overcome senescence at passage 4, possibly due to gaining suppressor mutations

3.2.4. Southern blot analysis of telomere length in strains with tagged Est2 and Est3 proteins

In order to verify the conclusions of the temperature sensitivity assay, I decided to assess telomere length equilibrium of strains with tagging constructs more directly in a telomere-specific Southern blot. Haploid strains with epitopes on Est2, Est3 or both proteins were passaged 4 times at 30°C (~80 generations), their genomic DNA (gDNA) was extracted, digested with KpnI and resolved in a 0.85% agarose gel. Y'-telomere length was then analysed by Y'-telomere-specific Southern blotting (see Figure 3.13 and section 2.8.8 for details).

As seen in Figure 3.14, among the combinations of tagging constructs that were tested for their impact on telomere length equilibrium at 30°C, Est3-$FLAG_3$ as well as Est2-myc_{13} (Figure 3.14B) or myc_{12}-Gly_6-Est2 (Figure 3.14C) exert the least effect on telomere length, corroborating the results of the temperature sensitivity assay.

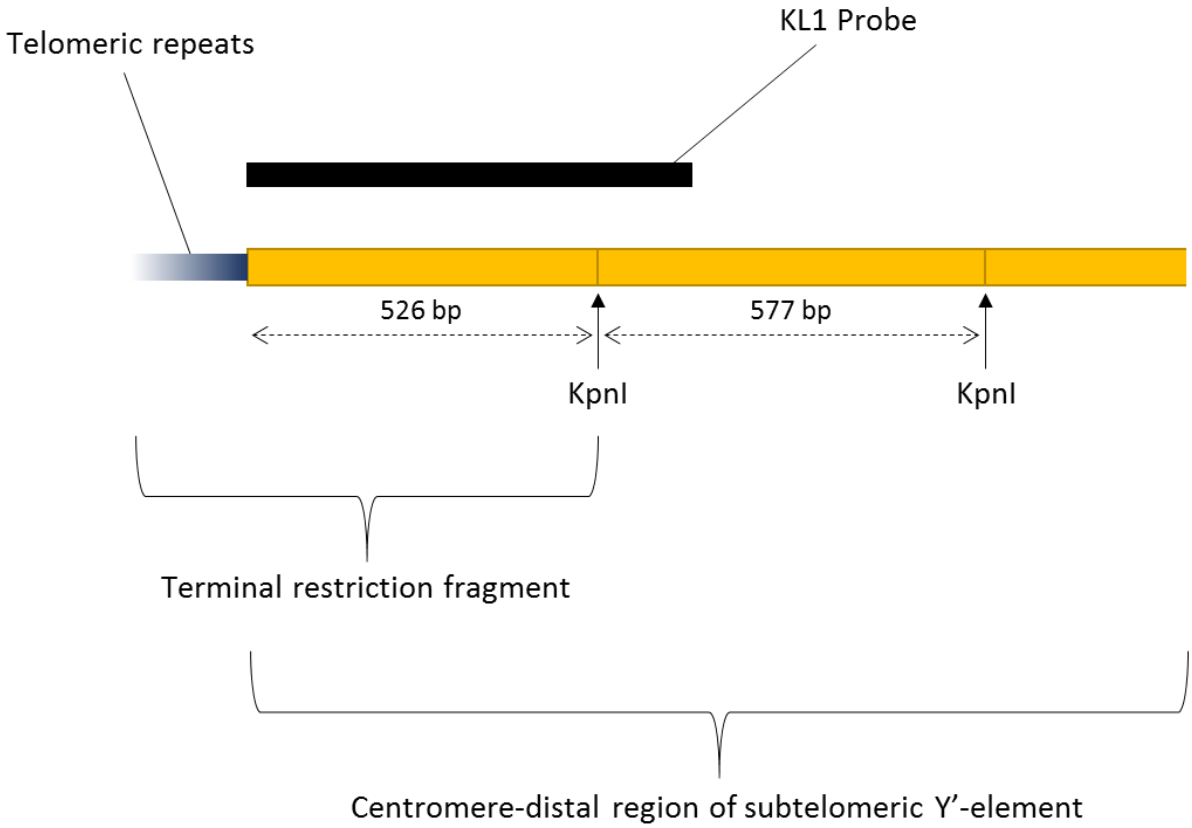

Figure 3.13: Schematic of the terminal region of a subtelomeric Y'-element showing the probe used in the telomere-specific Southern blot

The KL1 probe anneals to terminal restriction fragment (TRF) of the Y'-element that includes 526 bp of Y'-element sequence and a varying length of telomeric repeats (~300-350 bp in WT cells). The stretch of telomeric repeats is therefore 526 bp shorter than the terminal restriction fragment. The probe also anneals to the 577 bp-long fragment adjacent to the TRF

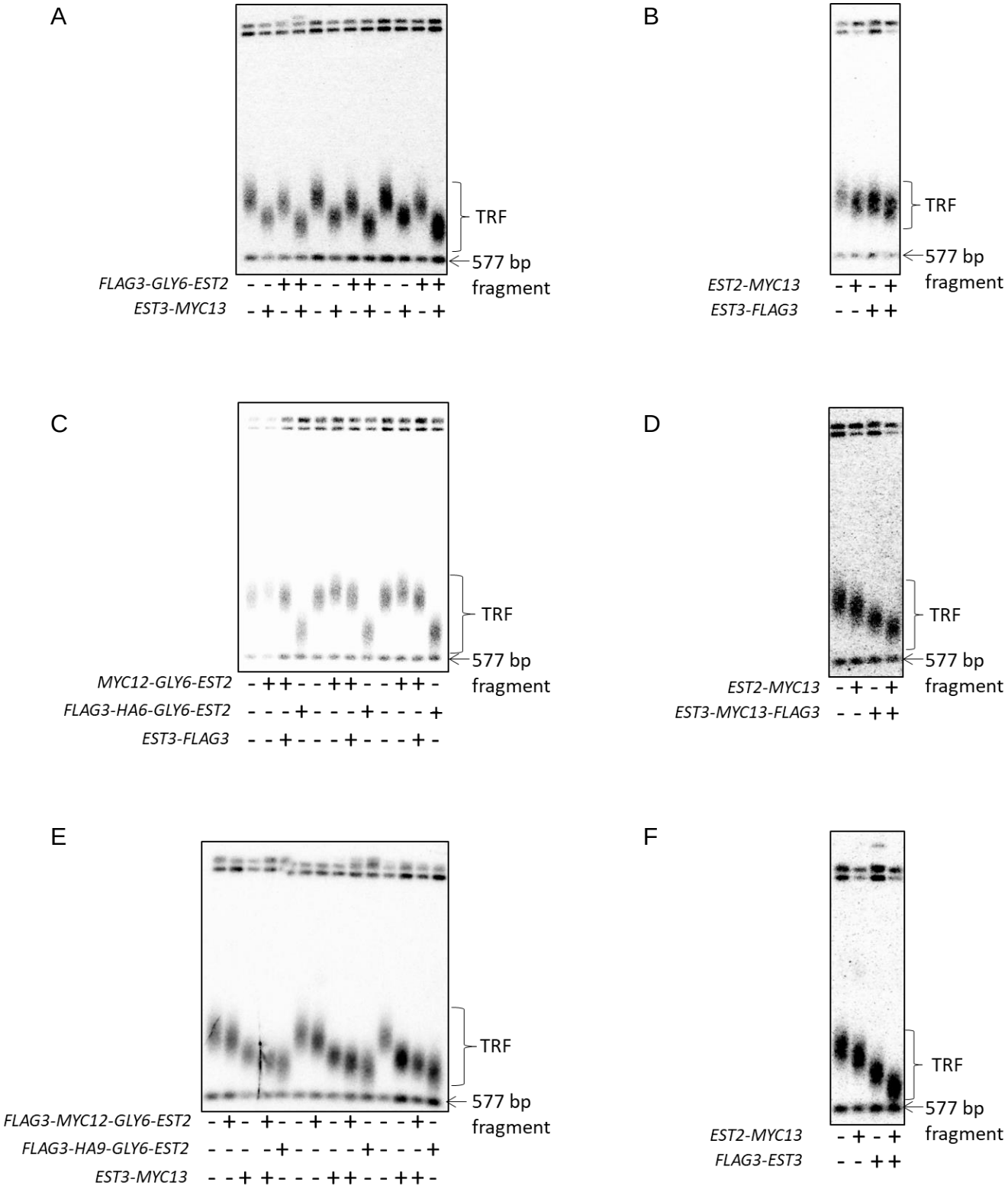

Figure 3.14: Southern blots showing Y' telomere length equilibrated at 30°C compared between WT cells and cells carrying tagging constructs on Est2 and/or Est3

TRF – terminal restriction fragment

3.2.5. Pilot co-immunoprecipitation of Est2-myc$_{13}$ with Est3-FLAG$_3$ from haploid cells grown at 30°C or at 38.5°C

The tagging constructs Est2-myc$_{13}$ and Est3-FLAG$_3$ were selected based on their low impact on telomerase function for a test co-immunoprecipitation of Est2-myc$_{13}$ with Est3-FLAG$_3$ from haploid cells, before the construction of the corresponding aneuploid and diploid strains. For the first pilot co-immunoprecipitation experiment, cells were grown at 30°C since the level of Est2-myc$_{13}$ is higher in the cells grown at this temperature, than at 38.5°C (Millet *et al.*, 2015), and therefore the protein is easier to detect. Once the cells were harvested from liquid cultures, washed and resuspended in lysis buffer, they were lysed by bead-beating to obtain total lysate. Total lysate was cleared by two subsequent centrifugation steps pelleting cellular debris (pellet 1) and chromatin (pellet 2) to obtain cleared lysate, from which Est3-FLAG$_3$ was pulled down using anti-FLAG affinity resin (see section 2.7.5 and Figure 3.15 for details). In this experiment the elution of Est3-FLAG$_3$ from the resin was performed by competitive displacement with an excess of 3X FLAG peptide.

I managed to successfully co-immunoprecipitate Est2-myc$_{13}$ with Est3-FLAG$_3$ from cells grown at 30°C (Figure 3.16C), however, ~28% of Est2-myc$_{13}$ remained bound to the resin after the elution (Figure 3.16C, lane 12), indicating that Est3-FLAG$_3$ was not completely displaced from the resin by competitive elution with the FLAG3 peptide. More than half of Est3-FLAG$_3$ was pulled-down from the cleared lysate, as evident from the comparison between the cleared lysate and the flow-through (Figure 3.16B, lanes 8 and 10; note, that the antibody light chain band obscures the Est3-FLAG$_3$ band in lane 12), while only about 5% of Est2-myc$_{13}$ was depleted from the cleared lysate (Figure 3.16A, lanes 8, 10 and 12), suggesting that only a small fraction of Est2-myc$_{13}$ was associated with Est3-FLAG$_3$. Approximately 16% of Est2-myc$_{13}$ was retained in the chromatin-containing pellet 2 (Figure 3.16A, lane 6), consistent with the previously published data, indicating that Est2 can bind to chromatin

independently of Est1 in G1 phase of the cell cycle (Chan, Boulé and Zakian, 2008).

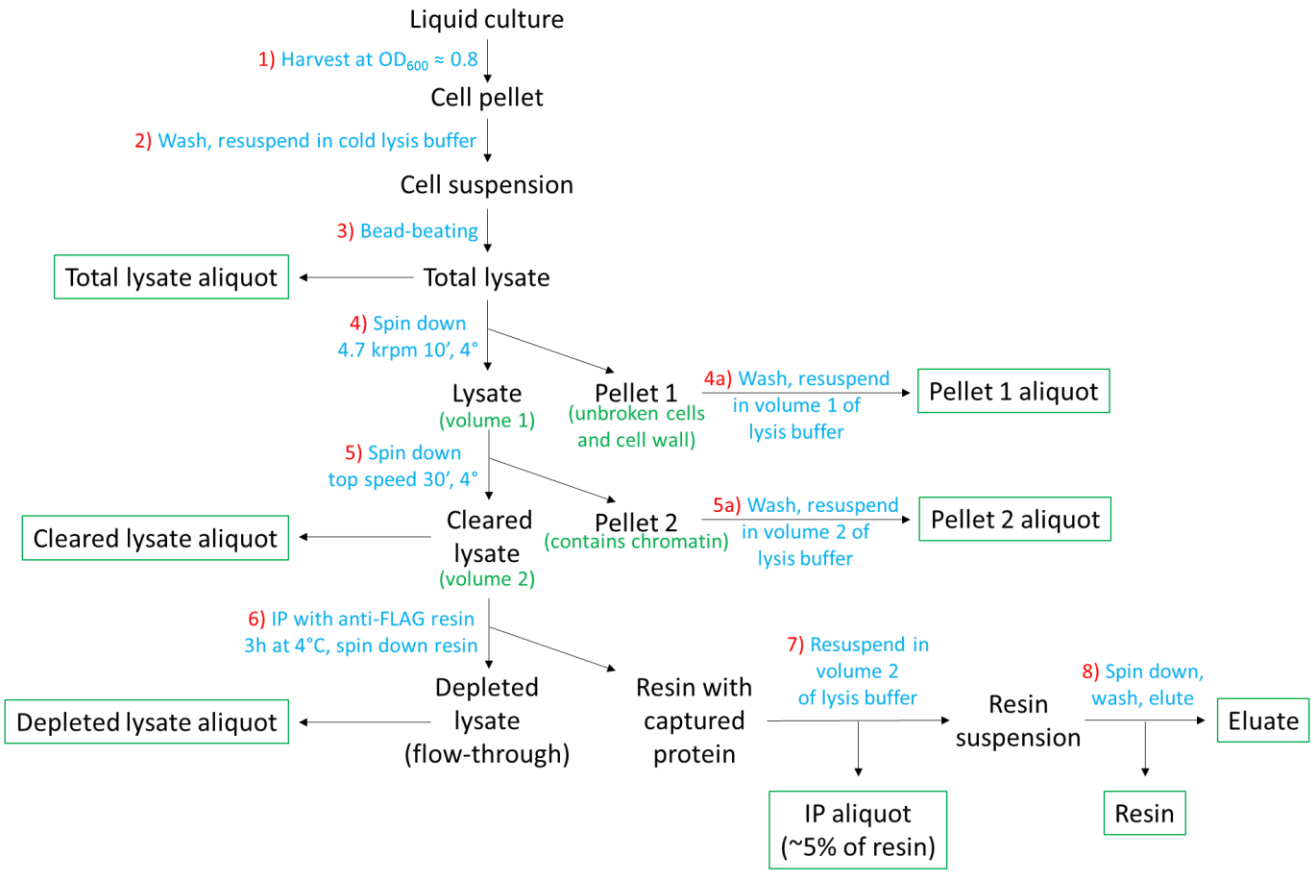

Figure 3.15: Outline of the protocol for co-immunoprecipitation of Est2 and Est3

The Protocol steps are in red and light blue, descriptive notes are in green, sample aliquots are in green boxes. To allow direct comparison of the amount of target proteins in the pellet and supernatant fractions, the pellets and resin were resuspended in the volumes of lysis buffer matching the volumes of the supernatants (see steps 4a, 5a and 7) and the respective sample aliquots were taken. The elution of the bound protein from the anti-FLAG resin was performed either by competitive displacement with 3XFLAG peptide or by incubating in 1% SDS at 65°C

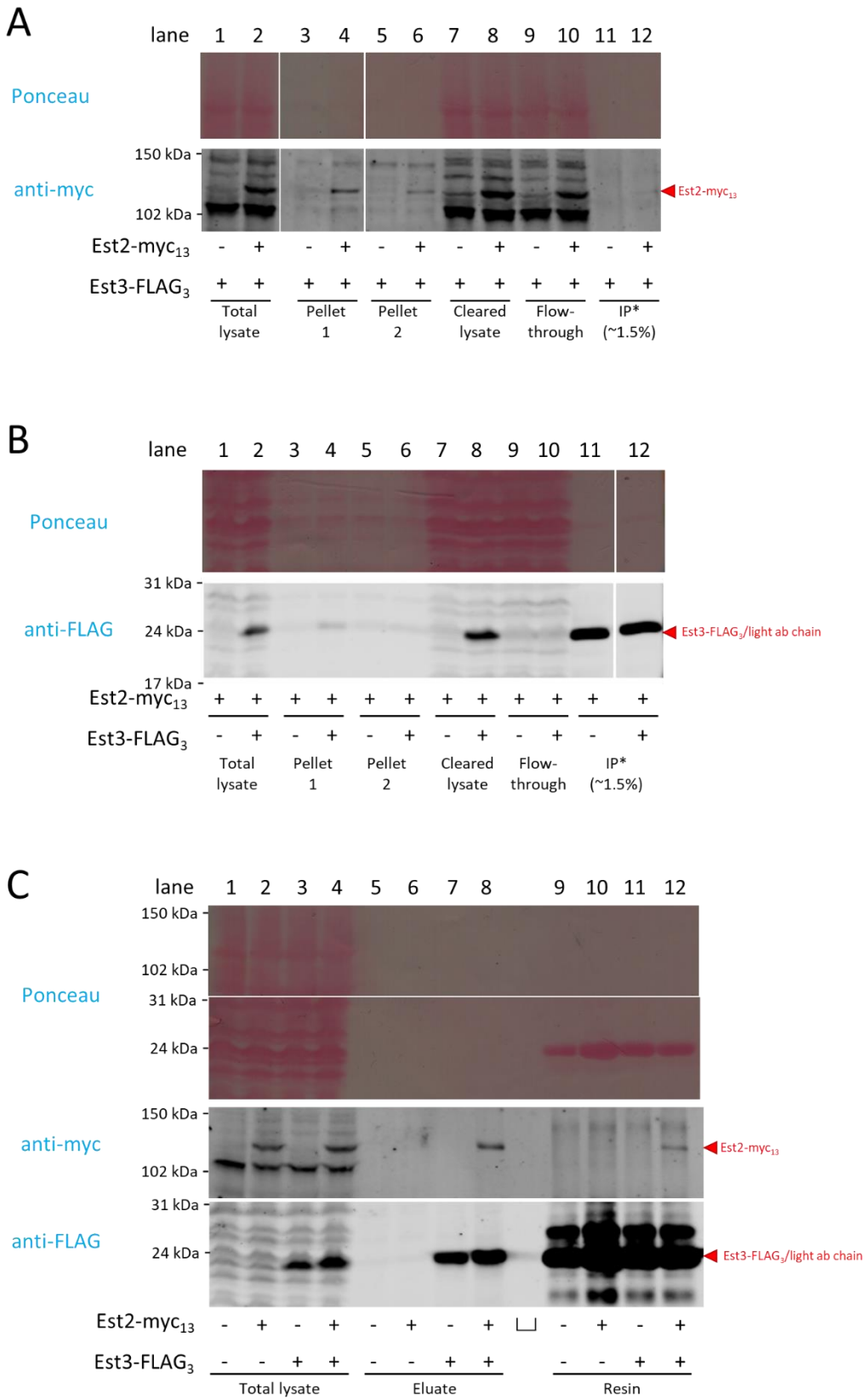

Figure 3.16: Pilot co-immunoprecipitation of Est2-myc$_{13}$ with Est3-FLAG$_3$ from haploid cells grown at 30°C

A – Est2-myc$_{13}$ in various fractions throughout the CoIP procedure, B – the same for Est3-FLAG$_3$, C – co-immunoprecipitation of Est2-myc$_{13}$ with Est3-FLAG$_3$. ␣ - empty lane. *IP samples represent a fraction of resin (~1.5%) taken before the elution (see Figure 3.15) and thus contain beads with the antibodies used for the pull down

I next set out to attempt a pilot co-immunoprecipitation from haploid cells grown at 38.5°C, since aneuploidy-dependent suppression of telomerase insufficiency had been discovered at this temperature. This time the elution was performed by incubating the resin in 1% SDS at 65°C for 10 minutes to maximize the release of the target proteins from the resin. As a result, I managed to co-immunoprecipitate Est2-myc$_{13}$ with Est3-FLAG$_3$ from cells grown at 38.5°C, albeit the with a lower yield of Est2, than at 30°C (Figure 3.17).

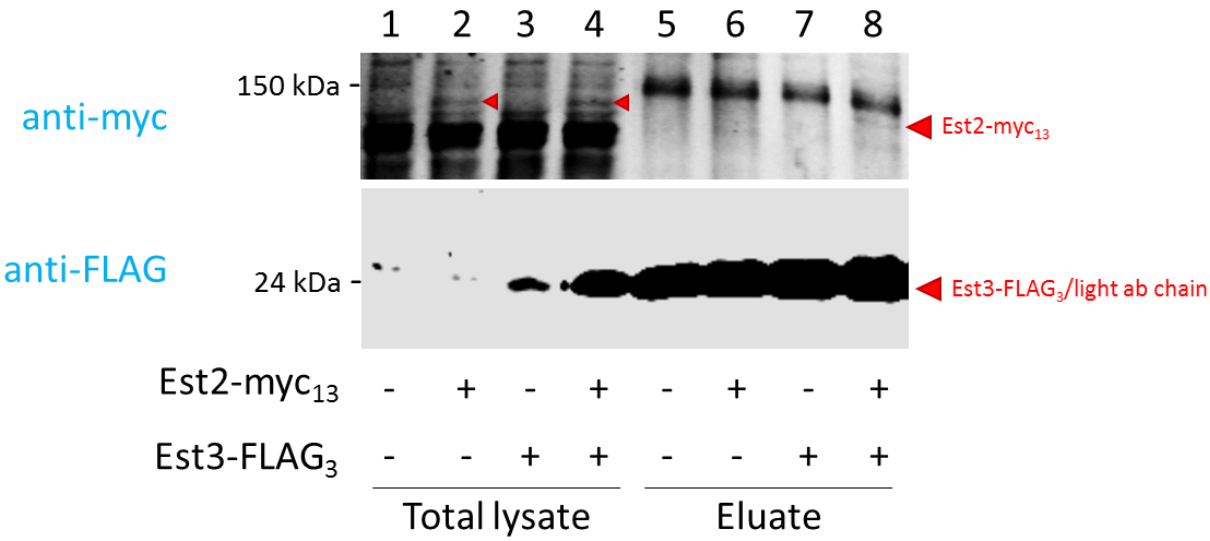

Figure 3.17: Pilot co-immunoprecipitation of Est2-myc$_{13}$ with Est3-FLAG$_3$ from haploid cells grown at 38.5°C

Small red arrowheads indicate Est2-myc$_{13}$ in the total lysate. Note, that because the elution was performed by treating the resin with 1% SDS at 65°C, the antibodies became released from the resin, resulting in a 50 kDa band (heavy chain, not shown) and a 25 kDa band (light chain) on the western blot. The 25 kDa band overlaps with Est3-FLAG$_3$ protein band, thus obscuring it in the eluate fraction

3.3. Optimization of the protocol for CoIP of Est2-myc$_{13}$ with Est3-FLAG$_3$

3.3.1. Testing benzonase treatment of lysate as means of the Est2-myc$_{13}$ release from chromatin-containing pellets

In the previous experiments, I have observed that some of Est2-myc$_{13}$ is associated with the chromatin-containing pellet 2 (see Figure 3.16A). There exists a chance that some of Est2-myc$_{13}$ found in the pellet 2 may be part of the telomere-bound telomerase complexes, which therefore would not be captured by the affinity resin, potentially resulting in a skewed output in the co-immunoprecipitation experiments. To determine whether Est2-myc$_{13}$ is associated with chromatin in pellet 2, I undertook an attempt to release Est2-myc$_{13}$ from the pellet 2 by treating the lysate with a chromatin-degrading enzyme Benzonase just prior to separating the pellet 2 from the cleared lysate (between steps 4 and 5 in Figure 3.15). Since Benzonase is inhibited by high Na^+ and K^+ concentrations (Figure 3.18), half of the cells were lysed in the lysis buffer with lower (100 mM) than previously used NaCl concentration, while the other half were lysed in the original buffer (300 mM NaCl).

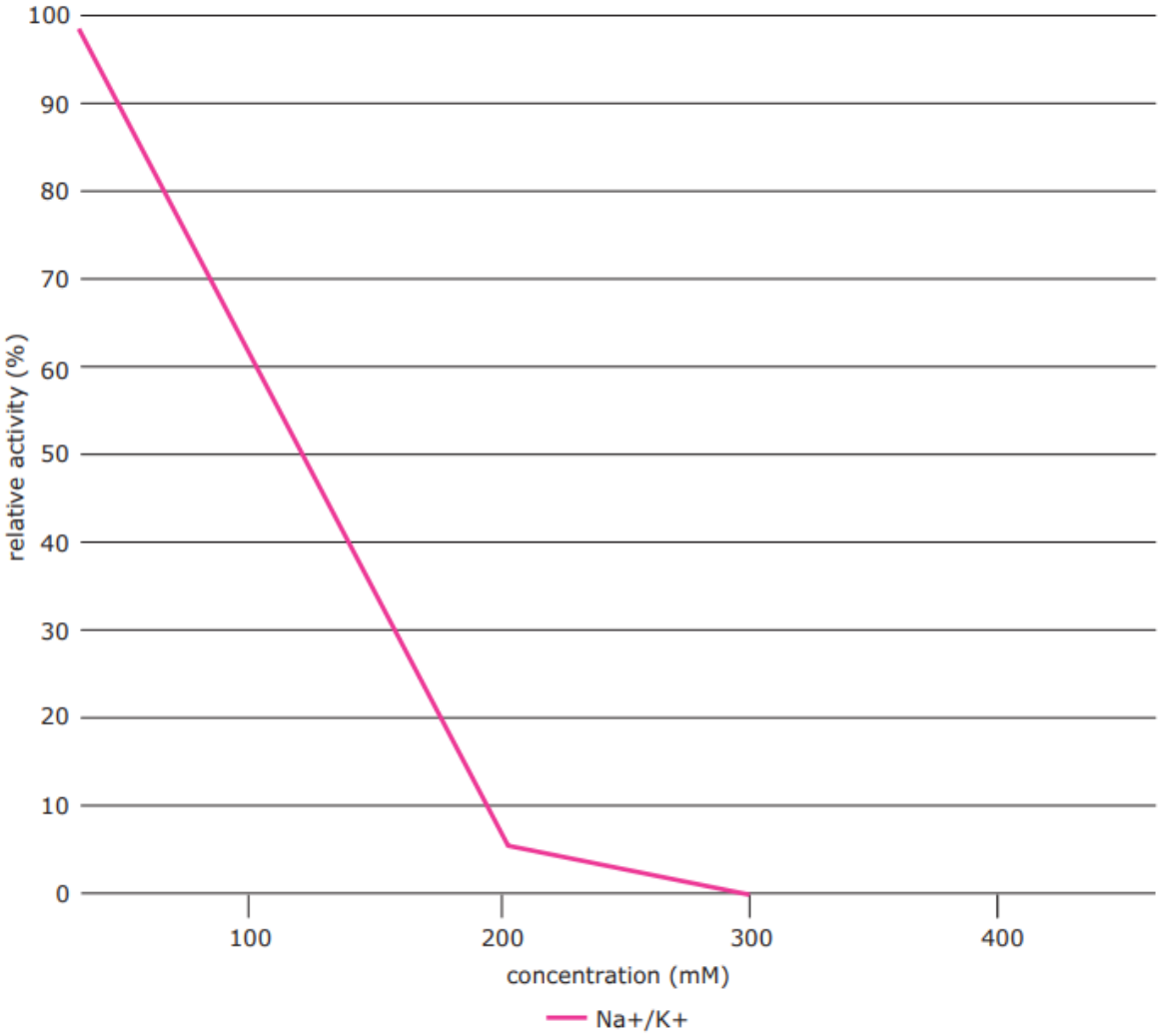

Figure 3.18: The effect of monovalent cations on Benzonase endonuclease activity

From http://www.merckmillipore.com/Web-DE-Site/de_DE/-/EUR/ShowDocument-Pronet?id=200411.164

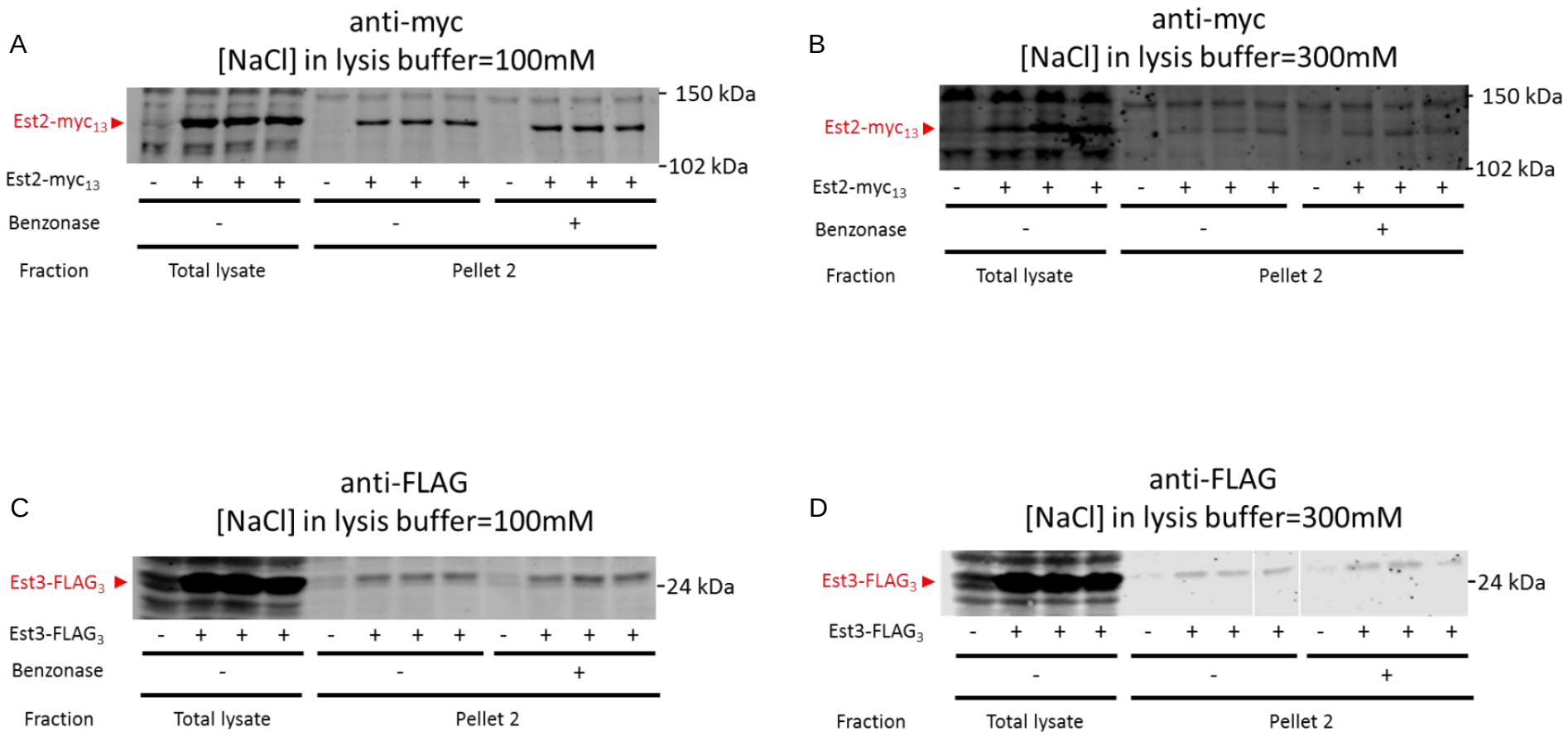

Figure 3.19: (beginning) The effect of Benzonase treatment on the proportion of Est2-myc$_{13}$ and Est3-FLAG$_3$ associated with pellet 2

A – anti-myc western blot of samples with 100 mM NaCl, B – anti-myc western blot of samples with 300 mM NaCl, C – anti-FLAG western blot of samples with 100 mM NaCl, D – anti-FLAG western blot of samples with 300 mM NaCl. Three biological repeats were analysed in each experiment

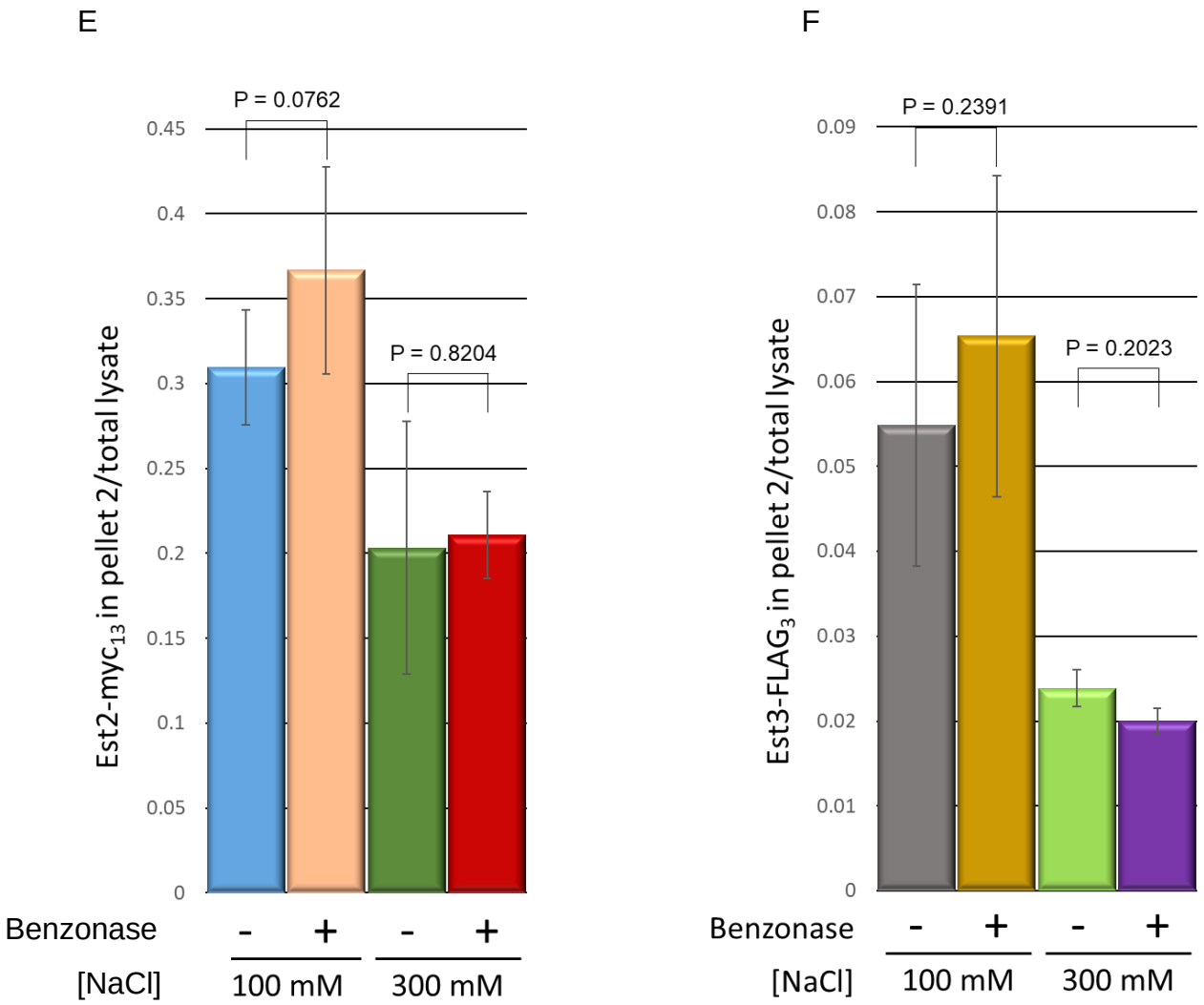

Figure 3.19: (continuation) The effect of Benzonase treatment on the proportion of Est2-myc$_{13}$ and Est3-FLAG$_3$ associated with pellet 2

E – mean Est2-myc$_{13}$ content in pellet 2 relative to total lysate in blots in A and B, F – mean Est3-FLAG$_3$ content in pellet 2 relative to total lysate in blots C and D. P value was calculated using paired T-test. Error bars correspond to standard deviation of the mean in three biological repeats

Once the cells were lysed and the cellular debris was removed from the lysate by centrifugation, half of the lysate was treated with benzonase and then the pellet 2 was collected from both the Benzonase-treated and untreated samples in the second round of centrifugation. The western blot analysis of the pellet 2 and total lysate samples performed in three parallel repeats demonstrated that Benzonase treatment does not significantly affect the fraction of either Est2-myc$_{13}$ or Est3-FLAG$_3$ proteins associated with the pellet 2, regardless of the NaCl concentration in the lysis buffer (Figure 3.19). Of note, the increase in the salt concentration in the lysis buffer correlated with a decrease in the Est2-myc$_{13}$ and Est3-FLAG$_3$ levels in the pellet 2. To assay chromatin degradation in the Benzonase-treated samples, (gDNA) was extracted from the pellet 2 samples and analysed by agarose gel electrophoresis (Figure 3.20). Degradation of gDNA was apparent in the Benzonase-treated samples at both NaCl concentrations, however it was more pronounced, when the lysis buffer with 100 mM NaCl was used. This is consistent with the inhibition of Benzonase activity by high concentrations of monovalent cations (see Figure 3.18).

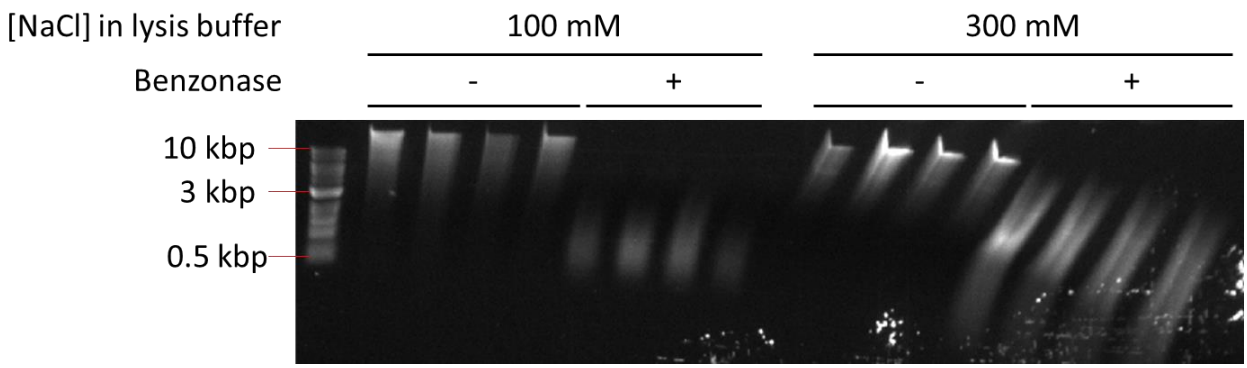

Figure 3.20: Agarose gel electrophoresis of gDNA extracted from the pellet 2 samples with and without the Benzonase treatment

The skew of the gDNA smears towards the left side of the gel is due to a defect in the wire of the gel-running apparatus. For each set of conditions 4 technical repeats were analysed

Telomeric heterochromatin may be less susceptible to the Benzonase treatment than the bulk of gDNA, thus preventing the release of the telomere-associated telomerase complexes. If that were the case, then the fraction of the telomeric sequences in gDNA would be increased in the samples treated with Benzonase. To test this hypothesis, the ratio of telomeric DNA to non-telomeric DNA was compared between Benzonase-treated and untreated pellet 2 samples in a dot-blot experiment. Telomere-specific probe signal was normalized to *URA3* probe signal.

A

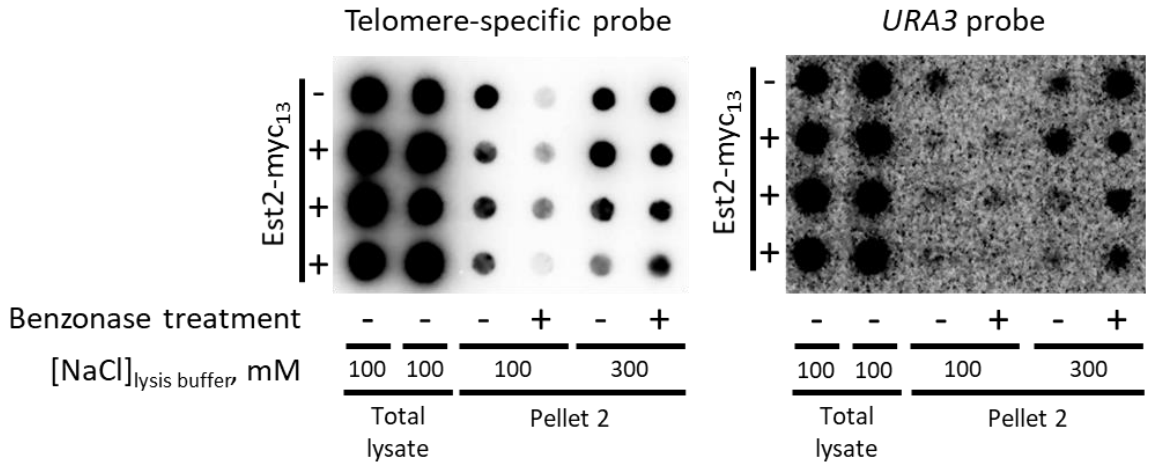

Figure 3.21: (beginning) Comparison of telomeric DNA content relative to *URA3* in benzonase-treated and untreated samples

A – a dot blot of yeast genomic DNA extracted from total lysate or pellet 2 hybridized to a telomere-specific probe (left) and a *URA3*-specific probe (right)

B

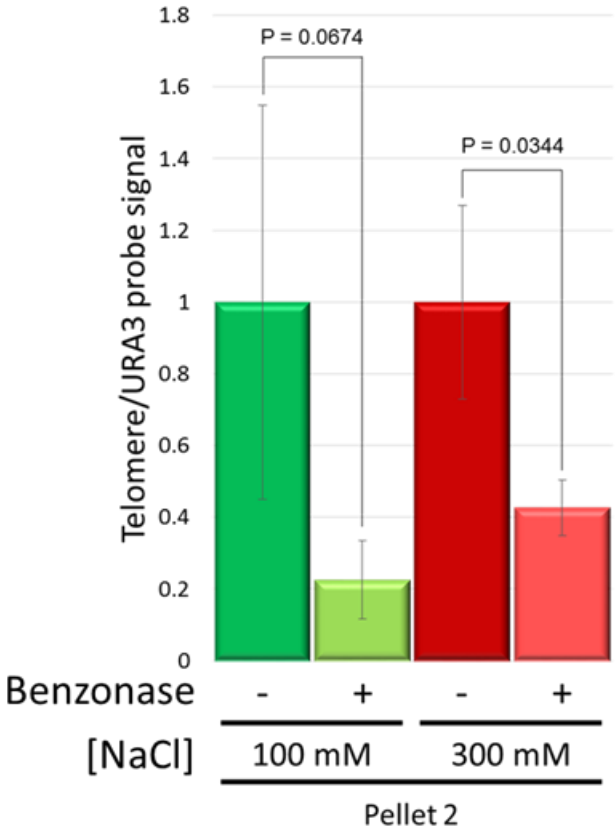

Figure 3.21: (continuation) Comparison of telomeric DNA content relative to *URA3* in benzonase-treated and untreated samples

B – mean ratio of the telomeric signal to the *URA3* signal for the dot blot images above. The telomere/*URA3* probe signal ratios were normalized to Benzonase-untreated samples for each NaCl concentration. P values were calculated using paired T-test. Error bars correspond to standard deviation of mean of four repeats

Dot blot analysis demonstrated that there had been no increase in telomeric DNA relative to *URA3* DNA in the Benzonase-treated pellet 2 samples (Figure 3.21). Combined with the agarose gel analysis of Benzonase-dependent degradation of bulk gDNA (see Figure 3.20) these results suggest that telomeric DNA was degraded by Benzonase more efficiently than the bulk of gDNA. Therefore, Est2-myc$_{13}$ associated with pellet 2 was not was not kept insoluble by association with telomeres.

3.3.2. Testing the effect of different NaCl concentrations on the distribution of Est2-myc$_{13}$ between chromatin-containing pellet and cleared lysate

The data obtained in the Benzonase-treatment experiment using two different NaCl concentrations for the lysis buffer suggest that Est2-myc$_{13}$ was increasingly released from pellet 2 with the higher salt concentration. To test whether a significant amount of Est2-myc$_{13}$ can be recovered from pellet 2 by further increase in NaCl concentration in the lysis buffer, I performed a western blot analysis of distribution of Est2-myc$_{13}$ between pellet 2 and cleared lysate at a range of NaCl concentrations in the lysis buffer. To that end, the cells were ruptured in lysis buffer containing 100 mM NaCl, cellular debris (pellet 1) was removed by centrifugation and the resulting lysate was split into several aliquots in which a range of desired NaCl concentrations was set by adding 0.25 volume of either isotonic or more concentrated NaCl solution. After an additional round of centrifugation, pellet 2 was separated from cleared lysate and the distribution of Est2-myc$_{13}$ between the two fractions was assayed in a western blot (Figure 3.22). Despite a steady decrease in the fraction of Est2-myc$_{13}$ remaining in pellet 2 with the increasing NaCl concentration in the samples, the extent of Est2-myc$_{13}$ release from pellet 2 was only marginally higher at 700 mM NaCl compared to 300 mM used in previous publications (Tucey and Lundblad, 2014). The steepest increase in the amount of Est2-myc$_{13}$ released into the cleared lysate was observed between the NaCl concentrations of 100 mM and 300 mM. Taking into account the potentially disruptive effect of increased NaCl concentration on telomerase complex stability, as well as negligible gain in the amount of Est2-myc$_{13}$ released into cleared lysate at such concentrations, it was deemed impractical to use NaCl concentrations higher than 300 mM for telomerase co-immunoprecipitation.

A

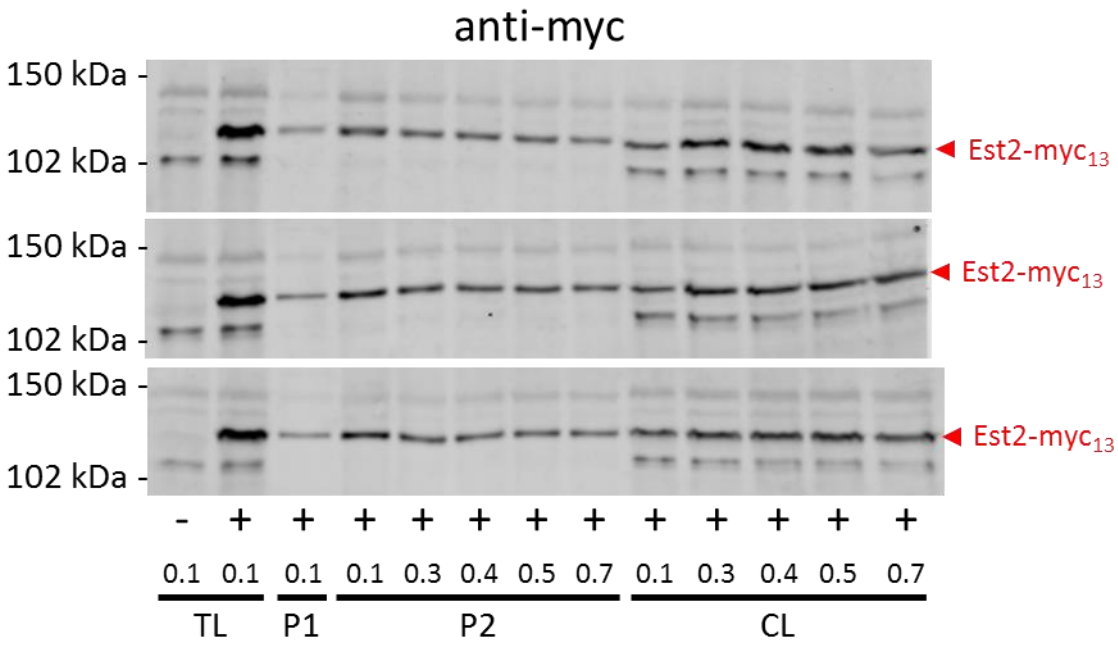

B

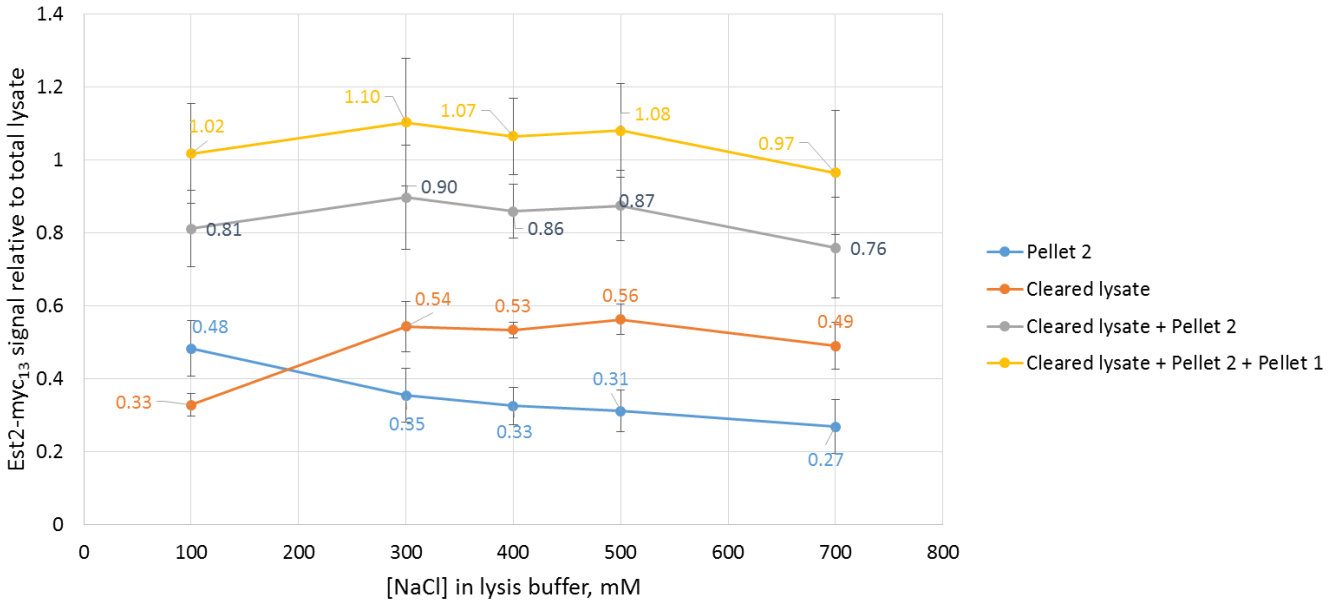

Figure 3.22: The effect of NaCl concentrations in lysis buffer on the distribution of Est2-myc$_{13}$ between pellet 2 and cleared lysate

A – western blots showing three biological repeats of the experiment, B – mean distribution of Est2-myc$_{13}$ among different fractions relative to total lysate. TL – total lysate, CL – cleared lysate, P1 – pellet 1 (cellular debris and unbroken cells), P2 – pellet 2 (contains chromatin). Error bars in B correspond to the standard deviation of mean

3.4. Factors affecting telomerase steady-state level in different species of yeast

3.4.1. Est2 steady state level is not dependent on Ku protein in *S. cerevisiae*

It has been previously noted that, when TLC1 is absent or unable to bind to Est2 (as in *tlc1-59* mutants), the steady-state level of the Est2 subunit decreases approximately two-fold (Taggart, Teng and Zakian, 2002; Lin and Blackburn, 2004; Tucey and Lundblad, 2014). A similar decrease was also observed in yeast grown at 38.5°C (Millet *et al.*, 2015), which prompted a speculation that the effect of the elevated temperature on Est2 steady-state level might be mediated by TLC1: TLC1 secondary structure might be disrupted at 38.5°C thereby mimicking the effect of the *tlc1-59* mutation on the TLC1-Est2 association and hence on the Est2 steady-state level.

Some preliminary data indicated that Est2 was destabilized in *tlc1Δ* mutants compared to wild type cells and that this destabilization was partially rescued by proteasome inhibition (Figure 3.23). Consequently, it has been hypothesised that the impact of *TLC1* deletion on the Est2 protein level is at least partially due to proteasome-dependent degradation. If melting of the TLC1 secondary structure is the actual reason for the decreased abundance of Est2 protein at high temperature, this effect might be to some extent mediated by the proteasome as well. Potentially, there could be at least two ways in which Est2 not bound to TLC1 is recognised and marked for subsequent degradation. In the first scenario, free Est2 subunit might be recognised *per se*. Alternatively, the Est2 degradation in the absence of TLC1 could be a secondary effect of the Est2 disrupted nuclear localization. TLC1 nuclear transport depends on binding to the Ku complex (Gallardo *et al.*, 2008) and it is possible that Est2 is translocated into the nucleus in a complex with TLC1 via a Ku-dependent mechanism. In this case, Est2 localized in the cytoplasm could be targeted for degradation. The two explanations are not mutually exclusive.

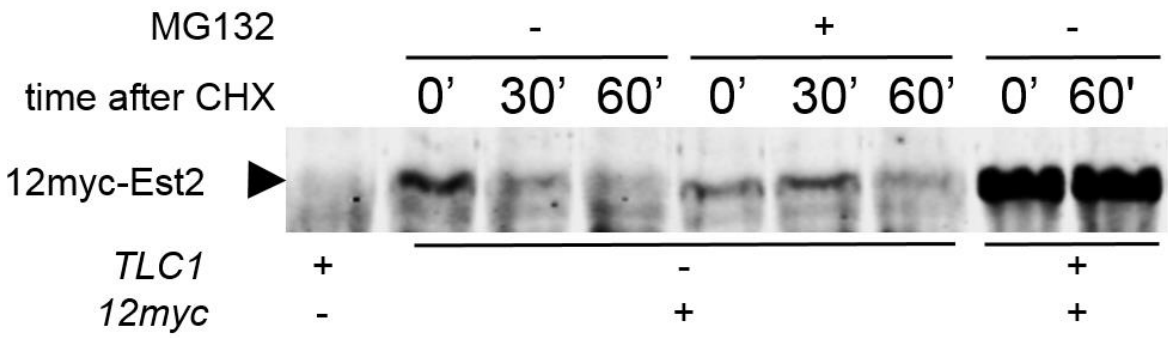

Figure 3.23: Telomerase catalytic subunit not bound to telomerase RNA TLC1 is degraded by proteasome

Analysis of Est2 stability by western blotting. Cells with myc-tagged Est2 subunit were grown to mid-log phase and proteasome inhibitor MG132 was added at 75 μM 30’ before protein synthesis was blocked with 100 μg/ml cycloheximide (CHX). Cell aliquots were collected at the time-points indicated above the gel. Equal amount of protein extract was loaded in each lane. Notice much lower steady state level of Est2 in the absence of *TLC1* (compare 0’ time-points)

If Est2 degradation in the absence of TLC1 was at least partially dependent on its cytoplasmic retention because of the abolished Ku-mediated transport, then I should have been able to observe some decrease in the Est2 steady-state level in *yku70/80Δ* and *tlc1Δ48* mutants in which TLC1 cannot bind to the Ku complex. I constructed the strains with a myc-tag fused to the Est2 protein combined with either *ykuΔ80* or *tlc1Δ48* mutation and compared the steady-state levels of Est2 in these strains to the corresponding WT strains (Figure 3.24). No statistically significant difference was observed in these comparisons, suggesting that either Est2 nuclear import does not depend on Yku80 or that the defect in Yku80-dependent nuclear import of Est2 does not significantly alter the Est2 steady-state levels.

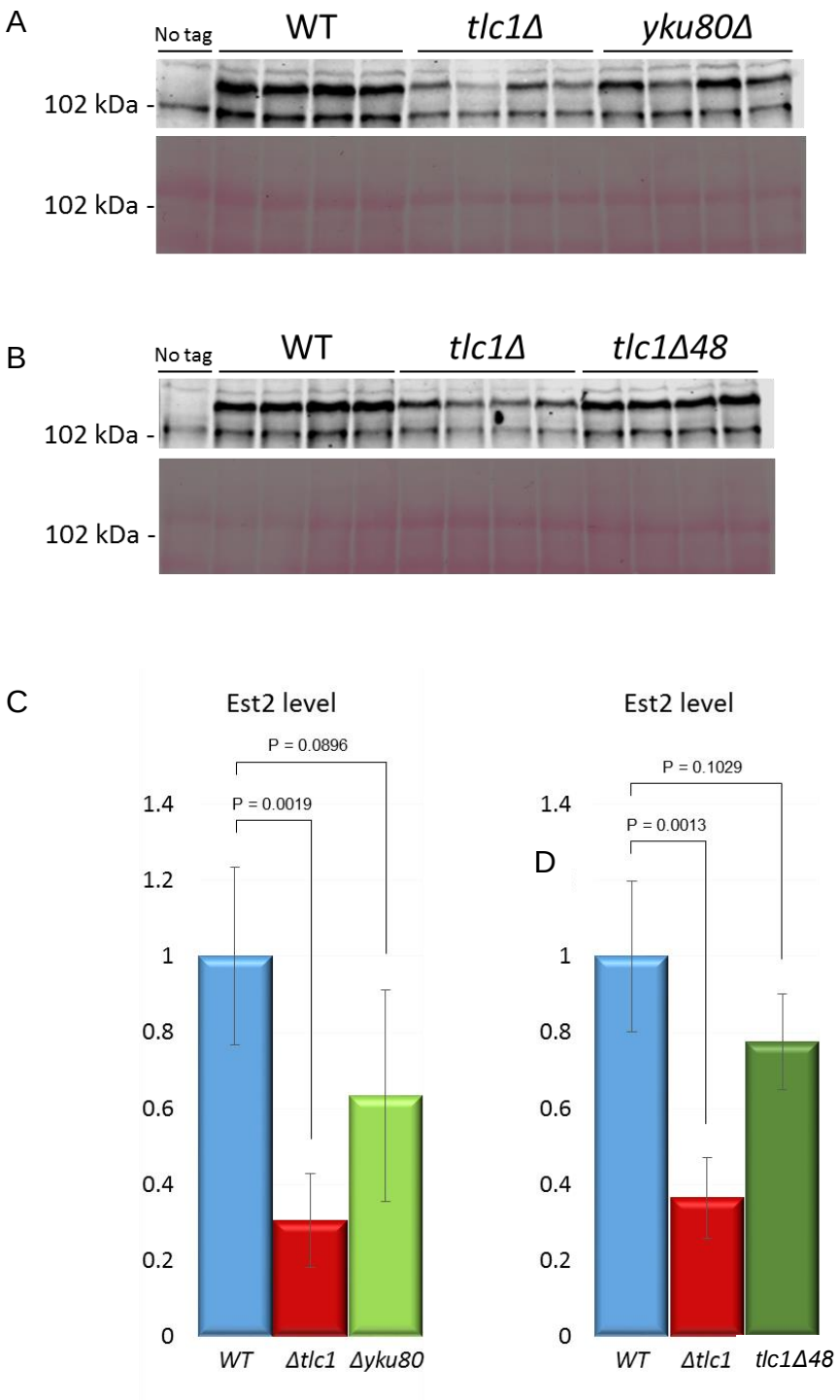

Figure 3.24: Analysis of the effect of the deletion of *YKU80* or the Yku70/80-binding stem-loop of TLC1 on the steady-state levels of Est2-myc$_{13}$

A – comparison of the Est2-myc$_{13}$ steady state level between WT, *tlc1Δ* and *yku80* cells, B – the same for WT, *tlc1Δ* and *tlc1Δ48* cells, C – mean Est2-myc$_{13}$ steady-state level from the western blot in A, D - mean Est2-myc$_{13}$ steady-state level from the western blot in B. Mean Est2-myc$_{13}$ band signals in *yku80* and *tlc1Δ48* mutants were normalized to a background band (not shown) and then to WT. The Error bars correspond to standard deviation of mean of four repeats. P values were calculated using unpaired T-test

3.4.2. Higher growth temperature decreases the steady-state level of the *S. pombe* Est2 homolog Trt1

Similarly to *S. cerevisiae* telomeres, *S. pombe* telomeres have been previously reported to equilibrate at progressively shorter length with increasing growth temperature (Millet *et al.*, 2015). If the underlying mechanism of temperature-dependent telomere shortening between these two evolutionarily divergent species is conserved, then the temperature-induced telomerase insufficiency might be relevant to and has implications for species other than *S. cerevisiae*.

Initially, I set out to test whether elevated growth temperatures are associated with a decrease in the steady-state level of the *S. pombe* telomerase catalytic subunit, as found previously for the *S. cerevisiae* telomerase reverse-transcriptase (Millet *et al.*, 2015). To that end, Trt1 – the *S. pombe* homolog of Est2 – was tagged with 13 myc repeats and the strains were grown either at 23°C or at 37°C, the proteins were extracted and analysed by anti-myc western blot. Ponceau red staining was used as loading control (Figure 3.25). Despite the fact that the samples originating from cultures grown at 37°C seem to have been overloaded compared to the samples from yeast grown at 23°C, there was a statistically significant decrease in the steady-state levels of Trt1-myc$_{13}$ in the cultures grown at the elevated temperature. This result is consistent with the hypothesis that the decrease in the telomere length observed in *S. pombe* grown at higher temperatures is due to a lower telomerase level.

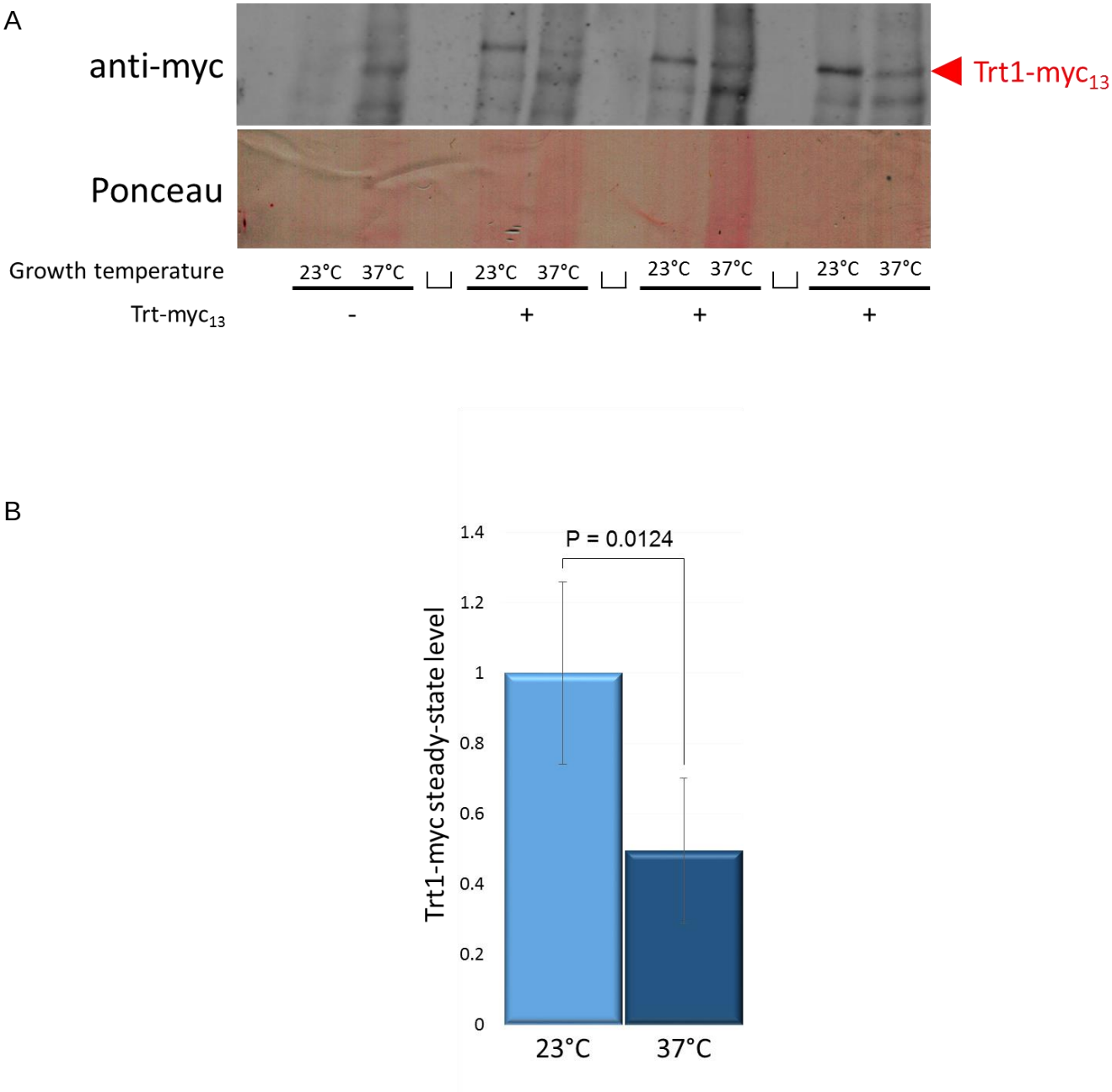

Figure 3.25: The steady-state level of Trt1 is decreased in *S. pombe* at an elevated temperature

A – comparison of the steady-state levels of Trt1-myc$_{13}$ at 23°C and 37°C in a western blot, B – quantification for A. Mean Trt1-myc$_{13}$ steady-state levels were calculated from three biological repeats and normalized to the average Trt1 level at 23°C. the P value was calculated using paired T-test. The error bars correspond to standard deviation of mean of three repeats. ␣ - empty lane

3.5. Discussion

3.5.1. Optimization of the co-immunoprecipitation of Est2 and Est3

The comparative quantitative co-immunoprecipitation of Est2 and Est3 is a direct way for assessing the relative amounts of telomerase complex in aneuploids and diploids.

Despite the protocol for co-immunoprecipitation of Est2 with Est3 having been previously established (Hughes *et al.*, 2000; Talley *et al.*, 2011; Tucey and Lundblad, 2014), it had to be optimized to avoid quantitative artifacts and increase sensitivity of the target protein detection. Pilot co-immunoprecipitation experiments revealed a number of problems, such as an overlapping of target protein bands with bands of antibodies (see Figure 3.2) or protein degradation products (see Figure 3.6) in western blots and low co-immunoprecipitation output in diploid strains heterozygous for the epitope-carrying alleles of *EST2* and *EST3* (see Figure 3.3). Moreover, it was discovered that *EST3-MYC13* cells have a shorter telomere length equilibrium (Figure 3.14A, also see Supplementary Material in Tucey and Lundblad, 2014), indicative of their suboptimal telomerase function, not unlikely due to an impaired interaction between modified Est3 protein and Est2 protein.

These considerations prompted me to use haploid strains for pilot experiments and seek an alternative set of tags for Est2 and Est3, with following properties:

1. Different tags for detection of Est2 and Est3 to prevent cross-reaction between Est2 degradation products and Est3.
2. Detectability in a western blot.
3. No significant effect on telomere length equilibrium (a commonly reported side-effect of telomerase tagging, e.g. Sabourin *et al.*, 2007; Tuzon *et al.*, 2011), to exclude tagging constructs that may impinge on telomerase complex stability and consequently skew the co-immunoprecipitation output.

Telomerase function of the strains bearing tags was assessed in a temperature-sensitivity assay (Figures 3.10-3.12) as well as in a Southern blot analysis to measure telomere length equilibrium (Figure 3.14). As a result of these tests, Est2-myc$_{13}$ and Est3-FLAG$_3$ were selected as constructs meeting the requirements laid out above. Subsequently, a pilot co-immunoprecipitation experiment was performed using haploid *EST2-MYC13 EST3-FLAG3* strains grown at 30°C, in which Est2-myc$_{13}$ was successfully co-IPed with Est3-FLAG$_3$ (Figure 3.16). When the same experiment was performed with strains grown at 38.5°C, Est2-myc$_{13}$ band, although much less intense, was still detected in the co-immunoprecipitate (Figure 3.17). The pilot co-immunoprecipitation however raised another technical concern as a perceptible proportion of Est2-myc$_{13}$ was found in the insoluble chromatin-containing fraction of pellet 2 (see Figure 3.16A). Considering, that maximum interaction between Est1 and Est2 occurs in S/G2 (Tucey and Lundblad, 2013), when all three protein subunits of telomerase show peak recruitment to the telomeres (Taggart, Teng and Zakian, 2002; Chan, Boulé and Zakian, 2008; Tuzon *et al.*, 2011), it is possible that a significant fraction of the overall mature telomerase complex is telomere-associated. To prevent a potential bias in the comparative assessment of the total amount of the telomerase complex in aneuploids and diploids caused by segregation of a sizeable proportion of telomerase holoenzyme from the lysate into chromatin pellet I attempted to release Est2-myc$_{13}$ into the supernatant using either DNA-degrading enzyme Benzonase or an increased NaCl concentration in the buffer. Despite evidence indicating degradation of the bulk of chromatin (Figure 3.20), and specifically telomeric chromatin (Figure 3.21), in pellet 2 upon benzonase treatment, a detectable release of Est2-myc$_{13}$ into cleared lysate was not achieved (Figure 3.19). Although increasing salt concentration in the lysis buffer was accompanied by a slight decrease in the proportion of Est2-myc$_{13}$ associated with pellet 2 (Figure 3.22), the relative extent of such dissociation at NaCl concentrations higher than 0.3 M appears to be negligible compared to the risk of destabilizing interactions between telomerase subunits in the conditions of high ionic strength.

The observed discrepancy between the extent of chromatin-degradation and the release of Est2-myc$_{13}$ from pellet 2 may have several explanations. For instance, Benzonase nucleolytic activity may not be sufficient under the conditions of NaCl concentration of 0.1 M or higher (Figure 3.18) to generate chromatin fragments small enough to remain the supernatant upon centrifugation. This, however, appears unlikely, given that the bulk of the chromatin smear from pellet 2 samples post Benzonase treatment concentrates in 0.5 kb area of the agarose gel in case of 0.1 M NaCl concentration in the lysis buffer (Figure 3.20). Moreover, bead-beating method of yeast extract preparation is believed to produce an extensive level of chromatin shear (Deutscher, 1990) resulting in solubilisation of a major part of chromatin fraction, which is consistent with a prominent reduction in both *URA3*- and telomere-specific probe signal in pellet 2 compared to total lysate (Figure 3.21A).

Alternatively, the presence of Est2-myc$_{13}$ in pellet 2 could be attributed to unspecific protein aggregation, a frequently encountered issue during protein extraction (Bondos and Bicknell, 2003). This explanation is agreement with the observed effect of increasing NaCl concentration on solubilisation of Est2-myc$_{13}$, since NaCl has been shown to reduce protein aggregation *in vitro* (Bondos and Bicknell, 2003). In yet another scenario, pelleting of Est2-myc$_{13}$ may be due to an unspecific hydrophobic interaction with the crude membrane fraction or nuclear scaffold that have been reported to precipitate at approximately the same centrifugation speed, as the one used in our protocol to remove chromatin (Navarre *et al.*, 2002; Xie, Bandhakavi and Griffin, 2005; Tran and Brodsky, 2012). In conclusion, Est2-myc$_{13}$ found in pellet 2 is not likely associated with telomeric chromatin.

3.5.2. The stability of the telomerase steady-state level in the context of genetic changes and telomerase functions and interacting partners

Chromosome VIII monosomy is associated with significant increases in the steady state levels of a host of non-ribosomal proteins, including Est1 and Est3. However the abundance of Est2 remains unaffected in the wake these proteome-wide changes (Millet *et al.*, 2015), implying a tight control of Est2 expression possibly via a yet-undiscovered negative-feedback loop.

The mechanisms responsible for the temperature-induced decrease in the amount of Est2 are equally obscure and are possibly related to the regulation of Est2 expression.

According to one view, Est2 level regulation could predominantly occur via control of its degradation, rather than synthesis. A cycloheximide assay performed by S. Makovets demonstrates that Est2 is destabilized in the absence of TLC1 and that this destabilization can be partially mitigated by inhibition of the proteasome (S. Makovets, personal communication; Figure 3.23). Given that RNA stem-loop structures can melt at higher temperatures (Krajewski and Narberhaus, 2014), it could be speculated that the temperature-induced decrease in Est2 levels might result from the melting of the TLC1 stem-loop regions responsible for Est2 binding, thus escalating the proteasome-dependent degradation of Est2.

Multiple explanations could be proposed as to why cells evolved a pathway that identifies and degrades RNA-free Est2 subunits.

A study performed in 2014 argued that the telomerase holoenzyme undergoes disassembly via dissociation of Est2 from the TLC1-Est1-Est3 complex (Tucey and Lundblad, 2014). Thus, free Est2 may represent an unwanted decay product of the telomerase complex which is dispensed with by the proteasome-dependent protein degradation pathway.

It could be similarly surmised, that the Est2 dissociation from the rest of the telomerase components could be a mandatory, yet reversible, step in the process leading to a full dismantling of telomerase complex and efficient cell-cycle dependent degradation of Est1, the latter being a well-characterized event considered to limit fully assembled telomerase to the S-phase (Taggart, Teng and Zakian, 2002; Osterhage, Talley and Friedman, 2006). Degradation of Est2 could therefore prevent its re-association with the TLC1-Est1-Est3 particle, thereby irreversibly sensitising Est1 to the subsequent clearance steps.

Alternatively, free Est2 could be removed to prevent off-target effects, the likes of which have been extensively documented for its human homolog hTERT (Saretzki, 2016). However, such effects may not be immediately obvious, since overexpression of Est2 does not seem to exert any effect on the cell growth rate (Teixeira *et al.*, 2002). It is possible that the selective disadvantage of yeast cells with an excess of telomerase manifests only under the conditions of stress. Also, in contrast to its mammalian homolog, Est2 lacks mitochondrial localization signal and has not been detected in mitochondria (Sickmann *et al.*, 2003). Given that human telomerase has been found to confer its adverse effect in mitochondria (Santos *et al.*, 2004), the lack of mitochondrial import of Est2 argues against extrapolation of human telomerase off-target properties onto Est2.

A. Bianchi and D. Shore have proposed that limiting the amount of telomerase is instrumental for ensuring preferential elongation of short telomeres (Bianchi and Shore, 2008), although whether such regulation necessitates degradation of free Est2 as opposed to Est2-TLC1 complex is an open question.

Finally, the degradation of free Est2 might result from its mislocalization from telomeres to a different compartment, where it is recognized as a foreign protein and marked for destruction. It has been shown, that in the absence of TLC1 overexpression, overexpressed Est2 accumulated in the nucleolus (Teixeira *et al.*, 2002). Est2 relies on TLC1 RNA for recruitment to telomeres throughout the cell cycle (Taggart, Teng and Zakian, 2002) and is sequestered

by a nucleolar protein PinX1 in *tlc1Δ* cells (Lin and Blackburn, 2004). Yeast Ku protein complex has been also implicated in the recruitment of telomerase to telomeres (Fisher, Taggart and Zakian, 2004; Chan, Boulé and Zakian, 2008), and Gallardo *et al.* reported a role of yKu in the nuclear import of TLC1 (Gallardo *et al.*, 2008), raising a possibility of yKu participation in the nuclear trafficking of Est2-TLC1 complex. Therefore, it could be the case, that when Est2 fails to efficiently localize to the telomeres in the absence of yKu complex, it is redistributed to the nucleolus, as in *tlc1Δ* cells, or retained in the cytoplasm, where it could be rendered for degradation. As the initial step in testing the connection between the localization of Est2 and its stability I analysed the effects of deletion of *YKU80* or yKu-interacting hairpin of TLC1 on Est2-myc$_{13}$ steady-state level. I discovered no statistically significant difference when comparing Est2-myc$_{13}$ levels in mutants to WT cells (Figure 3.24), suggesting that either Est2-myc$_{13}$ does not relocalize to the nucleolus in the absence of TLC1 interaction with yKu, or that such relocalization, if happens, does not confer instability to Est2. Alternatively, it could be argued, that the sample size of the experiment was insufficient to distinguish Est2-muc$_{13}$ levels between the mutants and the wild type strains.

3.5.3. The amount of *S. pombe* telomerase catalytic subunit is reduced at elevated growth temperature

Budding yeast proved to be a valuable model eukaryote for investigating telomere biology. Nevertheless, species-specific properties of *S. cerevisiae* inevitably limit the extent to which the conclusions drawn from studying budding yeast telomeres and telomerase can be applied to mammalian cells.

Understanding cancer and ageing is the ultimate goal of telomerase-related research in all species. The discovery of temperature-induced telomerase insufficiency and aneuploidy-dependent compensation of telomerase shortage in *S. cerevisiae* paved the way for establishing the first yeast model of telomerase reactivation (Millet *et al.*, 2015). Expanding such a model across other species may help to crystallize patterns relevant to the telomere biology

of the eukaryotes in general and facilitate understanding of the mechanisms underlying both telomerase insufficiency and its compensation in cancer cells.

S. pombe telomere length equilibrium responds to the growth temperature similarly to *S. cerevisiae* (Millet *et al.*, 2015), thus I tested the effect of temperature on the steady-state level of *S. pombe* telomerase catalytic subunit Trt1. I found that Trt1 level decreased in fission yeast grown at 37°C compared to 23°C (Figure 3.25), recapitulating the effect observed in *S. cerevisiae.* However, deletion of *ter1*$^{+}$ (the gene encoding *S. pombe* telomerase RNA), did not seem to produce a significant decrease in the level of Trt1 (data not shown), consistent with previously obtained data (Leonardi *et al.*, 2008). It remains to be elucidated, whether the nature of the temperature-induced decrease in the telomerase catalytic subunits in *S. pombe* and *S. cerevisiae* is the same. Given, that *S. pombe* haploid cells possess only 3 chromosomes, aneuploidy seems an unlikely possibility in fission yeast. For this reason telomerase reactivation in fission yeast might not be occurring by aneuploidy, which may limit the benefits of studying *S. pombe* telomere biology, or conversely, lead to a discovery of completely new aneuploidy-independent mechanisms of compensating telomerase insufficiency.

CHAPTER 4

Dna2 and Rad27 Affect the Efficiency of DSB Healing via BIR and DNTA

4.1. Introduction

RPA-coated ssDNA is a common feature of stalled replication forks and resected DSBs and is an important intermediate in homology repair, where it plays a vital role in the recruitment and activation of DNA damage checkpoint proteins. RPA-ssDNA tracts are also observed in the lagging-strand synthesis during normal DNA replication in the form of long 5'-flaps of Okazaki fragments (Rossi and Bambara, 2006; Rossi, Foiani and Giannattasio, 2018). 5'-flaps normally result from the displacement activity of Pol δ – the lagging strand polymerase – during the extension of an upstream Okazaki fragment (Maga *et al.*, 2001). Both Dna2 and Pif1 participate in the metabolism of 5'-flaps, whereby Pif1 promotes the formation of long flaps capable of binding to the RPA, which thus become refractory to the flap-endonuclease (Rad27) nucleolytic activity and require cleavage by Dna2 (Rossi *et al.*, 2008; Pike *et al.*, 2009). Once the role of Dna2 in the S-checkpoint signalling was discovered, it has been proposed that persistent RPA-coated 5'flaps could promote Dna2-dependent S-checkpoint signalling (Kumar and Burgers, 2013; Wanrooij and Burgers, 2015). In addition, some of the models of BIR propose, that the synthesis of the lagging strand occurs via Okazaki fragments, which may require processing by Dna2 (Saini *et al.*, 2013; Rossi, Foiani and Giannattasio, 2018). Thus, the metabolism of the 5'-flaps of Okazaki fragments might be relevant to homologous recombination and specifically to BIR, and the roles of Pif1 in BIR and Okazaki fragment maturation might be connected. Genetic studies of Dna2-related processes are somewhat difficult since the deletion of *DNA2* is lethal (unless some other genes are deleted, e.g. *PIF1*, *RAD9*, *POL32*) however a hypomorphic *dna2ΔN(1-248)* mutant is available which is characterized by decreased nuclear localization of Dna2 and the lack of the amino-acids of Dna2 responsible for S-checkpoint signalling (Budd *et al.*, 2006, 2011; Kumar and Burgers, 2013; Markiewicz-Potoczny, Lisby and Lydall, 2018). While looking into genetic interactions between *PIF1* and *DNA2* in BIR, S. Makovets and O. Kotenko have found that *dna2ΔN(1-248)* partially suppresses the BIR-defect incurred by the nuclear-null *pif1-m2* mutation (see

Figure 4.1). Unexpectedly, when introduced into WT cells, *dna2ΔN(1-248)* caused a decrease of BIR efficiency. Subsequent genetic experiments and Southern-blot analysis confirmed that in contrast to *pif1-m2* cells *pif1-m2 dna2ΔN(1-248)* cells are capable of Pif1-independent long-range BIR. It was also revealed that *dna2ΔN(1-248)* alleviates BIR-defect incurred by other mutant *pif1* alleles, such as *pif1-4A* (non-phosphorylatable), *pif1-4D* (phosphomimic) and *pif1-R3E* (deficient for the interaction with PCNA). In addition, *RAD27* effects on the BIR efficiency were found to partially recapitulate the effects of *DNA2*.

4.2. N-terminally truncated Dna2 (Dna2ΔN(1-248)) alleviates the requirement for Pif1 in BIR but not for Pol32

As mentioned previously, O. Kotenko and S. Makovets have discovered a suppression of BIR defect in *pif1-m2* cells by *dna2ΔN(1-248)* (Figure 4.1). The BIR efficiency in this experiment, as well as the experiments performed in this study, was assessed by a previously published plating assay (Vasianovich, Harrington and Makovets, 2014), wherein an inducible DSB was created by *GAL1* promoter-regulated HO-nuclease that introduced a cut at an ectopic HO-site (Figure 4.2). The HO-site was placed close to the *MNT2* gene on chrVIIL and was flanked by the *URA3* gene from the telomere-proximal side and by a 3'-fragment of *KAN* from the centromere-proximal side. The 3' *KAN* fragment shared 500 bp of homology with the 5' *KAN* fragment located approximately 100 kb away from the right end of chromosome II. The cells pre-grown on raffinose were plated in parallel on YPD and YPGal plates and the efficiency of BIR was calculated as the total number of $G418^R$ Ura^- colonies on YPGal plates relative to the cell titer. All the plating experiments in chapter 4 were done using this system, unless specified otherwise.

In order to test, whether *dna2ΔN(1-248)* increases the frequency of $G418^R$ Ura^- survivors upon induction of a DSB in *pif1-m2* cells through BIR rather than alternative mechanisms, the efficiency of BIR was analysed in *pol32Δ*

derivatives of *PIF1* or *pif1-m2* with *DNA2* or *dna2ΔN(1-248)*, which lack the Pol32 subunit of Pol δ essential for BIR (Lydeard *et al.*, 2007). In this background, *dna2ΔN(1-248)* was unable to suppress the BIR defect (Figure 4.3). Thus, *pif1-m2 dna2ΔN(1-248)* cells are partially proficient for BIR independently of Pif1.

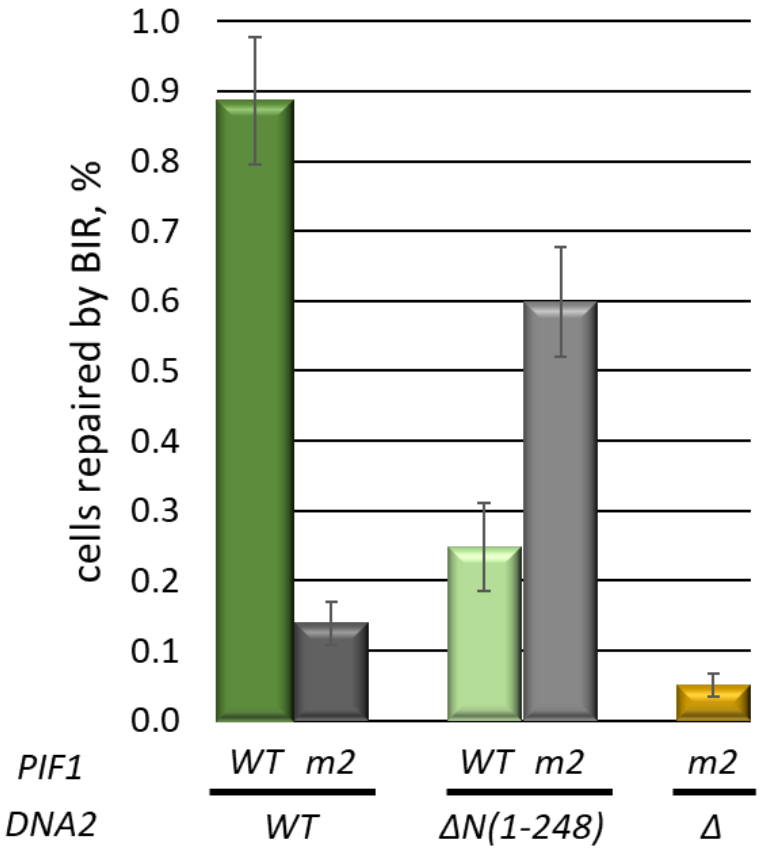

Figure 4.1: *dna2ΔN(1-248)* decreases BIR efficiency in WT cells, but partially suppresses BIR-defect in *pif1-m2* cells

Mean frequency of BIR was calculated from three technical repeats. Error bars correspond to standard deviation. *dna2Δ* strains are not viable and therefore could not be used in the assay. From Vasianovich, Harrington and Makovets, 2014, and O. Kotenko (personal communication)

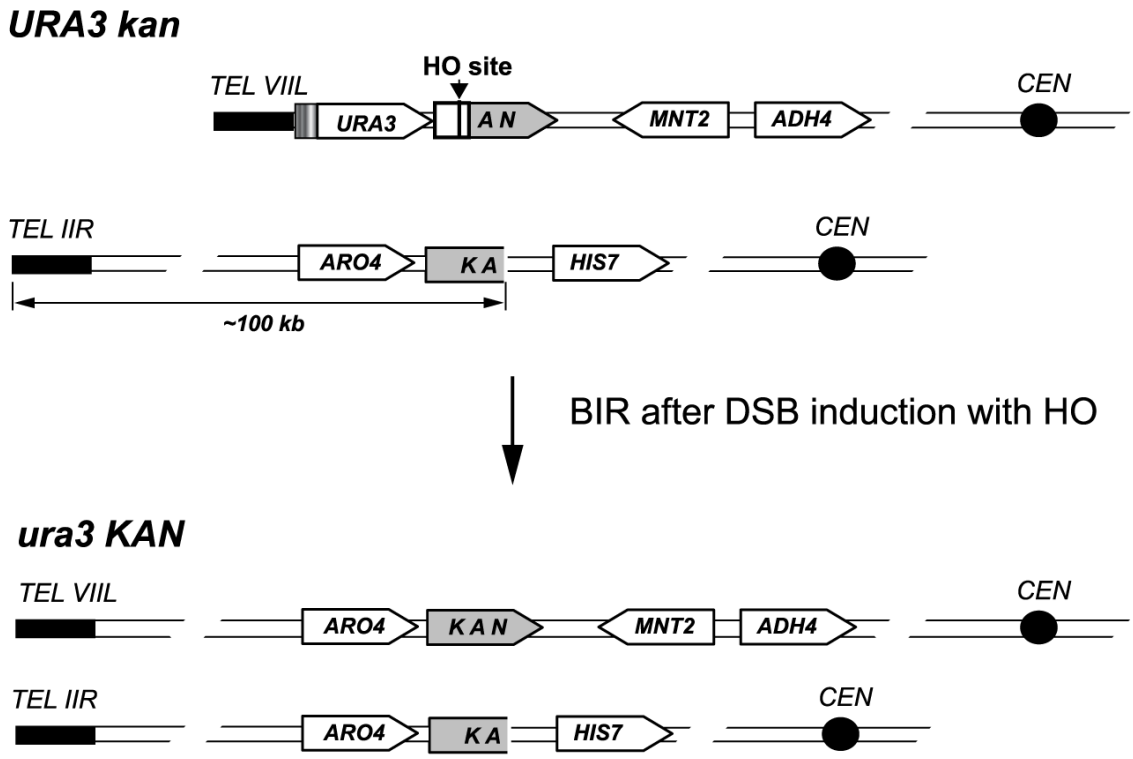

Figure 4.2: Schematic of the BIR assay

From Vasianovich, Harrington and Makovets, 2014

DNA combing experiments performed by Malkova's group have demonstrated that Pif1 is important for long-range (~100 kb) BIR, since in *pif1Δ* cells BIR terminated prematurely, resulting in half-crossover repair outcomes (Saini *et al.*, 2013). In order to test if *pif1-m2 dna2ΔN(1-248)* cells are capable of long-range BIR, I analysed several $G418^R$ Ura^- clones recovered after the DSB induction from *pif1-m2, dna2ΔN(1-248), pif1-m2 dna2ΔN(1-248)* and WT cells for the presence of long-range BIR products using PFGE in combination with Southern blotting using a probe specific to the distal part of the BIR donor chromosome (Figure 4.4). In case of successful BIR repair, this region is copied to the broken chromosome, i.e. chrVII. As seen from Figure 4.5 (also see Table 4.1), all ten *pif1-m2 dna2ΔN(1-248)* clones, that were assayed by PFGE-coupled Southern blotting, had successfully copied the distal region of chrII onto chrVII, indicating that the majority of $G418^R$ Ura^- clones result from

long-range BIR. In the *pif1-m2* strain, out of nineteen G418^{R} Ura^{-} clones selected for analysis, one clone failed to copy the aforementioned region onto chrVII, apparently as a result of prematurely terminated BIR. In WT and *dna2ΔN(1-248)* strains, all the analysed clones carried the sequence in question on both chrII and chrVII, indicating successfully-completed long-range BIR in the majority of G418^{R} Ura^{-} clones. Collectively, the results of the plating assay (see Figure 4.3) and the PFGE analysis of repair outcomes suggest that *pif1-m2 dna2ΔN(1-248)* cells are partially proficient for long-range Pif1-independent BIR.

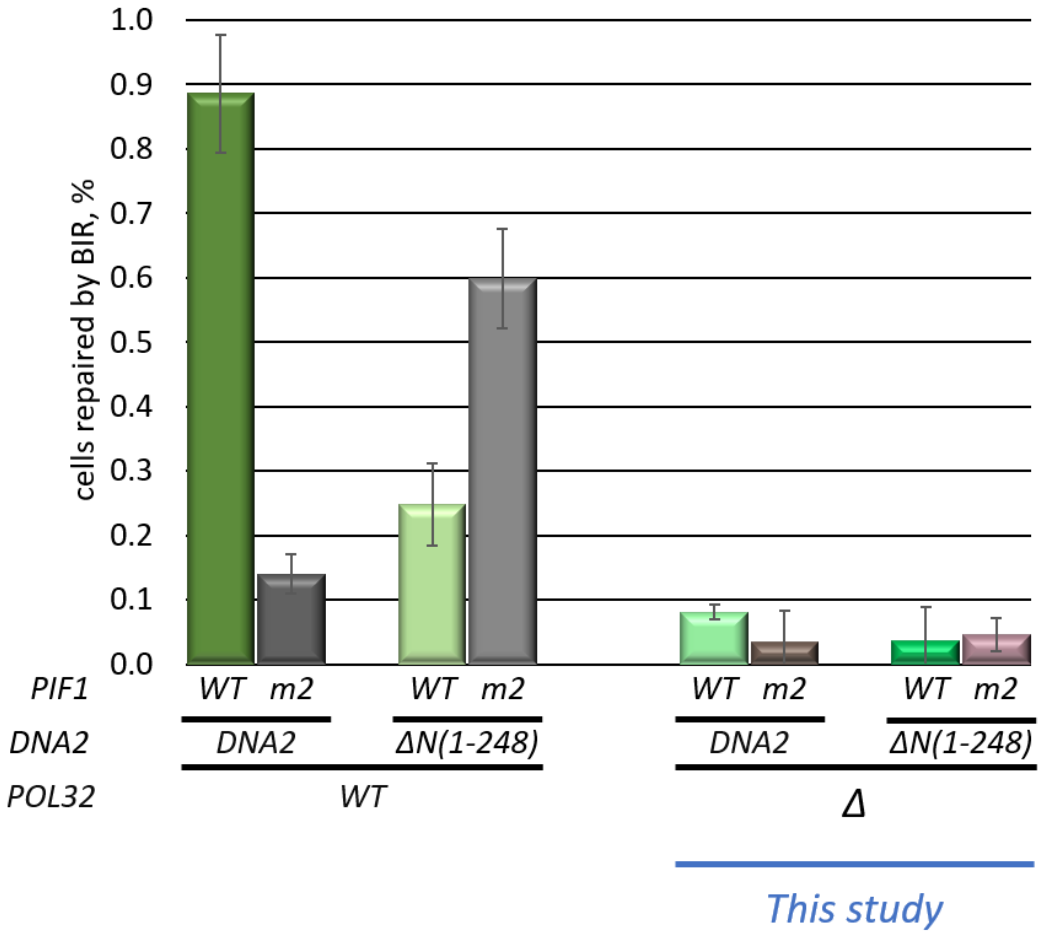

Figure 4.3: *dna2ΔN(1-248)* does not suppress the BIR deficiency in *pol32Δ* cells

Mean frequency of BIR was calculated from three technical repeats. Error bars correspond to standard deviation. Here and henceforth the plating assay results obtained in this study are indicated below the diagram. Data for *POL32* strains are from are Vasianovich, Harrington and Makovets, 2014 and O. Kotenko (personal communication)

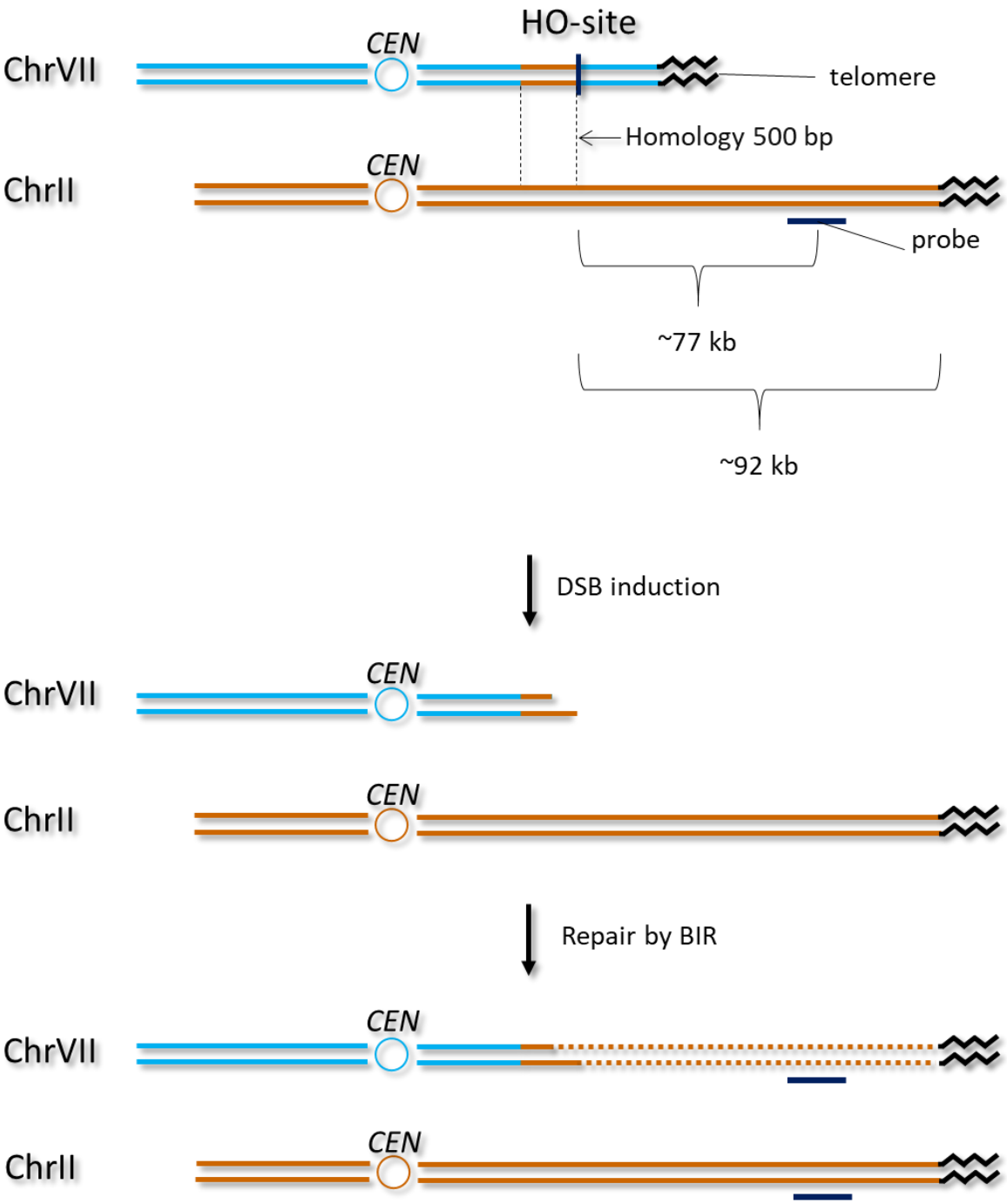

Figure 4.4: Schematic of the repair product resulting from the completion of long-range BIR, that can be detected by probing for the region ~77 kb downstream from the invasion point on chrII

The lengths of the chromosomes are not depicted to scale

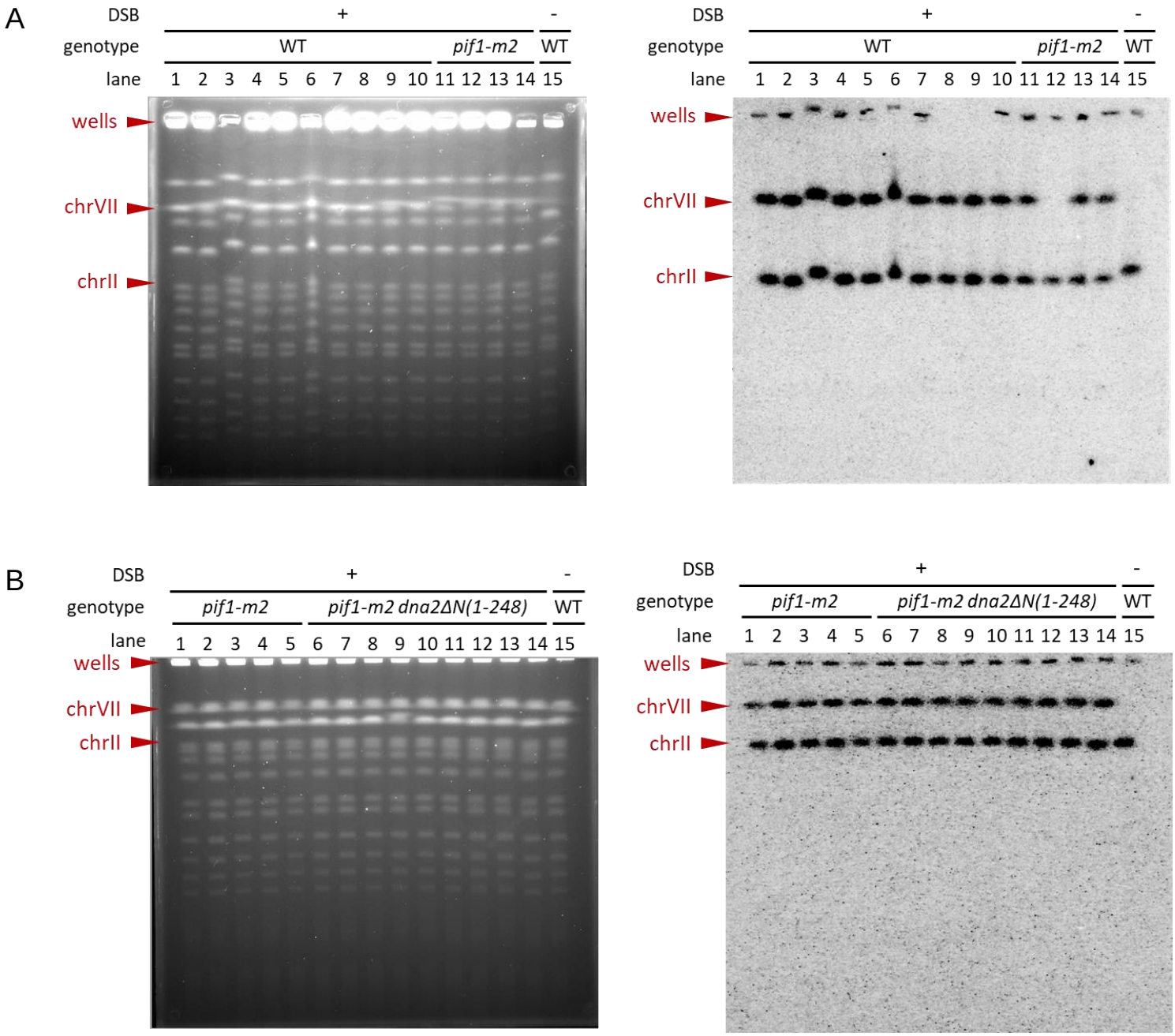

Figure 4.5: (beginning) Analysis of repair outcomes in G418^{R} Ura^{-} clones recovered upon DSB induction in WT, *dna2ΔN(1-248)*, *pif1-m2* or double-mutant strains

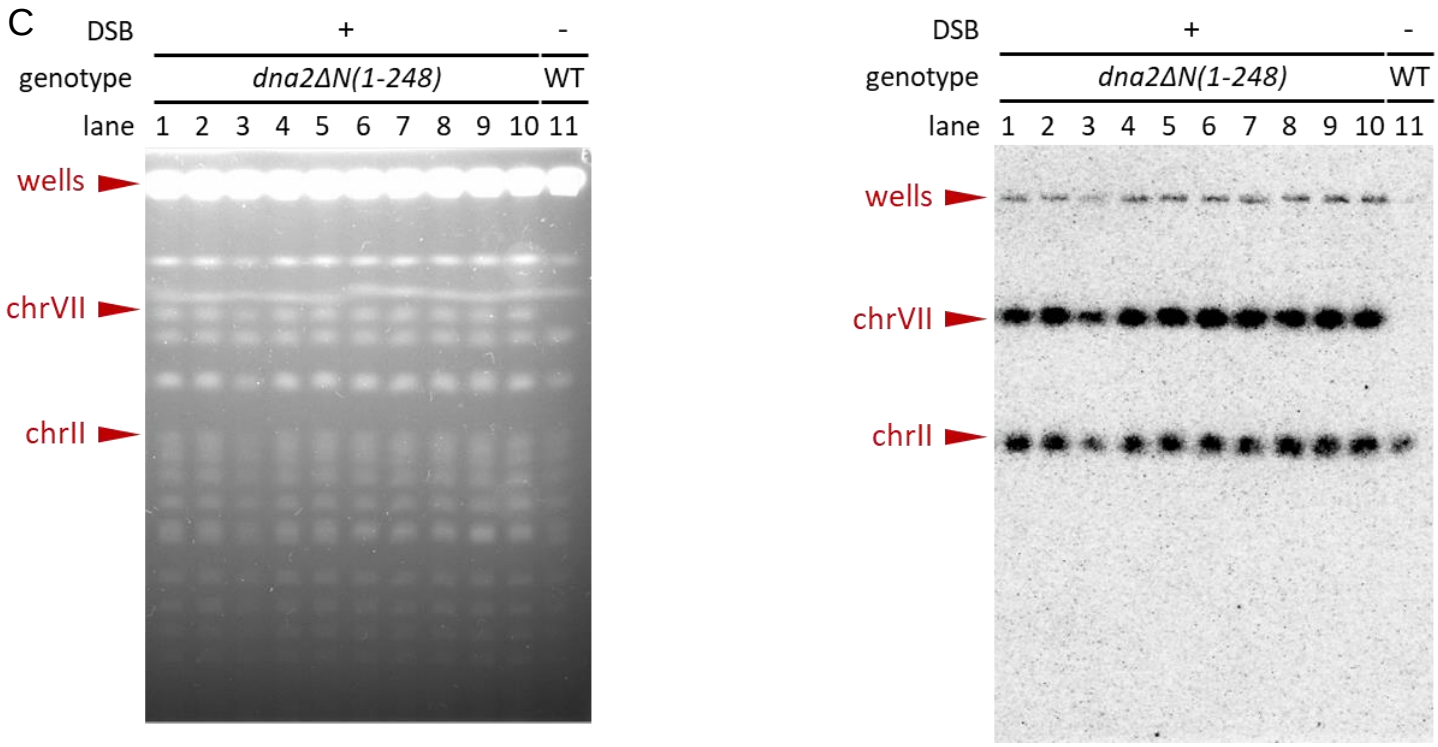

Figure 4.5: (continuation) Analysis of repair outcomes in G418^{R} Ura^{-} clones recovered upon DSB induction in WT, *dna2ΔN(1-248), pif1-m2* or double-mutant strains

Pulse-field gels are on the left and Southern blots are on the right. A WT strain with no DSB induction and a 5 kb homology between chrVII and chrII was used as a negative control for chrVII probing. The rest of the strains have 500 bp homology between chrVII and chrII. One *pif1-m2* clone failed to copy the region 77 kb downstream of the invasion point (A, right side, lane 12), indicating that the BIR either terminated prematurely or has never occurred. The rest of the analysed clones successfully copied the region in question onto chrVII upon DSB induction, consistent with the efficient long-range BIR

Table 4.1: Summary of the repair outcomes in different genotypes analysed by PFGE-coupled Southern blotting

Fractions indicate the number of clones that have copied the chrII fragment 77 kb downstream from the invasion point onto chrVII upon DSB induction relative to the total number of analysed $G418^R$ Ura^- clones

	WT	***dna2ΔN(1-248)***	***rad27Δ***
PIF1	10/10	9/9	10/10
pif1-m2	18/19	10/10	9/9
pif1-4A	13/17	Not assayed	Not assayed

4.3. The suppression of the BIR defect in *pif1-m2 dna2ΔN(1-248)* is dependent on the nuclease activity of Dna2

Dna2 possesses two enzymatic activities – a nuclease and a helicase one (Budd, Choe and Campbell, 1995). In an attempt to gain insights into the mechanism underlying the suppression of BIR deficiency in *pif1-m2 dna2ΔN(1-248)* cells, I analysed the effect of the missense mutations disrupting the catalytic functions of the truncated Dna2 protein on its ability to alleviate the BIR defect. In Dna2, the D657A amino acid substitution abolishes its nuclease activity, while the K1080E change inactivates the ATP-binding-motif, thus effectively eliminating the helicase activity (Budd, Choe and Campbell, 1995, 2000). The plating assay demonstrated that only the nuclease, but not the helicase activity of Dna2ΔN(1-248) was essential for rescuing the BIR deficiency in *pif1-m2* cells, since strains harbouring helicase-dead, but not helicase-,nuclease-dead *dna2ΔN(1-248)* were able to supress the BIR-defect (Figure 4.6).

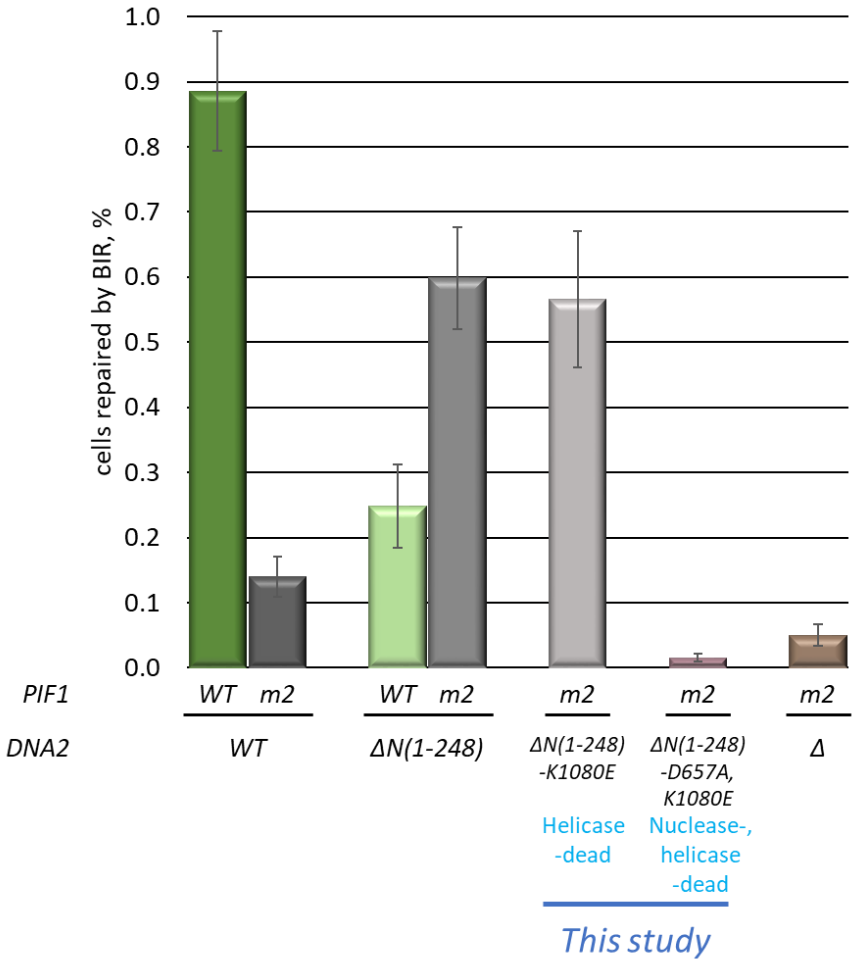

Figure 4.6: The helicase, but not the nuclease activity of Dna2ΔN is dispensable for the partial suppression of BIR defect in *pif1-m2 dna2ΔN(1-248)* cells

Mean frequency of BIR was calculated from three technical repeats. Error bars correspond to standard deviation. Data for the WT, *pif1-m2*, *dna2ΔN(1-248)*, *pif1-m2 dna2ΔN(1-248)* and *pif1-m2 dna2Δ* strains are from Vasianovich, Harrington and Makovets, 2014, Y. Vasianovich (personal communication) and O. Kotenko (personal communication)

4.4. *dna2ΔN(1-248)* partially suppresses the BIR defect in different *pif1* mutants

Elucidating the mechanism of the *dna2ΔN(1-248)*-mediated suppression of the BIR deficiency phenotype in *pif1-m2* may shed light on the Pif1 function in BIR and *vice versa*. Y. Vasianovich *et. al.* have demonstrated that the *pif1-4A* mutation, that abrogates the Rad53-dependent phosphorylation of the TLSSAES motif in Pif1, decreases the BIR efficiency in a similar to *pif1-m2* fashion (Vasianovich, Harrington and Makovets, 2014). Other BIR-deficient *pif1* mutants have been subsequently reported in the literature and also identified in our lab (Buzovetsky *et al.*, 2017 and O. Kotenko, personal communication), collectively suggesting that the engagement of Pif1 in BIR could involve several steps and/or molecular interactions. Identifying the *pif1* alleles that complement *dna2ΔN(1-248)* in BIR could help to pinpoint the specific step or process that is rescued by *dna2ΔN(1-248)*. It should be pointed out that in WT background *dna2ΔN(1-248)* inhibits BIR, raising a possibility of a competition between Pif1 and Dna2ΔN(1-248) for some third factor. Thus, if a particular *pif1* mutation happens to impair the Pif1 function in BIR without affecting the said competition with Dna2, it could potentially exacerbate the BIR defect observed in *PIF1 dna2ΔN(1-248)* cells.

Using the same plating assay as before (Figure 4.2), I analysed the genetic interaction of *dna2ΔN(1-248)* with the following nuclear *pif1* alleles: *pif1-m1-4A, pif1-m1-4D* (with the threonine and serine residues in the TLSSAES motif replaced by either alanines or phosphomimic aspartates, respectively; Makovets and Blackburn, 2009), *pif1-m1-R3E* (deficient for the interaction with PCNA; Buzovetsky *et al.*, 2017), *pif1-m1-4A-R3E* and *pif1-m1-4D-R3E*, all of which were co-expressed with an otherwise unaltered mitochondrial allele *pif1-m2* to avoid mitochondrial side-effects (Figure 4.7A). Comparable levels of the suppression of the BIR defects by *dna2ΔN(1-248)* were observed in all the studied *pif1* mutants (Figure 4.7B), including cells exclusively expressing the nuclear null allele *pif1-m2*, suggesting a shared nature of the BIR deficiency and its rescue by Dna2ΔN(1-248) in strains carrying these alleles.

A

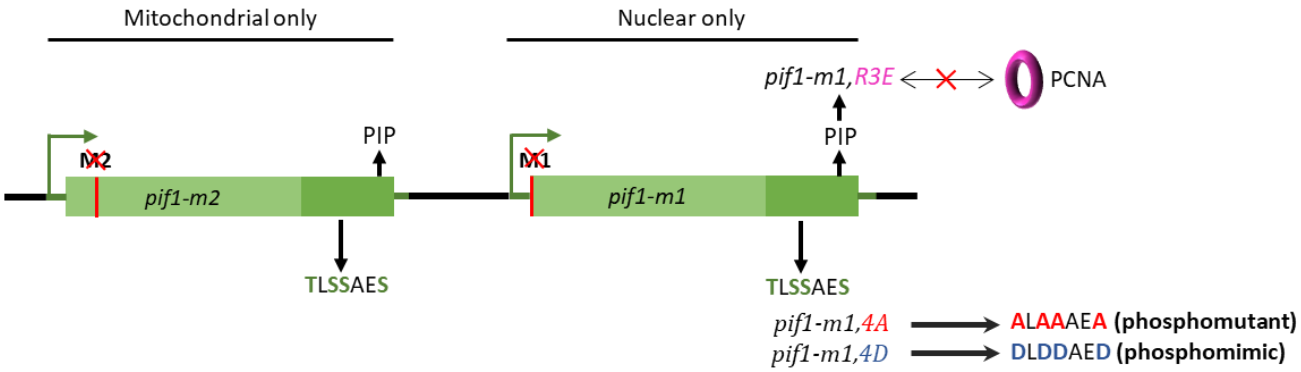

B

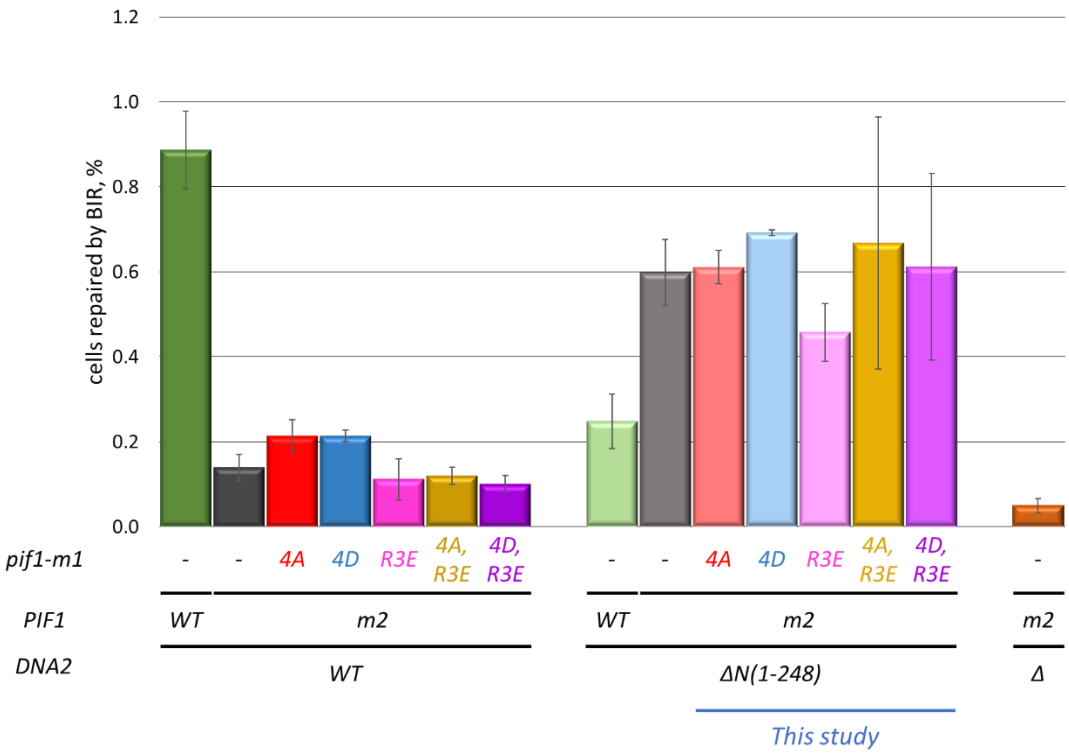

Figure 4.7: *dna2ΔN(1-248)* partially suppresses the BIR defect of different mutant *pif1* alleles to a similar extent

A – schematic of a tandem arrangement of nuclear-null and mitochondrial-null *pif1* alleles in the *PIF1* locus used in the BIR plating assay. PIP – PCNA interacting peptide, TLSSAES – a motif phosphorylated upon the DNA damage checkpoint activation. Amino acid sequence alterations introduced upon different mutations are indicated. B – BIR efficiency of the strains with different *PIF1* alleles and *DNA2*, *dna2ΔN(1-248)* or *dna2Δ*. Mutations in the PIP and/or the TLSSAES motifs were introduced into the *pif1-m1* (nuclear only) allele on an integration vector and the resultant mutant genes were co-expressed with *pif1-m2* (mitochondrial only) allele to avoid any effect on the mitochondrial function of Pif1. Mean frequency of BIR was calculated from at least three technical repeats (except for *pif1-m2 pif1-m1,4D dna2ΔN(1-248)* strain, where only two repeats were used). Error bars correspond to standard deviation. Data for WT, *pif1-m2*, *dna2ΔN(1-248)*, *pif1-m2 dna2ΔN(1-248)*, *pif1-m2 pif1-m1,4A*, *pif1-m2 pif1-m1,4D*, *pif1-m2 pif1-m1,4A,R3E*, *pif1-m2 pif1-m1,4D,R3E* and *pif1-m2 dna2Δ* strains is from Vasianovich, Harrington and Makovets, 2014, Y. Vasianovich (personal communication) and O. Kotenko (personal communication)

4.5. Overexpression of *DNA2* or its truncated forms affects both BIR and DNTA at DSBs

Dna2ΔN(1-248) has been found to have a decreased localization to DSBs compared to the full-length protein (Chen *et al.*, 2011), indicating that it might behave as a hypomorph in general and in BIR too. Of note, the efficiency of BIR is lower in *pif1-m2 dna2Δ* than in *pif1-m2 dna2ΔN(1-248)* cells and lower in *pif1-m2 dna2ΔN(1-248)-D6575A,K1080E* cells than in *pif1-m2 dna2ΔN(1-248)-K1080E* cells (see Figures 4.1 and 4.6), suggesting that a minimal level of the Dna2ΔN nuclease activity is essential for the efficient BIR in the *pif1-m2* background. At the same time, *dna2ΔN(1-248)* cells have a decreased BIR frequency compared to *pif1-m2 dna2ΔN(1-248)* cells, indicating a requirement for an intricate balance between the activities of Pif1 and Dna2 for efficient BIR. Such a balance is supposedly upset whenever the activity of Pif1 exceeds that of Dna2ΔN(1-248) (however it is not clear whether the same is true for an inverse situation). If this hypothesis is correct, then *dna2Δ* cells could be expected to demonstrate even lower BIR efficiency, than *dna2ΔN(1-248)* cells, however *DNA2* loss is lethal in the presence of Pif1 (Budd *et al.*, 2006), preventing such strains from being constructed and analysed in the BIR assay. On the other hand, removal of the first 405 amino acids of Dna2 has been reported to increase the *in vitro* nuclease activity of Dna2 (Bae, 2001). This suggests an alternative interpretation of the BIR assay data obtained from the *dna2ΔN(1-248)* strains. The increased nuclease activity of the Dna2ΔN(1-248) protein might be compensating for the lack of Pif1 in *pif1-m2 dna2ΔN(1-248)* cells by an unknown mechanism. However in the presence of functional Pif1 an excess of Dna2ΔN(1-248) nuclease activity might be somehow detrimental for BIR, possibly upsetting a finely tuned coordination between the many processes that underlie the progress of the repair. In an attempt to determine whether the efficiency of BIR in *dna2ΔN(1-248)* cells is limited by insufficient Dna2ΔN(1-248) activity, I assessed the effect of ectopic *DNA2* and *dna2ΔN(1-248)* overexpression on BIR in the WT and *pif1-m2* backgrounds. *DNA2* overexpression inhibited BIR more than threefold in WT background and did

not significantly alter the BIR efficiency in *pif1-m2* cells (Figure 4.8). Overexpression of the ectopic *dna2ΔN(1-248)* in cells with the WT endogenous copy of *DNA2* did not bring about a noticeable change in the BIR efficiency in either WT or *pif1-m2* background. Surprisingly, overexpression of the ectopic *dna2ΔN(1-248)* in *dna2ΔN(1-248)* cells was associated with an almost 14-fold increase in the BIR frequency compared to the strain with no overexpression, whereas in *pif1-m2 dna2ΔN(1-248)* cells, the ectopic *dna2ΔN(1-248)* overexpression failed to produce an appreciable difference in BIR efficiency (P = 0.2; Figure 4.9). Collectively, these results indicate, that the full-length Dna2, whether endogenous or ectopic, limits the BIR efficiency, whereas Dna2ΔN(1-248) facilitates BIR, when its amount is sufficient, the threshold for the required level of Dna2ΔN(1-248) apparently being elevated in the presence of Pif1. Interestingly, ectopic overexpression of the first 405 amino acid residues of Dna2 (*dna2-N(1-405)*), that lacks both the nuclease and the helicase domains, resulted in an approximately 1.5-fold increase in BIR in WT cells, suggesting that there might be more than one mechanism of the Dna2-related increase in the BIR efficiency.

An unanticipated effect of *DNA2* overexpression was discovered upon the induction of a DSB while analysing the frequency of $G418^S$ Ura^- colonies, which were expected to form in case of addition of a telomere to the DSB by DNTA (see Figures 4.10 and 4.11). Specifically, ectopic overexpression of *DNA2* produced an almost 4-fold increase in DNTA in *pif1-m2* cells (up to 4% frequency), which lack Pif1 normally responsible for inhibiting DNTA (Schulz and Zakian, 1994). Overexpression of *dna2-N(1-405)*, but not *dna2ΔN(1-248)* in *pif1-m2* cells resulted in a similar rise of DNTA frequency, suggesting that the observed effect is specific to the N-terminal part of Dna2, rather than its catalytic domains. Y. Vasianovich has previously observed a 2-fold increase in DNTA frequency (up to 3.5% of total colonies) upon deletion of *SGS1* in *pif1-4A* cells (Y. Vasianovich, personal communication) and a 1.5-fold increase in BIR upon deletion of SGS1 in WT cells had been previously reported in a system with 1157 bp homology (Lydeard *et al.*, 2010). Dna2 has been known to interact physically and genetically with Sgs1; the two proteins jointly act in

the same pathway of DNA resection at DSBs (Cejka, Cannavo, *et al.*, 2010) and the resection has been reported to inhibit DNTA, especially in *pif1-m2* cells (Chung *et al.*, 2010). Therefore, it could be hypothesised, that the ectopic overexpression of *DNA2* or *dna2-N(1-405)* in *pif1-m2* cells results in the sequestration of Sgs1 from the DSB, thereby abrogating the Sgs1-dependent resection and consequently attenuating the resection-dependent inhibition of DNTA.

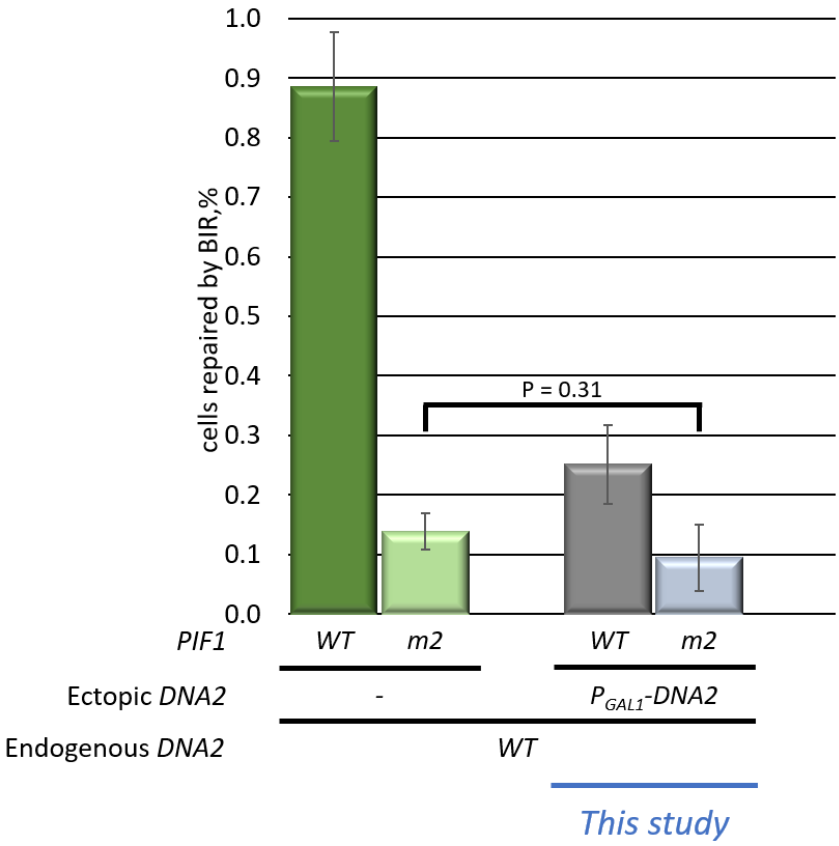

Figure 4.8: Overexpression of *DNA2* decreases the efficiency of BIR in WT cells

Mean frequency of BIR was calculated from three technical repeats, except for *pif1-m2* P_{GAL1}-*DNA2* strains, where two technical repeats were used. Error bars correspond to standard deviation. Data for WT and *pif1-m2* a strains is from Vasianovich, Harrington and Makovets, 2014

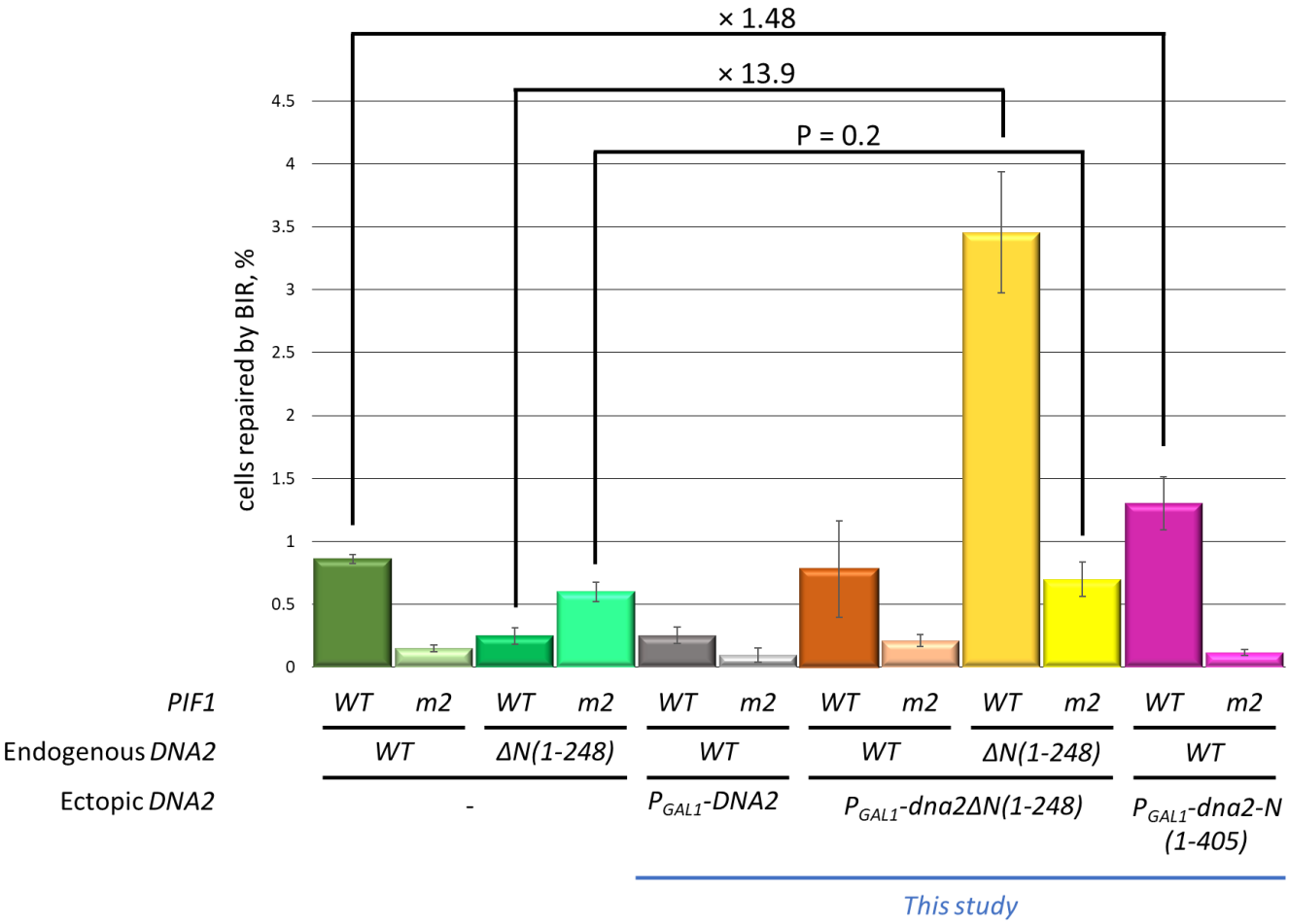

Figure 4.9: The effect of ectopic overexpression of either *DNA2* or its truncated forms on the BIR efficiency (combined data)

Mean frequency of BIR was calculated from at least three technical repeats, except for the *pif1-m2* P_{GAL1}*-DNA2* strains, where 2 repeats were used. Error bars correspond to standard deviation. Data for WT, *pif1-m2, dna2ΔN(1-248)* and *pif1-m2 dna2ΔN(1-248)* strains is from Vasianovich, Harrington and Makovets, 2014 and O. Kotenko (personal communication)

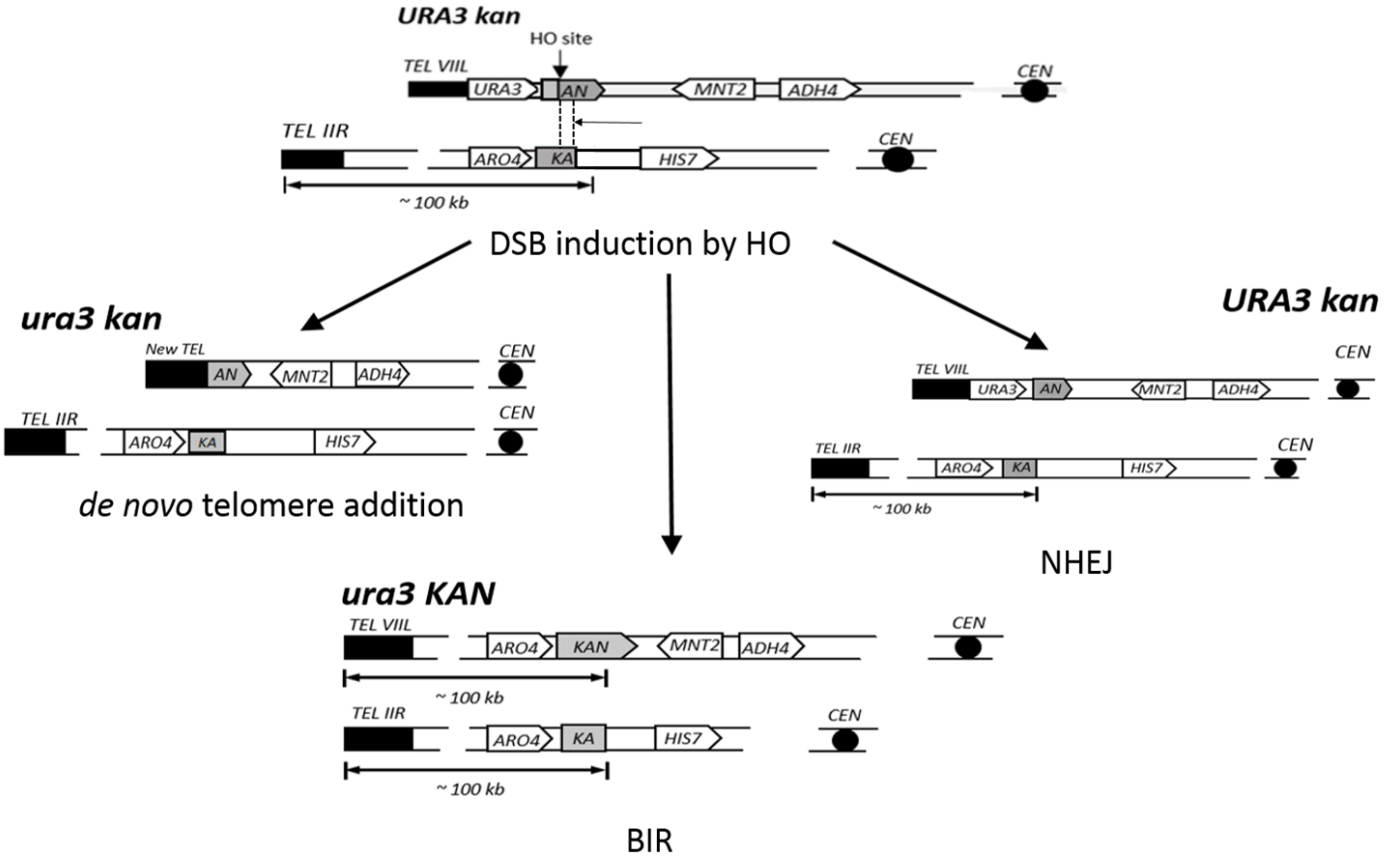

Figure 4.10: Schematic of possible genetic outcomes upon the induction of a DSB in the genetic system used for the plating assay of the BIR efficiency

Modified from Vasianovich, Harrington and Makovets, 2014

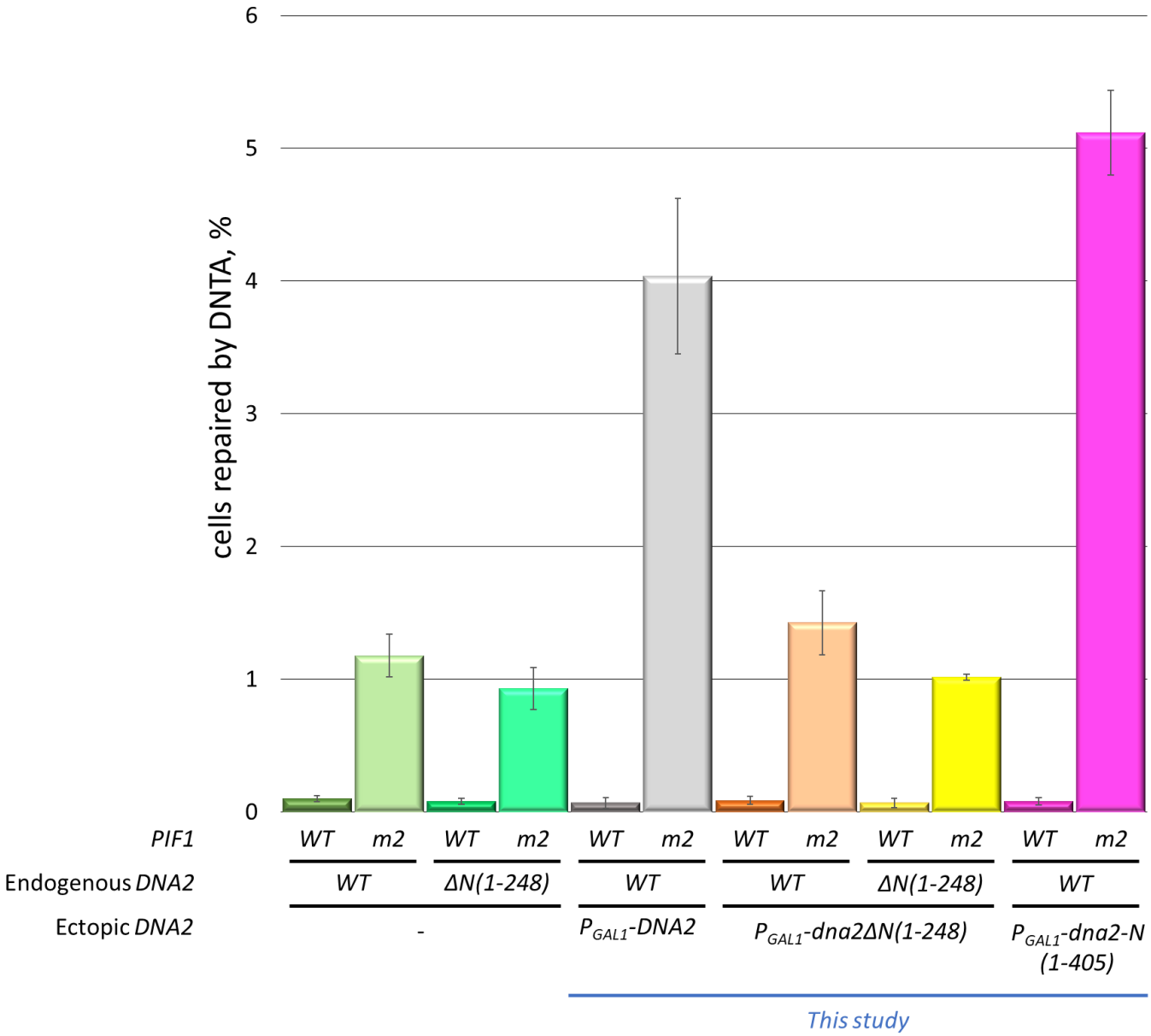

Figure 4.11: The effect of ectopic overexpression of either *DNA2* or its truncated forms on DNTA efficiency (combined data)

Mean frequency of DNTA was calculated from at least three technical repeats, except for *pif1-m2* P_{GAL1}-*DNA2* strains, where 2 repeats were used. Error bars correspond to standard deviation. Data for WT, *pif1-m2*, *dna2ΔN(1-248)* and *pif1-m2 dna2ΔN(1-248)* strains is from Y. Vasianovich (personal communication) and O. Kotenko (personal communication)

4.6. The effect of the overexpression of mutant *DNA2* alleles on checkpoint activation

As noted before (see section 4.5), overexpression of the full-length *DNA2* caused a decrease in the efficiency of BIR in the WT background and no increase in *pif1-m2* background. In an effort to find out, whether this effect could be linked to a specific catalytic activity of Dna2, the strains with the inducible DSB, carrying helicase-, nuclease- or catalytically-dead versions of ectopic *DNA2* under *GAL1* promoter were created and tested in the BIR plating assay. However, all the strains overexpressing mutant *DNA2* failed to form colonies on YPGal plates in both WT and *pif1-m2* backgrounds (data not shown). The lethality of *dna2Δ* has been previously attributed to persistent checkpoint activation due to the accumulation of long RPA-coated 5'-flaps generated by Pif1 out of the Okazaki fragments during DNA-replication in the absence of Dna2 needed to remove them (Budd *et al.*, 2011). It could therefore be proposed, that P_{GAL1}*-dna2-D657A* and P_{GAL1}*-dna2-K1080E* exert a dominant-negative effect by producing an excess of dysfunctional Dna2 protein that displaces the WT Dna2 from the RPA-coated flaps, thus inhibiting their cleavage and promoting the checkpoint activation. However, this explanation does not account for the inviability of the *pif1-m2* strains overexpressing dysfunctional *DNA2*, considering that *pif1-m2* has been shown to suppress *dna2Δ* lethality (Budd *et al.*, 2006).

To test whether the overexpression of the mutant versions of *DNA2* results in the checkpoint activation, the phosphorylation status of Rad53 was analysed in the strains with the overexpression of either the WT or the mutant *DNA2* variants (including the truncated versions). To that end, the cells were pre-grown in YPRaf media at 30°C and then the overexpression of the ectopic *DNA2* variants was induced by the addition of galactose and further incubation for three hours at 30°C. A detectable Rad53 mobility shift was observed in the cells overexpressing either the nuclease-dead *dna2-D657A* in both the WT and *pif1-m2* backgrounds or the nuclease- and helicase-dead *dna2-D657A,E1080K* in the WT background (Figure 4.12), indicating the DNA

damage checkpoint activation in the corresponding strains. Neither the full-length WT *DNA2*, nor its truncated versions produced any noticeable Rad53 band shift, consistent with the ability of the cells overexpressing these constructs to form colonies on YPGal plates. The lack of a detectable checkpoint activation upon overexpression of *dna2-N(1-405)* suggests, that Dna2-N(1-405) does not prevent the endogenous full-length Dna2 from cleaving the 5'-flaps of the Okazaki fragments during replication. Thus, the inviability of the cells overexpressing *DNA2* with disrupted nuclease activity may be due to persistent checkpoint.

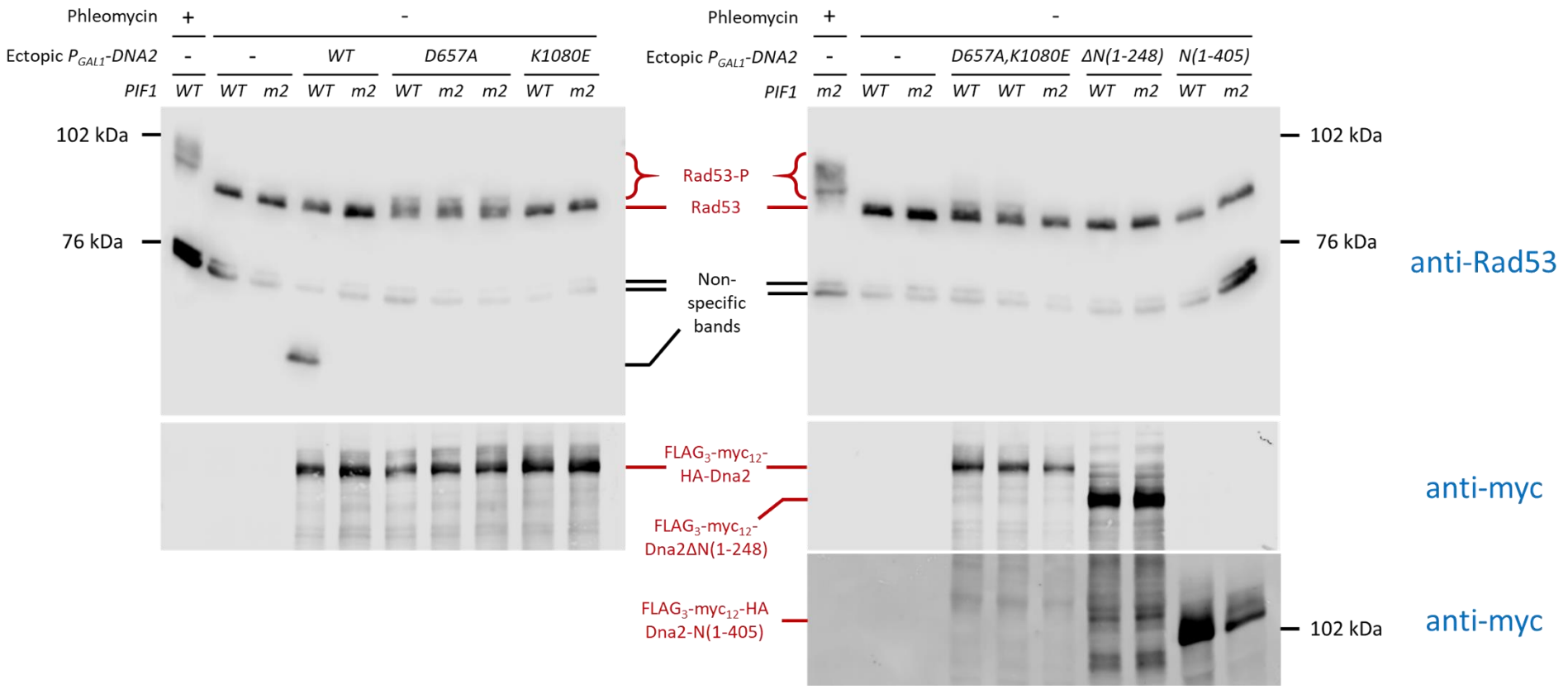

Figure 4.12: Overexpression of nuclease-dead *DNA2* (*dna2-D657A*) leads to Rad53 phosphorylation in WT and *pif1-m2* cells

Phleomycin was added to the final concentration of 2µg/mL (for 3 hours) to two cultures used as the positive control of Rad53 phosphorylation. *dna2-D657A* – nuclease-dead, *dna2-K1080E* – ATPase(helicase)-dead, *dna2-D657A,K1080E* – nuclease- and helicase-dead

4.7. *RAD27* overexpression inhibits BIR in both the WT and *pif1-m2* backgrounds

Both Rad27 and Dna2 play a role during DNA replication by removing 5'-flaps of the Okazaki fragments (Bae *et al.*, 2001). In contrast to Dna2, Rad27 is not essential for cell viability, although *rad27Δ* causes accumulation of single-stranded DNA and destabilization of telomeric repeats in yeast (Parenteau and Wellinger, 2015). Rad27 has been shown to physically interact with Dna2 in cells that overexpress both proteins (Budd and Campbell, 1997). However, the subsequent attempts to reconstitute the Dna2-Rad27 complex *in vitro* were unsuccessful, suggesting that either the interaction between the proteins is weak or it requires an additional bridging protein (Bae and Seo, 2000). It was later discovered by the Makovets' group that *rad27Δ* affects BIR similarly to *dna2ΔN(1-248)* in that it partially suppresses the BIR defect incurred by *pif1-m2*, but reduces the efficiency of BIR in WT cells (Figure 4.13). To further delineate the role of Rad27 in BIR, I assayed the effect of *RAD27* overexpression on BIR. Similarly to *DNA2* overexpression, an excess of the Rad27 nuclease resulted in a significant decrease in the BIR efficiency, in both WT and *pif1-m2* cells (Figure 4.13). Just as with *pif1-m2 dna2ΔN(1-248)* cells before and in contrast to *pif1-m2* cells no incidents of premature BIR termination were discovered in the PFGE-coupled Southern blot analysis of repair outcomes in nine $G418^R$ Ura^- clones (Figure 4.14), indicating proficiency for long-range BIR. Overall, the effects of *RAD27* on BIR were reminiscent of the effects exerted by *DNA2* (see Figure 4.13), raising a possibility of a common mechanism/complex underlying the functions of the two proteins in BIR.

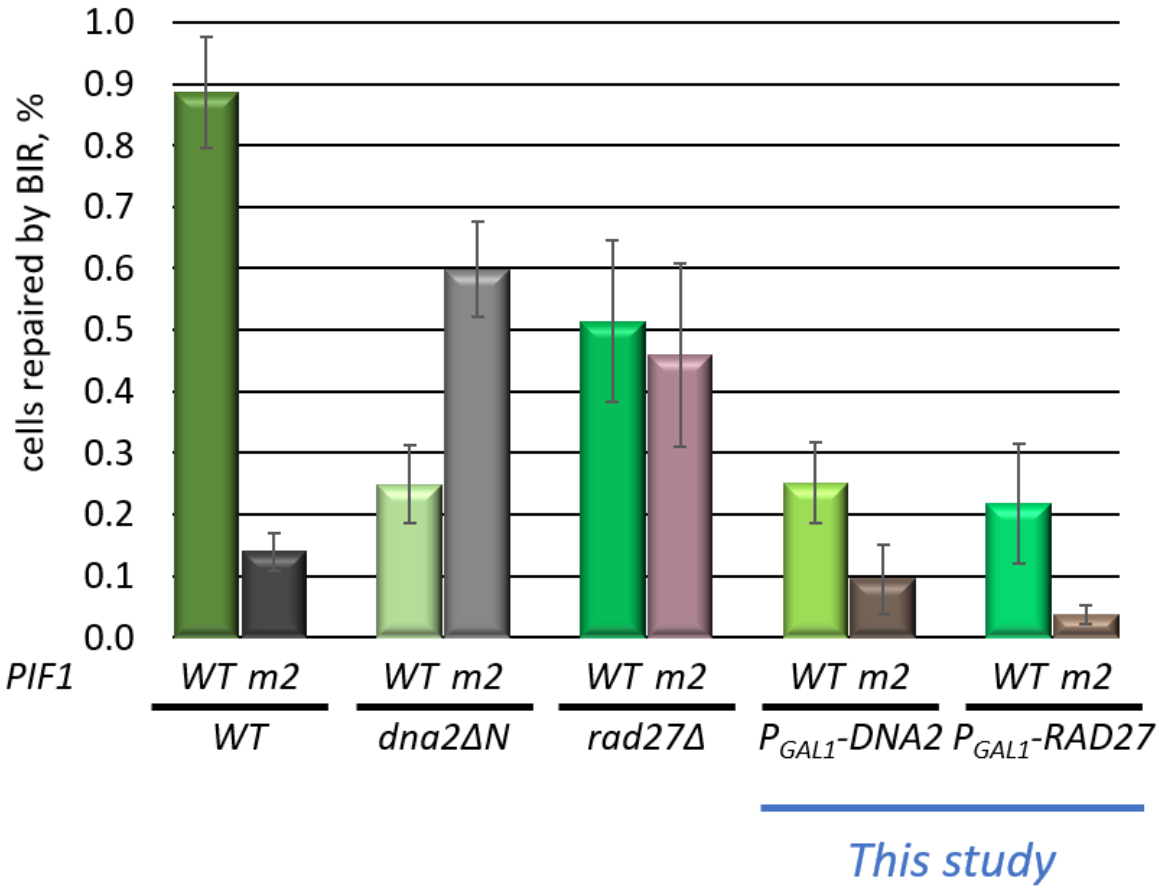

Figure 4.13: *RAD27* affects BIR similarly to *DNA2*

Combined data on the effects of *DNA2* and *RAD27* loss or overexpression on the efficiency of BIR in WT and *pif1-m2* cells. Data for WT, *pif1-m2*, *rad27Δ*, *pif1-m2 rad27Δ, dna2ΔN(1-248)* and *pif1-m2 dna2ΔN(1-248)* strains are from Vasianovich, Harrington and Makovets, 2014 and O. Kotenko (personal communication)

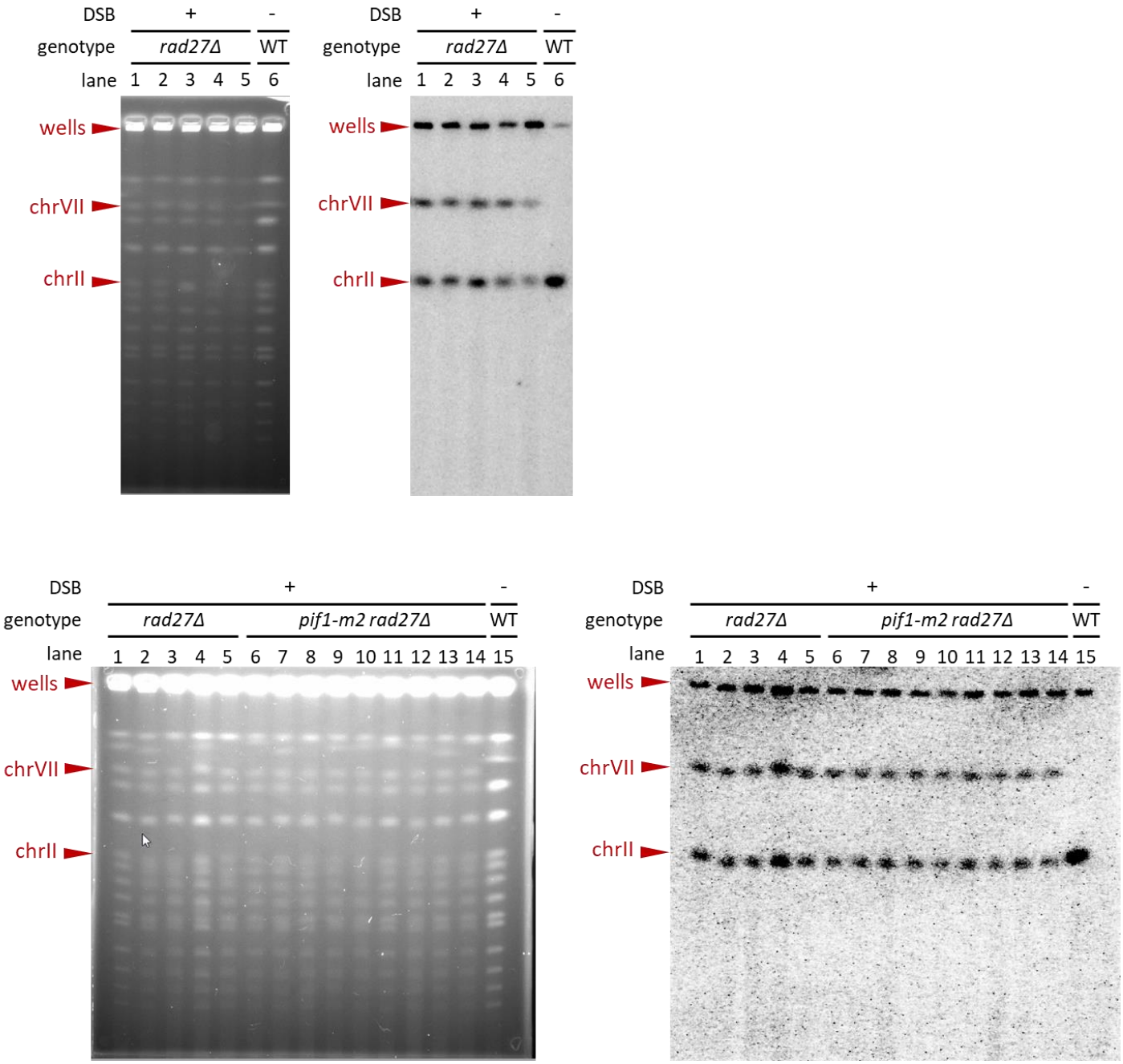

Figure 4.14: *rad27Δ* and *pif1-m2 rad27Δ* strains are capable of long-range BIR

Left side – pulse-field gels, right side – Southern blots. A WT strain with no DSB induction and 5 kb homology between chrVII and chrII was used as a negative control for chrVII probing. The rest of the strains have 500 bp homology between chrVII and chrII. All of the analysed clones successfully copied the probed region onto chrVII upon DSB induction, consistent with efficient long-range BIR

4.8. Sgs1 interacts with the N-terminus of Dna2

Dna2 is involved in a wide variety of functions in eukaryotic cells (Wanrooij and Burgers, 2015). Among these functions is the 5'-strand resection of a DSB, which Dna2 performs jointly with Sgs1 helicase in one of the two partially redundant DNA resection pathways (Zhu *et al.*, 2008; Cejka, Cannavo, *et al.*, 2010). Recombinant Dna2 and Sgs1 interact *in vitro* (Cejka, Cannavo, *et al.*, 2010). Previously, I observed that overexpression of either the full-length *DNA2* or *dna2-N(1-405)*, but not *dna2ΔN(1-248)*, was associated with increased DNTA in cells with an inducible DSB (see Figure 4.11). This effect was similar to the 3.5-fold increase in DNTA observed upon deletion of *SGS1* (Y. Vasianovich, personal communication), which likely results from a decrease in resection, since the resection has been shown to decrease the efficiency of DNTA (Chung *et al.*, 2010). The effect of *DNA2* or *dna2-N(1-405)* overexpression could thus be potentially explained by a hypothesis where the corresponding Dna2 proteins sequester Sgs1 from the DSB, thereby preventing Sgs1 from participating in the resection. Conversely, ectopic Dna2ΔN(1-248) fails to elevate DNTA, possibly due to the loss of the interaction with Sgs1, thus not being able to drive Sgs1 away from the full-length Dna2 at the DSB site. To test whether Dna2-N(1-405) can interact with Sgs1 *in vivo*, I performed co-immunoprecipitation of either the full-length Dna2 or Dna2-N(1-405) with Sgs1 under the conditions where all the involved proteins were overexpressed. Sgs1 co-immunoprecipitated with both the full-length and the C-terminally truncated versions of the protein (Figure 4.15), consistent with the proposed hypothesis (also see Figure 4.11). This result is in line with the recently demonstrated interaction between Dna2-N(1-405) and Sgs1 helicase domain in a yeast-two-hybrid system (Mojumdar *et al.*, 2019). Dna2ΔN(1-248) also could interact with Sgs1 (Figure 4.16). It could therefore be concluded that either there are several redundant regions in Dna2 responsible for the interaction with Sgs1 or that the only such region is located in the stretch between the 248th and the 405th amino acid residues, shared by both Dna2ΔN(1-248) and Dna2-N(1-405).

Identifying specific amino acid residues of Dna2 important for the interaction with Sgs1 could facilitate the creation of separation-of-function *DNA2* mutants, which would allow to evaluate the role of the aforementioned interaction in the various effects that *DNA2* and its truncated versions exert on BIR efficiency. To that end a set of nested *DNA2* truncations expressed from the *GAL1* promotor was introduced into *exo1Δ* cells with the inducible DSB. The strains were tested for the frequency of DNTA upon DSB induction as the metric of Sgs1 sequestration by the truncated Dna2 proteins (in cells lacking Exo1-dependent resection sequestration of Sgs1 from the DSB would result in a complete abruption of long-range resection and a prominent increase in DNTA frequency). A steep decrease in the frequency of DNTA was observed between the strains overexpressing *dna2-N(2-370)* and *dna2-N(2-309)* (Figure 4.17), suggesting that the interaction with of Dna2-N(1-405) with Sgs1 requires the stretch located between the amino acids 309 and 370 of Dna2-N(1-405). The results of this plating assay and the co-immunoprecipitation of Sgs1 with full-length and truncated Dna2 isoforms are consistent with the presence of at least one Sgs1-interacting region between amino acids 248 and 370 of Dna2. However, the absence of an increase in DNTA in cells with ectopic Dna2ΔN(1-248) (see Figure 4.11) suggests that interaction with Sgs1 is not sufficient to produce an increase in DNTA upon overexpression of truncated Dna2, which means that DNTA frequency is not a reliable proxy of Sgs1-Dna2 interaction. Thus, additional co-immunoprecipitation experiments are required to conclusively identify the Sgs1-interacting region of Dna2.

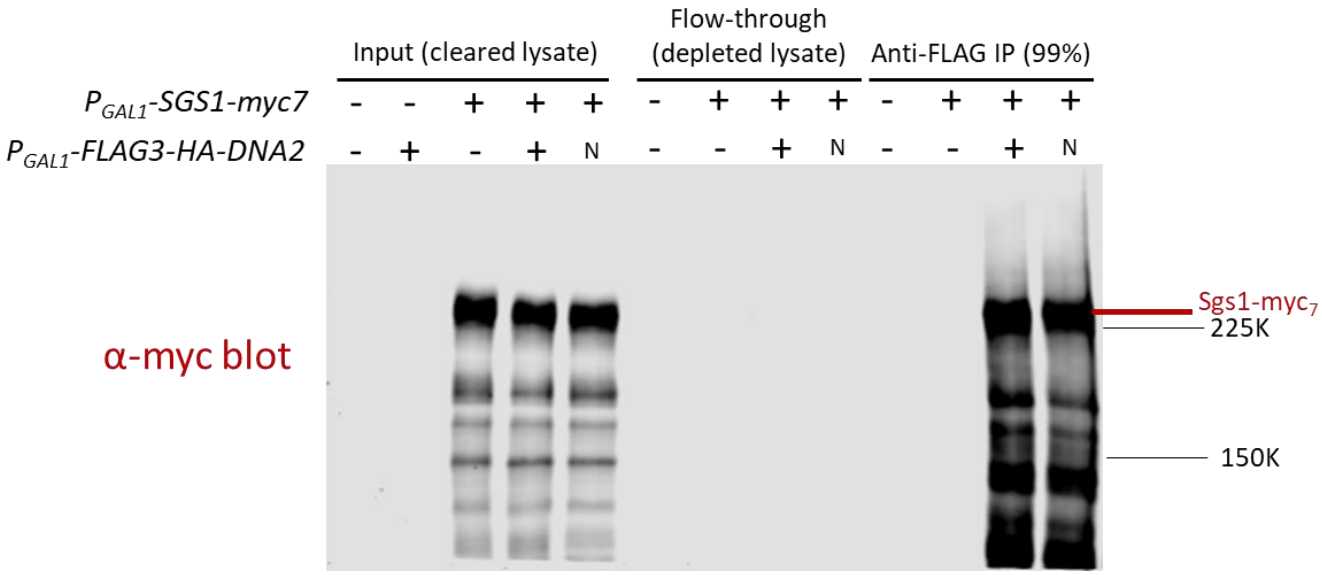

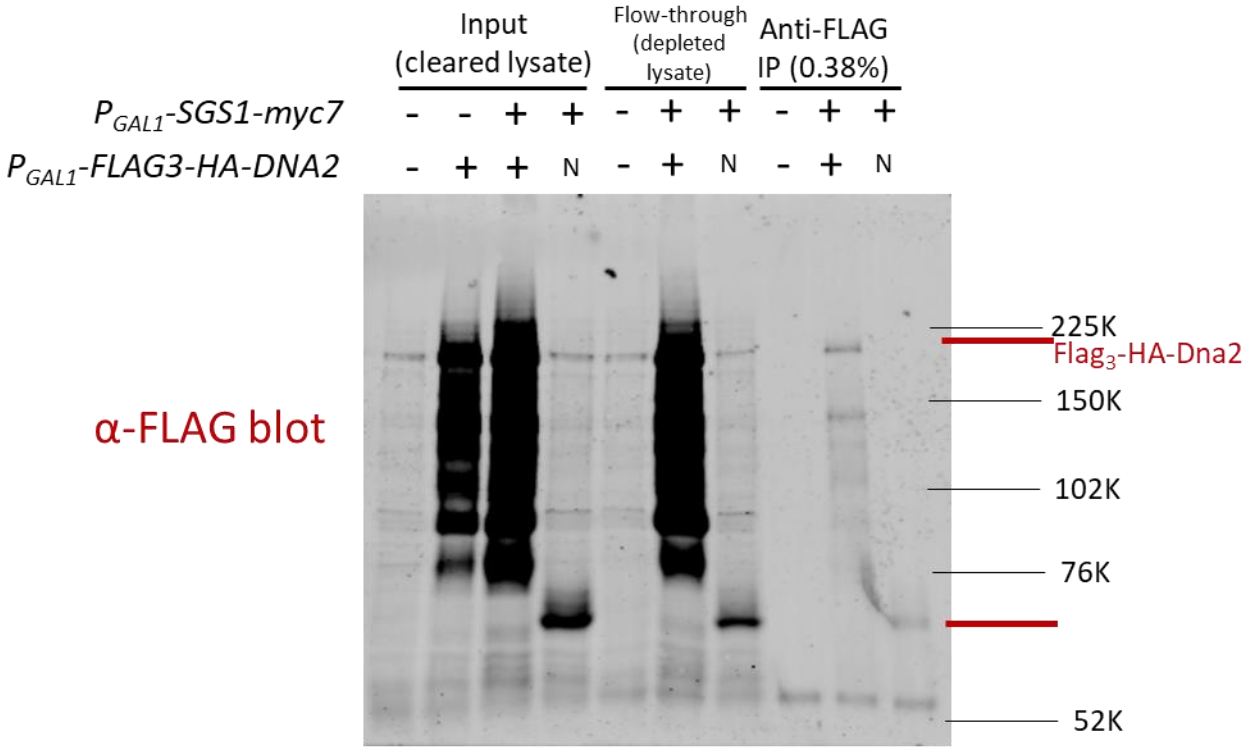

Figure 4.15: Sgs1 co-immunoprecipitates with Dna2 and Dna2-N(1-405)

N – P_{GAL1}-dna2-N(1-405)

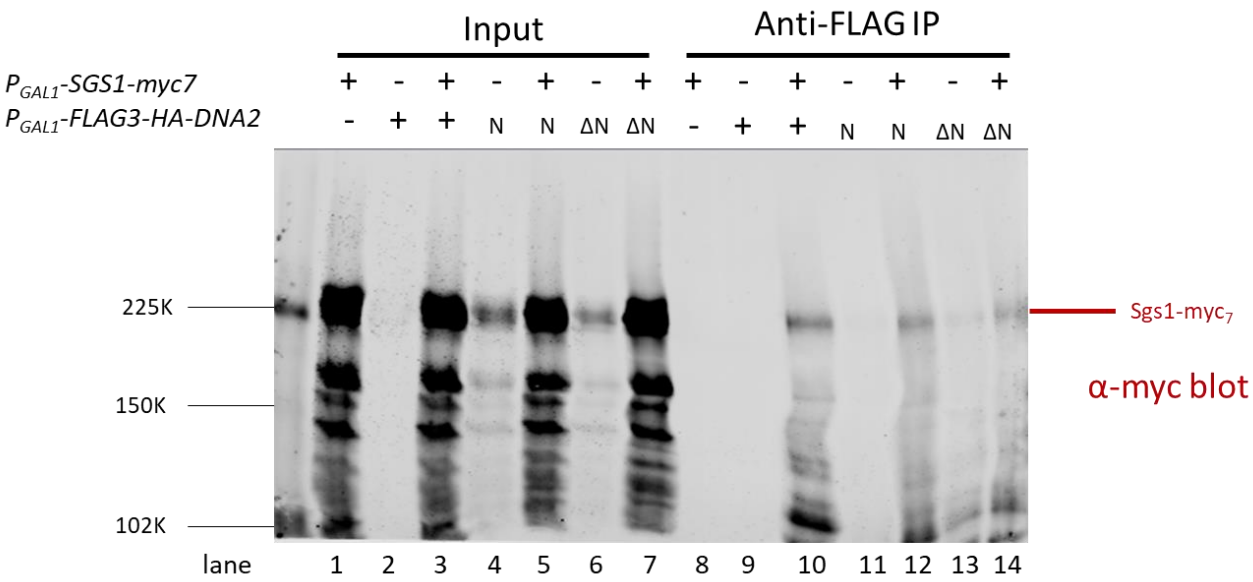

Figure 4.16: Sgs1 co-immunoprecipitates with Dna2, Dna2ΔN(1-248) and Dna2-N(1-405)

ΔN – *P_{GAL1}-dna2ΔN(1-248)*, N - *P_{GAL1}-dna2-N(1-405)*. Some degree of overflow from the neighboring lanes could be seen in lanes 4, 6 and 13

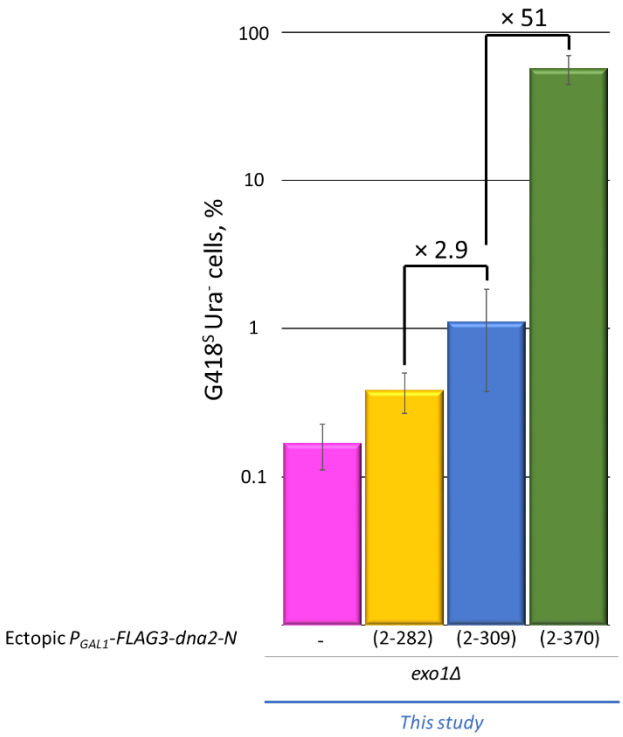

Figure 4.17: The frequency of DNTA in strains overexpressing various truncated versions of *DNA2*

Mean frequency of BIR was calculated from at least two technical repeats. Error bars correspond to standard deviation. Note the logarithmic scale of the vertical axis

4.9. Overexpression of Dna2 or its truncated forms does not affect the telomere length equilibrium in yeast

Both Dna2 and Pif1 are relevant to BIR. Given that overexpression of *DNA2* inhibits BIR (see Figure 4.9), it could be speculated, that Dna2 antagonizes Pif1. This speculation would be supported in case other instances of antagonism between Dna2 and Pif1 were found. Notably, the two proteins are also involved in the telomere biology. For instance, Pif1 inhibits telomerase at telomeres (Schulz and Zakian, 1994), while Dna2 has been found to associate with the telomeres throughout most of the cell cycle (Choe *et al.*, 2002) and proposed to modulate the DNA damage response at telomeres (Markiewicz-Potoczny, Lisby and Lydall, 2018). With the aim of getting a more detailed understanding of the genetic interaction between *DNA2* and *PIF1*, the effect of the ectopic overexpression of *DNA2* or its truncated forms on the telomere length equilibrium of WT and *pif1-m2* yeast grown at 30°C was investigated. Consistent with the previously reported observations (Schulz and Zakian, 1994), *pif1-m2* cells had elongated telomeres (Figure 4.18). The ectopic overexpression of *DNA2, dna2-D657A,E1080K* (nuclease- and helicase-dead), *dna2ΔN(1-248)* or *dna2-N(1-405)* did not produce any noticeable effect on the telomere length equilibrium in either the WT or the *pif1-m2* background. Thus, no genetic interaction between *DNA2* and *PIF1* was discovered at the level of telomeres.

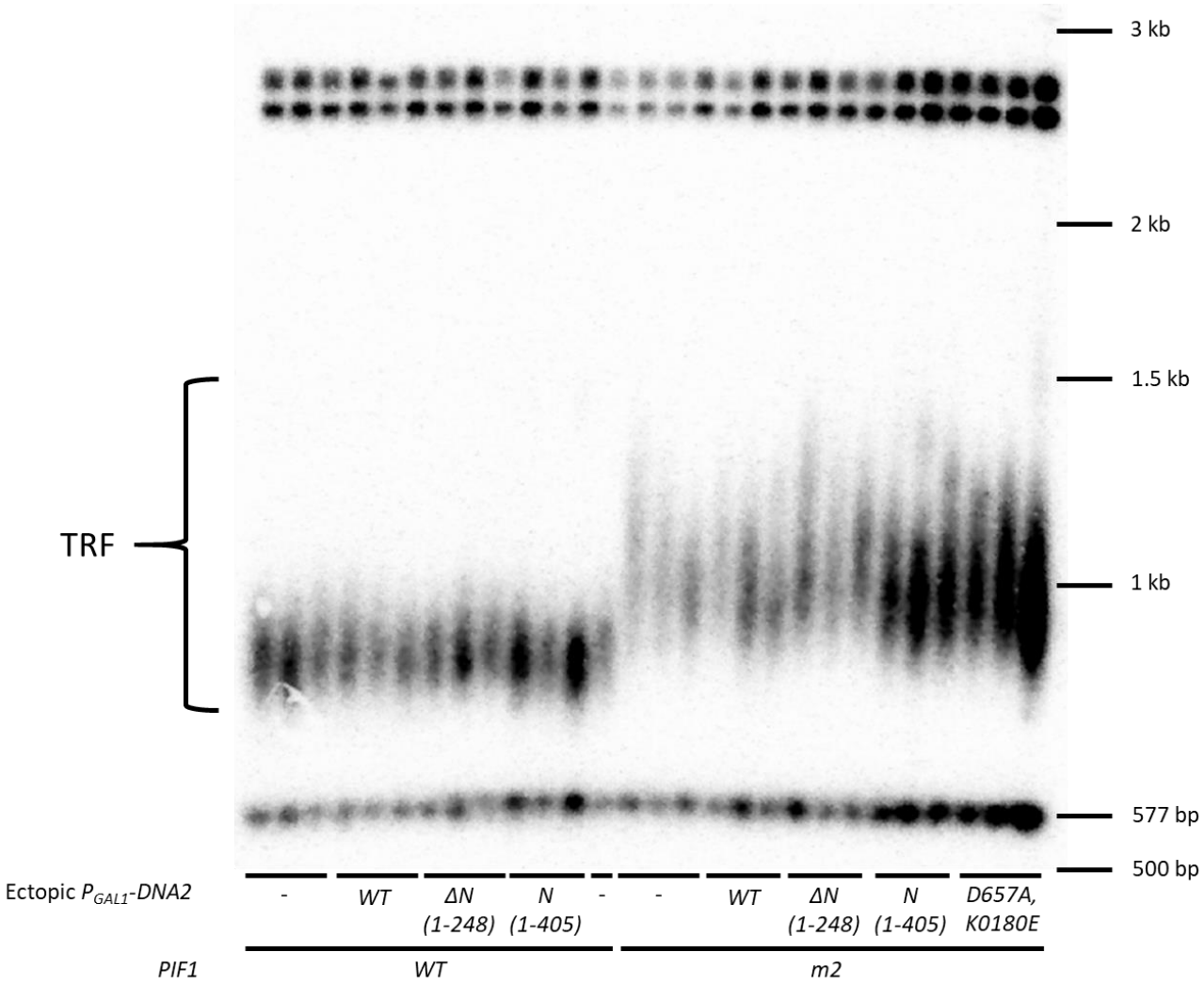

Figure 4.18: Telomere length equilibrium of strains continually overexpressing ectopic *DNA2* or its truncated/mutated forms at 30°C

Average Y-telomere length was analyzed after 5 passages on YPGal plates at 30°C. TRF – terminal restriction fragment. See section 2.8.10 and Figure 3.13 for the detailed method description

4.10. Discussion

Dna2 performs a variety of functions important for genome stability (Wanrooij and Burgers, 2015), increasing the chances that a mutation such as *dna2ΔN(1-248)* would have a pleiotropic effect. This might be one of the reasons behind the complex genetic interaction between *DNA2* and *PIF1* in BIR (see Figures 4.1 and 4.9). Several explanations could be brought forward to account for the results presented in this chapter.

4.10.1. The interplay between Pif1-dependent D-loop migration, the resection and the recombination execution checkpoint might determine BIR efficiency

The efficiency of BIR could be proposed to be the net result of a complex interplay between a number of factors and processes, as visualized in Figure 4.19. Such factors could include **recombination execution checkpoint (REC) (i)**, **DSB resection (ii)** and **Pif1-dependent D-loop migration (iii)**. Both DNA resection at a DSB and Pif1-dependent D-loop migration have been shown to promote BIR (Symington and Gautier, 2011; Wilson *et al.*, 2013). REC is performed by the Sgs1 and Mph1 helicases and exerts an inhibitory effect on BIR, possibly by destabilizing the D-loop (Jain *et al.*, 2009, 2016). Hypothetically, in WT cells Pif1 might strongly antagonize Sgs1 and Mph1 in the execution of the REC (Pif1 has the opposite polarity to Sgs1 and Mph1 and hence might displace them from the DNA strand, see Figure 4.19A and B). Consequently, in cells lacking nuclear Pif1 REC could be rampant (Figure 4.19C), further inhibiting BIR that is already down due to the lack of Pif1 D-loop migration function (Wilson *et al.*, 2013).

(i). The possible effects of *DNA2* alleles on recombination execution checkpoint in the context of BIR

A possible explanation for the partial suppression of BIR defect by *dna2ΔN(1-248)* in *pif1-m2* cells stems from the hypothetical effect of *dna2ΔN(1-248)* on

REC. The co-immunoprecipitation experiments performed in this study demonstrated that Dna2ΔN(1-248) interacts with Sgs1 (see Figure 4.16). It could be speculated, that Dna2ΔN(1-248), which has a lower-than WT level of recruitment to the DSB site (Chen *et al.*, 2011), causes reduced localization of Sgs1 to the D-loop, thereby hindering the Sgs1-dependent REC (Figure 4.19D). Thus in *pif1-m2* background *dna2ΔN(1-248)* may promote BIR by inhibiting runaway REC.

It could also be proposed that the increase in BIR upon *dna2ΔN(1-248)* or *dna2-N(1-405)* overexpression in *dna2ΔN(1-248)* background (Figure 4.9) is due to intensified sequestration of Sgs1 from the D-loop by ectopic truncated Dna2 species, causing a severe REC defect (see Figure 4.19F).

(ii). The possible effects of *DNA2* alleles on resection

However, if REC inhibition by *dna2ΔN(1-248)* promotes BIR, it is not clear why *dna2ΔN(1-248)* does not increase the efficiency of BIR in WT background and instead decreases it. Here I propose a model, which links the decrease of BIR efficiency upon introduction of *dna2ΔN(1-248)* into WT cells to a hypothetical increase in the interaction between Pif1 and Dna2ΔN(1-248) following the removal of Dna2 N-terminus (Figure 4.19E). The postulated strong Pif1-Dna2ΔN(1-248) interaction might result from the removal of the part of Dna2, responsible for favoring the interaction with Sgs1 over the interaction with Pif1. Correspondingly, in *dna2ΔN(1-248)* cells the competition between Pif1 and Sgs1 for the association with Dna2ΔN(1-248) might be exacerbated compared to WT cells, dampening functions depending on the interaction between Dna2ΔN(1-248) and Sgs1.

One of such functions could be Sgs1-dependent resection at the DSB. It is reasonable to assume that attenuated Sgs1-resection would reduce BIR efficiency, given the importance of resection for BIR and that Sgs1 and Dna2 act together in the major pathway for the long-range resection (Zhu *et al.*, 2008). On a separate note, the importance of the Sgs1-dependent resection for BIR could also be the reason why the Dna2ΔN(1-248) nuclease activity is required for the suppression of the BIR defect in *pif1-m2* cells (see Figure 4.6),

since the removal of nuclease activity of Dna2ΔN(1-248) would completely abrogate any Sgs1-dependent resection.

Meanwhile, the absence of the nuclease domain in Dna2-N(1-405) prevents Dna2-N(1-405)-Sgs1 complex from participating in the resection, possibly accounting for the less pronounced gain in the BIR efficiency observed in *dna2ΔN(1-248)* cells overexpressing *dna2-N(1-405)* instead of *dna2ΔN(1-248)*.

The hypothesis stating that some effects of *dna2ΔN(1-248)* on BIR are mediated by changes in resection efficiency is subject to several caveats. First of all, the helicase activity of Dna2ΔN(1-248) appears to be dispensable for its suppressive effect on BIR in *pif1-m2* cells (see Figure 4.6), but recently P. Cejka's group have discovered a noticeable drop in the Sgs1-dependent resection efficiency in cells harboring helicase-dead *dna2-K1080E*, albeit in an *exo1Δ* background (Levikova, Pinto and Cejka, 2017). Secondly, the overall significance of the Sgs1-dependent resection for BIR in cells expressing *EXO1* and possessing only 500 bp of homology between the broken end and an ectopic template may itself be questionable.

(iii). The possible effects of *DNA2* alleles on D-loop migration in the context of BIR

Intensified interaction between Pif1 and Dna2ΔN(1-248), proposed above, might also hamper Pif1-dependent D-loop migration due to the sequestration of Pif1 away from the D-loop by Dna2ΔN(1-248) deficient in nuclear localization (see Figure 4.19E and F). However, the effect of overexpression of *dna2ΔN(1-248)* on BIR in *dna2ΔN(1-248)* background (see Figure 4.9) is not consistent with this notion, as ectopic Dna2ΔN(1-248) would be expected to decrease BIR through sequestration of Pif1 from the D-loop, when, in fact, ectopic Dna2ΔN(1-248) promotes BIR in the presence of Pif1.

(iv). Why *DNA2* overexpression inhibits BIR. Explanations from the viewpoint of REC and DSB resection

The inhibitory effect of *DNA2* overexpression on BIR (Figure 4.9) may be due to the enhanced recruitment of Sgs1 to the D-loop that leads to a stricter recombination execution checkpoint. Alternatively, BIR inhibition could result from excessive resection upon overexpression of *DNA2*, as could be inferred with the previously published decrease in BIR efficiency upon overexpression of *EXO1* or *SGS1* (Lydeard *et al.*, 2010). This idea also provides an alternative viewpoint as to the nature of the partial BIR rescue by *dna2ΔN(1-248)*, which could stem from the possibility of a less extensive resection upon removal of the N-terminus of Dna2 being more optimal for efficient BIR in *pif1-m2* cells. However the elevation of DNTA (see Figure 4.11) argues strongly against the possibility of intensified resection upon overexpression of *DNA2*, considering that resection inhibits DNTA (Chung *et al.*, 2010).

A

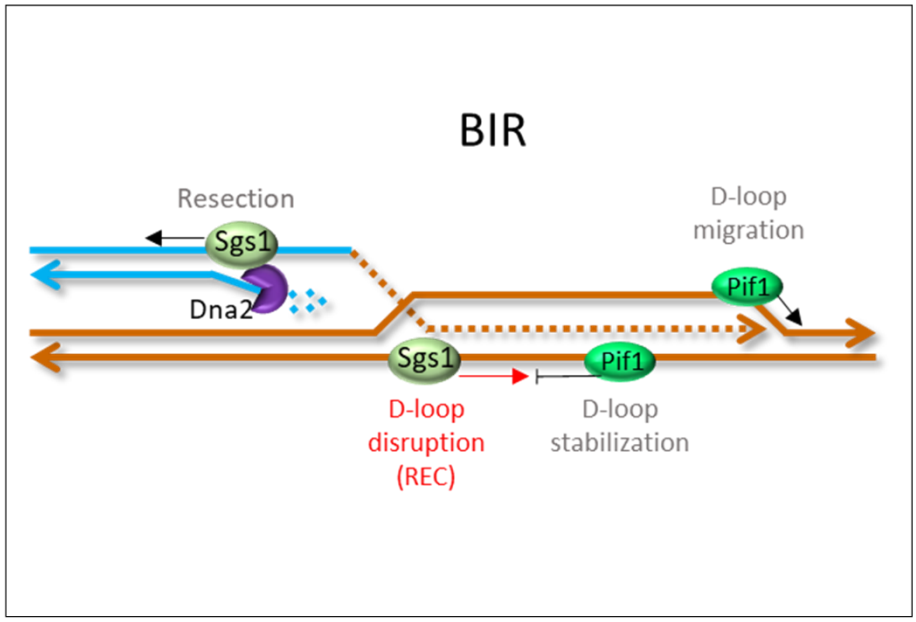
BIR
Resection
Sgs1
Dna2
D-loop
migration
Pif1
Sgs1
Pif1
D-loop
disruption
(REC)
D-loop
stabilization

B

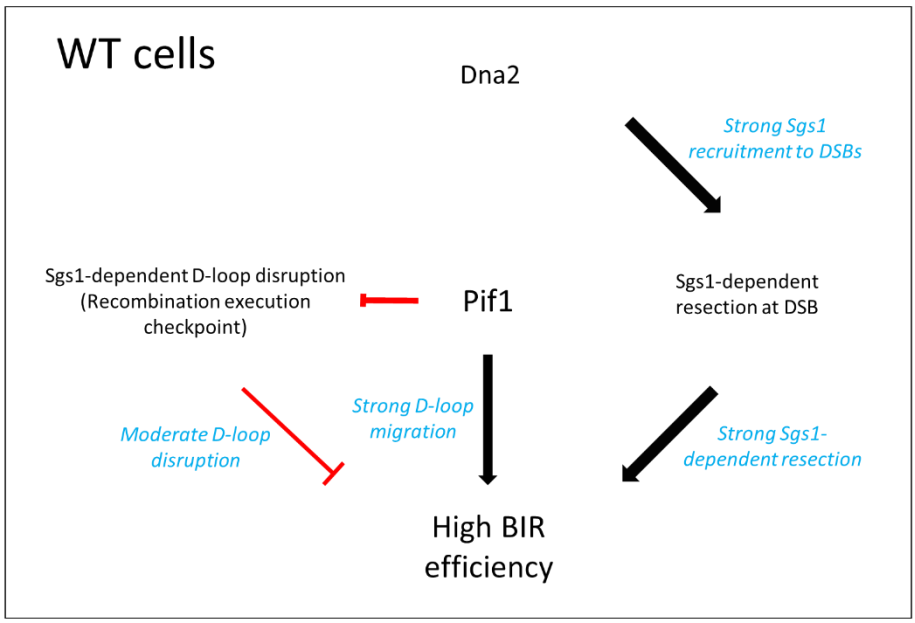
WT cells
Dna2
Strong Sgs1
recruitment to DSBs
Sgs1-dependent D-loop disruption
(Recombination execution
checkpoint)
Pif1
Sgs1-dependent
resection at DSB
Moderate D-loop
disruption
Strong D-loop
migration
Strong Sgs1-
dependent resection
High BIR
efficiency

C

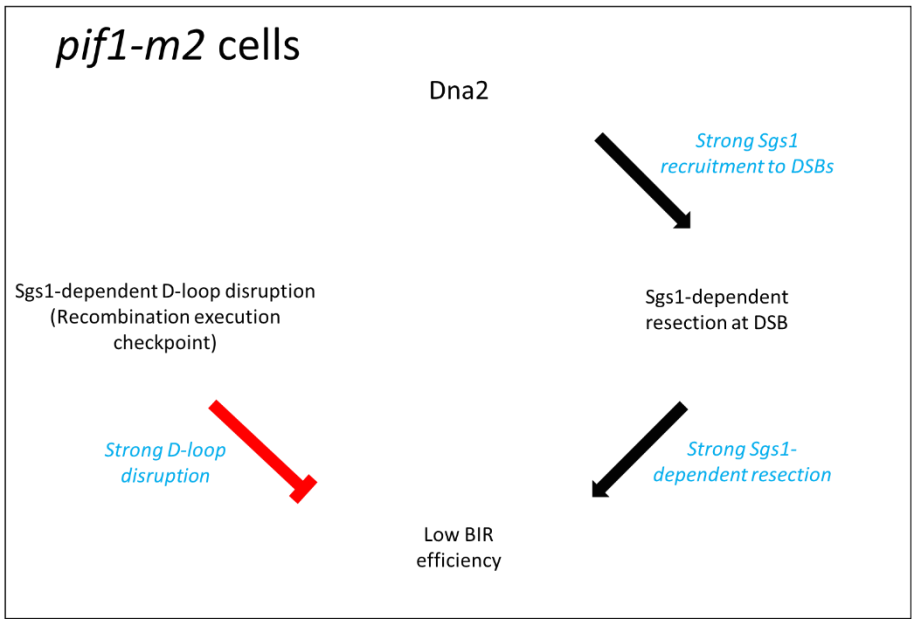
pif1-m2 cells
Dna2
Strong Sgs1
recruitment to DSBs
Sgs1-dependent D-loop disruption
(Recombination execution
checkpoint)
Sgs1-dependent
resection at DSB
Strong D-loop
disruption
Strong Sgs1-
dependent resection
Low BIR
efficiency

D

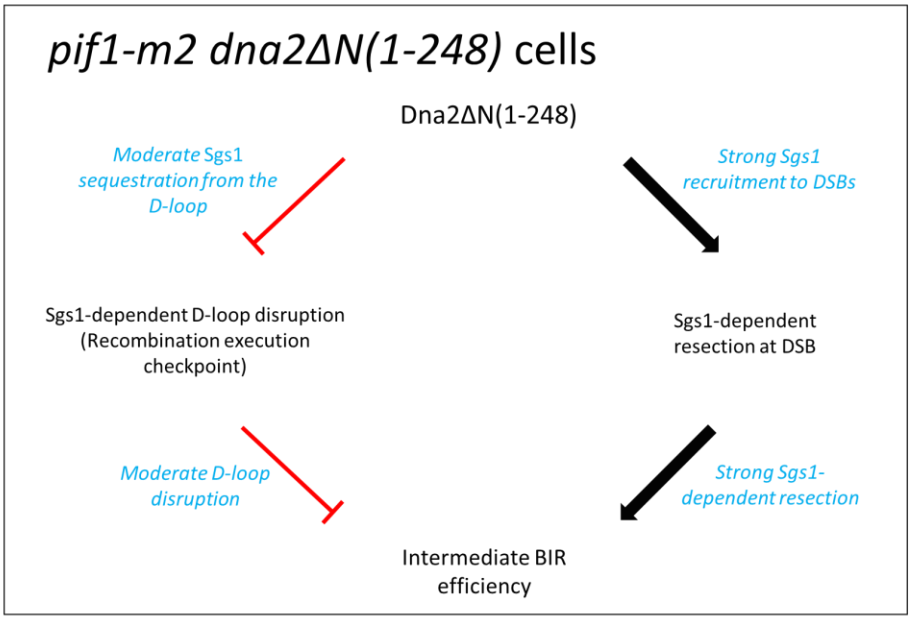
pif1-m2 dna2ΔN(1-248) cells
Dna2ΔN(1-248)
Moderate Sgs1 sequestration from the D-loop
Strong Sgs1 recruitment to DSBs
Sgs1-dependent D-loop disruption (Recombination execution checkpoint)
Sgs1-dependent resection at DSB
Moderate D-loop disruption
Strong Sgs1-dependent resection
Intermediate BIR efficiency

E

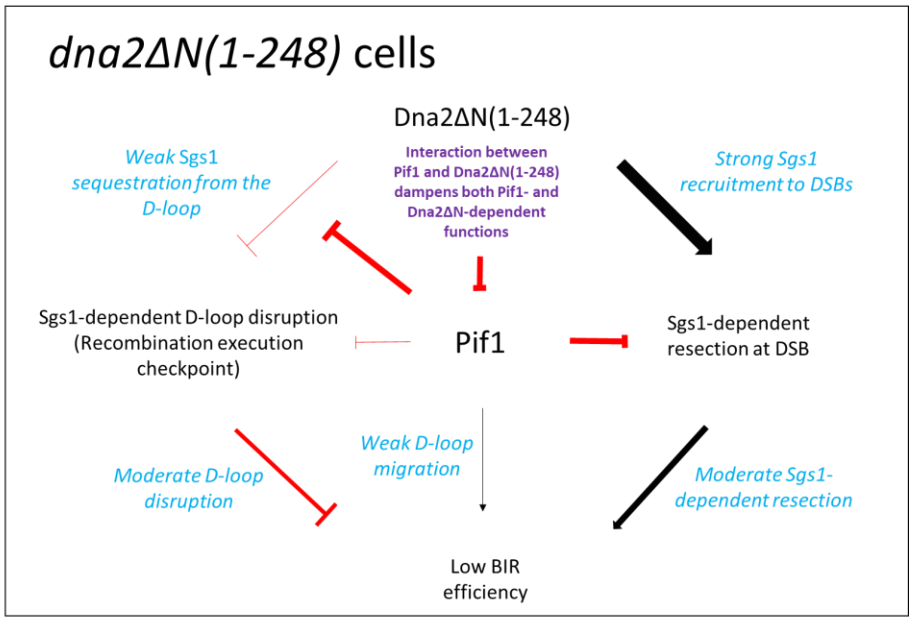
dna2ΔN(1-248) cells
Dna2ΔN(1-248)
Weak Sgs1 sequestration from the D-loop
Interaction between Pif1 and Dna2ΔN(1-248) dampens both Pif1- and Dna2ΔN-dependent functions
Strong Sgs1 recruitment to DSBs
Sgs1-dependent D-loop disruption (Recombination execution checkpoint)
Pif1
Sgs1-dependent resection at DSB
Moderate D-loop disruption
Weak D-loop migration
Moderate Sgs1-dependent resection
Low BIR efficiency

F

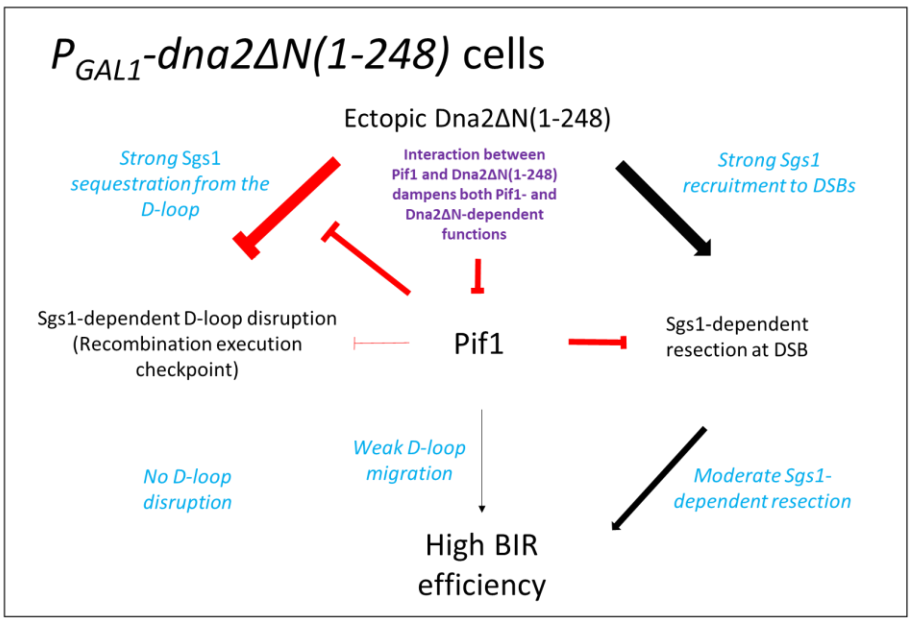
P GAL1 -dna2ΔN(1-248) cells
Ectopic Dna2ΔN(1-248)
Strong Sgs1 sequestration from the D-loop
Interaction between Pif1 and Dna2ΔN(1-248) dampens both Pif1- and Dna2ΔN-dependent functions
Strong Sgs1 recruitment to DSBs
Sgs1-dependent D-loop disruption (Recombination execution checkpoint)
Pif1
Sgs1-dependent resection at DSB
No D-loop disruption
Weak D-loop migration
Moderate Sgs1-dependent resection
High BIR efficiency

Figure 4.19: Hypothetical model of the interplay between resection, REC and D-loop migration in BIR in cells with different genotypes

A – an overview of factors affecting BIR. Both resection by Sgs1-Dna2 and Pif1-facilitated D-loop migration promote BIR. Sgs1-dependent D-loop disruption inhibits BIR, but is being counteracted by Pif1. B-F – Models depicting different contributions of the three factors to BIR efficiency depending on genetic background. B – in WT cells both DSB resection and D-loop migration are efficient and Sgs1-dependent D-loop disruption is moderate due to Pif1-dependent removal of Sgs1 from the D-loop. C – in *pif1-m2* cells lack of nuclear Pif1 leads to both inefficient D-loop migration and unrestrained Sgs1-dependent D-loop disruption. D – in *pif1-m2 dna2ΔN(1-248)* cells BIR is partially rescued due to sequestration of Sgs1 away from the D-loop resulting in lower level of Sgs1-dependet D-loop disruption. E – in *dna2ΔN(1-248)* cells there is an antagonism between Pif1 and Dna2ΔN(1-248) due to their strong association. Pif1 outcompetes Sgs1 from the complex with Dna2ΔN(1-248), thus hampering Sgs1-dependent resection. However, Pif1 also decreases the extent of Dna2ΔN(1-248)-dependent sequestration of Sgs1 from the D-loop, resulting in stronger REC. In addition, Dna2ΔN(1-248) sequesters Pif1 from the D-loop, thus hindering D-loop migration. F – overexpression of *dna2ΔN(1-248)* in *dna2ΔN(1-248)* background abrogates Sgs1-dependet D-loop disruption resulting in BIR upregulation

4.10.2. The BIR efficiency might be affected by the competition between Pol δ and either Dna2 or Rad27 for PCNA.

It could be the case, that an excess of Dna2 or Rad27, both of which associate physically with PCNA (Gomes and Burgers, 2000; Krogan *et al.*, 2006; Levikova and Cejka, 2015), inhibits BIR by competitive displacement of the Pol32 subunit of Pol δ from PCNA. Earlier, John R. Lydeard *et al.* have observed an almost two-fold decrease in BIR repair upon the removal of the PCNA-interacting domain of Pol32, indicating the importance of Pol32-PCNA interaction for BIR (Lydeard *et al.*, 2007). Meanwhile, another group has discovered that pcna-90 and pcna-79 mutants, in which the PCNA protein is defective for the interaction with Pol32 and the other two subunits of Pol δ, respectively, result in lower DNA polymerization processivity when combined with Pol δ *in vitro* compared to the combination of WT PCNA and Pol δ (Johansson, Garg and Burgers, 2004).

4.10.3. Okazaki-fragment flaps might serve as recruitment pads for BIR-promoting factors

The parallels between the effects exerted on BIR efficiency in WT and *pif1-m2* cells by *dna2ΔN(1-248)* and *rad27Δ* as well as the matching levels of BIR inhibition upon overexpression of either *DNA2* or *RAD27* (see Figure 4.13) may indicate that the two proteins share a common function in BIR. More to the point, the two proteins have been co-immunoprecipitated (Budd and Campbell, 1997), although their direct physical interaction has been questioned, since the attempts to reconstitute Dna2-Rad27 complex *in vitro* were unsuccessful (Bae and Seo, 2000). Given the lack of any reported participation of Rad27 in DNA resection and considering the highly-documented role of the two proteins in Okazaki fragment metabolism (Ayyagari *et al.*, 2003; Zheng and Shen, 2011; Balakrishnan and Bambara, 2013), it stands to reason to suggest that Okazaki fragment metabolism may be the key to the roles of Dna2 and Rad27 in BIR. Dna2 and Rad27 cleave 5'-

flaps of Okazaki fragments. Interestingly, Pif1 plays an opposite role in Okazaki fragment metabolism promoting the formation of long flaps (Pike *et al.*, 2009). It could be the case, that one of the roles of Pif1 in BIR is generation of long flaps, which may be somehow involved in BIR, e.g. by recruiting proteins participating in the lagging strand synthesis. Accordingly, Rad27 and Dna2 might be inhibiting BIR by removal of the flaps along with BIR-promoting factors from the lagging strand.

References

Abreu, E. *et al.* (2010) 'TIN2-Tethered TPP1 Recruits Human Telomerase to Telomeres In Vivo', *Molecular and Cellular Biology*. doi: 10.1128/mcb.00240-10.

Agmon, N. *et al.* (2009) 'Analysis of repair mechanism choice during homologous recombination', *Nucleic Acids Research*, 37(15), pp. 5081–5092. doi: 10.1093/nar/gkp495.

Amiard, S. *et al.* (2007) 'A topological mechanism for TRF2-enhanced strand invasion', *Nature Structural and Molecular Biology*. doi: 10.1038/nsmb1192.

Andriuskevicius, T., Kotenko, O. and Makovets, S. (2018) 'Putting together and taking apart: assembly and disassembly of the Rad51 nucleoprotein filament in DNA repair and genome stability', 2(5), pp. 96–112. doi: 10.15698/cst2018.05.134.

Arat, N. Ö. and Griffith, J. D. (2012) 'Human Rap1 interacts directly with telomeric DNA and regulates TRF2 localization at the telomere', *Journal of Biological Chemistry*. doi: 10.1074/jbc.M112.415984.

Artandl, S. E. *et al.* (2000) 'Telomere dysfunction promotes non-reciprocal translocations and epithelial cancers in mice', *Nature*. doi: 10.1038/35020592.

Ayyagari, R. *et al.* (2003) 'Okazaki fragment maturation in yeast: I. Distribution of functions between FEN1 and DNA2', *Journal of Biological Chemistry*. doi: 10.1074/jbc.M209801200.

Bae, S.-H. *et al.* (2001) 'RPA governs endonuclease switching during processing of Okazaki fragments in eukaryotes', *Nature*. Nature Publishing Group, 412(6845), pp. 456–461. doi: 10.1038/35086609.

Bae, S.-H. (2001) 'Tripartite structure of Saccharomyces cerevisiae Dna2 helicase/endonuclease', *Nucleic Acids Research*. doi: 10.1093/nar/29.14.3069.

Bae, S.-H. and Seo, Y.-S. (2000) 'In vitro evidence that purified yeast Rad27

and Dna2 are not stably associated with each other suggests that an additional protein (s) is required for a complex formation', *BMB Reports*. Korean Society for Biochemistry and Molecular Biology, 33(2), pp. 155–161.

Bajon, E., Laterreur, N. and Wellinger, R. J. (2015) 'A Single Templating RNA in Yeast Telomerase', *Cell Reports*, 12(3), pp. 441–448. doi: 10.1016/j.celrep.2015.06.045.

Balakrishnan, L. and Bambara, R. A. (2013) 'Okazaki fragment metabolism', *Cold Spring Harbor Perspectives in Biology*. doi: 10.1101/cshperspect.a010173.

Bardwell, A. J. *et al.* (1994) 'Specific cleavage of model recombination and repair intermediates by the yeast Rad1-Rad10 DNA endonuclease', *Science*. doi: 10.1126/science.8091230.

Baumann, P. and Cech, T. R. (2001) 'Pot1, the putative telomere end-binding protein in fission yeast and humans', *Science*. doi: 10.1126/science.1060036.

Beattie, T. L. *et al.* (2001) 'Functional multimerization of the human telomerase reverse transcriptase', *Mol Cell Biol*, 21(18), pp. 6151–6160.

Bhargava, R., Onyango, D. O. and Stark, J. M. (2016) 'Regulation of Single-Strand Annealing and its Role in Genome Maintenance', *Trends in Genetics*. doi: 10.1016/j.tig.2016.06.007.

Bianchi, A. *et al.* (1997) 'TRF1 is a dimer and bends telomeric DNA', *EMBO Journal*. doi: 10.1093/emboj/16.7.1785.

Bianchi, A. and Shore, D. (2008) 'How Telomerase Reaches Its End: Mechanism of Telomerase Regulation by the Telomeric Complex', *Molecular Cell*, 31(2), pp. 153–165. doi: 10.1016/j.molcel.2008.06.013.

Bishop, D. K. *et al.* (1992) 'DMC1: A meiosis-specific yeast homolog of E. coli recA required for recombination, synaptonemal complex formation, and cell cycle progression', *Cell*. doi: 10.1016/0092-8674(92)90446-J.

Biswas, H. *et al.* (2019) 'Ddc2ATRIP promotes Mec1ATR activation at RPA-

ssDNA tracts', *PLOS Genetics*. doi: 10.1371/journal.pgen.1008294.

Bondos, S. E. and Bicknell, A. (2003) 'Detection and prevention of protein aggregation before, during, and after purification', *Analytical Biochemistry*. doi: 10.1016/S0003-2697(03)00059-9.

Bonetti, D. *et al.* (2010) 'Shelterin-like proteins and Yku inhibit nucleolytic processing of Saccharomyces cerevisiae telomeres', *PLoS Genetics*, 6(5), p. 1. doi: 10.1371/journal.pgen.1000966.

Borde, V. and de Massy, B. (2013) 'Programmed induction of DNA double strand breaks during meiosis: Setting up communication between DNA and the chromosome structure', *Current Opinion in Genetics and Development*. doi: 10.1016/j.gde.2012.12.002.

Boulton, S. J. and Jackson, S. P. (1996) 'Identification of a Saccharomyces cerevisiae Ku80 homologue: roles in DNA double strand break rejoining and in telomeric maintenance.', *Nucleic acids research*, 24(23), pp. 4639–48. doi: 10.1093/nar/24.23.4639.

Bressan, D. A., Baxter, B. K. and Petrini, J. H. J. (1999) ' The Mre11-Rad50-Xrs2 Protein Complex Facilitates Homologous Recombination-Based Double-Strand Break Repair in Saccharomyces cerevisiae ', *Molecular and Cellular Biology*. doi: 10.1128/mcb.19.11.7681.

Broach, J. R. (2012) 'Nutritional control of growth and development in yeast', *Genetics*, 192(1), pp. 73–105. doi: 10.1534/genetics.111.135731.

Broccoli, D. *et al.* (1997) 'Human telomeres contain two distinct Myb-related proteins, TRF1 and TRF2', *Nature Genetics*. doi: 10.1038/ng1097-231.

Brown, T. (2001) 'Dot and slot blotting of DNA.', *Current protocols in molecular biology / edited by Frederick M. Ausubel ... [et al.]*, Chapter 2, p. Unit2.9B. doi: 10.1002/0471142727.mb0209bs21.

Budd, M. E. *et al.* (2006) 'Evidence Suggesting that Pif1 Helicase Functions in DNA Replication with the Dna2 Helicase/Nuclease and DNA Polymerase ', *Molecular and Cellular Biology*. doi: 10.1128/MCB.26.7.2490-2500.2006.

Budd, M. E. *et al.* (2011) ‘Inviability of a DNA2 deletion mutant is due to the DNA damage checkpoint’, *Cell Cycle*. doi: 10.4161/cc.10.10.15643.

Budd, M. E. and Campbell, J. L. (1997) ‘A yeast replicative helicase, Dna2 helicase, interacts with yeast FEN-1 nuclease in carrying out its essential function.’, *Molecular and Cellular Biology*. doi: 10.1128/mcb.17.4.2136.

Budd, M. E., Choe, W. C. and Campbell, J. L. (1995) ‘DNA2 encodes a DNA helicase essential for replication of eukaryotic chromosomes’, *Journal of Biological Chemistry*, 270(45), pp. 26766–26769. doi: 10.1074/jbc.270.45.26766.

Budd, M. E., Choe, W. C. and Campbell, J. L. (2000) ‘The nuclease activity of the yeast Dna2 protein, which is related to the RecB-like nucleases, is essential in vivo’, *Journal of Biological Chemistry*. doi: 10.1074/jbc.M909511199.

Buzovetsky, O. *et al.* (2017) ‘Role of the Pif1-PCNA Complex in Pol δ-Dependent Strand Displacement DNA Synthesis and Break-Induced Replication’, *Cell Reports*. doi: 10.1016/j.celrep.2017.10.079.

Cannavo, E. and Cejka, P. (2014) ‘Sae2 promotes dsDNA endonuclease activity within Mre11-Rad50-Xrs2 to resect DNA breaks’, *Nature*. doi: 10.1038/nature13771.

Cejka, P., Cannavo, E., *et al.* (2010) ‘DNA end resection by Dna2-Sgs1-RPA and its stimulation by Top3-Rmi1 and Mre11-Rad50-Xrs2’, *Nature*. doi: 10.1038/nature09355.

Cejka, P., Plank, J. L., *et al.* (2010) ‘Rmi1 stimulates decatenation of double Holliday junctions during dissolution by Sgs1-Top3’, *Nature Structural and Molecular Biology*. doi: 10.1038/nsmb.1919.

Celli, G. B., Denchi, E. L. and de Lange, T. (2006) ‘Ku70 stimulates fusion of dysfunctional telomeres yet protects chromosome ends from homologous recombination’, *Nature Cell Biology*. doi: 10.1038/ncb1444.

Celli, G. B. and de Lange, T. (2005) ‘DNA processing is not required for ATM-

mediated telomere damage response after TRF2 deletion', *Nature Cell Biology*. doi: 10.1038/ncb1275.

Cesare, A. J. *et al.* (2008) 'Telomere Loops and Homologous Recombination-Dependent Telomeric Circles in a Kluyveromyces lactis Telomere Mutant Strain', *Molecular and Cellular Biology*. doi: 10.1128/mcb.01122-07.

Chabes, A. *et al.* (2003) 'Survival of DNA damage in yeast directly depends on increased dNTP levels allowed by relaxed feedback inhibition of ribonucleotide reductase', *Cell*. doi: 10.1016/S0092-8674(03)00075-8.

Chan, A., Boulé, J. B. and Zakian, V. A. (2008) 'Two pathways recruit telomerase to Saccharomyces cerevisiae telomeres', *PLoS Genetics*. doi: 10.1371/journal.pgen.1000236.

Chan, C. S. M. and Tye, B. K. (1983) 'Organization of DNA sequences and replication origins at yeast telomeres', *Cell*. doi: 10.1016/0092-8674(83)90437-3.

Chen, H., Lisby, M. and Symington, L. (2013) 'RPA Coordinates DNA End Resection and Prevents Formation of DNA Hairpins', *Molecular Cell*. doi: 10.1016/j.molcel.2013.04.032.

Chen, L.-Y., Liu, D. and Songyang, Z. (2007) 'Telomere Maintenance through Spatial Control of Telomeric Proteins', *Molecular and Cellular Biology*. doi: 10.1128/mcb.00603-07.

Chen, X. *et al.* (2011) 'Cell cycle regulation of DNA double-strand break end resection by Cdk1-dependent Dna2 phosphorylation', *Nature Structural and Molecular Biology*. Nature Publishing Group, 18(9), pp. 1015–1019. doi: 10.1038/nsmb.2105.

Cheng, X., Dunaway, S. and Ivessa, A. S. (2007) 'The role of Pif1p, a DNA helicase in Saccharomyces cerevisiae, in maintaining mitochondrial DNA', *Mitochondrion*. doi: 10.1016/j.mito.2006.11.023.

Chin, L. *et al.* (1999) 'p53 deficiency rescues the adverse effects of telomere loss and cooperates with telomere dysfunction to accelerate carcinogenesis',

Cell. doi: 10.1016/S0092-8674(00)80762-X.

Choe, W. *et al.* (2002) 'Dynamic Localization of an Okazaki Fragment Processing Protein Suggests a Novel Role in Telomere Replication', *Molecular and Cellular Biology*. doi: 10.1128/mcb.22.12.4202-4217.2002.

Chung, J., Khadka, P. and Chung, I. K. (2012) 'Nuclear import of hTERT requires a bipartite nuclear localization signal and Akt-mediated phosphorylation', *Journal of cell science*, 125(Pt 11), pp. 2684–2697. doi: 10.1242/jcs.099267 [doi].

Chung, W. H. *et al.* (2010) 'Defective resection at DNA double-strand breaks leads to de Novo telomere formation and enhances gene targeting', *PLoS Genetics*. doi: 10.1371/journal.pgen.1000948.

Clémenson, C. and Marsolier-Kergoat, M. C. (2009) 'DNA damage checkpoint inactivation: Adaptation and recovery', *DNA Repair*. doi: 10.1016/j.dnarep.2009.04.008.

Clerici, M. *et al.* (2006) 'The Saccharomyces cerevisiae Sae2 protein negatively regulates DNA damage checkpoint signalling', *EMBO Reports*. doi: 10.1038/sj.embor.7400593.

Clerici, M. *et al.* (2008) 'The Yku70-Yku80 complex contributes to regulate double-strand break processing and checkpoint activation during the cell cycle', *EMBO Reports*. doi: 10.1038/embor.2008.121.

Conway, A. B. *et al.* (2004) 'Crystal structure of a Rad51 filament', *Nature Structural and Molecular Biology*. doi: 10.1038/nsmb795.

Counter, C. M. *et al.* (1997) 'The catalytic subunit of yeast telomerase.', *Proceedings of the National Academy of Sciences of the United States of America*, 94(17), pp. 9202–7. doi: 10.1073/pnas.94.17.9202.

Court, R. *et al.* (2005) 'How the human telomeric proteins TRF1 and TRF2 recognize telomeric DNA: A view from high-resolution crystal structures', *EMBO Reports*. doi: 10.1038/sj.embor.7400314.

D'Adda Di Fagagna, F. *et al.* (2003) 'A DNA damage checkpoint response in telomere-initiated senescence', *Nature*. doi: 10.1038/nature02118.

Dahan, D. *et al.* (2018) 'Pif1 is essential for efficient replisome progression through lagging strand G-quadruplex DNA secondary structures', *Nucleic Acids Research*. Oxford University Press, Accepted f(Avalable upon request), pp. 1–11. doi: 10.1093/nar/gky1065.

Daley, J. M. *et al.* (2005) 'DNA joint dependence of Pol X family polymerase action in nonhomologous end joining', *Journal of Biological Chemistry*. doi: 10.1074/jbc.M505277200.

Danilowicz, C. *et al.* (2014) 'The differential extension in dsDNA bound to Rad51 filaments may play important roles in homology recognition and strand exchange', *Nucleic Acids Research*. doi: 10.1093/nar/gkt867.

Davis, A. P. and Symington, L. S. (2001) 'The yeast recombinational repair protein Rad59 interacts with Rad52 and stimulates single-strand annealing', *Genetics*.

Davis, A. P. and Symington, L. S. (2004) 'RAD51-Dependent Break-Induced Replication in Yeast', *Molecular and Cellular Biology*. doi: 10.1128/mcb.24.6.2344-2351.2004.

Davoli, T., Denchi, E. L. and de Lange, T. (2010) 'Persistent Telomere Damage Induces Bypass of Mitosis and Tetraploidy', *Cell*. doi: 10.1016/j.cell.2010.01.031.

Davoli, T. and de Lange, T. (2011) 'The Causes and Consequences of Polyploidy in Normal Development and Cancer', *Annual Review of Cell and Developmental Biology*. doi: 10.1146/annurev-cellbio-092910-154234.

Davoli, T. and de Lange, T. (2012) 'Telomere-Driven Tetraploidization Occurs in Human Cells Undergoing Crisis and Promotes Transformation of Mouse Cells', *Cancer Cell*. doi: 10.1016/j.ccr.2012.03.044.

Deem, A. *et al.* (2011) 'Break-induced replication is highly inaccurate', *PLoS Biology*. doi: 10.1371/journal.pbio.1000594.

Denchi, E. L. and De Lange, T. (2007) ‘Protection of telomeres through independent control of ATM and ATR by TRF2 and POT1’, *Nature*. doi: 10.1038/nature06065.

Deng, S. K. *et al.* (2014) ‘RPA antagonizes microhomology-mediated repair of DNA double-strand breaks’, *Nature Structural and Molecular Biology*. doi: 10.1038/nsmb.2786.

Deutscher, M. P. (1990) *Guide to protein purification*. Academic Press.

Dilley, R. L. *et al.* (2016) ‘Break-induced telomere synthesis underlies alternative telomere maintenance’, *Nature*. Nature Publishing Group, 539(7627), pp. 54–58. doi: 10.1038/nature20099.

Doksani, Y. *et al.* (2013) ‘Super-resolution fluorescence imaging of telomeres reveals TRF2-dependent T-loop formation’, *Cell*. doi: 10.1016/j.cell.2013.09.048.

Donnianni, R. A. and Symington, L. S. (2013) ‘Break-induced replication occurs by conservative DNA synthesis’, *Proceedings of the National Academy of Sciences*. doi: 10.1073/pnas.1309800110.

Downs, J. A., Lowndes, N. F. and Jackson, S. P. (2000) ‘A role for Saccharomyces cerevisiae histone H2A in DNA repair’, *Nature*. doi: 10.1038/35050000.

Dragon, F. *et al.* (2002) ‘A large nucleolar U3 ribonucleoprotein required for 18S ribosomal RNA biogenesis.’, *Nature*, 417(6892), pp. 967–970. doi: 10.1038/nature00769.

Dumur, C. I. *et al.* (2003) ‘Genome-wide detection of LOH in prostate cancer using human SNP microarray technology’, *Genomics*. doi: 10.1016/S0888-7543(03)00020-X.

Emerson, C. H. and Bertuch, A. A. (2016) ‘Consider the workhorse: Nonhomologous end-joining in budding yeast 1’, *Biochemistry and Cell Biology*. doi: 10.1139/bcb-2016-0001.

Emili, A. (1998) ‘MEC1-dependent phosphorylation of Rad9p in response to DNA damage’, *Molecular Cell*. doi: 10.1016/S1097-2765(00)80128-8.

Evans, S. K. and Lundblad, V. (1999) ‘Est1 and Cdc13 as comediators of telomerase access.’, *Science (New York, N.Y.)*, 286(5437), pp. 117–20. doi: 10.1126/science.286.5437.117.

Feng, J. *et al.* (1995) ‘The RNA component of human telomerase’, *Science*. doi: 10.1126/science.7544491.

Fisher, T. S., Taggart, A. K. P. and Zakian, V. A. (2004) ‘Cell cycle-dependent regulation of yeast telomerase by Ku.’, *Nature structural & molecular biology*, 11(12), pp. 1198–205. doi: 10.1038/nsmb854.

Fishman-Lobell, J., Rudin, N. and Haber, J. E. (1992) ‘Two alternative pathways of double-strand break repair that are kinetically separable and independently modulated.’, *Molecular and Cellular Biology*. doi: 10.1128/mcb.12.3.1292.

Friedman, K. L. *et al.* (2003) ‘N-terminal domain of yeast telomerase reverse transcriptase: recruitment of Est3p to the telomerase complex.’, *Molecular biology of the cell*, 14(1), pp. 1–13. doi: 10.1091/mbc.E02-06-0327.

Fulcher, N. *et al.* (2014) ‘If the cap fits, wear it: An overview of telomeric structures over evolution’, *Cellular and Molecular Life Sciences*, pp. 847–865. doi: 10.1007/s00018-013-1469-z.

Furuse, M. *et al.* (1998) ‘Distinct roles of two separable in vitro activities of yeast Mre11 in mitotic and meiotic recombination’, *EMBO Journal*. doi: 10.1093/emboj/17.21.6412.

Galipeau, P. C. *et al.* (1996) ‘17p (p53) allelic losses, 4N (G2/tetraploid) populations, and progression to aneuploidy in Barrett’s esophagus’, *Proceedings of the National Academy of Sciences of the United States of America*. doi: 10.1073/pnas.93.14.7081.

Gallardo, F. *et al.* (2008) ‘TLC1 RNA nucleo-cytoplasmic trafficking links telomerase biogenesis to its recruitment to telomeres’, *The EMBO Journal*, pp.

748–757. doi: 10.1038/emboj.2008.21.

Gallardo, F. and Chartrand, P. (2008) ‘Telomerase biogenesis: The long road before getting to the end.’, *RNA biology*, 5(4), pp. 212–5. doi: 7115 [pii].

Garcia, V. *et al.* (2011) ‘Bidirectional resection of DNA double-strand breaks by Mre11 and Exo1’, *Nature*. doi: 10.1038/nature10515.

Geuting, V., Reul, C. and Löbrich, M. (2013) ‘ATM Release at Resected Double-Strand Breaks Provides Heterochromatin Reconstitution to Facilitate Homologous Recombination’, *PLoS Genetics*. doi: 10.1371/journal.pgen.1003667.

Gilbert, C. S., Green, C. M. and Lowndes, N. F. (2001) ‘Budding yeast Rad9 is an ATP-dependent Rad53 activating machine’, *Molecular Cell*. doi: 10.1016/S1097-2765(01)00267-2.

Gilson, E. and Géli, V. (2007) ‘How telomeres are replicated.’, *Nature reviews. Molecular cell biology*, 8(10), pp. 825–38. doi: 10.1038/nrm2259.

Gobbini, E. *et al.* (2013) ‘Interplays between ATM/Tel1 and ATR/Mec1 in sensing and signaling DNA double-strand breaks’, *DNA Repair*. doi: 10.1016/j.dnarep.2013.07.009.

Gomes, X. V. and Burgers, P. M. J. (2000) ‘Two modes of FEN1 binding to PCNA regulated by DNA’, *EMBO Journal*. doi: 10.1093/emboj/19.14.3811.

Gong, Y. and de Lange, T. (2010) ‘A Shld1-Controlled POT1a Provides Support for Repression of ATR Signaling at Telomeres through RPA Exclusion’, *Molecular Cell*. doi: 10.1016/j.molcel.2010.10.016.

Gorbunova, V. and Seluanov, A. (2009) ‘Coevolution of telomerase activity and body mass in mammals: From mice to beavers’, *Mechanisms of Ageing and Development*. doi: 10.1016/j.mad.2008.02.008.

Gottschling, D. E. *et al.* (1990) ‘Position effect at S. cerevisiae telomeres: Reversible repression of Pol II transcription’, *Cell*, 63(4), pp. 751–762. doi: 10.1016/0092-8674(90)90141-Z.

Greider, C. W. and Blackburn, E. H. (1985) ‘Identification of a specific telomere terminal transferase activity in Tetrahymena extracts.’, *Cell*, 43(2 Pt 1), pp. 405–13. doi: 10.1016/0092-8674(85)90170-9.

Griffith, J. D. *et al.* (1999) ‘Mammalian telomeres end in a large duplex loop’, *Cell*, 97(4), pp. 503–514. doi: 10.1016/S0092-8674(00)80760-6.

Haber, J. E. (1992) ‘Exploring the pathways of homologous recombination’, *Current Opinion in Cell Biology*. doi: 10.1016/0955-0674(92)90005-W.

Haber, J. E. (2018) ‘DNA Repair: The Search for Homology’, *BioEssays*. doi: 10.1002/bies.201700229.

Haber, J. E. and Leung, W. Y. (1996) ‘Lack of chromosome territoriality in yeast: Promiscuous rejoining of broken chromosome ends’, *Proceedings of the National Academy of Sciences of the United States of America*. doi: 10.1073/pnas.93.24.13949.

Hanaoka, S. *et al.* (2001) ‘NMR structure of the hRap1 Myb motif reveals a canonical three-helix bundle lacking the positive surface charge typical of Myb DNA-binding domains’, *Journal of Molecular Biology*. doi: 10.1006/jmbi.2001.4924.

Hanaoka, S., Nagadoi, A. and Nishimura, Y. (2009) ‘Comparison between TRF2 and TRF1 of their telomeric DNA-bound structures and DNA-binding activities’, *Protein Science*. doi: 10.1110/ps.04983705.

Hardy, C. F., Sussel, L. and Shore, D. (1992) ‘A RAP1-interacting protein involved in transcriptional silencing and telomere length regulation.’, *Genes & development*, 6(5), pp. 801–14. Available at: http://www.ncbi.nlm.nih.gov/pubmed/1577274 (Accessed: 24 July 2016).

Harley, C. B. *et al.* (1992) ‘The telomere hypothesis of cellular aging’, *Experimental Gerontology*, 27(4), pp. 375–382. doi: 10.1016/0531-5565(92)90068-B.

Harrison, J. C. and Haber, J. E. (2006) ‘Surviving the Breakup: The DNA Damage Checkpoint’, *Annual Review of Genetics*, 40(1), pp. 209–235. doi:

10.1146/annurev.genet.40.051206.105231.

Hawkins, C. and Friedman, K. L. (2014) ‘Normal telomere length maintenance in Saccharomyces cerevisiae requires nuclear import of the ever shorter telomeres 1 (Est1) protein via the importin alpha pathway.’, *Eukaryotic cell*. American Society for Microbiology (ASM), 13(8), pp. 1036–50. doi: 10.1128/EC.00115-14.

Hayflick, L. (1965) ‘The limited in vitro lifetime of human diploid cell strains’, *Experimental Cell Research*, 37(3), pp. 614–636. doi: 10.1016/0014-4827(65)90211-9.

Hemnani, T. and Parihar, M. S. (1998) ‘Reactive oxygen species and oxidative DNA damage’, *Indian journal of physiology and pharmacology*. DEPARTMENT OF PHYSIOLOGY ALL INDIAN INSTITUTE OF MEDICAL SCIENCES, 42, pp. 440–452.

Heyer, W. D. (2015) ‘Regulation of recombination and genomic maintenance’, *Cold Spring Harbor Perspectives in Medicine*, 5(8), pp. 1–24. doi: 10.1101/cshperspect.a016501.

Hockemeyer, D. *et al.* (2006) ‘Recent Expansion of the Telomeric Complex in Rodents: Two Distinct POT1 Proteins Protect Mouse Telomeres’, *Cell*. doi: 10.1016/j.cell.2006.04.044.

Hopfner, K. P. *et al.* (2000) ‘Mre11 and Rad50 from Pyrococcus furiosus: Cloning and biochemical characterization reveal an evolutionarily conserved multiprotein machine’, *Journal of Bacteriology*. doi: 10.1128/JB.182.21.6036-6041.2000.

Hopfner, Karl Peter *et al.* (2000) ‘Structural biology of Rad50 ATPase: ATP-driven conformational control in DNA double-strand break repair and the ABC-ATPase superfamily’, *Cell*. doi: 10.1016/S0092-8674(00)80890-9.

Hopfner, K. P. *et al.* (2001) ‘Structural biochemistry and interaction architecture of the DNA double-strand break repair Mre11 nuclease and Rad50-ATPase’, *Cell*. doi: 10.1016/S0092-8674(01)00335-X.

Hopfner, K. P. *et al.* (2002) 'The Rad50 zinc-hook is a structure joining Mre11 complexes in DNA recombination and repair', *Nature*. doi: 10.1038/nature00922.

Hu, C. *et al.* (2017) 'Structural and functional analyses of the mammalian TIN2-TPP1-TRF2 telomeric complex', *Cell Research*. doi: 10.1038/cr.2017.144.

Huang, M., Zhou, Z. and Elledge, S. J. (1998) 'The DNA replication and damage checkpoint pathways induce transcription by inhibition of the Crt1 repressor', *Cell*. doi: 10.1016/S0092-8674(00)81601-3.

Huertas, P. *et al.* (2008) 'CDK targets Sae2 to control DNA-end resection and homologous recombination', *Nature*. doi: 10.1038/nature07215.

Hughes, T. R. *et al.* (2000) 'The Est3 protein is a subunit of yeast telomerase', *Current Biology*. doi: 10.1016/S0960-9822(00)00562-5.

Ip, S. C. Y. *et al.* (2008) 'Identification of Holliday junction resolvases from humans and yeast', *Nature*. doi: 10.1038/nature07470.

Ira, G. *et al.* (2003) 'Srs2 and Sgs1-Top3 Suppress Crossovers during Double-Strand Break Repair in Yeast', *Cell*. doi: 10.1016/S0092-8674(03)00886-9.

Ira, G. and Haber, J. E. (2002) 'Characterization of RAD51-Independent Break-Induced Replication That Acts Preferentially with Short Homologous Sequences', *Molecular and Cellular Biology*. doi: 10.1128/mcb.22.18.6384-6392.2002.

Ivanov, E. L. *et al.* (1994) 'Mutations in XRS2 and RAD50 delay but do not prevent mating-type switching in Saccharomyces cerevisiae.', *Molecular and Cellular Biology*. doi: 10.1128/mcb.14.5.3414.

Ivanov, E. L. *et al.* (1996) 'Genetic requirements for the single-strand annealing pathway of double-strand break repair in Saccharomyces cerevisiae', *Genetics*.

Jacobs, J. J. L. and De Lange, T. (2004) 'Significant role for p16INK4a in p53-independent telomere-directed senescence', *Current Biology*. doi:

10.1016/j.cub.2004.12.025.

Jain, S. *et al.* (2009) ‘A recombination execution checkpoint regulates the choice of homologous recombination pathway during DNA double-strand break repair’, *Genes & Development*, 23(3), pp. 291–303. doi: 10.1101/gad.1751209.

Jain, S. *et al.* (2016) ‘Sgs1 and Mph1 helicases enforce the recombination execution checkpoint during DNA double-strand break repair in saccharomyces cerevisiae’, *Genetics*. doi: 10.1534/genetics.115.184317.

Johansson, E., Garg, P. and Burgers, P. M. J. (2004) ‘The Pol32 Subunit of DNA Polymerase δ Contains Separable Domains for Processive Replication and Proliferating Cell Nuclear Antigen (PCNA) Binding’, *Journal of Biological Chemistry*. doi: 10.1074/jbc.M310362200.

Karlseder, J. *et al.* (1999) ‘p53- and ATM-dependent apoptosis induced by telomeres lacking TRF2’, *Science*. doi: 10.1126/science.283.5406.1321.

Karlseder, J., Smogorzewska, A. and De Lange, T. (2002) ‘Senescence induced by altered telomere state, not telomere loss’, *Science*. doi: 10.1126/science.1069523.

Keeney, S. and Kleckner, N. (1995) ‘Covalent protein-DNA complexes at the 5′ strand termini of meiosis-specific double-strand breaks in yeast’, *Proceedings of the National Academy of Sciences of the United States of America*. doi: 10.1073/pnas.92.24.11274.

Kim et al., N. W. (1994) ‘Specific association of human telomerase activity with immortal cells and cancer’, *Science*, 266, pp. 2011–2015.

Kim, H. *et al.* (2009) ‘TRF2 functions as a protein hub and regulates telomere maintenance by recognizing specific peptide motifs’, *Nature Structural and Molecular Biology*. doi: 10.1038/nsmb.1575.

Krajewski, S. S. and Narberhaus, F. (2014) ‘Temperature-driven differential gene expression by RNA thermosensors’, *Biochimica et Biophysica Acta - Gene Regulatory Mechanisms*. doi: 10.1016/j.bbagrm.2014.03.006.

Krejci, L. *et al.* (2012) ‘Homologous recombination and its regulation’, *Nucleic Acids Research*, 40(13), pp. 5795–5818. doi: 10.1093/nar/gks270.

Krogan, N. J. *et al.* (2006) ‘Global landscape of protein complexes in the yeast Saccharomyces cerevisiae’, *Nature*. doi: 10.1038/nature04670.

Kumar, S. and Burgers, P. M. (2013) ‘Lagging strand maturation factor Dna2 is a component of the replication checkpoint initiation machinery’, *Genes and Development*. Cold Spring Harbor Laboratory Press, 27(3), pp. 313–21. doi: 10.1101/gad.204750.112.

Kupiec, M. (2014) ‘Biology of telomeres: lessons from budding yeast’, *FEMS Microbiology Reviews*, 38(2), pp. 144–171. doi: 10.1111/1574-6976.12054.

de Lange, T. (2018) ‘Shelterin-Mediated Telomere Protection’, *Annual Review of Genetics*. doi: 10.1146/annurev-genet-032918-021921.

De Lange, T. (2005) ‘Shelterin: The protein complex that shapes and safeguards human telomeres’, *Genes and Development*. doi: 10.1101/gad.1346005.

Lanz, M. C., Dibitetto, D. and Smolka, M. B. (2019) ‘DNA damage kinase signaling: checkpoint and repair at 30 years’, *The EMBO Journal*. John Wiley & Sons, Ltd. doi: 10.15252/embj.2019101801.

Laroche, T. *et al.* (1998) *Mutation of yeast Ku genes disrupts the subnuclear organization of telomeres*, *Current Biology*. doi: 10.1016/S0960-9822(98)70252-0.

Larrivée, M., LeBel, C. and Wellinger, R. J. (2004) ‘The generation of proper constitutive G-tails on yeast telomeres is dependent on the MRX complex’, *Genes and Development*, 18(12), pp. 1391–1396. doi: 10.1101/gad.1199404.

Le, S. *et al.* (1999) ‘RAD50 and RAD51 define two pathways that collaborate to maintain telomeres in the absence of telomerase.’, *Genetics*, 152(1), pp. 143–52. Available at: http://www.ncbi.nlm.nih.gov/pubmed/10224249.

Lee, C. S. *et al.* (2014) ‘Dynamics of yeast histone H2A and H2B

phosphorylation in response to a double-strand break', *Nature Structural and Molecular Biology*. doi: 10.1038/nsmb.2737.

Lejnine, S., Makarov, V. L. and Langmore, J. P. (1995) 'Conserved nucleoprotein structure at the ends of vertebrate and invertebrate chromosomes', *Proceedings of the National Academy of Sciences of the United States of America*. doi: 10.1073/pnas.92.6.2393.

Lendvay, T. S. *et al.* (1996) 'Senescence mutants of Saccharomyces cerevisiae with a defect in telomere replication identify three additional EST genes', *Genetics*, 144(4), pp. 1399–1412.

Leonardi, J. *et al.* (2008) 'TER1, the RNA subunit of fission yeast telomerase', *Nature Structural and Molecular Biology*. doi: 10.1038/nsmb1343.

Levikova, M. and Cejka, P. (2015) 'The Saccharomyces cerevisiae Dna2 can function as a sole nuclease in the processing of Okazaki fragments in DNA replication', *Nucleic Acids Research*. doi: 10.1093/nar/gkv710.

Levikova, M., Pinto, C. and Cejka, P. (2017) 'The motor activity of dna2 functions as an ssdna translocase to promote dna end resection', *Genes and Development*, 31(5), pp. 493–502. doi: 10.1101/gad.295196.116.

Levy, D. L. and Blackburn, E. H. (2004) 'Counting of Rif1p and Rif2p on Saccharomyces cerevisiae Telomeres Regulates Telomere Length', *Molecular and Cellular Biology*. doi: 10.1128/mcb.24.24.10857-10867.2004.

Li, Y. *et al.* (2014) 'Constitutional and somatic rearrangement of chromosome 21 in acute lymphoblastic leukaemia', *Nature*. doi: 10.1038/nature13115.

Liang, F. and Wang, Y. (2007) 'DNA Damage Checkpoints Inhibit Mitotic Exit by Two Different Mechanisms', *Molecular and Cellular Biology*. doi: 10.1128/mcb.00095-07.

Lin, J. and Blackburn, E. H. (2004) 'Nucleolar protein PinX1p regulates telomerase by sequestering its protein catalytic subunit in an inactive complex lacking telomerase RNA', *Genes and Development*, 18(4), pp. 387–396. doi: 10.1101/gad.1171804.

Lisby, M. *et al.* (2004) ‘Choreography of the DNA damage response: Spatiotemporal relationships among checkpoint and repair proteins’, *Cell*. doi: 10.1016/j.cell.2004.08.015.

Liu, D. *et al.* (2004) ‘PTOP interacts with POT1 and regulates its localization to telomeres’, *Nature Cell Biology*. doi: 10.1038/ncb1142.

Liu, J. *et al.* (2011) ‘Rad51 paralogues Rad55-Rad57 balance the antirecombinase Srs2 in Rad51 filament formation’, *Nature*. doi: 10.1038/nature10522.

Liu, J. *et al.* (2017) ‘Srs2 promotes synthesis-dependent strand annealing by disrupting DNA polymerase d-extending D-loops’, *eLife*. doi: 10.7554/eLife.22195.

Livengood, A. J., Cech, T. R. and Zaug, A. J. (2002) ‘Essential regions of Saccharomyces cerevisiae telomerase RNA: separate elements for Est1p and Est2p interaction.’, *Molecular and cellular biology*, 22(7), pp. 2366–74. doi: 10.1128/MCB.22.7.2366.

Loayza, D. *et al.* (2004) ‘DNA binding features of human POT1: A nonamer 5′-TAGGGTTAG-3′ minimal binding site, sequence specificity, and internal binding to multimeric sites’, *Journal of Biological Chemistry*. doi: 10.1074/jbc.M312309200.

Lobachev, K. *et al.* (2004) ‘Chromosome fragmentation after induction of a double-strand break is an active process prevented by the RMX repair complex’, *Current Biology*. doi: 10.1016/j.cub.2004.11.051.

Longtine, M. S. *et al.* (1998) ‘Additional modules for versatile and economical PCR-based gene deletion and modification in Saccharomyces cerevisiae’, *Yeast*, 14(10), pp. 953–961. doi: 10.1002/(SICI)1097-0061(199807)14:10<953::AID-YEA293>3.0.CO;2-U.

Luke-Glaser, S., Poschke, H. and Luke, B. (2012) ‘Getting in (and out of) the loop: regulating higher order telomere structures’, *Frontiers in Oncology*. doi: 10.3389/fonc.2012.00180.

Lundblad, V. and Szostak, J. W. (1989) ‘A mutant with a defect in telomere elongation leads to senescence in yeast’, *Cell*, 57(4), pp. 633–643. doi: 10.1016/0092-8674(89)90132-3.

Ly, H. *et al.* (2003) ‘A role for a novel “trans-pseudoknot” RNA-RNA interaction in the functional dimerization of human telomerase’, *Genes and Development*, 17(9), pp. 1078–1083. doi: 10.1101/gad.1060803.

Lydall, D. (2003) ‘Hiding at the ends of yeast chromosomes: telomeres, nucleases and checkpoint pathways.’, *Journal of cell science*, 116(Pt 20), pp. 4057–65. doi: 10.1242/jcs.00765.

Lydeard, J. R. *et al.* (2007) ‘Break-induced replication and telomerase-independent telomere maintenance require Pol32’, *Nature*. doi: 10.1038/nature06047.

Lydeard, J. R. *et al.* (2010) ‘Sgs1 and Exo1 redundantly inhibit break-induced replication and de Novo telomere addition at broken chromosome ends’, *PLoS Genetics*, 6(5), p. 25. doi: 10.1371/journal.pgen.1000973.

Maciejowski, J. *et al.* (2015) ‘Chromothripsis and Kataegis Induced by Telomere Crisis’, *Cell*. doi: 10.1016/j.cell.2015.11.054.

Maciejowski, J. and De Lange, T. (2017) ‘Telomeres in cancer: Tumour suppression and genome instability’, *Nature Reviews Molecular Cell Biology*. doi: 10.1038/nrm.2016.171.

Maga, G. *et al.* (2001) ‘Okazaki fragment processing: Modulation of the strand displacement activity of DNA polymerase by the concerted action of replication protein A, proliferating cell nuclear antigen, and flap endonuclease-1’, *Proceedings of the National Academy of Sciences*. doi: 10.1073/pnas.251193198.

Majka, J. and Burgers, P. M. J. (2003) ‘Yeast Rad17/Mec3/Ddc1: A sliding clamp for the DNA damage checkpoint’, *Proceedings of the National Academy of Sciences of the United States of America*. doi: 10.1073/pnas.0437148100.

Makarov, V. L., Hirose, Y. and Langmore, J. P. (1997) ‘Long G tails at both

ends of human chromosomes suggest a C strand degradation mechanism for telomere shortening', *Cell*. doi: 10.1016/S0092-8674(00)81908-X.

Makovets, S. and Blackburn, E. H. (2009) 'DNA damage signalling prevents deleterious telomere addition at DNA breaks', *Nature Cell Biology*. doi: 10.1038/ncb1985.

Makovets, S., Herskowitz, I. and Blackburn, E. H. (2004) 'Anatomy and Dynamics of DNA Replication Fork Movement in Yeast Telomeric Regions', *Molecular and Cellular Biology*. doi: 10.1128/mcb.24.9.4019-4031.2004.

Malkova, A. *et al.* (2005) 'RAD51-Dependent Break-Induced Replication Differs in Kinetics and Checkpoint Responses from RAD51-Mediated Gene Conversion', *Molecular and Cellular Biology*. doi: 10.1128/mcb.25.3.933-944.2005.

Malkova, A., Ivanov, E. L. and Haber, J. E. (1996) 'Double-strand break repair in the absence of RAD51 in yeast: A possible role for break-induced DNA replication', *Proceedings of the National Academy of Sciences of the United States of America*. doi: 10.1073/pnas.93.14.7131.

Mantiero, D. *et al.* (2007) 'Dual role for Saccharomyces cerevisiae Tel1 in the checkpoint response to double-strand breaks', *EMBO Reports*. doi: 10.1038/sj.embor.7400911.

Marcand, S. *et al.* (2008) 'Multiple pathways inhibit NHEJ at telomeres', *Genes and Development*, 22(9), pp. 1153–1158. doi: 10.1101/gad.455108.

Maringele, L. and Lydall, D. (2004) 'EXO1 Plays a Role in Generating Type I and Type II Survivors in Budding Yeast', *Genetics*, 166(4), pp. 1641–9. doi: 10.1534/genetics.166.4.1641.

Markiewicz-Potoczny, M., Lisby, M. and Lydall, D. (2018) 'A critical role for Dna2 at unwound telomeres', *Genetics*, 209(1), pp. 129–141. doi: 10.1534/genetics.118.300809.

Maser, R. S. and DePinho, R. A. (2002) 'Connecting chromosomes, crisis, and cancer', *Science*. doi: 10.1126/science.297.5581.565.

Mason, J. M., Frydrychova, R. C. and Biessmann, H. (2008) 'Drosophila telomeres: An exception providing new insights', *BioEssays*. doi: 10.1002/bies.20688.

Mateos-Gomez, P. A. *et al.* (2015) 'Mammalian polymerase θ promotes alternative NHEJ and suppresses recombination', *Nature*. doi: 10.1038/nature14157.

Matsuoka, S., Huang, M. and Elledge, S. J. (1998) 'Linkage of ATM to cell cycle regulation by the Chk2 protein kinase', *Science*. doi: 10.1126/science.282.5395.1893.

Mayle, R. *et al.* (2015) 'Mus81 and converging forks limit the mutagenicity of replication fork breakage', *Science*. doi: 10.1126/science.aaa8391.

Mehta, A. and Haber, J. E. (2014) 'Sources of DNA double-strand breaks and models of recombinational DNA repair', *Cold Spring Harbor Perspectives in Biology*. doi: 10.1101/cshperspect.a016428.

Melo, J. A., Cohen, J. and Toczyski, D. P. (2001) 'Two checkpoint complexes are independently recruited to sites of DNA damage in vivo', *Genes and Development*.

Meyerson, M. *et al.* (1997) 'hEST2, the putative human telomerase catalytic subunit gene, is up- regulated in tumor cells and during immortalization', *Cell*. doi: 10.1016/S0092-8674(00)80538-3.

Millet, C. *et al.* (2015) 'Cell populations can use aneuploidy to survive telomerase insufficiency.', *Nature communications*. Nature Publishing Group, 6, p. 8664. doi: 10.1038/ncomms9664.

Mimitou, E. P. and Symington, L. S. (2008) 'Sae2, Exo1 and Sgs1 collaborate in DNA double-strand break processing', *Nature*. doi: 10.1038/nature07312.

Mimitou, E. P. and Symington, L. S. (2010) 'Ku prevents Exo1 and Sgs1-dependent resection of DNA ends in the absence of a functional MRX complex or Sae2', *EMBO Journal*. doi: 10.1038/emboj.2010.193.

Mojumdar, A. *et al.* (2019) 'Nej1 Interacts with Mre11 to Regulate Tethering and Dna2 Binding at DNA Double-Strand Breaks', *Cell Reports*. doi: 10.1016/j.celrep.2019.07.018.

Morafraile, E. C. *et al.* (2015) 'Checkpoint-dependent RNR induction promotes fork restart after replicative stress', *Scientific Reports*. doi: 10.1038/srep07886.

Mordes, D. A., Nam, E. A. and Cortez, D. (2008) 'Dpb11 activates the Mec1-Ddc2 complex', *Proceedings of the National Academy of Sciences of the United States of America*. doi: 10.1073/pnas.0806621105.

Moreau, S., Ferguson, J. R. and Symington, L. S. (1999) 'The Nuclease Activity of Mre11 Is Required for Meiosis but Not for Mating Type Switching, End Joining, or Telomere Maintenance', *Molecular and Cellular Biology*. doi: 10.1128/mcb.19.1.556.

Moretti, P. *et al.* (1994) 'Evidence that a complex of SIR proteins interacts with the silencer and telomere-binding protein RAP1', *Genes and Development*, 8(19), pp. 2257–2269. doi: 10.1101/gad.8.19.2257.

Morin, G. B. (1989) 'The human telomere terminal transferase enzyme is a ribonucleoprotein that synthesizes TTAGGG repeats', *Cell*. doi: 10.1016/0092-8674(89)90035-4.

Morin, I. *et al.* (2008) 'Checkpoint-dependent phosphorylation of Exo1 modulates the DNA damage response', *EMBO Journal*. doi: 10.1038/emboj.2008.171.

Morrical, S. W. (2015) 'DNA-pairing and annealing processes in homologous recombination and homology-directed repair', *Cold Spring Harbor Perspectives in Biology*. doi: 10.1101/cshperspect.a016444.

Motamedi, M. R., Szigety, S. K. and Rosenberg, S. M. (1999) 'Double-strand-break repair recombination in Escherichia coli: Physical evidence for a DNA replication mechanism in vivo', *Genes and Development*. doi: 10.1101/gad.13.21.2889.

Mozdy, A. D., Cech, T. R. and Podell, E. R. (2008) 'Multiple yeast genes,

including Paf1 complex genes, affect telomere length via telomerase RNA abundance.', *Molecular and cellular biology*, 28(12), pp. 4152–61. doi: 10.1128/MCB.00512-08.

Nakada, D., Matsumoto, K. and Sugimoto, K. (2003) 'ATM-related Tel1 associates with double-strand breaks through an Xrs2-dependent mechanism', *Genes and Development*. doi: 10.1101/gad.1099003.

Nakamura, T. M. *et al.* (1997) 'Telomerase catalytic subunit homologs from fission yeast and human', *Science*. doi: 10.1126/science.277.5328.955.

Navadgi-Patil, V. M. and Burgers, P. M. (2009) 'The Unstructured C-Terminal Tail of the 9-1-1 Clamp Subunit Ddc1 Activates Mec1/ATR via Two Distinct Mechanisms', *Molecular Cell*. doi: 10.1016/j.molcel.2009.10.014.

Navarre, C. *et al.* (2002) 'Subproteomics: Identification of plasma membrane proteins from the yeast Saccharomyces cerevisiae', *Proteomics*. doi: 10.1002/1615-9861(200212)2:12<1706::AID-PROT1706>3.0.CO;2-K.

Neale, M. J., Pan, J. and Keeney, S. (2005) 'Endonucleolytic processing of covalent protein-linked DNA double-strand breaks', *Nature*. doi: 10.1038/nature03872.

Ngo, G. H. P. and Lydall, D. (2015) 'The 9-1-1 checkpoint clamp coordinates resection at DNA double strand breaks', *Nucleic Acids Research*. doi: 10.1093/nar/gkv409.

Nicolette, M. L. *et al.* (2010) 'Mre11-Rad50-Xrs2 and Sae2 promote 5′ strand resection of DNA double-strand breaks', *Nature Structural and Molecular Biology*. doi: 10.1038/nsmb.1957.

Nimonkar, A. V., Sica, R. A. and Kowalczykowski, S. C. (2009) 'Rad52 promotes second-end DNA capture in double-stranded break repair to form complement-stabilized joint molecules', *Proceedings of the National Academy of Sciences of the United States of America*. doi: 10.1073/pnas.0813247106.

Niu, H. *et al.* (2010) 'Mechanism of the ATP-dependent DNA endresection machinery from Saccharomyces cerevisiae', *Nature*. doi:

10.1038/nature09318.

Nugent, C. I. *et al.* (1996) ‘Cdc13p: a single-strand telomeric DNA-binding protein with a dual role in yeast telomere maintenance.’, *Science (New York, N.Y.)*, 274(5285), pp. 249–52. doi: 10.1126/science.274.5285.249.

O’Hagan, R. C. *et al.* (2002) ‘Telomere dysfunction provokes regional amplification and deletion in cancer genomes’, *Cancer Cell*. doi: 10.1016/S1535-6108(02)00094-6.

Oh, B. K. *et al.* (2008) ‘High telomerase activity and long telomeres in advanced hepatocellular carcinomas with poor prognosis’, *Laboratory Investigation*. doi: 10.1038/labinvest.3700710.

Olovnikov, A. M. (1973) ‘A theory of marginotomy: the incomplete copying of template margin in enzymatic synthesis of poynucleotides and biological significance of the phenomenon’, *Journal of Theoretical Biology*, 41(1), pp. 181–190. doi: 10.1016/0022-5193(73)90198-7.

Osterhage, J. L., Talley, J. M. and Friedman, K. L. (2006) ‘Proteasome-dependent degradation of Est1p regulates the cell cycle-restricted assembly of telomerase in Saccharomyces cerevisiae’, *Nature Structural and Molecular Biology*. doi: 10.1038/nsmb1125.

Paciotti, V. *et al.* (2000) ‘The checkpoint protein Ddc2, functionally related to S. pombe Rad26, interacts with Mec1 and is regulated by Mec1-dependent phosphorylation in budding yeast’, *Genes and Development*.

Palladino, F. *et al.* (1993) ‘SIR3 and SIR4 proteins are required for the positioning and integrity of yeast telomeres’, *Cell*. Elsevier, 75(3), pp. 543–555. doi: 10.1016/0092-8674(93)90388-7.

Palm, W. and de Lange, T. (2008) ‘How Shelterin Protects Mammalian Telomeres’, *Annual Review of Genetics*, 42(1), pp. 301–334. doi: 10.1146/annurev.genet.41.110306.130350.

Pardo, B., Crabbé, L. and Pasero, P. (2017) ‘Signaling pathways of replication stress in yeast’, *FEMS Yeast Research*. doi: 10.1093/femsyr/fow101.

Pardo, B. and Marcand, S. (2005) ‘Rap1 prevents telomere fusions by nonhomologous end joining.’, *The EMBO journal*, 24(17), pp. 3117–3127. doi: 10.1038/sj.emboj.7600778.

Parenteau, J. and Wellinger, R. J. (2015) ‘ Accumulation of Single-Stranded DNA and Destabilization of Telomeric Repeats in Yeast Mutant Strains Carrying a Deletion of RAD27 ’, *Molecular and Cellular Biology*. doi: 10.1128/mcb.19.6.4143.

Paschini, M. *et al.* (2012) ‘A naturally thermolabile activity compromises genetic analysis of telomere function in Saccharomyces cerevisiae.’, *Genetics*, 191(1), pp. 79–93. doi: 10.1534/genetics.111.137869.

Paull, T. T. and Gellert, M. (1998) ‘The 3′ to 5′ exonuclease activity of Mre11 facilitates repair of DNA double-strand breaks’, *Molecular Cell*. doi: 10.1016/S1097-2765(00)80097-0.

Peifer, M. *et al.* (2015) ‘Telomerase activation by genomic rearrangements in high-risk neuroblastoma’, *Nature*. doi: 10.1038/nature14980.

Pennaneach, V., Putnam, C. D. and Kolodner, R. D. (2006) ‘Chromosome healing by *de novo* telomere addition in *Saccharomyces cerevisiae*’, *Molecular Microbiology*. Wiley/Blackwell (10.1111), 59(5), pp. 1357–1368. doi: 10.1111/j.1365-2958.2006.05026.x.

Peterson, S. E. *et al.* (2001) ‘The function of a stem-loop in telomerase RNA is linked to the DNA repair protein Ku.’, *Nature genetics*. Nature Publishing Group, 27(1), pp. 64–7. doi: 10.1038/83778.

Petreaca, R. C., Chiu, H.-C. and Nugent, C. I. (2007) ‘The role of Stn1p in Saccharomyces cerevisiae telomere capping can be separated from its interaction with Cdc13p.’, *Genetics*, 177(3), pp. 1459–74. doi: 10.1534/genetics.107.078840.

Petukhova, G., Sung, P. and Klein, H. (2000) ‘Promotion of Rad51-dependent D-loop formation by yeast recombination factor Rdh54/Tid1’, *Genes and Development*. doi: 10.1101/gad.826100.

Pfingsten, J. S. *et al.* (2012) ‘Mutually exclusive binding of telomerase RNA and DNA by Ku alters telomerase recruitment model’, *Cell*. Elsevier Inc., 148(5), pp. 922–932. doi: 10.1016/j.cell.2012.01.033.

Pike, J. E. *et al.* (2009) ‘Pif1 helicase lengthens some Okazaki fragment flaps necessitating Dna2 nuclease/helicase action in the two-nuclease processing pathway’, *Journal of Biological Chemistry*. doi: 10.1074/jbc.M109.023325.

Poli, J. *et al.* (2012) ‘dNTP pools determine fork progression and origin usage under replication stress’, *EMBO Journal*. doi: 10.1038/emboj.2011.470.

Polotnianka, R. M., Li, J. and Lustig, a J. (1998) ‘The yeast Ku heterodimer is essential for protection of the telomere against nucleolytic and recombinational activities.’, *Current biology : CB*, 8(14), pp. 831–834.

Poulet, A. *et al.* (2009) ‘TRF2 promotes, remodels and protects telomeric Holliday junctions’, *EMBO Journal*. doi: 10.1038/emboj.2009.11.

Prescott, J. and Blackburn, E. H. (1997) ‘Functionally interacting telomerase RNAs in the yeast telomerase complex’, *Genes and Development*, 11(21), pp. 2790–2800. doi: 10.1101/gad.11.21.2790.

Pryde, F. E. and Louis, E. J. (1999) ‘Limitations of silencing at native yeast telomeres’, *EMBO Journal*, 18(9), pp. 2538–2550. doi: 10.1093/emboj/18.9.2538.

Puddu, F. *et al.* (2008) ‘Phosphorylation of the Budding Yeast 9-1-1 Complex Is Required for Dpb11 Function in the Full Activation of the UV-Induced DNA Damage Checkpoint’, *Molecular and Cellular Biology*. doi: 10.1128/mcb.00330-08.

Rai, R. *et al.* (2016) ‘TRF2-RAP1 is required to protect telomeres from engaging in homologous recombination-mediated deletions and fusions’, *Nature Communications*. doi: 10.1038/ncomms10881.

Ramsden, D. A. and Gellert, M. (1995) ‘Formation and resolution of double-strand break intermediates in V(D)J rearrangement’, *Genes and Development*. doi: 10.1101/gad.9.19.2409.

Rao, T. *et al.* (2014) ‘Structure of Est3 reveals a bimodal surface with differential roles in telomere replication.’, *Proceedings of the National Academy of Sciences of the United States of America*, 111(1), pp. 214–8. doi: 10.1073/pnas.1316453111.

Ribeyre, C. *et al.* (2009) ‘The yeast Pif1 helicase prevents genomic instability caused by G-quadruplex-forming CEB1 sequences in vivo’, *PLoS Genetics*. doi: 10.1371/journal.pgen.1000475.

Riboni, R. *et al.* (1997) ‘Telomeric fusions in cultured human fibroblasts as a source of genomic instability’, *Cancer Genetics and Cytogenetics*. doi: 10.1016/S0165-4608(96)00248-8.

Richardson, C. and Jasin, M. (2000) ‘Frequent chromosomal translocations induced by DNA double-strand breaks’, *Nature*. doi: 10.1038/35015097.

Rine, J. *et al.* (1979) ‘A suppressor of mating-type locus mutations in Saccharomyces cerevisiae: Evidence for and identification of cryptic mating-type loci’, *Genetics*.

Roger, L. *et al.* (2013) ‘Extensive telomere erosion in the initiation of colorectal adenomas and its association with chromosomal instability’, *Journal of the National Cancer Institute*. doi: 10.1093/jnci/djt191.

Rosen, D. M. *et al.* (2013) ‘Fragile Site Instability in Saccharomyces cerevisiae Causes Loss of Heterozygosity by Mitotic Crossovers and Break-Induced Replication’, *PLoS Genetics*. doi: 10.1371/journal.pgen.1003817.

Rossi, M. L. *et al.* (2008) ‘Pif1 helicase directs eukaryotic okazaki fragments toward the two-nuclease cleavage pathway for primer removal’, *Journal of Biological Chemistry*. doi: 10.1074/jbc.M804550200.

Rossi, M. L. and Bambara, R. A. (2006) ‘Reconstituted Okazaki fragment processing indicates two pathways of primer removal’, *Journal of Biological Chemistry*. doi: 10.1074/jbc.M604805200.

Rossi, S. E., Foiani, M. and Giannattasio, M. (2018) ‘Dna2 processes behind the fork long ssDNA flaps generated by Pif1 and replication-dependent strand

displacement', *Nature Communications*. Springer US, 9(1), p. 4830. doi: 10.1038/s41467-018-07378-5.

Rouse, J. and Jackson, S. P. (2002) 'Lcd1p recruits Mec1p to DNA lesions in vitro and in vivo', *Molecular Cell*. doi: 10.1016/S1097-2765(02)00507-5.

Sabourin, M. *et al.* (2007) 'A flexible protein linker improves the function of epitope-tagged proteins in Saccharomyces cerevisiae', *Yeast*. doi: 10.1002/yea.1431.

Sabourin, M., Tuzon, C. T. and Zakian, V. A. (2007) 'Telomerase and Tel1p Preferentially Associate with Short Telomeres in S. cerevisiae', *Molecular Cell*, 27(4), pp. 550–561. doi: 10.1016/j.molcel.2007.07.016.

Saini, N. *et al.* (2013) 'Migrating bubble during break-induced replication drives conservative DNA synthesis', *Nature*. Nature Publishing Group, 502(7471), pp. 389–392. doi: 10.1038/nature12584.

Sakofsky, C. J. *et al.* (2014) 'Break-induced replication is a source of mutation clusters underlying kataegis', *Cell Reports*. doi: 10.1016/j.celrep.2014.04.053.

Sanchez, Y. *et al.* (1999) 'Control of the DNA damage checkpoint by Chk1 and Rad53 protein kinases through distinct mechanisms', *Science*. doi: 10.1126/science.286.5442.1166.

Santos, J. H. *et al.* (2004) 'Mitochondrial hTERT exacerbates free-radical-mediated mtDNA damage', *Aging Cell*. doi: 10.1111/j.1474-9728.2004.00124.x.

Saretzki, G. (2016) 'Extra-telomeric Functions of Human Telomerase : Cancer , Mitochondria and Oxidative Stress Extra-telomeric Functions of Human Telomerase : Cancer , Mitochondria and', (June 2014). doi: 10.2174/1381612820666140630095606.

Sartori, A. A. *et al.* (2007) 'Human CtIP promotes DNA end resection', *Nature*. doi: 10.1038/nature06337.

Schmutz, I. *et al.* (2017) 'TRF2 binds branched DNA to safeguard telomere

integrity', *Nature Structural and Molecular Biology*. doi: 10.1038/nsmb.3451.

Schulz, V. P. and Zakian, V. A. (1994) 'The saccharomyces PIF1 DNA helicase inhibits telomere elongation and de novo telomere formation', *Cell*. doi: 10.1016/0092-8674(94)90179-1.

Schwartz, M. F. *et al.* (2002) 'Rad9 phosphorylation sites couple Rad53 to the Saccharomyces cerevisiae DNA damage checkpoint', *Molecular Cell*. doi: 10.1016/S1097-2765(02)00532-4.

Sfeir, A. and De Lange, T. (2012) 'Removal of shelterin reveals the telomere end-protection problem', *Science*. doi: 10.1126/science.1218498.

Shampay, J., Szostak, J. W. and Blackburn, E. H. (1984) 'DNA sequences of telomeres maintained in yeast.', *Nature*, 310(5973), pp. 154–7. doi: 10.1038/310154a0.

Sharples, G. J. and Leach, D. R. F. (1995) 'Structural and functional similarities between the SbcCD proteins of Escherichia coli and the RAD50 and MRE11 (RAD32) recombination and repair proteins of yeast', *Molecular Microbiology*. doi: 10.1111/j.1365-2958.1995.mmi_17061215_1.x.

Shay, J. W. and Bacchetti, S. (1997) 'A survey of telomerase activity in human cancer.', *European Journal of Cancer Part A*, 33(5), pp. 787–91. doi: 10.1016/S0959-8049(97)00062-2.

Shcherbakova, D. M. *et al.* (2009) 'Telomerase from yeast Saccharomyces cerevisiae is active in vitro as a monomer.', *Biochemistry. Biokhimiia*, 74(7), pp. 749–55. doi: Doi 10.1134/S0006297909070074.

Shi, I. *et al.* (2009) 'Role of the Rad52 amino-terminal DNA binding activity in DNA strand capture in homologous recombination', *Journal of Biological Chemistry*, 284(48), pp. 33275–33284. doi: 10.1074/jbc.M109.057752.

Shibata, A. *et al.* (2014) 'DNA Double-Strand Break Repair Pathway Choice Is Directed by Distinct MRE11 Nuclease Activities', *Molecular Cell*. doi: 10.1016/j.molcel.2013.11.003.

Shim, E. Y. *et al.* (2010) 'Saccharomyces cerevisiae Mre11/Rad50/Xrs2 and Ku proteins regulate association of Exo1 and Dna2 with DNA breaks', *EMBO Journal*. doi: 10.1038/emboj.2010.219.

Shinohara, A., Ogawa, H. and Ogawa, T. (1992) 'Rad51 protein involved in repair and recombination in S. cerevisiae is a RecA-like protein', *Cell*. doi: 10.1016/0092-8674(92)90447-K.

Sickmann, A. *et al.* (2003) 'The proteome of Saccharomyces cerevisiae mitochondria', *Proceedings of the National Academy of Sciences*. doi: 10.1073/pnas.2135385100.

Signon, L. *et al.* (2001) 'Genetic Requirements for RAD51 - and Replication Repair of a Chromosomal Double-Strand Break Genetic Requirements for RAD51 - and RAD54 -Independent Break-Induced Replication Repair of a Chromosomal Double-Strand Break', 21(6), pp. 2048–2056. doi: 10.1128/MCB.21.6.2048.

Singer, M. S. and Gottschling, D. E. (1994) 'TLC1: Template RNA component of Saccharomyces cerevisiae telomerase', *Science*. doi: 10.1126/science.7545955.

Sinha, S. *et al.* (2016) 'Risky business: Microhomology-mediated end joining', *Mutation Research - Fundamental and Molecular Mechanisms of Mutagenesis*. Elsevier B.V., 788, pp. 17–24. doi: 10.1016/j.mrfmmm.2015.12.005.

Smogorzewska, A. and De Lange, T. (2002) 'Different telomere damage signaling pathways in human and mouse cells', *EMBO Journal*. doi: 10.1093/emboj/cdf433.

Song, K. *et al.* (2000) 'Interaction of human Ku70 with TRF2', in *FEBS Letters*. doi: 10.1016/S0014-5793(00)01958-X.

Soulier, J. and Lowndes, N. F. (1999) 'The BRCT domain of the S. cerevisiae checkpoint protein Rad9 mediates a Rad9-Rad9 interaction after DNA damage', *Current Biology*. doi: 10.1016/S0960-9822(99)80242-5.

Spingola, M. *et al.* (1999) ‘Genome-wide bioinformatic and molecular analysis of introns in Saccharomyces cerevisiae’, *RNA*. doi: 10.1017/S1355838299981682.

Stansel, R. M., De Lange, T. and Griffith, J. D. (2001) ‘T-loop assembly in vitro involves binding of TRF2 near the 3′ telomeric overhang’, *EMBO Journal*. doi: 10.1093/emboj/20.19.5532.

Van Steensel, B., Smogorzewska, A. and De Lange, T. (1998) ‘TRF2 protects human telomeres from end-to-end fusions’, *Cell*. doi: 10.1016/S0092-8674(00)80932-0.

Stewart, S. A. *et al.* (2003) ‘Erosion of the telomeric single-strand overhang at replicative senescence’, *Nature Genetics*. doi: 10.1038/ng1127.

Stracker, T. H., Usui, T. and Petrini, J. H. J. (2009) ‘Taking the time to make important decisions: The checkpoint effector kinases Chk1 and Chk2 and the DNA damage response’, *DNA Repair*. doi: 10.1016/j.dnarep.2009.04.012.

Sugawara, N., Wang, X. and Haber, J. E. (2003) ‘In vivo roles of Rad52, Rad54, and Rad55 proteins in Rad51-mediated recombination’, *Molecular Cell*. doi: 10.1016/S1097-2765(03)00269-7.

Sugiyama, T. and Kowalczykowski, S. C. (2002) ‘Rad52 protein associates with replication protein A (RPA)-single-stranded DNA to accelerate Rad51-mediated displacement of RPA and presynaptic complex formation’, *Journal of Biological Chemistry*. doi: 10.1074/jbc.M203494200.

Sugiyama, T., New, J. H. and Kowalczykowski, S. C. (1998) ‘DNA annealing by Rad52 protein is stimulated by specific interaction with the complex of replication protein A and single-stranded DNA’, *Proceedings of the National Academy of Sciences of the United States of America*. doi: 10.1073/pnas.95.11.6049.

Sugiyama, T., Zaitseva, E. M. and Kowalczykowski, S. C. (1997) ‘A single-stranded DNA-binding protein is needed for efficient presynaptic complex formation by the Saccharomyces cerevisiae Rad51 protein’, *Journal of*

Biological Chemistry. doi: 10.1074/jbc.272.12.7940.

Sun, Z. *et al.* (1998) 'Rad53 FHA domain associated with phosphorylated Rad9 in the DNA damage checkpoint', *Science*. doi: 10.1126/science.281.5374.272.

Sung, P. (1994) 'Catalysis of ATP-dependent homologous DNA pairing and strand exchange by yeast RAD51 protein', *Science*. doi: 10.1126/science.8066464.

Sung, P. and Robberson, D. L. (1995) 'DNA strand exchange mediated by a RAD51-ssDNA nucleoprotein filament with polarity opposite to that of RecA', *Cell*. doi: 10.1016/0092-8674(95)90434-4.

Symington, L. S. (2014) 'End resection at double-strand breaks: Mechanism and regulation', *Cold Spring Harbor Perspectives in Biology*. doi: 10.1101/cshperspect.a016436.

Symington, L. S. (2016) 'Mechanism and regulation of DNA end resection in eukaryotes', *Critical Reviews in Biochemistry and Molecular Biology*. doi: 10.3109/10409238.2016.1172552.

Symington, L. S. and Gautier, J. (2011) 'Double-Strand Break End Resection and Repair Pathway Choice', *Annual Review of Genetics*, 45(1), pp. 247–271. doi: 10.1146/annurev-genet-110410-132435.

Symington, L. S., Rothstein, R. and Lisby, M. (2014) 'Mechanisms and regulation of mitotic recombination in saccharomyces cerevisiae', *Genetics*. doi: 10.1534/genetics.114.166140.

Szostak, J. W. *et al.* (1983) 'The double-strand-break repair model for recombination', *Cell*. doi: 10.1016/0092-8674(83)90331-8.

Taggart, A. K. P., Teng, S.-C. and Zakian, V. A. (2002) 'Est1p as a cell cycle-regulated activator of telomere-bound telomerase.', *Science (New York, N.Y.)*, 297(5583), pp. 1023–6. doi: 10.1126/science.1074968.

Talley, J. M. *et al.* (2011) 'Stimulation of yeast telomerase activity by the ever

shorter telomere 3 (Est3) subunit is dependent on direct interaction with the catalytic protein Est2', *Journal of Biological Chemistry*. doi: 10.1074/jbc.M111.228635.

Tatsumoto, N. *et al.* (2000) 'High telomerase activity is an independent prognostic indicator of poor outcome in colorectal cancer', *Clinical Cancer Research*.

Teixeira, M. T. *et al.* (2002) 'Intracellular trafficking of yeast telomerase components', *EMBO Reports*, 3(7), pp. 652–659. doi: 10.1093/embo-reports/kvf133.

Teng, S. C. and Zakian, V. A. (1999) 'Telomere-telomere recombination is an efficient bypass pathway for telomere maintenance in Saccharomyces cerevisiae.', *Molecular and cellular biology*, 19(12), pp. 8083–93. Available at: http://www.ncbi.nlm.nih.gov/pubmed/10567534.

Tittel-Elmer, M. *et al.* (2009) 'The MRX complex stabilizes the replisome independently of the S phase checkpoint during replication stress', *EMBO Journal*. doi: 10.1038/emboj.2009.60.

Toh, G. W. L. *et al.* (2006) 'Histone H2A phosphorylation and H3 methylation are required for a novel Rad9 DSB repair function following checkpoint activation', *DNA Repair*. doi: 10.1016/j.dnarep.2006.03.005.

Tomaska, L. *et al.* (2004) 'Taz1 binding to a fission yeast model telomere: Formation of telomeric loops and higher order structures', *Journal of Biological Chemistry*. doi: 10.1074/jbc.M409790200.

Tran, J. R. and Brodsky, J. L. (2012) 'Assays to Measure ER-Associated Degradation in Yeast', in. Humana Press, pp. 505–518. doi: 10.1007/978-1-61779-474-2_36.

Tsaponina, O. *et al.* (2011) 'Ixr1 is required for the expression of the ribonucleotide reductase Rnr1 and maintenance of dNTP pools', *PLoS Genetics*. doi: 10.1371/journal.pgen.1002061.

Tsubouchi, H. and Ogawa, H. (2000) 'Exo1 roles for repair of DNA double-

strand breaks and meiotic crossing over in Saccharomyces cerevisiae', *Molecular Biology of the Cell*. doi: 10.1091/mbc.11.7.2221.

Tucey, T. M. and Lundblad, V. (2013) 'A yeast telomerase complex containing the Est1 recruitment protein is assembled early in the cell cycle', *Biochemistry*, 52(7), pp. 1131–1133. doi: 10.1021/bi3015218.

Tucey, T. M. and Lundblad, V. (2014) 'Regulated assembly and disassembly of the yeast telomerase quaternary complex', *Genes and Development*, 28(19), pp. 2077–2089. doi: 10.1101/gad.246256.114.

Tuzon, C. T. *et al.* (2011) 'The saccharomyces cerevisiae telomerase subunit Est3 binds telomeres in a cell cycle- and Est1-dependent manner and interacts directly with Est1 in vitro', *PLoS Genetics*, 7(5), pp. 1–12. doi: 10.1371/journal.pgen.1002060.

Usui, T. *et al.* (1998) 'Complex formation and functional versatility of Mre11 of budding yeast in recombination', *Cell*. doi: 10.1016/S0092-8674(00)81640-2.

Usui, T., Foster, S. S. and Petrini, J. H. J. (2009) 'Maintenance of the DNA-Damage Checkpoint Requires DNA-Damage-Induced Mediator Protein Oligomerization', *Molecular Cell*. doi: 10.1016/j.molcel.2008.12.022.

VanHulle, K. *et al.* (2007) 'Inverted DNA Repeats Channel Repair of Distant Double-Strand Breaks into Chromatid Fusions and Chromosomal Rearrangements', *Molecular and Cellular Biology*. doi: 10.1128/mcb.01740-06.

Vasan, S. *et al.* (2014) 'Cascades of Genetic Instability Resulting from Compromised Break-Induced Replication', *PLoS Genetics*. doi: 10.1371/journal.pgen.1004119.

Vasianovich, Y., Harrington, L. A. and Makovets, S. (2014) 'Break-Induced Replication Requires DNA Damage-Induced Phosphorylation of Pif1 and Leads to Telomere Lengthening.', *PLoS Genetics*, 10(10), p. e1004679. doi: 10.1371/journal.pgen.1004679.

Vega, L. R. *et al.* (2007) 'Sensitivity of yeast strains with long G-tails to levels

of telomere-bound telomerase', *PLoS Genetics*, 3(6), pp. 1065–1075. doi: 10.1371/journal.pgen.0030105.

Venclovas, Č. and Thelen, M. P. (2000) 'Structure-based predictions of Rad1, Rad9, Hus1 and Rad17 participation in sliding clamp and clamp-loading complexes', *Nucleic Acids Research*. doi: 10.1093/nar/28.13.2481.

Vialard, J. E. *et al.* (1998) 'The budding yeast Rad9 checkpoint protein is subjected to Mec1/Tel1-dependent hyperphosphorylation and interacts with Rad53 after DNA damage', *EMBO Journal*. doi: 10.1093/emboj/17.19.5679.

Vijayraghavan, U., Company, M. and Abelson, J. (1989) 'Isolation and characterization of pre-mRNA splicing mutants of Saccharomyces cerevisiae.', *Genes & development*, 3(8), pp. 1206–1216. doi: 10.1101/gad.3.8.1206.

Vilenchik, M. M. and Knudson, A. G. (2003) 'Endogenous DNA double-strand breaks: Production, fidelity of repair, and induction of cancer', *Proceedings of the National Academy of Sciences of the United States of America*. doi: 10.1073/pnas.2135498100.

Villarreal, D. D. *et al.* (2012) 'Microhomology Directs Diverse DNA Break Repair Pathways and Chromosomal Translocations', *PLoS Genetics*. doi: 10.1371/journal.pgen.1003026.

Van Vugt, M. A. T. M., Brás, A. and Medema, R. H. (2004) 'Polo-like kinase-1 controls recovery from a G2 DNA damage-induced arrest in mammalian cells', *Molecular Cell*. doi: 10.1016/j.molcel.2004.07.015.

Wang, H. *et al.* (2001) 'Pds1 phosphorylation in response to DNA damage is essential for its DNA damage checkpoint function', *Genes and Development*. doi: 10.1101/gad.893201.

Wang, H. *et al.* (2012) 'CtIP protein dimerization is critical for its recruitment to chromosomal DNA double-stranded breaks', *Journal of Biological Chemistry*. doi: 10.1074/jbc.M112.355354.

Wang, R. and Brattain, M. G. (2007) 'The maximal size of protein to diffuse through the nuclear pore is larger than 60 kDa', *FEBS Letters*, 581(17), pp.

3164–3170. doi: 10.1016/j.febslet.2007.05.082.

Wang, X. and Haber, J. E. (2004) ‘Role of Saccharomyces single-stranded DNA-binding protein RPA in the strand invasion step of double-strand break repair’, *PLoS Biology*. doi: 10.1371/journal.pbio.0020021.

Wanrooij, P. H. and Burgers, P. M. (2015) ‘Yet another job for Dna2: Checkpoint activation’, *DNA Repair*. Elsevier B.V., 32, pp. 17–23. doi: 10.1016/j.dnarep.2015.04.009.

Weinert, T. A. and Hartwell, L. H. (1993) ‘Cell cycle arrest of cdc mutants and specificity of the RAD9 checkpoint.’, *Genetics*. Genetics Society of America, 134(1), pp. 63–80. Available at: http://www.ncbi.nlm.nih.gov/pubmed/8514150 (Accessed: 25 July 2016).

Wellinger, R. J. R. J. and Zakian, V. A. V. A. (2012) ‘Everything you ever wanted to know about Saccharomyces cerevisiae telomeres: Beginning to end’, *Genetics*, 191(4), pp. 1073–1105. doi: 10.1534/genetics.111.137851.

Wellinger, R. J., Wolf, A. J. and Zakian, V. A. (1993) ‘Saccharomyces telomeres acquire single-strand TG1-3 tails late in S phase’, *Cell*, 72(1), pp. 51–60. doi: 10.1016/0092-8674(93)90049-V.

Wenz, C. *et al.* (2001) ‘Human telomerase contains two cooperating telomerase RNA molecules’, *EMBO Journal*, 20(13), pp. 3526–3534. doi: 10.1093/emboj/20.13.3526.

Wilson, M. A. *et al.* (2013) ‘Pif1 helicase and Polδ promote recombination-coupled DNA synthesis via bubble migration’, *Nature*. doi: 10.1038/nature12585.

Wiltzius, J. J. W. *et al.* (2005) ‘The Rad50 hook domain is a critical determinant of Mre11 complex functions’, *Nature Structural and Molecular Biology*. doi: 10.1038/nsmb928.

Wu, D., Topper, L. M. and Wilson, T. E. (2008) ‘Recruitment and dissociation of nonhomologous end joining proteins at a DNA double-strand break in Saccharomyces cerevisiae’, *Genetics*. doi: 10.1534/genetics.107.083535.

Wu, P., Takai, H. and De Lange, T. (2012) 'Telomeric 3′ overhangs derive from resection by Exo1 and apollo and fill-in by POT1b-associated CST', *Cell*. doi: 10.1016/j.cell.2012.05.026.

Wyman, C. and Kanaar, R. (2006) 'DNA Double-Strand Break Repair: All's Well that Ends Well', *Annual Review of Genetics*. doi: 10.1146/annurev.genet.40.110405.090451.

Xie, H., Bandhakavi, S. and Griffin, T. J. (2005) 'Evaluating preparative isoelectric focusing of complex peptide mixtures for tandem mass spectrometry-based proteomics: A case study in profiling chromatin-enriched subcellular fractions in Saccharomyces cerevisiae', *Analytical Chemistry*. doi: 10.1021/ac0482256.

Ye, J. Z. S. *et al.* (2004) 'POT1-interaction protein PIP1: A telomere length regulator that recruits POT1 to the TIN2/TRF1 complex', *Genes and Development*. doi: 10.1101/gad.1215404.

Yu, X. and Gabriel, A. (2004) 'Reciprocal Translocations in Saccharomyces cerevisiae Formed by Nonhomologous End Joining', *Genetics*. doi: 10.1534/genetics.166.2.741.

Zappulla, D. C. *et al.* (2011) 'Ku can contribute to telomere lengthening in yeast at multiple positions in the telomerase RNP.', *RNA (New York, N.Y.)*, 17, pp. 298–311. doi: 10.1261/rna.2483611.

Zheng, L. and Shen, B. (2011) 'Okazaki fragment maturation: Nucleases take centre stage', *Journal of Molecular Cell Biology*. doi: 10.1093/jmcb/mjq048.

Zhu, X. D. *et al.* (2000) 'Cell-cycle-regulated association of RAD50/MRE11/NBS1 with TRF2 and human telomeres', *Nature Genetics*. doi: 10.1038/77139.

Zhu, Z. *et al.* (2008) 'Sgs1 Helicase and Two Nucleases Dna2 and Exo1 Resect DNA Double-Strand Break Ends', *Cell*. doi: 10.1016/j.cell.2008.08.037.

Zou, L. and Elledge, S. J. (2003) 'Sensing DNA damage through ATRIP recognition of RPA-ssDNA complexes', *Science*. doi:

10.1126/science.1083430.

Zou, L., Liu, D. and Elledge, S. J. (2003) ‘Replication protein A-mediated recruitment and activation of Rad17 complexes’, *Proceedings of the National Academy of Sciences of the United States of America*. doi: 10.1073/pnas.2336100100.

Zou, Y. *et al.* (2004) ‘Does a sentinel or a subset of short telomeres determine replicative senescence?’, *Molecular Biology of the Cell*. doi: 10.1091/mbc.E04-03-0207.

Zubko, M. K., Guillard, S. and Lydall, D. (2004) ‘Exo1 and Rad24 differentially regulate generation of ssDNA at telomeres of Saccharomyces cerevisiae cdc13-1 mutants’, *Genetics*, 168(1), pp. 103–115. doi: 10.1534/genetics.104.027904.